MRI biomarkers of recovery for acute stroke

D.Phil. thesis, University of Oxford

Davide Carone

MD

Linacre College, Oxford

MRI biomarkers of recovery for acute stroke

DPhil thesis, Davide Carone, Linacre College

Trinity Term, 2021

Abstract

Predicting stroke recovery is challenging. Imaging biomarkers might help address this unmet need. However, the majority of studies to date have been performed in the post-acute period or used simplistic biomarkers such as infarct volume and have largely ignored the dynamic processes that occur immediately after stroke such as the contribution of oedema.

This Thesis set out to address these issues in a systematic manner in a cohort of patients recruited to a clinical imaging study at the John Radcliffe Hospital. Serial imaging data were acquired starting from the first hours following symptom onset.

The first part of this Thesis focused on improving measurement accuracy. A machine learning approach was developed and validated to segment stroke lesion and separately quantify infarct volume and anatomical distortion (oedema ± haemorrhagic transformation). An independent component analysis (ICA) based approach was used for the first time to denoise arterial spin labeling (ASL) perfusion data. Minimising the potential confounding factors present in the early stroke stages enabled the robust analysis and interpretation of the results obtained.

The second part of this Thesis used Topological Data Analysis (TDA) to analyse structural (DTI tractography) and functional data (rs-fMRI). TDA allows the study of higher order complex relationships between brain regions using spatially insensitive metrics. TDA metrics showed that both structural and functional connectivity were independent predictors of recovery. The changes in functional connectivity were independent of perfusion metrics, either BOLD or ASL derived. At 1-week, oedema was associated with symptom severity and recovery. Oedema was linked to presenting vasodilation and vasoconstriction, the latter providing supporting evidence for the glymphatic theory.

The results of this Thesis open the opportunity for further work to validate TDA metrics as biomarkers of recovery and to understand whether they may play a role in clinical trial design. In addition, a greater understanding of how post-stroke oedema reflects the balance of injury and repair mechanisms is needed to guide what treatment might be appropriate and when following acute stroke. These biomarkers could allow personalised treatment.

Table of Contents

Abstract *2*

Table of Contents *3*

List of publications *10*

Acknowledgements *11*

Chapter 1. Introduction *12*

1. Stroke Background **12**

2. Injury and recovery are more closely related than initially thought **12**

3. The potential role of recovery biomarkers **19**

4. Analytical approaches: the brain as a complex network **31**

5. Aim **36**

Chapter 2. MRI Biomarkers of Recovery in Acute Stroke: Systematic Review *37*

1. Introduction **37**

2. Methods **38**

3. Results **43**

4. Discussion **54**

Chapter 3. General Methods *60*

1. Overview **60**

2. Study participants **60**

3. Study procedures **61**

4. Imaging **63**

5. Measures of recovery **67**

6. Recruitment results **68**

Chapter 4. Improving accuracy of measurements: Automating Infarct and Oedema quantification ……..……..70

1. **Introduction** **70**
2. **Methods** **72**
3. **Results** **80**
4. **Discussion** **87**
5. **Conclusion** **89**

Chapter 5. Improving accuracy of measurements: an ICA based approach to denoise ASL……..90

1. **Introduction** **90**
2. **Methods** **92**
3. **Results** **101**
4. **Discussion** **111**
5. **Conclusion** **113**

Chapter 6. Topological Data Analysis of Functional Connectivity 115

1. **Introduction** **115**
2. **Methods** **117**
3. **Results** **125**
4. **Discussion** **137**
5. **Conclusions** **140**

Chapter 7. Local and Whole brain metrics of Residual Integrity 142

1. **Introduction** **142**
2. **Methods** **144**
3. **Results** **151**
4. **Discussion** **158**
5. **Conclusions** **161**

Chapter 8. The impact of haemodynamic status on functional connectivity and oedema……..…….163

1. Introduction 163

2. Methods 165

3. Results 170

4. Discussion 178

Chapter 9. Summary and Conclusions 183

1. Summary 183

2. General considerations and future work 185

Appendix A: Example Search Strategy used in Chapter 2 190

Appendix B: Studies included in Chapter 2 193

Appendix C: Studies included in Chapter 2 210

Appendix D 223

Appendix E 224

References 225

Abbreviations

AD	Anatomical Distortion
ADC	Apparent Diffusion Coefficient
AF	Atrial Fibrillation
AMICI	Acute Magnetic Resonance Imaging In Cerebral Ischaemia
ANOVA	Analysis Of Variance
ASL	Arterial Spin Labeling
ASPECTS	Alberta Stroke Programme Early CT Score
ATP	Adenosine Triphosphate
ATT	Arterial Transit Time
AUC	Area Under The Curve
BASIL	Bayesian Inference For Arterial Spin Labeling
BBB	Blood–Brain Barrier
BBR	Boundary-Based Registration
BIANCA	Brain Intensity Abnormality Classification Algorithm
BOLD	Blood-Oxygen-Level Dependent
CASL	Continuous Arterial Spin Labeling
CBF	Cerebral Blood Flow
CBV	Cerebral Blood Volume
CCD	Chronic Cerebrovascular Disease
CEST	Chemical Exchange Saturation Transfer
CI	Confidence Interval
CMRO2	Cerebral Blood Oxygen Consumption
CMS	Clique Maximum Size
CNR	Contrast-To-Noise Ratio
CSF	Cerebrospinal Fluid
CST	Cortical Spinal Tract
CT	X-Ray Computed Tomography
CVD	Cardiovascular Disease
DC	Davide Carone, Thesis Author
DER	Detection Error Rate
DSC	Dynamic Susceptibility Contrast
DSI	Dice Similarity Index
DTI	Diffusion Tensor Imaging
DWI	Diffusion Weighted Imaging
ENABLE	Enhancement Of Automated Blood Flow Estimates
EPI	Echo Planar Imaging
FA	Fractional Anisotropy
FAST	Fmrib's Automated Segmentation Tool

FDR	False Discovery Rate
FDT	Fmrib's Diffusion Toolbox
FIX	FMRIB's ICA-Based Xnoiseifier
FLAIR	Fluid-Attenuated Inversion Recovery
FLIRT	FSL Linear Registration Tool
FMRIB	Functional Magnetic Resonance Imaging Of The Brain
FN	False Negative
FNIRT	FSL Non-Linear Registration Tool
FNR	False-Negative Rate
FP	False Positive
FSL	Fmrib Software Library
GABA	Gamma Aminobutyric Acid
GLM	Generalized Linear Model
HCP	Human Connectome Project
IAT	Intra-Arterial Thrombolysis
IC	Independent Component
ICA	Independent Component Analysis
ICC	Intraclass Correlation Coefficient
k-NN	K-Nearest Neighbour
LAA	Large Artery Atherosclerosis
LHI	Large Hemispheric Infarctions
LOWESS	Locally Weighted Scatterplot Smoothing
LVO	Large Vessel Occlusion
MAP	Mean Arterial Pressure
MB	Multi Band
MCA	Middle Cerebral Artery
MD	Mean Diffusivity
MELODIC	Multivariate Exploratory Linear Optimized Decomposition Into Independent Components
MPRAGE	Magnetization-Prepared Rapid Gradient Echo
MR	Magnetic Resonance
MRA	Magnetic Resonance Angiogram
MRI	Magnetic Resonance Imaging
MRS	Magnetic Resonance Spectroscopy
mRS	Modified Rankin Scale
MT	Mechanical Thrombectomy
MTT	Mean Transit Time
NetMat	Network-Matrix
NHS	National Health Service
NIHSS	National Institutes Of Health Stroke Scale
NMR	Nuclear Magnetic Resonance

NODDI	Neurite Orientation Dispersion And Density Imaging
nTPT	Number Of Topological Phase Transitions
OER	Outline Error Rate
PASL	Pulsed Arterial Spin Labeling
PCA	Principal Component Analysis
PCASL	Pseudo Continuous Arterial Spin Labeling
PET	Positron Emission Tomography
PH2	Parenchymal Haematoma Type 2
PI	Pulsatility Index
PLD	Post Labeling Delay
PRISMA	Preferred Reporting Items For Systematic Reviews And Meta-Analyses
PVE	Partial Volume Estimate
PVS	Perivascular Space Size
PWI	Perfusion Weighted Imaging
QUADAS	Quality Assessment Of Diagnostic Accuracy Studies
QUAPAS	Quality Assessment Of Prognostic Accuracy Studies
rAD	Relative Anatomical Distortion
RCT	Randomized Controlled Trial
RF	Radiofrequency
RI	Resistivity Index
ROC	Receiver Operating Characteristic
ROI	Region Of Interest
RS	Resting State
rs-fMRI	Resting State Functional Magnetic Resonance Imaging
RSN	Resting State Network
SD	Standard Deviation
SL	Stroke Lesion
sLFO	Systemic Low-Frequency Oscillations
SNR	Signal To Noise Ratio
SVD	Small Vessel Disease
SVZ	Subventricular Zone
SW	Small-Worldness
SWI	Susceptibility Weighted Imaging
T1	Longitudinal Recovery
T2	Transverse Decay
TDA	Topological Data Analysis
TE	Echo Time
TIA	Transient Ischaemic Attack
TCD	Trans-Cranial Doppler
TNR	True Negative Ratio

TPR	True Positive Ratio
TR	Repetition Time
TTP	Time To Peak
VEPCASL	Vessel-Encoded Pseudocontinuous Arterial Spin Labeling
WMH	White Matter Hyperintensities

List of publications

Publications arising from this thesis:

Carone D, Harston GWJ, Garrard J, De Angeli F, Griffanti L, Okell TW, Chappell MA, Kennedy J. ICA-based denoising for ASL perfusion imaging. Neuroimage. 2019 Oct 15;200:363-372. doi: 10.1016/j.neuroimage.2019.07.002. Epub 2019 Jul 2. PMID: 31276796; PMCID: PMC6711457.

Presented abstracts arising from this thesis (DC as first author):

European Stroke Organisation Conference 2017 (Prague):

Carone D, Harston GWJ, Filippini N, Kennedy J. Adaptative changes in the insula network match functional recovery following acute stroke**. -**poster presentation- European Stroke Journal, vol. 2, 1_suppl: pp. 496-562. , First Published May 16, 2017.

International Society for Magnetic Resonance in Medicine Conference 2018 (Paris):

Carone D, Harston GWJ, Okell TO, Chappell M, Kennedy J. Impact of ICA-based denoising of ASL data in clinical settings -poster presentation-

European Stroke Organisation Conference 2019 (Milan):

Carone D, De Angeli F, Griffanti L, Sheerin F. Jenkinson M, Harston GWJ. Automated infarct definition using a volume-dependent machine learning approach –poster presentation-

Acknowledgements

I am indebted to a large number of individuals for their help and support in the writing of this thesis. In particular I must thank my supervisor, Professor James Kennedy for his support and guidance over many years. I have benefited enormously from his knowledge and wisdom in both the clinical and research settings. I am also grateful to Dr. George Harston. His enthusiasm and guidance over the duration of my research fellowship has proved invaluable.

I must also thank my clinical fellow colleagues for the help I have received. Dr. Fausto De Angeli and Dr. James Garrard both collected data that was used in this thesis, and provided the complementary delineation of the follow up lesions used in Chapter 3 and 4. Dr. James Garrard also contributed to the systematic review in Chapter 2.

I am grateful to the Acute Stroke Service at the Oxford University Hospitals NHS Trust for facilitating the recruitment of patients under their care into. I am indebted to the stroke consultants at the John Radcliffe Hospital, Rocel Espinosa, and Rachel Teal for their advice and support. I am also grateful to the team in the Oxford Acute Vascular Imaging Centre, Alison Fletcher, Peter Manley, and Carol Davey, without whom it would not have been possible to deliver acute clinical research imaging in this cohort of patients. From the Department of Neuroradiology, I am thankful to Dr. Fintan Sheerin, not only for providing MRI reports, but also for reviewing the manually delineated follow up lesion definitions in Chapter 4.

I have received invaluable support and advice from the research groups of Professors Jezzard, Jenkinson and Chappell. The regular input provided by the group leaders has ensured the technical integrity of this work. I am indebted to Dr. Thomas Okell, Dr. Ludovica Griffanti, Martin Craig, and Professor Michael Chappell, for the insight on the postprocessing strategies described in Chapter 4 and 5. For the work in Chapter 6 and 7, I am indebted to Prof. Nobrega Santos for his guidance on applying Topological Data Analysis to functional and structural data.

Finally, I would like thank my family and in particular my partner, Lise, for her support, and my brother and parents, for their lifelong inspiration and encouragement.

This work was financially supported by the National Institute for Health Research Oxford Biomedical Research Centre Programme, the Dunhill Medical Trust and the Centre of Excellence for Personalized Healthcare funded by the Wellcome Trust and Engineering and Physical Sciences Research Council.

Chapter 1.

Introduction

1. Stroke Background

Stroke remains a leading cause of mortality and morbidity in developed nations.[1] In England stroke affects 110,000 people each year, and the prevalence of stroke survivors with moderate to severe disability is approximately 300,000.[2] It is estimated that stroke care costs the NHS £2.8 billion per year and the wider economy £1.8 billion in lost productivity and care.[3]

Functional recovery following stroke is dependent on the balance between injury and recovery mechanisms.[4] Limiting injury progression through recanalisation treatments remains the only approach demonstrated to improve outcome. However, only a minority of patients are eligible for this treatment.[5] Neuroprotective and neurorestorative strategies aimed at preventing salvageable neurons from dying and promoting repair have failed in clinical trials.[6,7]

2. Injury and recovery are more closely related than initially thought

Stroke research has mainly addressed injury and recovery separately, with most of the work investigating the latter set weeks or months after the event.[4,8] However, increasing evidence suggests that right after stroke onset, injured tissue is not just passively dying over time. It is also actively recovering.[9] Multiple processes of endogenous repair and remodelling are triggered after stroke, and many molecular targets mediating injury also mediate neurovascular remodelling during recovery.[9]

Neuroprotective approaches have concentrated on blocking injury mechanisms without considering the potential detrimental effects on repair/recovery.[9] Neurorestorative strategies have been tested too late,[10, 11] and have not excluded patients with insufficient residual structural and functional cerebral architecture to recover.[12]

2.1. Injury mechanisms

This transition from injury to recovery is not limited to the initial area of focal damage. Injury and recovery processes affect both peri-infarct tissue and more remote areas.

2.1.1. Infarct Core

Ischaemia is the imbalance between the energy requirements of the cell and its blood supply. This imbalance causes the resting membrane potential to collapse. As a result, neurons depolarise, releasing glutamate, which induces massive intracellular calcium entry. Calcium-mediated proteolysis, lipolysis, and DNA degradation lead to necrotic cell death. In addition, free radical formation, mitochondrial dysfunction and apoptosis also contribute to the initial neuronal cell death.[13]

Hours after the infarct, all cells in the infarct core die. Tissue repair and recovery depend on what happens in the tissue surrounding the infarct and in the connected areas.[14]

2.1.2. Penumbra and Peri-infarct

Over time, injury progresses from the infarct core to the surrounding areas.[14] It is useful to distinguish here two terms, ischaemic penumbra and peri-infarct, that have been used in stroke research to describe tissue surrounding the infarct.

- The concept of *ischaemic penumbra* has been pivotal in stroke reperfusion/recanalisation research. The penumbra was originally defined physiologically as the region of electrical silence in initially intact but hypoxic tissue at the onset of ischaemia.[15] Over the years, the ischaemic penumbra has come to mean the brain tissue that will progress to infarction over time if not treaated.[14]
- *Peri-infarct* is a term that has been used in stroke recovery research, as it constitutes a crucial region for tissue recovery.[14] *Peri-infarct* is a topographical term, it refers to the tissue next to the infarct core that has experienced partial damage.[14] Penumbra tissue that dies will become part of the infarct core, and the peri-infarct tissue will border the now enlarged infarct core. Penumbra tissue salvaged by reperfusion will remain part of the peri-infarct tissue.[14]

Secondary injury cascades mediate injury progression from the infarct core to the surrounding tissue.[14] Prolonged ischaemia, reperfusion[16] and inflammation[17] cause delayed cell injury and death mediated by free radical production and release of cytokines. Spreading depolarisation, recurrent waves of intense neuronal and glial mass-depolarisations further exacerbate tissue injury, as they are energetically highly costly and worsen the already compromised supply-demand mismatch.[18, 19]

Days to weeks after stroke, the peri-infarct cortex loses its initial response to afferent inputs neuronal excitability, further contributing to impaired circuit function and symptom severity.[20] This is caused by both an increased tonic GABA inhibition, a neuroprotective mechanism limiting depolarisations, and a net loss of dendritic spines in peri-infarct cortex.[20, 21]

The time course for the different pathological processes range from minutes to weeks,[13, 22] and are dependent on the reperfusion dynamics of the tissue, which can be either beneficial, or deleterious (e.g. in the context of reperfusion injury).[16]

2.1.3. Remote areas

The effects of focal stroke are relayed to remote brain areas through loss of neuronal connections, secondary axonal degeneration, and microglial and astrocyte activation. Minutes following stroke, axons projecting from the infarct lose their synaptic connections to distant sites. The disconnected cortical areas will also suffer delayed damage and neuronal death.[23] These remote brain areas, once deprived of their input or output, can no longer subserve behaviour and cognition, contributing to symptoms severity. Accordingly, network analyses in human and animal models of stroke have shown widespread disconnection of functional brain networks following stroke.[24-26] The degree of disconnection observed goes well beyond the original concept of diaschisis, a remote metabolic disturbance in one brain region produced from a stroke in another.[14]

2.2. Secondary injury mechanisms trigger recovery

Molecules playing an active role in injury have also been shown to play an essential role in neurovascular remodelling during recovery.[9] Free radicals generated in the penumbra and peri-infarct tissue activate growth factor signalling pathways [27] and promote neurogenesis.[27, 28] Inflammatory cytokines[29] induce the formation of new connections through axonal sprouting and dendritic growth[30]; promote angiogenesis,[31] neurogenesis and neuronal migration to areas of damage after stroke,[29, 32, 33] and activate endothelial and glial cells response, which in turn promotes the expression of nerve growth factors and neurotransmitter receptors[34, 35]

Days after stroke, synchronised low-frequency neuronal discharges replace spreading depolarisation.[36] The synchronised activity induces a downstream molecular program for neuronal growth, stimulates plasticity in specific regions of neurons, and induces axonal sprouting and the formation of new connections[36, 37]

These effects not only occur in the vicinity of the lesion but also in remote areas.[14] Electrical and molecular signals induce cytokines and growth factors in the contralateral cortex, basal ganglia, thalamus, brain stem, and spinal cord. They activate astrocytes and microglia and also trigger tissue regeneration**.**

2.3. Recovery mechanisms

Although the term recovery is used to describe the improvement in neurological deficits following stroke,[38] the re-emergent post-stroke behaviour is unlikely to be identical to the pre-stroke state.[39] This behavioural compensation is provided by remaining and newly developed brain connections.[39] Recovery after stroke involves complex interrelated systems of repair.

2.3.1. Injury resolution and recovery of function of the peri-infarct tissue

The acute normalisation of blood flow can facilitate early recovery by restoration of excitability and network responsiveness to previously non-functioning neurons. The benefit from reperfusion is not limited to saving penumbra tissue at risk of dying. Decreased perfusion in the peri-infarct areas can persist for weeks after stroke, contributing to symptom severity.[40, 41] The restoration of blood supply through spontaneous recanalisation or vascular remodelling alleviates these behavioural deficits and contributes to neurological improvement.[42, 43] Additionally, adequate tissue perfusion in the area surrounding the infarct can hasten or augment synaptic plasticity and functional recovery after stroke.[44]

Anatomical distortions secondary to the presence of oedema can also disrupt nearby neuronal functioning. As oedema subsides, these neurons may regain function, allowing for early recovery. In the first weeks after stroke, normalisation of the tonic GABA inhibition and restoration of dendritic spines in peri-infarct cortex allow for a differential return of neuronal activation within the peri-infarct cortex.[20, 21, 43, 45]

2.3.2. Reorganisation

Brain reorganisation plays a major role in the recovery process. It enables spared regions to take over the function of the damaged area. This process occurs both through activation of already existing, redundant connections, and through the ability of new circuits to form. To this end, surviving neurons undergo active structural and functional remodelling, which is associated with a remapping of lost function[20, 39, 43] and restoration of disconnected regions.

Reorganisation through the activation of redundant connections: some degree of remapping of function can occur within minutes after acute stroke.[46] Such a brief timescale is inconsistent with axonal sprouting and synaptogenesis.[47-49] Reorganisation is likely mediated by the unmasking of latent functional connections. During brain development and learning, widespread connections are created across brain regions. The more efficient pathways are then gradually strengthened,[50, 51]whilst the remaining are progressively inhibited. This process leaves redundant pathways well-positioned to compensate in the event of injury.

Reorganisation through new connections: structural plasticity plays a major role in recovery.[39] Axonal sprouting[52, 53] and dendritic spine turnover[20, 43] enable the rewiring of surviving tissue in both the peri-infarct tissue and connected areas. Neurons in regions 1–2 mm distant from the infarct gain synaptic connections,[43] indicating these neurons form

new connections after stroke. The branches of dendrites also remodel after stroke, with retraction and growth that is maximal 2 weeks after the infarct. These new axonal connections from neurons in the peri-infarct cortex are initiated in the first week after stroke and are reliably present 1 month after stroke[52-54]

The reorganisation site depends on the extent of the injury: The recovery process aims for efficiency in circuit utilisation.[55] A focusing stage follows the activation of redundant connections.[56] The more cost-efficient connections will be strengthened whilst the remaining will be progressively inhibited.

Areas with shared connectivity to the site of injury are more efficient in taking over the function of the damaged region than unrelated structures. Following small strokes, recovery will incorporate proximal circuits in functionally related structures (spared peri-infarct tissue with function and connectivity that is similar to the infarct)[20, 57]. In larger strokes, there may not be enough surviving cortical neurons for reorganisation in the peri-infarct. Therefore, less efficient and more distally located (e.g., supplementary areas in the injured hemisphere,[55, 58] and homotopic regions in the contralateral hemisphere[55, 59]) will be recruited to mediate recovery.

2.3.3. Tissue regeneration

Neurogenesis, gliogenesis, and angiogenesis may also play a role in repair, although the role these mechanisms play in recovery seems to be more limited in humans compared to rodents and primates.

Ischaemia induces proliferation and migration of neural and glial progenitors. The subventricular zone (SVZ) is the largest germinal matrix in the brain for neural progenitors. Stroke triggers an increased proliferation in the SVZ and neuroblasts migration to the

damaged regions.[14, 60] Post-stroke angiogenesis begins days after stroke and is a key mechanism of tissue recovery and regeneration. Angiogenesis and vascular remodelling occur most prominently in peri-infarct tissue. Angiogenic vessels secrete growth factors, proteases, and cytokines that modulate the local tissue environment and induce migration of neuroblasts after stroke[14, 60-62]

3. The potential role of recovery biomarkers

The development of treatments for promoting recovery of stroke survivors has been hampered by the inability to stratify which patients could benefit from intervention.[63-65] This is partly due to the heterogeneity in the residual structural and functional post-stroke brain architecture and the impact this has on recovery.[65, 66]

Stroke recovery biomarkers are defined as indicators of disease state that can be used clinically as a measure reflecting underlying molecular/cellular processes that may be difficult to measure directly in humans, and could be used to predict recovery/treatment response.[38] Identifying early biomarkers of recovery would allow stratifying patients based on their potential ability to recover, rationalising rehabilitation goals and improving the design of clinical trials.[38] Recovery biomarkers could be beneficial in identifying new potential therapeutic targets and define when a neuroprotective or a neurorestorative strategy would be more beneficial.[38]

Biomarkers can inform on domain-specific or global end points.[67] Domain-specific endpoints are assessments that correspond to the output of individual neural systems.[67] Global end points combine several attributes into a single score and are useful for capturing broad treatment effects in a summary way.[67] Domain-specific biomarkers are useful for capturing treatment effects on specific behaviours (e.g motor, sensory or language

recovery). However, they are often developed for selected stroke subpopulations (e.g. patients with isolated upper motor weakness) and as a result might not be generalisable to the broader stroke population. By contrast, biomarkers of overall recovery are usually more generalisable but might be less sensitive to changes in specific behaviours.

There are limited validated markers of stroke recovery, but promising potential targets exist.[38] Blood-genetic biomarkers consist of molecular signatures (brain-derived molecules such as micro-RNAs, lipids, short peptide chains, and exosomes that cross the blood brain barrier) and genetic profiles associated to post-stroke recovery.[68, 69] Despite many potential targets, there is limited evidence available at this time for their use.[38]

Another potential recovery biomarker is neurophysiological status. There is broad consensus that the presence of an upper limb motor evoked potential (MEP) in response to transcranial magnetic stimulation relates to motor outcome.[70] Prediction of recovery is more challenging for patients without a MEP,[71] and additional biomarkers might be required as for the PREP algorithm.[70] Magnetoencephalography (MEG) is potentially sensitive to alterations in both GABAergic and glutamatergic signalling that are important for plasticity and recovery after stroke.[72, 73] However, MEG is not yet of common use, possibly due to the elevated costs and the need of a dedicated multidisciplinary team.[38,73]

Considerable resources have focused on brain imaging to define post-stroke patterns of recovery. MRI represents an ideal approach for investigating this transition from injury to recovery following acute stroke. It is non-invasive, accessible, and, unlike neurophysiology techniques, allows simultaneous investigation of brain structure, function and chemistry. By manipulating multiple proprieties of protons in nuclei, several tissue properties can be probed.[74-78]

3.1. Principles of MRI

MRI exploits nuclear magnetic resonance (NMR) to generate images.[79] NMR usually involves three sequential steps:

Alignment: an MRI scanner consists of a high strength magnetic field aligned in the bore of an electromagnet to create the homogeneous resting field, B_0. The B_0 field causes a net alignment of protons along the longitudinal axis (M_z).[79]

Perturbation: by exciting the protons using a weak oscillating magnetic field, usually referred to as a radio-frequency (RF) pulse, the net alignment of protons is deflected from the longitudinal axis (M_z) towards the transverse plane ($M_{X/Y}$). The oscillation frequency required for significant perturbation is dependent upon the static magnetic field (B_0) and the nuclei of observation. Protons rotate around the B_0 axis (precession), the rate of which is also determined by the magnetic field strength. After the initial RF pulse, spins are completely in phase and produce a maximal amount of signal on the transverse plane.[79]

Readout: the NMR signal is detected during or after the RF pulse, due to the voltage induced in a detection coil by precession of the nuclear spins around B_0.[79]

Over time the deflected protons realign with the B_0 field, a process called longitudinal relaxation. The half-life of the longitudinal relaxation is denoted by T1. After the initial RF pulse, spins are completely in phase and produce a maximal amount of signal on the transverse plane. Due to local differences in the microenvironment magnetic field, the protons gradually dephase, causing a drop in signal on the transverse plane. This is called transverse relaxation, and the half-life of this is denoted by T2.[79]

In addition to the differences in the microenvironment magnetic field that lead to T2 transverse decay, larger scale inhomogeneities in the B_0 field lead to additional dephasing. As a result, the drop in signal measured is the sum of T2 relaxation and B_0 inhomogeneity dephasing and is referred to as T2*. This is most apparent in regions of the brain where the B_0 field is distorted, such as near large veins or haemorrhages. In order to isolate the T2 effect from the T2* signal, the proton spins are inverted 180° halfway between the RF pulse and the image readout. This is known as a spin-echo sequence as to opposed the gradient echo sequence. [79]

To acquire a signal the protons are repeatedly excited by RF pulses. The time in-between pulses is denominated repetition time, TR. During each TR and after each RF pulse the signal is acquired at a time known as the echo time, TE. Manipulation of the TR and TE leads to different properties of the protons influencing the signal to different degrees.[79]

By applying gradients across the B_0 field during the readout, the spin frequencies of the protons are manipulated in such a way that spatial frequencies of the signal intensity are generated. The spatial frequency information creates a k-space image that following a Fourier transform generates a conventional MRI picture.[79]

3.2. Diffusion-weighted imaging

Diffusion-weighted imaging (DWI) exploits the ability of magnetic gradients to change the precession frequency of a proton allowing to determine how much that proton has moved.[79]

DWI is a T2-weighted sequence with two opposite magnetic gradients applied at the beginning and end of the TE.[79] The first gradient is transiently applied after the RF pulse. As a result, the precession frequency changes across the gradient. When the gradient is removed the protons return to precessing at the same frequency, but are now systematically

out of phase.[79] Before readout, an opposite gradient is applied for an equal duration causing the protons to rephase. However, in protons that have traslated due to diffusion the rephasing will be imperfect, causing a drop in signal. By repeating this process with the diffusion gradient in different planes, it becomes possible to understand the directional information regarding proton diffusion. The signal measured is considered to provide information about the diffusion of water, as water accounts for the majority of protons in the brain.[79]

Conventional DWI acquires diffusion-weighted data in three orthogonal planes and averages the signal to give a directionless measure of water diffusion. This is known as the trace diffusion-weighted image.[79] If data are acquired in more than three planes then a vector can be generated to provide additional information about any anisotropy of diffusion. This is diffusion tensor imaging (DTI).[79]

3.2.1. Conventional DWI

The diffusion weighting of a sequence is quantified using a b-value, with higher numbers representing greater diffusion sensitivity. A b = 0 image is a T2-weighted image with no diffusion weighting.[79] In stroke, DWI typically uses two b-values of around 1000 s/mm^2 and 0. The trace DWI represents both diffusion- and T2-weighted signal. In order to remove the contribution of the T2-weighted signal, an apparent diffusion coefficient (ADC) image is calculated from the trace DWI and b = 0 images. The ADC value is a measure of how easily water can diffuse with lower values representing restricted diffusion.

Restricted diffusion of water is thought to occur in cerebral ischaemia due to net movement of water from the extracellular to the intracellular space and increased tortuosity of the extracellular compartment.[80] This occurs as a result of the energetic failure of the cells which become unable to maintain ionic gradients across the cell membrane. This causes a net influx

of sodium ions into the cell. The increased osmotic pressures draw water in from the extracellular space (cytotoxic oedema). The net intracellular movement of water restricts the ability of water to diffuse freely, increasing the trace DWI intensity and reducing the ADC values.

3.2.2. Diffusion Tensor Imaging

The mobility of water molecules is restricted by microstructural barriers. In white matter tracts, diffusion will mainly follow the direction of the fibres whilst being restricted in the perpendicular direction[81] Diffusion tensor imaging exploits this anisotropic diffusion behaviour. By estimating the preferred diffusion direction (fractional anisotropy) in each voxel, this approach not only enables the detection of disease-associated changes in diffusion properties but also allows the reconstruction of entire fibre tracts.[82]

A key factor affecting brain networks after stroke is the anatomical damage sustained. Lesion location rather than the size of the lesion accounts for symptom severity after stroke.[83, 84] DTI has been successfully used to characterise the degree of residual integrity of white matter tracts. Metrics such as the corticospinal tract integrity, are quantified using the overlap between the structure of interest and the stroke lesion, and have shown a moderate to strong relationship with motor impairment.[85]

3.2.3. DWI Limitations

There is currently no standardised objective method to define sub-acute ischaemic lesions on DWI imaging. Infarct segmentation is obtained through manual delineation despite being time-consuming and having low inter/intra rater reproducibility. Machine learning techniques might allow automating this process and removing the inconsistencies due to human error. Additionally, the lesion segmented in the early stages of stroke does not

represent only infarcted tissue, but also anatomical distortion secondary to cerebral oedema and haemorrhagic transformation.[86]

A limitation of DTI is that at standard magnetic resonance field strengths (1·5–3·0 Tesla) it provides a voxel resolution of 1–2 mm edge length. This means that diffusion-tensor imaging values do not show single fibres but rather information pooled along thousands of axons.[87]

3.3. Perfusion-weighted imaging

Perfusion is measured by tracking a contrast agent in the blood and quantifying its arrival in the brain tissue.[88] Contrast agents can be exogenous (e.g. gadolinium, Gd) or endogenous (e.g. arterial spin labeled blood).

3.3.1. Exogenous contrast perfusion

In clinical practice, MRI measures of cerebral perfusion are most commonly achieved by dynamic susceptibility contrast perfusion-weighted imaging (DSC-PWI).[89] An intravenous paramagnetic contrast (typically Gd-based) is injected, and its passage is measured through the cerebral vasculature. The concentration profile of the tracer is estimated by repeatedly measuring the effect of Gd on the T2* relaxivity as the bolus passes through the vasculature. Endogenous contrasts typically remain in the vasculature. A deconvolution algorithm is required to estimate the amount of blood reaching the tissue. This process allows to estimate several metrics such as cerebral blood volume (CBV, area under the curve), CBF (peak of the curve), and mean transit time (MTT, CBV/CBF), TTP is the time from the first detection of the arrival of contrast to the peak signal, and T_{max} is the deconvolved equivalent.[90]

3.3.2. Arterial spin labeling

Arterial spin labelling (ASL) is a non-contrast MRI technique, which quantifies CBF by measuring the passage of magnetically labelled water in blood as it arrives in the cerebral parenchyma.[75]

The labelled water freely diffuses into the tissue compartments, allowing a more straightforward quantification of perfusion.[88] CBF is measured by subtracting an image where there is no arterial labeling from one where blood has been tagged. The difference is the signal from the inflowing blood. Approximately 2% of the grey matter water is replaced by inflowing blood-borne water every second. Including the signal losses from magnetic decay, this results in a signal of less than 1% of the background.[91]

There are three options for labelling the inflowing blood: pulsed, continuous, and pseudocontinuous ASL (PASL, CASL and PCASL). PASL involves the labelling of a thick slab over the neck in a short period of time. CASL and PCASL label a single slice in the neck over a longer period of time, with PCASL providing a superior labelling efficiency. PASL has a lower signal-to-noise ratio than the other techniques. Therefore, PCASL is the preferred imaging technique for clinical use.[91]

3.3.3. PWI Limitations

The major concern with using exogenous contrast agents is their accumulation in brain tissue following their repeated administration,[92] and the risk of nephrogenic systemic fibrosis. Other disadvantages include the difficulty in determining absolute quantification of perfusion, and susceptibility artifacts (i.e., blood product, calcification, metal, air, and bone).[93]

The main drawback of ASL is that the generated image has an intrinsically low signal to noise ratio (SNR). Multiple measurements are routinely acquired and averaged to compensate for this,[94] though at a penalty of increased scan duration and, hence, opportunity for motion artefacts.

In addition, the PLD needs to be sufficiently long to ensure that the bolus of labelled blood has completely arrived in the brain by the time of image acquisition. However, if the PLD is too long then signal will be lost due to magnetisation decay. In patients with cerebrovascular disease, arrival times can be delayed resulting in CBF underestimation. Measuring the signal using a combination of different PLDs can overcome this problem. A model is fitted which incorporates both delays in the bolus arrival and signal decay into the quantification of CBF extending the range of arrival delays that can be accurately measured.[75, 95] Still, even using multiple PLDs, there is a theoretical bolus arrival time limit of approximately 3.5s, beyond which ASL cannot measure perfusion.[96]

3.4. Blood-oxygen-level-dependent (BOLD) functional MRI (fMRI)

The magnetic properties of blood are dependent on its oxygenation level. Oxyhaemoglobin and deoxyhaemoglobin have different magnetic susceptibilities: oxyhaemoglobin is weakly diamagnetic, whilst deoxyhaemoglobin is paramagnetic.[77, 97, 98] Increases in the concentration of deoxyhaemoglobin cause the magnetic field to be perturbed. As a result, the water-bound protons in both the blood and surrounding tissue experience increased dephasing, leading to a drop in signal. This change in signal (which is in the order of 1-5%) is quantified by repeatedly measuring T2* in time. [77, 97, 98]

The BOLD contrast in functional magnetic resonance imaging (fMRI) has been widely applied to investigate brain activity [99, 100] and to study cerebral haemodynamics.

3.4.1. Neuronal activity and functional organisation

Neuronal activity and vascular supply are tightly coupled. Cellular processes of neurons, such as the restoration of ionic gradients and neurotransmitter recycling, require energy in the form of adenosine triphosphate (ATP). In the brain, ATP is mainly synthesised by oxidative glucose metabolism, an aerobic process. Therefore, cerebral metabolism depends on cerebral blood perfusion (CBF) maintaining a constant supply of glucose and oxygen.

During neural activity, increases in oxygen and glucose consumption are followed by an increase in CBF termed functional hyperaemia. The increase in CBF far exceeds the oxygen demands of the neural activity, leading to a local increase in blood oxygenation level.

Only a small amount of oxygen (O_2) delivered to the tissue can be extracted from the blood. Increases in CBF negatively impact the relative amount of O_2 extracted (oxygen extraction fraction) due to a decreased capillary transit time. Large increases in CBF are required to support small increases in oxygen consumption.[101]

BOLD fMRI has been used both to localise neural activity and to explore how activity in one region is related to activity in another region. This relation is referred to as functional connectivity,[102] and is based on the assumption that two or more regions belong to the same functional network if their activation timecourses correlate with each other.

Functional connectivity can be measured in two different states: during a particular task; or at rest (in the absence of a structured task),[103] by analysing the spontaneous correlated low-frequency (<0·1 Hz) fluctuations across brain regions. The advantage of resting-state measurements do not impose particular demands on the patient's ability to comply, making this approach well suited to study acute stroke patients.[104]

These measurements can be used to describe how brain function is affected by injury, and the adaptations in brain network connectivity underlying functional recovery.[105]

3.4.2. Cerebral haemodynamics

The BOLD contrast is inherently sensitive to alterations in cerebral blood flow (CBF), cerebral blood volume (CBV) and cerebral blood oxygen consumption ($CMRO_2$)[106, 107] Extracting the vascular information contained in the rs-BOLD can inform on different aspects of cerebral haemodynamics.

Systemic low-frequency oscillations (sLFOs) are non-neuronal fluctuations contained in the BOLD signal. These fluctuations have an extracerebral origin and are likely related to carbon dioxide (CO_2) fluctuations in the blood, vasomotion and Mayer wave.[20] sLFOs share the same frequency range (0.01 to 0.1Hz) of neuronal signal but differ from the latter due to their ability to travel through the vasculature.[108-110] Disturbances of local blood flow are reflected in these sLFOs as a localised delay relative to areas of normal flow. This lag in the BOLD signal can be used to study tissue perfusion and can detect hypoperfusion in acute stroke[109-111]and chronic cerebrovascular disease.[112] Direct comparisons between perfusion modalities have shown that BOLD delay correlates with measures of perfusion derived from DSC-MRI[109, 110]and are associated to aspects of arterial spin labelling signal.[113]

The amplitude of the BOLD signal contains information on cerebral blood volume and vascular density.[109, 114] This property of the BOLD signal has been used to study changes in cerebrovascular reactivity following respiratory challenges[114-117] or study vessel status following the administration of vasoconstrictive drugs.[118, 119] Additional information related to arterial compliance and vascular resistance might be also derived by analysing the cardiac waveform extracted from the BOLD signal.[120]

3.4.3. BOLD Limitations

BOLD fMRI is a secondary and indirect measure of neuronal activity. As a result, there are some limitations in terms of spatial and temporal resolution. First, the smallest unit of the brain that is able to have its blood flow individually regulated is in the order of millimetres in diameter. Second, there is a 2-6 second lag between increased neuronal activity and haemodynamic response.

Additionally, T2* sequences are susceptible to field inhomogeneity secondary to bone-gas interface, haemosiderin/blood products, rapid flow in large veins, or metal. As the change detected is small (1-5%) even small movement artefacts can lead to poor images. In acute stroke patients, multiple noise sources may be simultaneously more evident and heterogeneous than in subjects that are either healthy or have a chronic disease process such as dementia. Up to 35% of stroke patients present with aphasia,[121] which may impact their compliance with instruction in the MRI scanner with a likely increase in motion artefact. Noise secondary to modifications of cardiac/respiratory cycles is likely to be more prevalent given how common both cardiac arrhythmias (for example, atrial fibrillation), and alterations in breathing control, respiratory mechanics, and breathing pattern are in this population.[122,123]

Although using higher field strengths could theoretically help improve the SNR, this remains largely impractical in clinical research due to the limited availability of high field strength scanners. A different approach involves post-processing the data acquired to remove noise while preserving signal. Most commonly, this consists in applying filters or in the removal of volumes deemed corrupted.[124,125] However, filter thresholds are chosen arbitrarily, and the removal of entire volumes inevitably causes loss of signal and requires the collection of redundant data increasing the acquisition time. Independent Component Analysis (ICA) is

a computational method for separating a multivariate signal into additive subcomponents. It is particularly effective in separating true signal from artefacts in fMRI, achieving a significant improvement on results obtained with traditional processing techniques.[126,127]

4. Analytical approaches: the brain as a complex network

The brain is comprised of specialised regions interconnected with each other. As a result, following stroke both injury and recovery processes are not limited to the area of focal injury but affect the whole brain. In order to better describe these effects, the brain can be modelled as a network, also referred as connectome.

4.1.1. Nodes and edges

Networks are comprised of nodes and edges. In brain networks, nodes represent functionally uniform neurons, grouped together to perform the same function. Nodes can correspond to neuronal populations or macroscopic brain regions. Analyses can focus either on a small set of nodes that only cover part of the brain (for example, the regions of a specific system of interest), or a larger set of nodes covering the entire brain.

An edge is defined as a connection between a pair of nodes. Edges can be directed or undirected, weighted or binary.

A first approach to network analysis is to separately investigate its smaller constituents. Group-level analyses have been used to compare the strength of connectivity in edges across subjects. This approach allows localising differences or changes in specific connections. It can be an ideal approach when studying conditions or diseases where changes are expected to happen in the same location (e.g. Alzheimer disease, schizophrenia), but it might be more

difficult to apply to heterogeneous diseases where affected nodes and edges vary across patients.

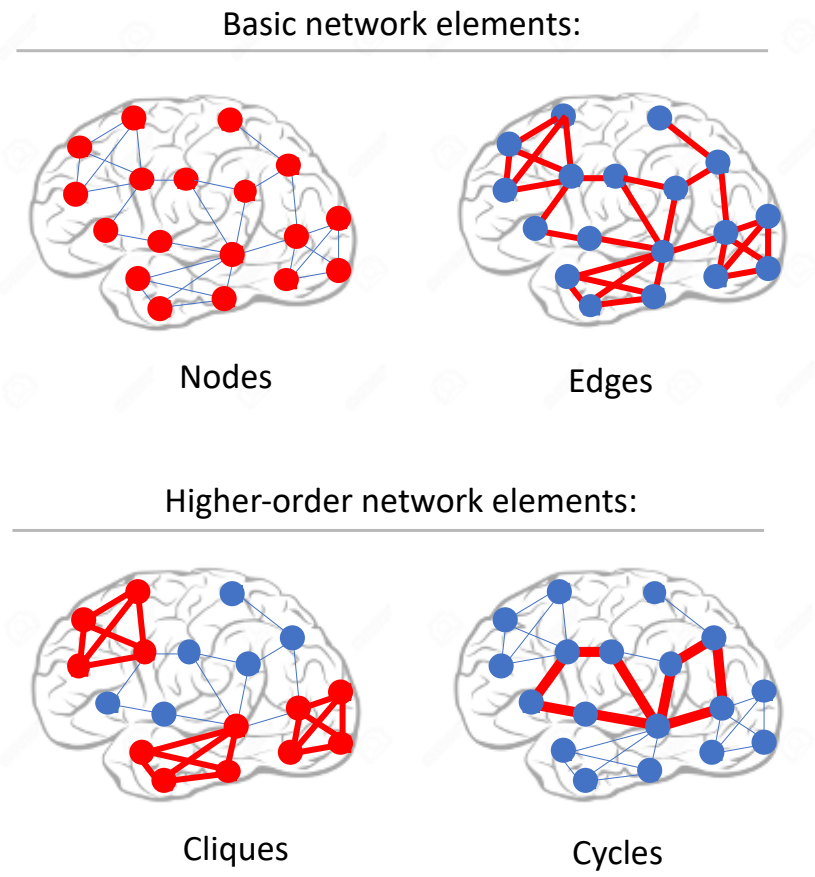


Figure 1-1Network components. Nodes and Edges represent the smallest constituents of a Network. Cliques and cycles represent higher order network structures.

Approaches more geared toward complexity (e.g. graph theory, TDA) focus on how interactions in the network drive the system.

4.1.2. Graph Theory

Graph theory is one of the main theoretical frameworks from complex network science used to model, estimate, and simulate brain networks. [128] Graph theory approaches extract

summary measures that describe aspects of network functioning, instead of directly comparing nodes and edges. [128]

Networks are represented as adjacency matrices (graphs), mathematical structures used to model pairwise relations between objects. Typically, graph theory analysis use correlation to calculate the network matrix edges, and subsequently threshold the network matrix into a binary matrix.

This binarised network matrix can be used to extract several metrics describing the brain network's features. Examples include the node degree (the total number of connections of a node) and the path length (number of intermediate edges between two nodes). [128] Using graph theory, important insights have been gathered on the brain organisation.[129] The brain follows a 'small-world network' architecture.[130, 131] The brain network obeys a balance between the ability to perform local processing (segregation) and combining of information streams on a global level (integration) to minimise wiring cost while maintaining optimal efficiency. [130, 131]

A limitation of graph theory is that due to the binarisation process only 10–20% of the edges with the strongest connectivity are retained. Additionally, graph theory metrics still focus on the pairwise interaction across regions, which might not adequtatly capture the complexity of brain behaviour.

4.1.3. Topological data analysis

Topological data analysis (TDA) is a novel, alternative framework for studying complex datasets and networks.

In TDA, a network is modelled as a multidimensional structure called simplicial complex. Simplicial complexes are not only made up of the set of nodes (0-simplex) and edges (1-simplex) but also of triangles (2-simplex), tetrahedrons (3-simplex), and higher *k*-dimensional structures (a *k*-simplex is an object in *k*-dimensions and is formed by a subset of *k+1* nodes of the network). Modelling the network as a multidimensional structure allows investigating higher order interactions in a network beyond the pairwise connections used in graph theory.[132, 133]

The number and dimension of simplices provide insight into how a system functions, as it reflects the size of its functional units.[134, 135]Among simplicial complexes, k-cliques (a subset of the network with *k* all-to-all connected nodes.) and k-cycles (looped patterns of *k*-simplices) are of particular interest from a computational perspective. Cliques represent highly interconnected areas for specialised data processing. Cycles represent paths along which data is disseminated to and collected from cliques.[134]

Another advantage TDA offers is that it allows the simultaneous investigation of both strong and weak connections. In contrast to graph theory, TDA does not require binarising matrices. Instead, it investigates connectivity over all possible thresholds, a process termed filtration.

TDA describes the shape of data and its properties (termed topological invariants).[133, 136] Examples of topological invariants are the Euler characteristic (defined as the numbers of vertices minus edges plus faces of the considered polyhedral), the topological phase transitions (the topological equivalent of a thermodynamic phase transitions), the Betti numbers (β k, the number of linearly independent k-dimensional cycles in the simplicial

complex[137]), and persistent homology (the persistence of cycles across the evolving simplicial complexes during the filtration process).

Although TDA has only recently been adopted to network neuroscience, promising results have been shown,[138] Group-level differences in network topology have been identified between healthy subjects that ingested psilocybin (psychedelic prodrug),[139] in attention-deficit/hyperactivity disorder children,[140]and in glioma patients.[141]

A limitation of TDA is the computational power required for some analyses. The computation of cliques may require exponential time as the size of the cliques or networks grows, resulting in an enormous time to compute all cliques. Additionally, given the early stage of TDA approaches in clinical network neuroscience, the neurobiological meaning of its metrics is still not well defined.

	Node/Edges	**Graph Theory**	**TDA**
Represented as	Graph	Graph	Simplicial complex
Spatial information	Retained	Partial loss	Partial loss
Sensitive to spatial coordinates	Yes	No	No
Requires Binarising	No	Yes	No
Interactions	pairwise	pairwise	Higher order (>2D)
Robustness to noise	Low	Medium	High
Computational Power	Low	Medium	High

Table 1-1 Summary of the differences between different network analytical approaches. TDA=Topological Data Analysis

5. Aim

The aim of this Thesis was to investigate MRI biomarkers in the understanding of the transition from injury to recovery in a cohort of acute stroke patients.

The Thesis plan was to carry out a systematic literature review to understand how and which MRI biomarkers to predict recovery following acute stroke. Strategies to deal with confounding factors were developed by improving measurement accuracy. Novel analysis approaches were used to study functional and structural changes and how these related to recovery. Finally, the relationship between cerebral haemodynamics and the biomarkers identified was explored.

Chapter 2.

MRI Biomarkers of Recovery in Acute Stroke: Systematic Review

1. Introduction

There has been little progress in the development of treatments focusing on recovery of stroke survivors, partly due to the inability to stratify which patients could benefit from intervention.[63-65] Predicting an individual's outcome following stroke remains challenging. Validated biomarkers of recovery are needed to improve clinical trial design and personalising rehabilitation goals [63-65]

1.1. MRI biomarkers of recovery

Magnetic Resonance Imaging (MRI) represents an ideal modality for investigating the transition from injury to recovery following acute stroke. It is non-invasive, readily accessible, and it allows the simultaneous investigation of brain structure and function. MRI biomarkers have the potential to describe changes in the brain at different levels. They can describe injury-related features. They can characterise specific cortical areas or white matter tracts. They can provide insight on how connections across different brain regions give rise to a complex network.

Identifying imaging biomarkers of recovery, particularly in the early stages following stroke, would allow stratifying patients based on their potential ability to recover, personalising rehabilitation goals and improving the design of clinical trials.[63-65]

1.2. Aim

This chapter aimed to systematically review the evidence available on how MRI biomarkers collected in the first month following stroke have been used to predict recovery.

2. Methods

The protocol of the complete systematic review is available in PROSPERO (registration number: CRD42021175408).

2.1. PICO

Population: adult patients (18 years or older) with an acute stroke (< 30 days from onset). Studies including transient ischaemic attack were excluded.

Index Test: MRI biomarkers obtained up to 30 days after stroke onset

Comparison: demographical or clinical data

Outcome: the main outcome was recovery defined as either:

- improvement in neurological impairment (change between baseline and follow-up assessment).
- Neurological outcome at follow-up, adjusted for baseline severity.

In order for studies to be included, MRI biomarker collection had to precede follow-up assessment.

2.2. Search strategy

A comprehensive search strategy containing words in the title/abstract or text words across the record and the medical subject heading (MeSH) was developed in collaboration with an experienced information specialist. MEDLINE (via OVID) and EMBASE (via OVID) were searched to retrieve potentially eligible studies from inception to January 2020 (see Appendix for example search terms).

2.3. Study selection

Search results of the two databases were merged and deduplicated using Endnote. Title and abstracts were screened by two independent reviewers (DC and one other fellow) using Rayyan QCRI (http://rayyan.qcri.org). Full texts of potentially eligible studies were retrieved for evaluation against a pre-specified inclusion criterion by the same two reviewers (Figure 2.1). Any discrepancies were resolved by discussion.

2.4. Inclusion and exclusion criteria

The search included studies published in peer-reviewed journals where MRI biomarkers (index test) were used to predict future recovery following acute stroke. Searches were limited to English language papers and adult human subjects. Imaging and baseline assessment had to be acquired within 30 days of symptom onset in all subjects included in the analysis. Studies that used imaging solely as inclusion/exclusion criteria were not included. Studies exploring the use of imaging to select patients that could benefit from recanalisation treatment (e.g. penumbral imaging, DWI-FLAIR mismatch) were not included. Studies including transient ischaemic attack were also excluded. Studies where patients underwent experimental interventions were also excluded. Where two or more

papers described the same populations, both studies were included, provided different imaging biomarkers were used in each.

2.5. Data extraction

Data extracted included: year, study characteristics, clinical characteristics, index test features, outcome features (if applicable), and study results. Data were independently extracted and cross-checked by two independent reviewers (DC and one other fellow).

MRI biomarkers were classified based on the following:

- **Class of biomarker**:
    - *Injury-related biomarkers*. Biomarkers included in this subgroup provided information on injury extent. This category included metrics related to the acute lesion (e.g. lesion volume, ASPECTS), measures of injury progression (e.g. penumbra volume, infarct growth, oedema, vasculature status), and pre-existing abnormalities (e.g. SVD burden).
    - *Biomarkers of residual integrity/function of specific regions*. Included in this subgroup were MRI descriptors localising the effects of stroke or estimating how specific brain regions were affected by stroke. Regions of interest could be either predefined or defined through data-driven approaches (e.g. lesion mapping).
    - *Network biomarkers*. This class of metrics aimed at quantifying the effects of stroke on the functional or structural organisation of the brain. Descriptors of the connection (structural or functional) between 2 brain regions (edges) or summary metrics obtained by employing network analysis.
- **Scan Timing**: the time of imaging acquisition from stroke onset was classified as *hyperacute* (<24h), *acute* (24 h to 1-week), and *subacute* (1 week to 30 days).[38]

- **MRI sequence**:
    - MRI sequences routinely used in stroke clinical practice were termed *routine imaging.* These included Diffusion-Weighted Imaging (DWI), Perfusion Weighted Imaging (PWI), Susceptibility Weighted Imaging (SWI) and Magnetic Resonance Angiography (MRA).
    - *Advanced imaging* included Magnetic Resonance Spectroscopy (MRS), Diffusion Tensor Imaging (DTI) and Blood Oxygenation Level Dependent functional MRI (BOLD-fMRI).

Recovery was classified based on the following:

- **Endpoint type**: recovery was dichotomised in *global* (e.g. mRS, NIHSS) and *domain-specific* (e,g motor: Fugl-Meyer).
- **Time of recovery assessment** was classified as < 7 days, 1 month, 3 months or later than 3 months. In studies predicting recovery at discharge, recovery was considered to be assessed at 3 months.

If a paper evaluated the performance of more than one MRI biomarker, each was separately extracted.

2.6. Quality assessment

2.6.1. QUAPAS

The Quality Assessment of Prognostic Accuracy Studies (QUAPAS) tool was used to assess the methodological quality and risk of bias in the included studies.[142] In short, QUAPAS is a modification of the existing Quality Assessment of Diagnostic Accuracy Studies (QUADAS-2) tool,[143] revised to account for items unique to prognostic accuracy study

designs. QUAPAS follows the same domain-based framework as QUADAS-2. Two independent reviewers (DC and one other fellow) evaluated the risk of bias using five domains (participant recruitment, index test, outcome (o target event), study flow, analysis), assigning each study with a judgement of 'low', 'high', or 'unclear' risk.

2.6.2. Additional quality metrics

The design of each study was classified based on data collection (prospective or retrospective) and analysis plan (pre-planned or post-hoc)

Additional items evaluating how cofounding factors specific for some radiological biomarkers were recorded. These included:

- what approach was used to carry out segmentation or rating of imaging features: manual, semi-automated or fully automated. If the task was carried manually, the number of raters was also recorded.
- If volumes were corrected for brain swelling or/and brain size.
- If denoising strategies were used when biomarkers were derived from sequences with low-SNR (e.g. BOLD, ASL)

2.7. Generalisability

The inclusion criteria of each study were reviewed to understand if the study population was selected based on:

- lesion location (e.g. anterior or posterior circulation).
- Recanalisation treatment received (r-tPA and/or mechanical thrombectomy, no recanalisation treatment).

- Mention of the presence or absence of specific symptoms (e.g. aphasia, motor weakness).

2.8. Biomarker performance

The ability of imaging biomarkers to independently predict recovery (or not) was reported for only studies at low risk of bias according to the QUAPAS criteria. If studies reported discrepant results for the same biomarker, then those studies were reviewed for differences in study design.

2.9. Statistical Analysis

Given the anticipated heterogeneity between studies, a meta-analysis was not considered.

3. Results

3.1. Search Results

The electronic search yielded 46129 titles, of which 11665 were duplicates. Screening of the remaining studies and additional manual searching produced 1539 to be appraised. 1349 were excluded following the full-text review, leaving 190 to be included in the study (see Figure 2-1). The complete list of studies is available in Appendix B.

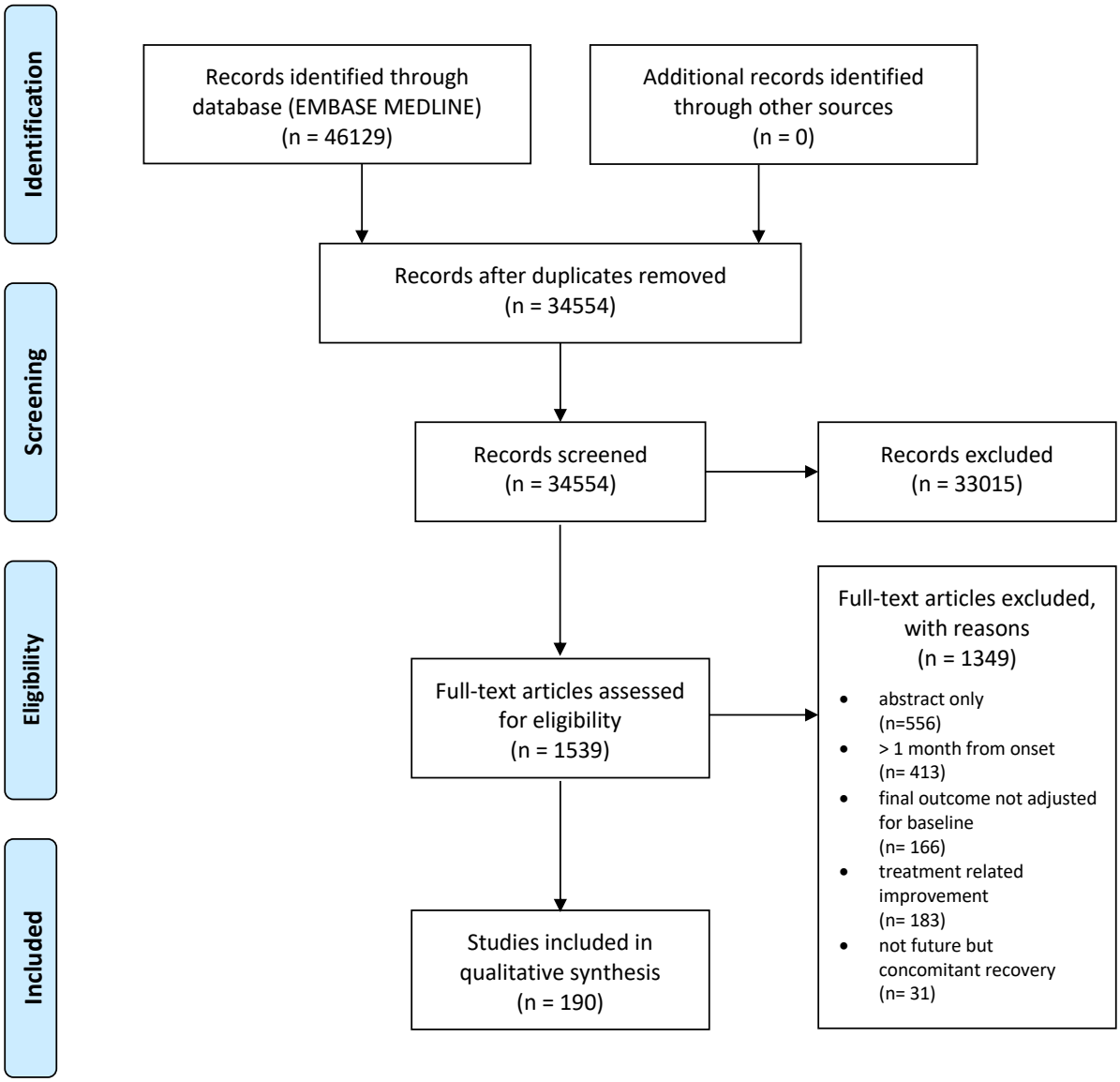


Figure 2-1 PRISMA flow chart[144]

3.2. Characteristics of included studies

Summary characteristics of the studies included are presented in Table 2-1 and Table 2-2. The data extracted for each individual study are included in Appendix C.

		Injury	Specific region	Network
	n studies	146	42	9
	n overall patients	29678	2464	287
Scan Timing	**Hyperacute**	71	3	0
	Acute	62	24	3
	Subacute	12	15	6
Imaging	**Routine**	144	13	0
	Advanced	4	29	9
Recovery	**Global**	130	6	4
	Domain-specific	15	36	5
Recovery Assessed at:	**7 d**	13	1	0
	1 month	6	2	0
	3 months	111	27	7
	>3 months	14	12	2

Table 2-1 Summary characteristics. Hyperacute (<24h), acute (24 h to 1-week), and subacute (1 week to 30 days)

3.2.1. Biomarker class

Injury-related biomarkers were used in 146 studies. These included metrics related to the acute lesion (n=71 studies), injury progression (n=95 studies), and pre-existing abnormalities (n=36 studies).

Among descriptors of injury, lesion size estimated using either quantitative or semi-quantitative (e.g. ASPECTS) methods, was the most frequently employed (n=67 studies). A limited number of studies (n=4 studies) employed indirect measures of infarct severity (e.g. rADC, the relative apparent diffusion coefficient).

Biomarkers of injury progression included penumbra descriptors (volume n=14 studies, perfusion status n=10 studies, metabolic profile n=2 studies), metrics capturing secondary injury processes (oedema n=7 studies, and infarct growth n=10 studies) and vascular descriptors (collateral status n=28 studies, occlusion site n=17 studies, and vessel appearance on SWI n=8 studies).

Among biomarkers capturing pre-existing abnormalities, SVD burden estimated using either volumetric or semi-quantitative (e.g. Fazekas scale) approaches, was the most commonly used (n= 33 studies). In a small number of studies, pre-existing damage was investigated using microstructural integrity metrics (n=3 studies).

Biomarkers characterising specific brain regions were used in 42 studies. These included both measures of function (n=10 studies) and residual integrity (n=32 studies). Among the specific regions, the CST (n=23 studies) and other motor-related areas were the most commonly investigated.

Nine studies employed network biomarkers. Six focused on the basic network constituents (nodes or edges), whilst 3 implemented graph theory analytical approaches to describe a sub-network or the brain as a whole.

3.2.2. Imaging

Routine imaging included DWI (n=99 studies), FLAIR (n=54 studies), PWI (n=11 studies), SWI (n=21 studies) and MRA (n=15 studies). Advanced imaging comprised of BOLD-fMRI (n=19 studies), DTI (n=23 studies) and MRS (n=2 studies).

In 144 studies, injury-related biomarkers were derived from routine imaging. DTI was used in 3 studies to estimate white matter microstructural integrity, whilst a further 2 studies used MRS to describe the metabolic profile of the penumbra.

Among biomarkers characterising specific brain regions, activation studies were all carried out using task BOLD-fMRI. Residual integrity was measured directly using DTI in 20 studies or estimated by quantifying the degree of overlap between the lesion and the region of interest (n=12 studies).

Network biomarkers required the use of advanced sequences (BOLD-fMRI or DTI).

3.2.3. Scan Timing

In 72 studies, imaging data were collected in the <24 (hyperacute stage), in 86 studies between 24h and 1 week (acute stage), and in 32 studies between 1 week and 1 month (subacute stage).

Biomarkers collected in the first days after stroke were generally derived using routine imaging, whilst advanced sequences were used later. Injury-related biomarkers were more frequently acquired in the hyperacute stage (n=71 studies) or acute stage (n=62 studies). Biomarkers of specific brain regions and network biomarkers were collected later (acute n=27 studies or subacute n=21 studies).

3.2.4. Recovery

In 140 studies, the predicted outcome was a measure of global recovery. The scale more frequently used to assess this was the mRS, followed by the NIHSS (Figure 2.2). In 51 studies, the predicted outcome was domain-specific. Motor recovery was the domain more frequently investigated (Figure 2.2).

Injury-related biomarkers were used more frequently to predict global recovery (n=130 studies), whilst biomarkers of specific regions were mainly used to investigate domain-specific recovery (n=36 studies). Network biomarkers were used to predict either equally (see Table 2-1).

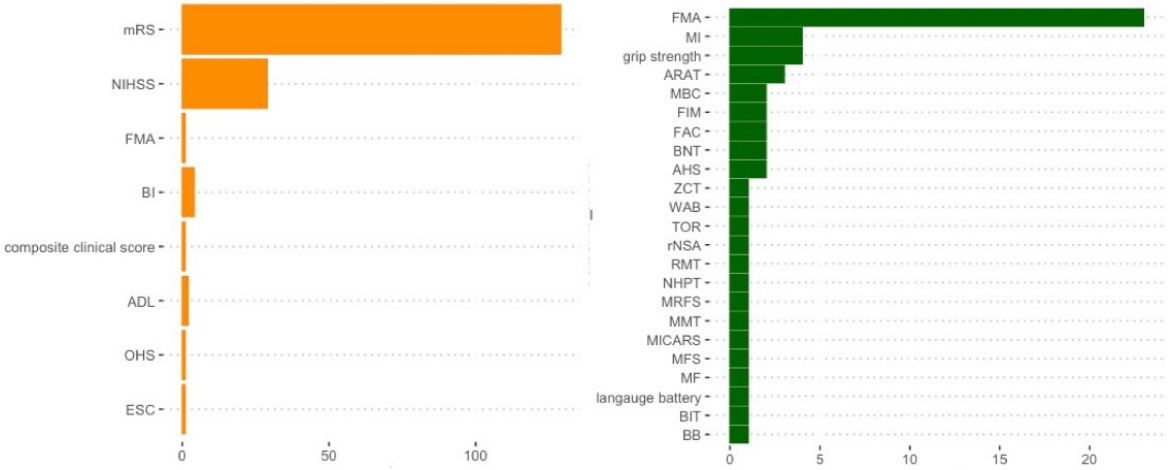


Figure 2-2 Outcome Metrics (absolute number). Acronyms are listed in the abbreviation table.

3.2.5. Time of recovery assessment

Recovery was assessed at 3 months in 129 studies. In 13 studies, recovery was assessed at <1 week, whilst in 8 studies, it was assessed at 1 month from symptom onset. The remaining studies employed a longer follow-up (>3 months). In 12 studies (10 using injury-related biomarkers and 2 using specific brain regions biomarkers), recovery was assessed at discharge.

		n studies	n patients	Stroke population restricted by:		
				Lesion location	Treatment	Symptom
Acute Lesion	**Size**	67	8487	46	38	8
	Severity	4	403	2	1	0
Injury progression	**Penumbra Volume**	14	1130	10	11	0
	Penumbra Perfusion	10	724	6	6	1
	Penumbra MRS	2	170	2	1	0
	Infarct Growth	10	2595	4	5	0
	Oedema	7	552	3	3	0
	Collaterals	28	2256	23	24	1
	Occlusion	17	2514	10	14	0
	Vessel appearance on SWI	8	496	6	4	0
Pre-existing abnormalities	**SVD**	33	16109	18	11	3
	Microstructure	3	574	2	1	0
Integrity	**CST**	23	1022	14	3	14
	other motor tract/area	3	99	3	1	2
	language tract/area	3	111	3	1	3
	other tract/area	4	352	1	0	1
	multiple tracts/areas	9	1711	5	1	2
Activation	**motor task**	9	170	4	0	8
	language task	1	21	1	0	1
Specific Connection		6	240	4	1	2
Whole network/subnetwork		3	47	1	0	3

Table 2-2 Number, size and generalisability of studies. Penumbra MRS: metabolic profile of the penumbra obtained using MR spectroscopy.

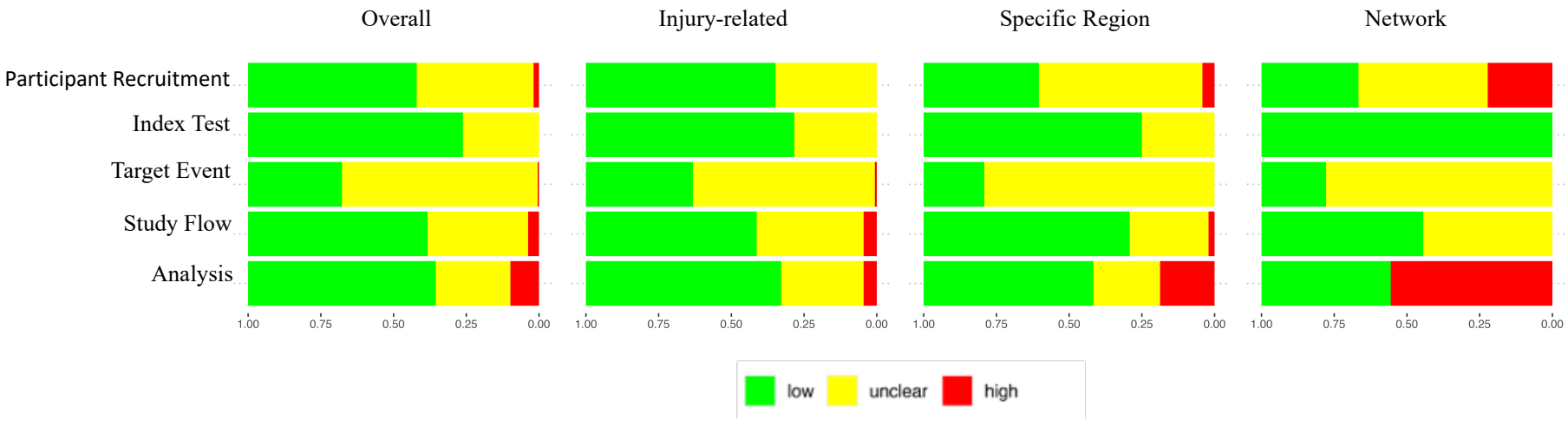


Figure 2-3 QUAPAS. Risk of bias. Risk of bias for Injury-related, Specific Region and Network biomarkers.

	Overall	Injury-related	Specific Region	Network
Low Risk	55	51	4	0
Unclear	108	78	27	3
High Risk	27	17	11	6

Table 2-3 QUAPAS. Risk of bias for Injury-related, Specific Region and Network biomarkers

3.3. Quality assessment

3.3.1. QUAPAS

QUAPAS summary results can be found in Figure 2-3 and Table 2-3. Injury-related biomarkers were investigated by a larger number of studies that had a low risk of bias. Studies using biomarkers of specific regions or network biomarkers had a higher risk of bias. Concerns about bias mainly related to patient recruitment and analysis strategies.

3.3.2. Additional quality metrics

In 140 studies, data were collected prospectively, whilst in 50 data were collected retrospectively. Among the studies with a prospective design, analyses were conducted post-hoc in 52 studies whilst 88 analyses were predefined.

Among studies requiring segmentation or rating, 110 were conducted manually, 3 studies used a semi-automated approach, and 5 used a fully automated approach. When tasks were performed manually only in 34 studies, the use of multiple raters was specified.

Image registration details were specified only in 4 studies; of these, only 2 used non-linear registration accounting for oedema. Three studies adjusted acute or chronic lesion volumes for brain size.

Among studies implementing ASL or BOLD-fMRI, only 1 implemented denoising strategies to minimise motion-related artefacts.

3.4. Generalisability

In 126 studies, the inclusion criteria restricted patient enrolment based on lesion location. In 85 studies, patients were included based on recanalisation treatment (r-tPA, MT, no

recanalisation treatment). In 44 studies, patients were eligible based on the presence or absence of specific symptoms. Details are presented in Table 2-2 and Table 2-4.

	Injury-related	Specific Region	Network
Lesion location	96	25	5
Treatment	80	4	1
Symptoms	12	27	5
No restrictions	28	7	1

Table 2-4 Biomarker Generalisability. Generalisability of Injury-related, Specific Region and Network biomarkers. Number of studies in which inclusion criteria restricted patient inclusion based on Lesion location, Treatment or Symptoms. No restriction refers to the more generalisable studies based on inclusion criteria.

3.1. Biomarker Performance

Biomarker performance was summarised only for studies with a low risk of bias.

3.1.1. Injury related biomarkers

- **Acute Lesion**:

  Lesion size was an independent predictor of recovery in 9 out of 22 studies.

  - Out of the 13 studies where lesion size was an independent predictor, 12 studies predicted global recovery. 12 studies restricted the study population using lesion location or treatment.
  - Out of the 7 studies where lesion size was not an independent predictor, 3 studies investigated domain-specific recovery. One study restricted the study population to patients with an ASPECTS > 4. Three studies predicted recovery in the general stroke population. Tw studies predicted recovery in an untreated population.

Only in one study out of two, an indirect measure of ischemia severity was associated to recovery.

- **Measure of Injury progression:**

  Metrics capturing or predicting injury progression were found to be independent predictors of recovery (penumbra volume 2/2 studies, infarct growth 6/6 studies, oedema 1/2 studies. collaterals 6/6 studies; susceptibility vessel sign on SWI 3/4 studies). Occlusion site was an independent predictor of recovery only in three out of seven studies.

- **Pre-existing abnormalities**:

  SVD burden and microstructural integrity were found to be independent predictors of recovery in 10 out of 14 studies.

  - Out of the 11 positive studies, 10 did not restrict the study cohort based on treatment.
  - Out of the 4 negative studies, 2 studies investigated recovery in MT/IAT cohorts. One study restricted the study population to LAA (large artery atherosclerosis). One study used a covariate already capturing white matter microstructural integrity using DWI.

3.1.2. Biomarkers of specific regions

- **Residual Integrity**

  Biomarkers of the residual integrity of the CST were independent predictor of recovery in 3 studies out of 5. Of notice, in the two studies where a biomarker of CST integrity was not found to be an independent predictor, this was due to the presence of covariates already capturing CST integrity (e.g. motor evoked potential,

other MRI CST integrity marker). Lesion location was also found to be an independent predictor of recovery (2/2).

- **Activation**.

  One study had a low risk of bias. activation patterns in motor areas were found to be independent predictors of recovery.

3.1.3. Network biomarkers

Among network biomarkers no study had a low risk of bias.

4. Discussion

The majority of studies focused on using injury-related metrics to predict patients' global recovery. This class of biomarkers offers a number of advantages. Injury-related biomarkers can be derived from imaging routinely collected in the hyperacute and acute stages of stroke. They do not require stratifying patients by symptoms. They are simple to derive and do not require complex analytical approaches.

Although injury-related biomarkers were found to be independent predictors of global recovery, results often varied across studies. A combination of inconsistent biomarkers definitions and different subgroups of stroke patients (based on lesion location and treatment received) is likely responsible for this.

Biomarkers focused on specific brain regions were preferred when predicting domain-specific recovery. Biomarkers were generally derived from advanced imaging (DTI or BOLD). Imaging data were collected later, outside the hyperacute stage. Studies mainly focused on recovery of motor function. Results were less clear when attempting to replicate this framework in language and somatosensory deficits. Targeting specific regions might

not be a strategy generalisable to subjects presenting with non-motor strokes or presenting with multi-domain impairment.

The use of network biomarkers to predict recovery is still in a preliminary stage, and only limited evidence is currently available. Network biomarkers derived using network analysis offer the theoretical advantage of predicting recovery without the need for stratifying for symptoms or lesion location. Network biomarkers were derived using advanced imaging (DTI or fMRI), which was collected outside the hyperacute stage.

4.1. Injury-related biomarkers

In the general stroke population, lesion size strongly correlated with symptom severity,[145, 146] and therefore did not provide added value over clinical scales such as the NIHSS.[145, 146] However, in selected subgroups of patients, clinical scales are less precise in quantifying damage extent. A first example of this are posterior circulation strokes, where small strategic lesions can cause disproportionally severe symptoms. A second example are patients undergoing recanalisation treatments, where hypoperfused but salvageable tissue also contributes to symptom severity. In these subpopulations of patients, lesion size was shown to improve prediction models,[147-151] as it is likely to better quantify damage compared to clinical scales.

Other injury-related biomarkers have shown similar results. Measures of reduced secondary injury, early reperfusion and good collaterals were associated with greater recovery. Measures of injury progression are likely informative on the potential to integrate areas surrounding the lesion into the recovery process.

Biomarker quantifying pre-existing abnormalities were also found to predict recovery. Both SVD burden and DTI metrics of white matter microstructural integrity improved prognostic

models.[152-154] Knowledge of the white matter integrity is likely informative on the possibility to recruit remote but connected areas that mediate recovery.

4.2. Biomarkers of specific regions

The integrity of white matter tracts was estimated either directly, by using DTI tractography, or indirectly, by using templates derived from a control population and measuring the degree of overlap with the lesion (lesion load).[71, 155] The use of templates allows estimating the residual integrity of a region using imaging modalities routinely collected in clinical practice. The downside of this approach is that a template cannot take into account inter-individual anatomical variability or pre-existent abnormalities. Both direct and indirect measures of CST residual integrity were found to predict motor recovery.[71, 155] Whilst other studies have focused on tracts other than the CST, less evidence is currently available.

A small number of studies has explored changes in function rather than the integrity of a specific region. Task-fMRI showed changes in the activation of directly damaged and contralateral areas associated with recovery.[156, 157] However, only exploratory studies, performed in small samples of selected patients, were available.

Multivariate machine learning methods have recently been applied to neuroimaging data (structural and functional) in an attempt to improve prognostication by integrating features extracted from brain voxels from multiple brain areas. [158] Despite encouraging results, more evidence is required.

4.3. Network biomarkers

Analyses focused on single connections suggested that interhemispheric connectivity is of particular importance for recovery. Ipsilesional primary motor cortex to contralesional

thalamus, supplementary motor area and medial frontal gyrus interhemispheric M1-M1 were associated with motor recovery.[159, 160]

Biomarkers derived using more advanced analytical approaches (e.g. graph theory) allowed capturing the broader effect stroke has on brain organisation. Current studies have predominantly used this approach to characterise the effects on a whole sub-network (motor).[161, 162] More evidence is required to understand if a similar framework could be used to investigate other sub-networks of interest or if it could be applied to the whole brain. Such an approach would allow describing common patterns of connectivity in heterogenous stroke patients

4.4. Strategies to minimize the potential confounding factors

Only a minority of studies adopted strategies to minimise the confounding factors present in acute stroke patients.

Both quantitative or semi-quantitative measurements (e.g., ASPECTS, Fazekas scale) have predominantly relied on manual raters. Manual lesion segmentation, in particular, is known to suffer from high intra- and inter-observer differences.[163-165] Even where there is an excellent interrater agreement between neuroradiologists, substantial measurement errors can still exist that affect sample size calculation for a RCT.[166] Machine learning techniques might allow automating this process and removing the inconsistencies due to human error.

Volumes and ROIs were rarely corrected for oedema. Sequences with low SNR (e.g. BOLD, ASL) were used for analysis without attempting to minimise the noise introduced by motion or vascular artefacts.

The relationship between biomarkers and recovery can change over time. Part of this might be driven by infarct growth, cerebral oedema and haemorrhagic transformation. Similarly, activation patterns associated with recovery have been reported to differ in time.[56]As a result, acquiring the same biomarker at different times can produce different results. Acquiring data longitudinally could help better understand how time affects the relationship between biomarkers and recovery and what biomarker to use at what stage.

4.5. Generalisability

Stroke is a heterogeneous condition. Patients vary greatly for symptoms, lesion location, and size. The effect of injury might be differently related to recovery depending on lesion location and what structures are affected. At the same time, it is unlikely that the same areas or connections relate to recovery in such a heterogeneous group. Studies have attempted to minimise the effects of these challenges by grouping patients presenting with similar features.[128, 130, 167] The results of such studies may have limited generalisability to a broader stroke population. Novel analysis strategies, able to detect common patterns of change unrelated to where these changes occur, might offer an alternative and more generalisable solution.[136]

4.6. Conclusions

The majority of studies have focused on injury-related and specific brain region MRI biomarkers. These metrics are limited in their generalisability across stroke subgroups that differ according to symptoms, lesion location or recanalisation treatment. Whilst network biomarkers are a theoretically more generalisable alternative, there is only limited evidence of their use to date.

Only a minority of studies adopted strategies to minimise the confounding factors present in acute stroke patients. Lesion segmentation was mainly obtained through single rater manual delineation, despite being time-consuming and suffering from low reproducibility. Volumes and ROIs were rarely corrected for oedema. Sequences with low SNR (e.g. BOLD, ASL) were used for analysis without attempting to minimise the noise introduced by motion or vascular artefacts.

Chapter 3.

General Methods

1. Overview

This thesis was nested within the Acute Magnetic Resonance Imaging in Cerebral Ischaemia (AMICI) study. The AMICI study is an MRI-based imaging prospective observational cohort study recruiting patients with acute stroke following informed consent or agreement from a representative. Ethical approval for this study was given by the National Research Ethics Service Committee South Central (Oxford C) under references 12/SC/0292 and 13/SC/0362.

2. Study participants

Participants were recruited from patients admitted to the John Radcliffe Hospital with ischaemic stroke between October 2013 and October 2019. Recruitment was considered for all patients who met the study criteria and who could be scanned in the operating hours of the Oxford Acute Vascular Imaging Centre (Monday to Friday, 8 am until 6 pm).

Inclusion criteria were as follows:

- Clinical diagnosis of stroke within 24 hours of symptom onset;
- Patient or representative able to give a clear medical history and participate in the consent process;
- Age over 18.

Patients with contraindication to MRI or severely impaired conscious level (score greater than 1 on question 1a of the National Institute for Health Stroke Scale (NIHSS)) were excluded. Patients with intracranial haemorrhage on CT or MRI at presentation were recruited into the AMICI cohort study, but the data are not included in this thesis.

3. Study procedures

A flow diagram of the study procedures is detailed in Figure 3.1. Patients were identified and screened either in the Emergency Department or on the Stroke Unit once the clinical team had assessed whether the patient or their family was agreeable to being approached by a member of the research team. Clinically indicated imaging and treatments were initiated prior to research scanning. Non-contrast CT was the standard imaging modality used by the clinical stroke service. Patients recruited within 6 hours of symptom onset were admitted to the Recovery Area in the Oxford Acute Vascular Imaging Centre directly from the Emergency Department. Upon completion of pre-MRI safety checks, patients underwent the first research MRI as soon as possible. The participants then returned to the Recovery Area where and underwent continuous transcranial doppler (TCD) to monitor the blood flow in the brain when possible. The second MRI scan was performed after 2 hours whenever possible. After the second MRI was complete, the patient was transferred to the Acute Stroke Unit to continue routine clinical care.

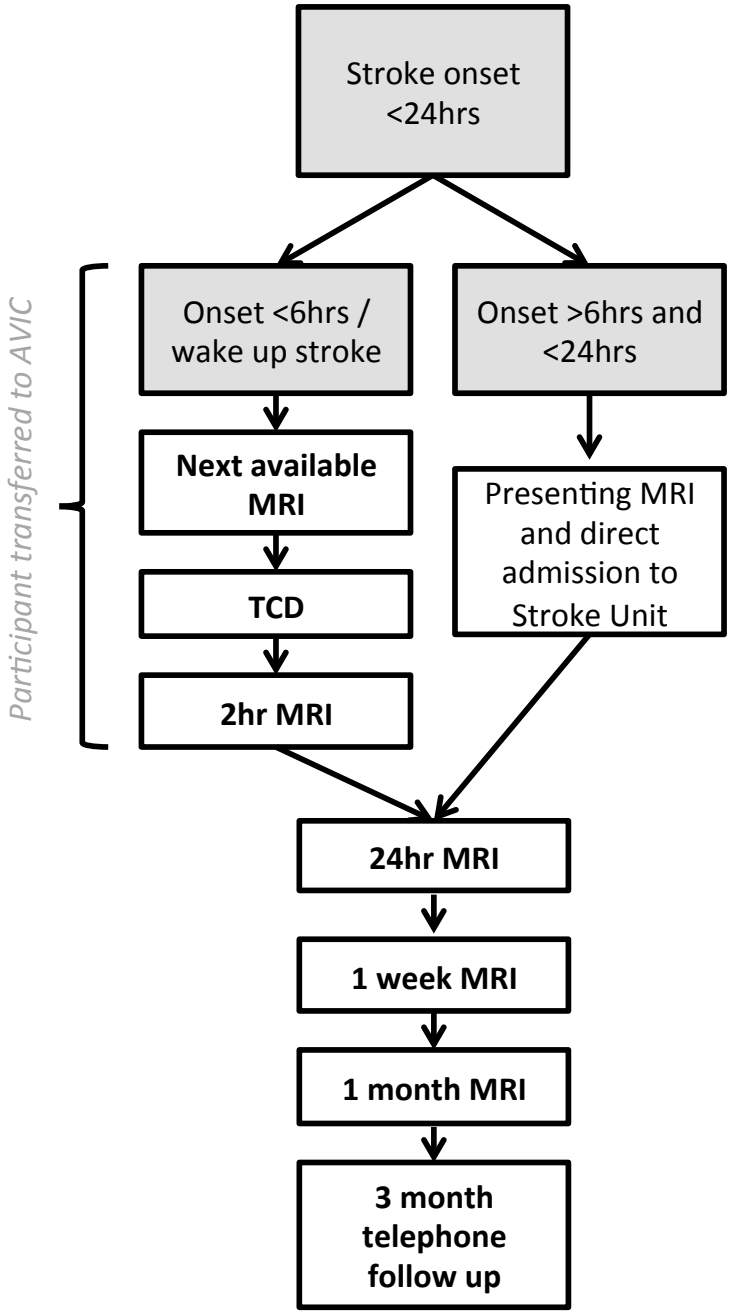


Figure 3. 1 – **Patient flow as part of the AMICI study**. Note that for the AMICI feasibility study, patients were only recruited within 6 hours of symptom onset.

Patients presenting between 6 and 24 hours underwent a similar pathway to those presenting within 6 hours, but assessments did not include a 2-hour scan.

Further MRI scanning was performed at 24 hours (24-48 hours), at 1 week (5-9 days) and at 1 month (21-42 days). Transport arrangements were made from home or community hospitals to acquire follow up imaging whenever possible.

Demographic data were collected at presentation. Clinical assessments were made at each scan time point. These included blood pressure, oxygen saturations and NIHSS. Patients were followed up by telephone assessment at 3 months. This consisted of a short conversation to establish the modified Rankin scale (mRS).[168]

4. Imaging

4.1. Patient imaging time points

Imaging time points were defined as follows:

- Presenting imaging: the first MRI performed within 24 hours of symptom onset.
- Acute imaging: a subgroup of the presenting MRIs performed within 6 hours of symptom onset. If thrombolysis was indicated, the initial MRI occurred during the infusion of tPA.
- 2-hour imaging: a second MRI performed 1-3 hours following acute imaging.
- 24-hour imaging: MRI performed between 24 and 48 hours from stroke onset.
- 1-week imaging: MRI performed between 5 and 9 days after stroke onset.
- 1-month imaging: MRI performed between 21 and 42 days after stroke onset.

4.2. Imaging protocols

All scans were acquired using the 3.0T Siemens Verio scanner in the Acute Vascular Imaging Centre, University of Oxford, using a 32-channel head coil. The total duration of scanning was 30 minutes.

The imaging protocol included a core set of sequences acquired at every time point:

- DWI (3 directions, 1.8×1.8×2.0mm, FoV=240mm, 4 averages, b=0 and 1000s/mm^2 TR=9000ms, TE=98ms);
- T1-weighted structural imaging (MPRAGE, 1.8×1.8×1.0mm, FoV=228mm, TR=2040ms, TE=4.55ms);
- Gradient and magnitude fieldmaps (3.0×3.0×5.0mm, FoV = 240mm, TR = 488ms, TE = 5.19ms and 7.65ms);
- T2-weighted turbo spin-echo fluid-attenuated inversion recovery sequence (FLAIR) (1.9×1.9×2.0mm, FoV=240mm, TR=9000ms, TE=96ms) at 1 week and 1-month time points; and
- Short, low resolution planning sequences, including localising scans to plan the main imaging sequences and time of flight imaging of the feeding arteries in the neck used to plan the perfusion sequence.

In addition to the core imaging, additional sequences were collected depending on the research question.

4.2.1. From 2013 to 2017

Depending on the volume and location of the presenting lesion visualised on DWI, one of two imaging protocols for ischaemic stroke was selected: lacunar (<15mm in axial diameter and subcortical) or large-volume

The lacunar imaging protocol, in addition to the core sequences above, acquired a 12-direction diffusion tensor image and a blood oxygen level dependent (BOLD) imaging for functional MRI assessment.

Patients imaged using the large-volume protocol had VEPCASL perfusion images acquired and a single slice CEST sequence localised to the DWI lesion. These sequences will not be discussed further.

4.2.2. From 2017 to 2019

In January 2017, the imaging protocol was standardised for all patients. In addition to the standard imaging sequences, all patients had a high-resolution PCASL perfusion sequence, a multiband BOLD, and a multiband DTI. Specific details of the PCASL, BOLD and DTI preparation and acquisition protocols are detailed in Chapters 5, 6 and 7, respectively.

4.3. Image processing

All image analysis was performed using FSL (Oxford Centre for Functional MRI of the Brain Software Library), Freesurfer, in-house UNIX shell scripts, R (https://www.R-project.org), and MATLAB 7.14 software (The Mathworks Inc.).[169-171] Details of the specific image processing and analysis are outlined in the relevant Chapters.

All analysis, other than postprocessing of the conventional imaging modalities, was performed offline and did not influence patient management.

4.4. ROI

Binary infarct definitions were created in the native image space. The following regions of interest (ROIs) for patients were used:

- *Infarct core (<24h)*: at <24h infarct volume was defined using semiautomated delineation of apparent diffusion coefficient below an externally validated threshold of 620×10^{-6} mm^2/s.[172]
- *Final Infarct (1-week)*: at 1-week the stroke lesion was defined by two stroke clinical research fellows, who independently defined stroke lesion on follow-up FLAIR. Any discrepancies (defined as Dice Similarity Index[173] <0.8) were resolved independently by a consultant neuroradiologist.
- *Peri-infarct* ROIs were generated by dilating the infarct mask using a 3×3×3 kernel centred on each voxel of the infarct mask. The infarct mask was subtracted from the dilated mask to leave the peri-infarct ROI.[174] Peri-infarct at <24h was generated by dilating the <24h infarct mask. Peri-infarct at 1-week was generated by dilating the 1-week infarct mask.
- *Gray matter* ROIs. Tissue segmentation of the structural T1-weighted image using FMRIB's Automated Segmentation Tool (FAST[175]) defined grey matter partial volume estimates, which were registered into perfusion image space. Grey matter masks were generated using a partial volume estimate (PVE) threshold of ≥70% unless otherwise specified.

Additional ROIs specific to each Chapter are outlined in the respective Methods sections.

Contralateral ROIs were created by non-linear registration of the masks to standard MNI152 space,[176] reflection in the sagittal plane, and returning to structural image space.

Masks were registered to the required image space for analysis before thresholding at 0.5 to minimize registration-induced error.

5. Measures of recovery

Among endpoints explicitly suggested by the European Medicines Agency for use in stroke trials, the National Institutes of Health Stroke Scale (NIHSS) provides information about neurological deficits.

The NIHSS was specifically designed for the assessment of interventions in clinical trials. It operates a 15-item ordinal, neurological impairment scale covering consciousness, ocular movement, vision, coordination, speech and language, sensory function, upper and lower limb strength, facial muscle function, and hemineglect.[177] The scale has exhibited excellent inter (ICC = 0.95) and intra-observer reliability (ICC = 0.93).[178]

There are some limitations to be aware of when using the NIHSS. The focus of the scale is weighted toward limb and speech impairments with reduced attention to cranial nerve-related lesions[179] and appears to have reduced validity non-dominant hemisphere strokes.[178]

Recovery was assessed by measuring changes in NIHSS over time.

- Overall recovery was defined as the change in NIHSS between <24h and 1-month.
- Acute recovery was defined as the change in NIHSS between <24h and 1-week.
- Sub-acute recovery at 1-month was defined as the change in NIHSS between 1-week and 1-month.

Recovery has also been treated as a binary outcome in previous studies. Overall and acute recovery were dichotomised using a value of 4. Sub-acute recovery was dichotomised around a value of 2 due to the more modest recovery rate observed between 1-week and 1-month.

Patients experiencing early neurological deterioration were removed from analyses aimed at predicting recovery only when this was caused by stroke recurrence, development of a symptomatic parenchymal hematoma (PH2 of the Heidelberg Bleeding Classification) or large hemispheric infarctions (LHI).[180]

6. Recruitment results

6.1. Summary details

Two hundred twenty-seven patients were recruited between August 2012 and October 2019. Summary demographic are presented in Table 3.1 and are comparable to other imaging-based acute stroke studies.[181-183] Data for individual patients is presented in Table 3.2.

6.2. Recruitment rate

Approximately 600 patients with stroke are admitted to the John Radcliffe hospital each year. Recruitment only occurred when acute MRI scanning was available during working hours. Recruitment was not possible at the weekend or on public holidays, during scanner service and repair, and when a radiographer or clinical research fellow was not available.

Between 23/04/2017 (beginning of my DPhil) and 31/12/2019, 79 patients were recruited, matching the recruitment rate witnessed in the previous years.

In 2020/21, recruitment was halted due to the restrictions in place for the SARS-COVID pandemic.

		AMICI participants	Stroke admissions
	Number	227	2604
Age	Mean (SD)	70.7 (14.7)	75.4 (13.5)
Sex F	% (n)	41.0 (93)	49.4 (1286)
M	% (n)	59.0 (134)	50.6 (1317)
Hypertension	% (n)	52.0 (118)	47.9 (1247)
Diabetes	% (n)	13.2 (30)	17.9 (466)
Atrial Fibrillation	% (n)	29.1 (66)	22.8 (59)
presenting NIHSS	Mean (SD)	8.8 (7.3)	8.6 (7.3)
mRS pre-stroke < 3	% (n)	93.0 (211)	80.7 (2101)
r-tPA	% (n)	48.5 (110)	21.1 (549)
MT	% (n)	6.6 (15)	3.2 (83)

Table 3. 1 – **Summary demographic data**. Summary clinical and demographic data for patients enrolled in the AMICI study and patients admitted in the same period. SD = standard deviation**.**

Chapter 4.

Improving accuracy of measurements:

Automating Infarct and Oedema quantification

1. Introduction

Studies investigating recovery using MRI frequently require segmenting stroke lesions on imaging. This task is necessary for quantifying infarct volume, defining ROIs (e.g. infarct, peri-infarct, and non-injured white matter) and estimating lesion load metrics.

As shown in Chapter 2, lesion segmentation was mainly obtained through single rater manual delineation, despite being time-consuming and having low reproducibility.[163,164] Additionally, the lesion segmented in the early stages of stroke does not represent only infarcted tissue but also anatomical distortion secondary to cerebral oedema and haemorrhagic transformation.[86]

An accurate and reproducible definition of infarct is needed to study recovery.

1.1. Current machine learning approaches

Machine learning techniques might allow automating lesion segmentation, removing the inconsistencies due to human error. Various approaches to automatically segment stroke lesion on follow-up imaging have been tested. However, promising results have been challenging to reproduce in clinically relevant settings and validate in different cohorts.[173] Despite the number of proposed methods, no automated solution is currently

widely used in clinical or research practice. Methods are often developed using limited or selected data, which does not reflect the heterogeneity of stroke lesions.[184]

1.2. Brain Intensity AbNormality Classification Algorithm (BIANCA)

BIANCA (Brain Intensity AbNormality Classification Algorithm),[185] is an open-access, fully automated supervised method for lesion detection based on a k-nearest neighbour (k-NN) algorithm.

The ability of BIANCA to process multimodal MRI data and the flexibility to be tailored to the imaging characteristics make it appealing to segment acute stroke lesions. Supervised algorithms such as BIANCA require less training data and are less computationally expensive than deep learning approaches allowing for a potentially more straightforward translation to clinical practice.

BIANCA has been shown to accurately segment white matter hyperintensities in large cohorts of patients with vascular stroke/TIA.[186] In a comparative study, BIANCA performance in segmenting multiple sclerosis lesions was comparable to convolutional neural networks (CNN) strategies,[187] outperforming commonly used untrained lesion segmentation methods.[187]

1.3. Anatomical Distortion (AD)

Infarct evolution over time involves swelling (oedema ± haemorrhagic transformation) in the initial stages, leading ultimately to atrophy. Approaches to estimating swelling contribution to the lesion have been developed to compensate for this. These involve measuring changes in density on CT (water uptake),[188] measuring CSF displacement, or directly measuring anatomical distortion (oedema ± haemorrhagic transformation)

using image registration techniques.[86, 189] (I am second author of reference 3; see Appendix D). Anatomical distortion was found to be superior in estimating swelling compared to CSF displacement approaches,[86] whilst water uptake cannot be applied to MRI.

Quantifying oedema not only allows to obtain a more accurate estimate of the actual infarct but can be used itself as an imaging biomarker or and outcome measure.[190] Separately quantifying infarct and anatomical distortion would allow to explore their relationship with recovery.

1.4. Aim

This Chapter aimed to evaluate the performance of an automated pipeline for the separate quantification of infarct and anatomical distortion. The proposed pipeline combines BIANCA with an image registration approach. Lesions of different volumes might benefit from different combination of settings. BIANCA was modified to automatically vary its parameters for different lesion volumes, helping in dealing with stroke heterogeneity.

2. Methods

2.1. Patients

Two separate datasets from two independent institutions were used for this Chapter analyses. The internal dataset was used to develop and validate the methodology for fully automated lesion segmentation and quantification of infarct and anatomical distortion. Patient data from the external dataset was used to replicate the approach in an institution with independent recruitment and imaging protocols.

The *internal dataset* included consecutive patients enrolled in the AMICI study from October 2013 to October 2019 with an anterior circulation ischaemic stroke and follow-up imaging (24h-48h from onset).

The *external dataset* was comprised of consecutive patients from a prospectively collected thrombectomy registry at a tertiary academic medical centre from March 2019 until July 2019. Only patients with an anterior circulation large vessel occlusion stroke (LVO) and follow-up MR imaging (24h-48h from onset) were included. The local institutional review board approved this study registry.

Internal and external datasets were each randomly divided into a training cohort (n=40) and a validation cohort (the remaining patients). Training cohorts were used to optimise the settings for automated lesion segmentation. Validation cohorts were used to evaluate the approach.

2.2. Imaging

Presenting imaging was either MRI (internal dataset) or CT (external dataset). Follow-up imaging was MRI in both datasets. MRI protocols included diffusion-weighted imaging (DWI) with b=0 and b=1000s/mm^2 acquisitions and apparent diffusion coefficient (ADC) calculation. Full details of the imaging protocols are reported in Table 4-1.

Dataset	Scanner	Imaging protocol
Internal	3.0T Siemens Verio scanner (Siemens Healthcare, Erlangen, Germany).	DWI, 3 directions, 1.8×1.8×2.0mm, FoV=240mm, 4 averages, b=0 and 1000s/mm2 (B=1000), TR=9000ms, TE=98ms, 50 slices, 2min53sec
External	1.5T Siemens Aera scanner (Siemens Healthcare, Erlangen, Germany).	DWI, 3 directions, 0.7×0.7×5.0mm, FoV=260mm, 3 averages, b=0 and 1000s/mm2 (B=1000), TR=9600ms, TE=90ms, 34 slices, 2min26sec

Table 4-1 Imaging protocols.

2.3. Image analysis

2.3.1. Volumes of interest

Volumes of interest were defined as:

- **Stroke lesion**: the uncorrected stroke lesion volume, segmented on follow-up imaging.
- **AD volume**: volume of anatomical distortion present in the lesion due to oedema or haemorrhagic transformation.
- **Corrected infarct**: volume of tissue infarcted corrected for oedema or haemorrhagic transformation, obtained by subtracting AD from the stroke lesion.

2.3.2. Manual lesion segmentation

Two stroke clinical research fellows independently defined stroke lesions on follow-up b=1000 diffusion-weighted imaging. Both raters were trained to segment using a dataset derived from 20 stroke patients not included in BIANCA performance analysis (training was deemed successful when the Dice Similarity Index[173] in the dummy dataset reached 0.8). Consensus masks were then created by combining masks from the

two stroke research fellows. Any discrepancies (defined as Dice Similarity Index[173] <0.8) were resolved independently by a consultant neuroradiologist. Consensus masks were used as the reference standard. Consensus masks were used for algorithm training and optimisation in the training cohorts, and performance evaluation in the validation cohorts.

To compare the performance of the automated pipeline to that of an individual rater, a third separate stroke research fellow manually defined infarction at follow-up, blind to the results of both the Consensus and the automated segmentation masks. These masks will be referred from now on as Individual-Rater masks. All raters had a minimum of two years of experience segmenting DWI lesions.

2.3.3. Automated lesion segmentation

BIANCA is a fully automated supervised method for lesion detection based on a k-nearest neighbour (k-NN) algorithm, where k is fixed at 40. The algorithm is trained at a voxel level, using lesion and non-lesion voxels from each patient within the training dataset. This allows it to obtain a large number of training examples even with a modest number of patients.

BIANCA performance can be optimised for different datasets through various options. It is possible to select different combinations of MRI modalities. Different weights can be given to the voxel spatial location (spatial weighting). Additional intensity features containing the local average intensity for each modality (patch, and patch-size) can be used. It is possible to customise the number of lesion and non-lesion training points. For an extensive description of each option, see Griffanti et al. 2016.[185] Two versions of a pipeline based on BIANCA were tested.

The *volume-independent pipeline* replicated the strategy described to segment white matter hyperintensities.[186] One set of options was applied equally to all images.

The *volume-dependent pipeline* automatically varied BIANCA settings for different ranges of estimated lesion volumes in an attempt to account for the heterogeneity of stroke lesions (results from an initial exploratory analysis suggested that lesion of different size might benefit from different settings).

This was achieved by integrating BIANCA with an automated pipeline that can:

1. Automatically determine the best combination of settings to estimate the volume of a stroke lesion (volume-independent BIANCA settings).
2. Automatically determine the best combination of settings for lesion of different sizes (volume-dependent BIANCA settings)
3. Automatically select, for any lesion to segment, the estimated best volume-dependent BIANCA settings

In order to determine the combination of settings that best estimates the volume of a generic stroke lesion, BIANCA tests all possible combination of a wide-range of pre-selected parameters (see Table 4-2). The combination of settings that yields the highest DSI on average across all subjects comprising the training dataset is then selected as the optimal *volume-independent BIANCA settings.* If more than one combination of settings yields the highest DSI the combination offering the lowest false negative rate is selected.

To determine the best combination of settings for stroke lesions of different volumes the data comprising the training dataset is ordered by volume (calculated from the reference-standard masks) and then automatically split in quantiles. The combination

of parameters giving the highest average DSI is then extracted for each subgroup. This allows the creation of a *reference-table* linking a stroke lesion volume range to its estimated optimal settings (*volume-dependent BIANCA settings*). This automated process was repeated using quantiles of different size (2-8) until the best partition was selected.

When masking a stroke lesion BIANCA uses the *volume-independent BIANCA settings* to obtain an initial estimation of the volume of the stroke lesion being masked. This is in turn used to select the best BIANCA option (*volume-dependent BIANCA settings*) in accordance to the *reference-table*.

BIANCA performance, when masking a lesion from the training dataset, was quantified by comparing its output against the manually defined Consensus mask using a leave-one-out approach.

Option	Values tested
MRI modalities	b=1000 only, b=1000 + ADC, b=1000 + b=0, b=1000 +ADC + b=0
Thresholds	0.3, 0.4, 0.5, 0.6, 0.7, 0.8, 0.9
Spatial weighting	0, 1, 2, 3, 4, 5
Patch size	0,3,6,9,12,15,18,21,24
Location of non-stroke lesions training points	any, no border, surround.
Training points	unbalanced: 2000 within mask, 5000 outside mask unbalanced: 2000 within mask, 10000 outside mask unbalanced: 2000 within mask, 15000 outside mask unbalanced: 2000 within mask, 20000 outside mask

Table 4-2 List of settings tested.

2.4. Quantification of Infarct and Anatomical Distortion

Anatomical distortion (AD) was quantified using a previously published registration-based approach.[86, 189]

Follow-up MRI were registered to the baseline MRI in the internal dataset (and to a template image in MNI152 space for the external dataset) both linearly (FMRIB's Linear Image Registration Tool-FLIRT) and non-linearly (FMRIB's Non-Linear Image Registration Tool-FNIRT).[9,10] Next, the stroke lesion mask obtained from the manual and automated segmentation were corrected for AD by applying the non-linear registration warp and further refined by applying a CSF exclusion mask generated from the baseline scan. AD was defined by subtracting the distortion-corrected mask from the uncorrected mask linearly registered to the baseline image.

2.5. Statistical Analysis

Clinical and demographic data were summarised using descriptive statistics. Performance was evaluated in terms of lesion segmentation accuracy and volumetric concordance.

The Dice Similarity Index (DSI)[173] was used as the principal metric to quantify lesion overlap between automated and manual masks. Additional overlap metrics were also calculated, including the false discovery rate, false-negative rate, the detection error rate and the outline error rate (see Table 4-3 for a description of each metric). DSI between Consensus masks and volume-dependent BIANCA masks, and between Consensus masks and Individual-Rater masks were compared using a paired t-test.

For each patient in the training cohort (internal dataset), the best 10 combinations of settings and the volume of the lesion to segment were extracted. Data from each patient were then pooled together. For each setting, the relationship between the best values for that setting and the stroke lesion volume was explored using a Spearman correlation.

Volumetric concordance between masks was quantified using the intraclass correlation coefficient (ICC, two-way mixed model with absolute agreement definition). ICC was computed for the overall stroke lesion volume and for corrected infarct and AD volumes separately.

Metric	Description
Dice Similarity Index (DSI)	calculated as 2 ∗ (true positive SL* voxels) / (true SL voxels + positive voxels).
Voxel-level false discovery rate (FDR)	number of voxels incorrectly labelled as SL (false positive, FP) divided by the total number of positive SL voxels (i.e. voxels labelled as SL by BIANCA).
Voxel-level false-negative rate (FNR)	number of voxels incorrectly labelled as non-SL (false negative, FN) divided by the total number of true SL voxels (i.e. voxels labelled as SI in the reference-standard mask).
Detection error rate (DER)	the detection error is the sum of voxels (SL volume) belonging to FP or FN clusters. The DER is obtained by dividing the detection error by the mean total area, calculated as the average total SL volume by the reference-standard mask and BIANCA output.
Outline error rate (OER)	the outline error is the sum of voxels belonging to true positive clusters (SL clusters detected by both manual and automated segmentation), excluding the overlapping voxels. The OER is obtained by dividing the outline error by the mean total area, calculated as the average total SL volume by the reference-standard mask and BIANCA output.
Intraclass correlation coefficient (ICC)	two-way mixed model with absolute agreement definition

Table 4-3 Metrics used to evaluate BIANCA performance. SL: Stroke Lesion

3. Results

3.1. Patient Details

Internal dataset: of the 83 patients meeting the inclusion criteria, 2 patients were excluded from the analysis due to severe motion artefacts. Stroke lesion volumes ranged from 0 to 390cm^3. Patients were randomly split into a training cohort (n=40) and a validation cohort (n=41).

External dataset: of the 103 patients included in the dataset, 3 patients were excluded from the analysis due to inadequate image quality (2 for motion artefact; 1 for severe dentistry artefact). Stroke lesion volumes ranged from 0 to 299cm^3. Patients were randomly split into a training cohort (n=40) and a validation cohort (n=60).

		Internal dataset	External dataset
n		81	100
Age	**Median (IQR)**	78 (76-78)	63 (53-71)
Sex	**n (%)**	F 38 (46%) M 43 (54%)	F 65 (65%) M 35 (35%)
Presenting NIHSS	**Median (IQR)**	7 (4-15)	17 (13-21)
mRS pre-stroke	**Median (IQR)**	0 (0-1)	0 (0-0.5)
Hemisphere affected	**n (%)**	R 46 (57%) L 35 (43%)	R 47 (47%) L 53 (53%)
r-tPA	**n (%)**	45 (56%)	33 (33%)
MT	**n (%)**	5 (6%)	100 (100%)
Hours from onset to follow-up imaging	**Median (IQR)**	28 (25-38)	29 (24-47)

Table 4-4 Summary of patient demographic and clinical characteristics. NIHSS: National Institutes of Health Stroke Scale; mRS: modified Rankin scale; r-tPA: recombinant tissue plasminogen activator; MT: mechanical thrombectomy.

The main characteristics for the overall cohort were as following: median (IQR) age 71 (60-78), median (IQR) NIHSS 14 (7-20), IV r-tPA use 43%, endovascular treatment

use 58%. Median (IQR) stroke onset to follow-up MRI was 29 (25-43). See Table 4-4 for each dataset summary characteristics and Fig.1 for representative lesions.

3.2. Optimisation process

The use of multiple MRI sequences improved overlap agreement in both registries. Optimum results using both b=1000 DWI and ADC imaging to segment stroke lesions (increase in DSI of 0.5 and 0.45 in the internal and external cohort, respectively), compared to using b=1000 imaging alone. Lesions in the lower volume quantiles benefitted from higher probability thresholds, higher numbers of non-lesion training points and lower patch sizes (see Table 4-5). Optimum BIANCA settings generated from the training cohort are presented in Table 4-6 and Table 4-7.

Setting	rho	p-value
MRI Modalities	n/a*	n/a*
Patch Size	0.26	0.004
Spatial Weighting	-0.34	0.001
Non-lesion training points	-0.30	0.001
Threshold	-0.79	0.001

Table 4-5 Correlation between best setting and volume. * the 10 best combination all implemented b=1000 + ADC in all patients.

	MRI modalities	Patch Size	Spatial Weighting	NL training points	Thr.	Quantile thresholds(cm3)
Volume independent settings	B=1000+ADC	06	1	20000	0.80	n/a
Volume dependent settings	B=1000+ADC	03	1	20000	0.90	0-1.4
	B=1000+ADC	01	3	20000	0.90	1.5-4.50
	B=1000+ADC	01	3	10000	0.80	4.5-22.4
	B=1000+ADC	09	1	5000	0.40	>22.4

Table 4-6 Reference Table internal dataset. Automatically estimated optimal settings across all volumes (volume-independent BIANCA settings) and for different stroke lesion volumes (volume-dependent BIANCA settings). NL training points: Non lesion training points. Thr: Threshold.

	MRI modalities	Patch Size	Spatial Weighting	NL training points	Thr.	Quantile thresholds(cm3)
Volume independent settings	B=1000+ADC	06	1	20000	0.70	n/a
Volume dependent settings	B=1000+ADC	01	3	20000	0.90	0-19.6
	B=1000+ADC	03	1	20000	0.80	19.7-39.3
	B=1000+ADC	03	1	20000	0.70	39.3-78.9
	B=1000+ADC	06	1	10000	0.30	> 78.9

Table 4-7 Reference Table external dataset. Automatically estimated optimal settings across all volumes (volume-independent BIANCA settings) and for different stroke lesion volumes (volume-dependent BIANCA settings). NL training points: Non lesion training points. Thr: Threshold

3.3. Performance

3.3.1. Lesion Segmentation

DSI between Individual-Rater stroke lesion masks and Consensus masks was 0.76 in the internal validation cohort and 0.73 in the external validation cohort.

Volume-dependent BIANCA settings significantly improved the automated segmentation performance in both datasets compared to the volume-independent masks. In the internal validation cohort, the DSI improved from 0.67 to 0.74 ($p<0.01$). In the external validation cohort, the DSI improved from 0.68 to 0.76 ($p<0.01$).

DSIs between automated volume-dependent and Consensus masks were not significantly different to DSIs between Individual-Rater and Consensus masks (Figure 4-2).

	DSI	FDR	FNR	DER	OER
Internal validation cohort	0.74	0.21	0.30	0.12	0.43
External validation cohort	0.76	0.20	0.24	0.13	0.36

Table 4-8 Summary Results. Lesion segmentation overlap metrics between BIANCA (volume-dependent) and Consensus masks. DSI=Dice Similarity Index, FDR=False-Discovery-Rate (voxelwise), FNR=False-Negative-Rate (voxelwise), DER=Detection error rate, OER=Outline error rate

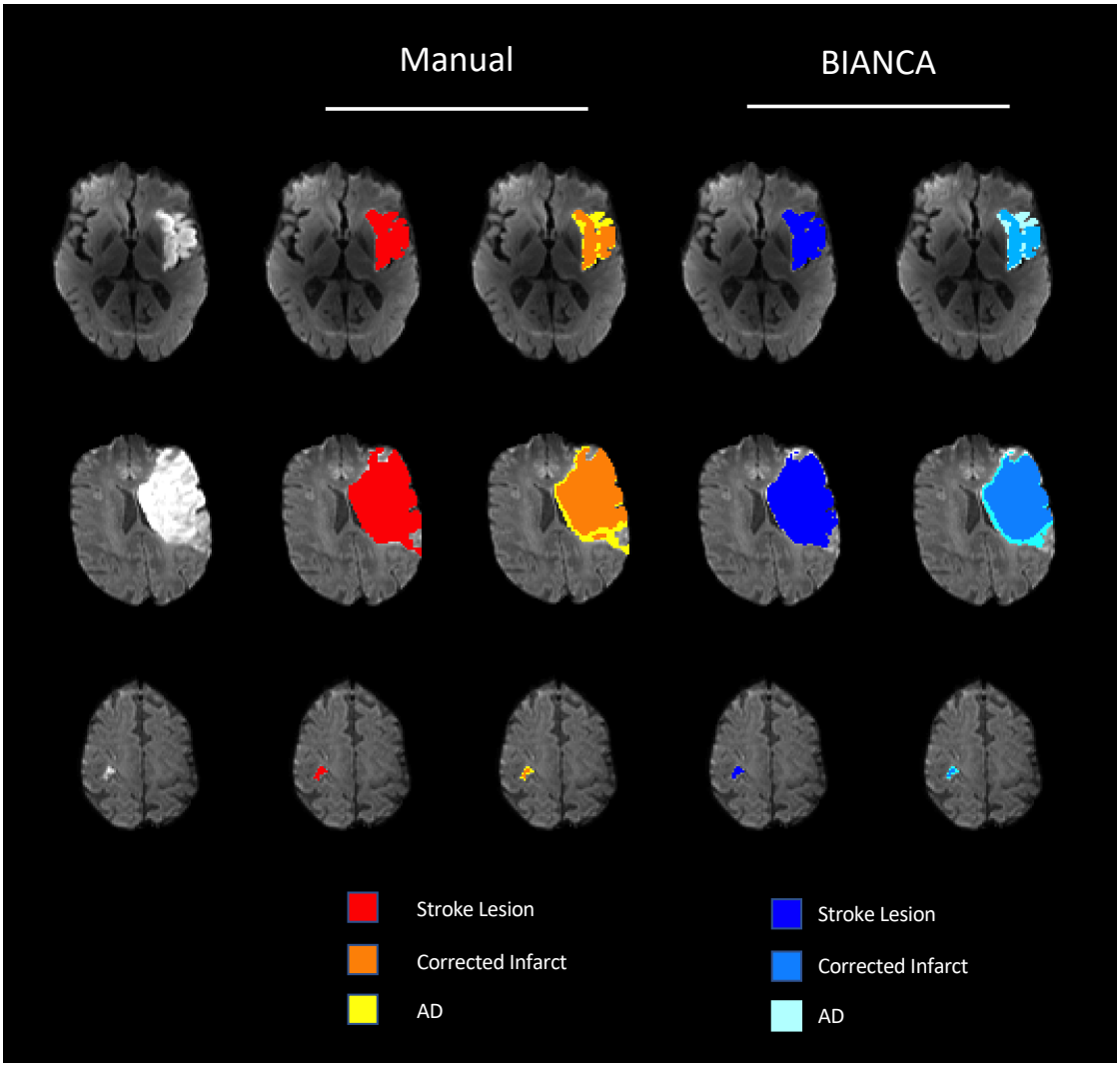


Figure 4-1 Representative stroke lesions. Representative stroke lesions with corresponding Consensus mask (red) and automatically generated masks using volume-dependent lesion segmentation (blue). AD and corrected infarct were estimated for both sets of masks.

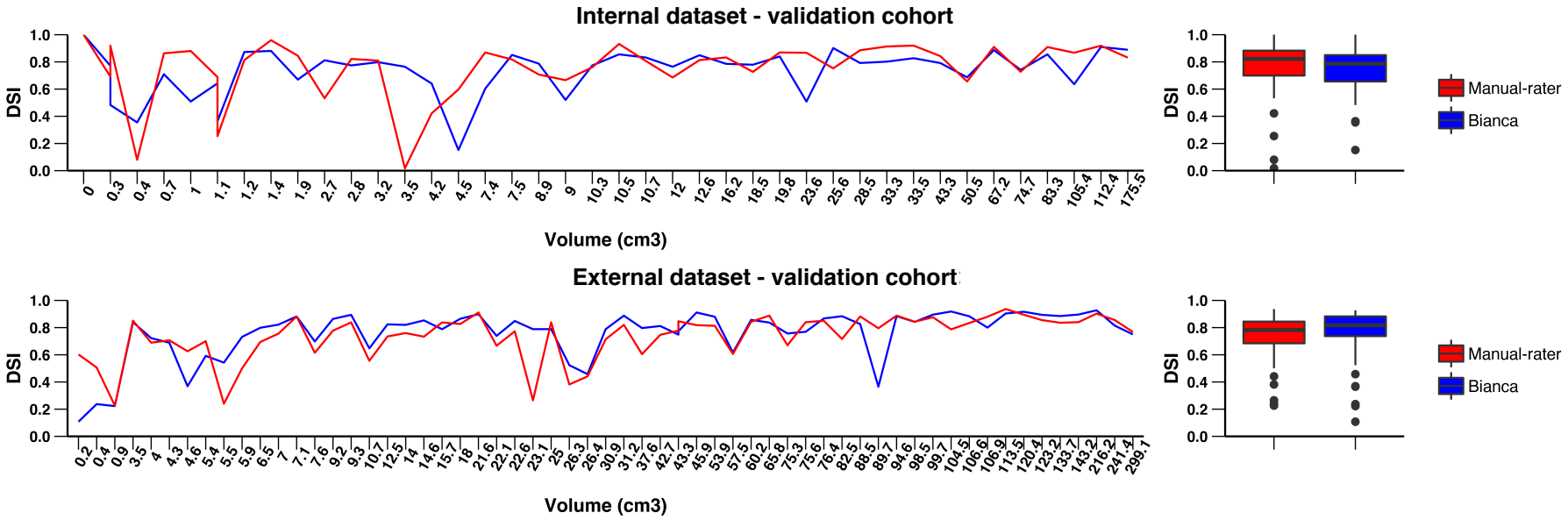


Figure 4-2 Dice Similarity Index. Comparison between the Dice Similarity Index (DSI) computed between mask generated by an individual rater and Consensus masks (red) and between masks generated by BIANCA and Consensus masks (blue)

3.3.2. Corrected Infarct and AD quantification

The concordance values (ICC) between stroke lesion, corrected infarct and AD volumes obtained using Individual-Rater and Consensus masks were respectively 0.94, 0.94 and 0.96 in the internal validation cohort and 0.95, 0.95 and 0.96 in the external validation cohort. (Table 4-9). When using volume-independent BIANCA setting stroke lesion, corrected infarct and AD volumes ICC with consensus values were respectively 0.90, 0.89 and 0.96 in the internal and 0.89, 0.89; and 0.88 in the external validation datasets. Volume-independent BIANCA stroke lesion, corrected infarct, and AD volumes achieved high ICC values compared to Consensus, all over 0.95 in both the internal and external validation cohorts (see Table 4-9).

		Stroke Lesion		Corrected Infarct		AD	
		ICC	**CI**	**ICC**	**CI**	**ICC**	**CI**
Internal validation cohort	**BIANCA**	0.96	0.94-0.98	0.96	0.93-0.97	0.99	0.98-0.99
	Individual rater	0.94	0.91-0.96	0.94	0.91-0.97	0.96	0.94-0.98
External validation cohort	**BIANCA**	0.95	0.93-0.97	0.96	0.93-0.97	0.97	0.95-0.98
	Individual rater	0.95	0.92-0.97	0.95	0.92-0.97	0.96	0.93-0.97

Table 4-9 Summary Results. Volumetric Concordance with Confidence Intervals (CI). Concordance between volumes obtained using volume-dependent BIANCA and Consensus masks; and between volumes obtained using Individual-Rater and Consensus masks.

4. Discussion

In this Chapter, a fully automated pipeline able to accurately quantify both corrected infarct volume and anatomical distortion was developed.

4.1. Segmentation accuracy

The automated pipeline was able to segment acute stroke lesions with accuracy comparable to an experienced individual rater. Overlap coefficients compared favourably to values from other studies described in the literature.[173,191] The validity of this fully automated approach is strengthened by the validation in separate datasets from different institutions with different imaging protocols.

The use of both b=1000 and ADC images improved infarct segmentation beyond that achieved using only a single image. This finding is in line with results from previous work,[191] and consistent with clinical radiology practice. The addition of ADC likely allowed better discrimination of acute changes in the b=1000 from chronic T2-weighted changes such as old infarcts or white matter hyperintensities.

4.2. Volume dependent approach improves segmentation accuracy

The volume-dependent pipeline improved lesion segmentation accuracy compared to volume-independent settings. Smaller lesions benefitted from higher probability thresholds, higher numbers of non-lesion training points, smaller patch sizes and greater spatial weighting.

Lesion volume is known to affect thresholds when binarising probability maps,[192, 193] whilst varying the number of lesion training points provides compensation for the class imbalance, which is more prominent in smaller lesions.

The spatial information allows voxels belonging to ventricles and sulci to be excluded. In large lesions, the degree of anatomical distortion can be so great as to remove any semblance of the normal anatomy (e.g. ventricular obliteration). Excessive reliance on the spatial information, therefore, can lead to misclassifying the displaced infarcted tissue.

In larger lesions, where whole vascular territories are affected, a greater patch size can be beneficial, whilst in smaller lesions, the surrounding voxels might have normal intensity. The implementation of the correct volume-dependent settings was enabled by BIANCA providing a good first estimate of the stroke lesion volume using volume-independent settings.

4.3. Anatomical distortion

In this Chapter, a fully automated process was used to quantify final infarct volume and the contribution to this from anatomical distortion, primarily due to subacute oedema. With a growing interest in the identification of patients at risk of clinically significant swelling for either medical or surgical intervention,[190, 194] this approach offers an opportunity for objective quantification of this pathological process, both to identify patients for inclusion in trials and, if successful, for use in clinical practice.

4.4. Limitations

The strength of this approach is that only a small number of training lesions are required, which can then be used to mask an unlimited number of follow-up scans. A limitation is that

the specific option settings are likely to differ for different cohorts, although the workflow to find them is generically applicable, as demonstrated in this study. Further testing in cohorts of patients where different imaging modalities are acquired on a variety of hardware would further validate the generalizability of these findings.

5. Conclusion

In the systematic review lesion segmentation was mainly obtained through single rater manual delineation, despite being time-consuming and having low reproducibility. The automated pipeline presented in this Chapter, is able to segment acute stroke lesions with accuracy comparable to an experienced individual rater, whilst at the same time removing the bias introduced by anatomical distortion.

Robust measurements of infarct and anatomical distortion allows better understanding of their separate relationship with recovery.

Chapter 5.

Improving accuracy of measurements: an ICA based approach to denoise ASL

1. Introduction

Arterial spin labelling (ASL)[195] represents an ideal tool for the longitudinal study of cerebral perfusion. Its key advantage is that it does not require the administration of an exogenous contrast agent. Instead, ASL generates an image by tracing the accumulation of magnetically labelled blood water in the brain, deriving a perfusion image by subtracting a magnetically labelled image from an unlabelled control image. The use of multiple post-labelling delays (PLD) in the acquisition allows the estimation of arterial transit time (ATT) values, which may not only improve the accuracy of the quantification of cerebral blood flow (CBF),[196,197] but may also provide relevant risk stratification information, for instance, in patients with carotid steno-occlusive arterial disease.[94]

1.1. ASL suffers from low SNR

The main drawback of ASL is that the generated image has an intrinsically low signal to noise ratio (SNR). Multiple measurements are routinely acquired and averaged to compensate for this,[94] though at a penalty of increased scan duration and, hence, opportunity for motion artefacts, whose adverse effect are further enhanced by the image subtraction process.[198]

1.2. Addressing ASL limitations

Methods have been proposed in the post-processing stage to remove structured noise arising from subtraction errors due to motion or other sources of difference between images while preserving as much signal as possible. Existing approaches include applying filters or removing image volumes deemed to be corrupted.[124,125] However, both strategies have their limitations. Filter thresholds are often chosen arbitrarily without reference to the imaging data. Removing entire volumes inevitably causes loss of signal and risks being counterproductive in the presence of limited measurements.

1.3. Independent Component Analysis based denoising

The challenges of low SNR and the presence of structured noise are not unique to ASL. BOLD-based functional MRI (fMRI) shares the same issues. Using Independent Component Analysis (ICA) in post-processing BOLD fMRI data has been shown to reliably separate signal from artefacts or structured noise,[127] allowing a significant improvement over results obtained with more traditional post-processing.[126,199,200,201] Prior to undertaking this thesis, I explored and demonstrated the benefits of this approach in denoising BOLD fMRI collected in acute stroke patients (see APPENDIX E).[198] The utility of ICA to improve SNR has also been explored in diffusion-weighted imaging,[202] and dynamic susceptibility contrast-MRI.[203] It has shown promising preliminary results when applied to pre-clinical ASL data.[204]

1.4. Aim

Building on my experience in denoising BOLD fMRI collected in acute stroke patients using an ICA-based approach, this Chapter investigates the use of a similar approach on clinical ASL data acquired in acute ischemic stroke patients. Its performance is compared to two

other denoising strategies: aCompCor,[205] a Principal Component-based method; and, Enhancement of Automated Blood Flow Estimates (ENABLE),[124] an algorithm based on the removal of corrupted volumes.

2. Methods

2.1. Patients and MRI data acquisition

Consecutive patients enrolled in the AMICI study from January 2017 to October 2019 with a clinical diagnosis of ischaemic stroke and in whom ASL data was collected were eligible for this Chapter analyses.

MRI data acquisition

ASL data were acquired using the following protocol: pseudo-continuous ASL; single-shot EPI readout; TR/TE 5386/14 ms; 3.4x3.4x4.5 mm; 24 slices using a matrix size 64x64; alternating control and label pairs acquired after 1.8 s of labelling at 5 different post-labelling delays: 400, 800, 1200, 1600, 2000 ms, varied in a looped fashion and repeated 6 times (total volumes acquired 60); background suppression; and, total acquisition time = 4 min 30 s. A calibration image with identical readout parameters but with no background suppression or ASL labelling was automatically collected within the same scan to allow quantification of CBF in absolute units. The vendor "pre-scan normalize" functionality used to remove the effects of receive coil non-uniformity.

2.2. Pre-processing

All ASL datasets underwent motion correction via rigid-body registration using the MCFLIRT tool,[206] brain extraction[207], and control-label subtraction.[208]

Tissue segmentation of the structural T1-weighted image using FMRIB's Automated Segmentation Tool (FAST[175]) defined grey matter partial volume estimates, which were registered into perfusion image space. Grey matter masks were generated using a partial volume estimate (PVE) threshold of ≥70% unless otherwise specified. Registration between perfusion and structural images was carried out using the BBR (Boundary-Based Registration) option of the FLIRT tool,[206, 209] which also allowed for simultaneous distortion correction using separately acquired fieldmaps. Registration between structural and standard-space (MNI152-2mm standard brain) was carried out using the FNIRT tool.[171]

2.3. ICA-based denoising

Each 4D ASL dataset after control-label subtraction (ASL-sub) was processed using single-subject spatial-ICA decomposition with automatic dimensionality estimation using the Multivariate Exploratory Linear Optimised Decomposition of Independent Components (MELODIC) tool.[210]

2.3.1. Manual Independent Component classification and artefactual component regression

Two independent raters manually classified the Independent Components (ICs) following a standardized procedure. Components were deemed as most likely representing signal (Figure 5-1) when at least two of the following characteristics were present:

- spatial maps consistent with the expected location of perfusion signal (i.e. grey matter).
- a time course congruous with the variation in post-labelling delays across the acquisition.
- most of the signal in the power spectrum at frequencies (in cycles per scan) corresponding to the number of repetitions or its multiple.

If a component had none or only one of these characteristics, it was labelled as noise (Figure 5-2) and regressed out of the data using a non-aggressive approach so that only the unique variance related to the artefacts was removed.[211] Disagreements were resolved by reference to a third rater.

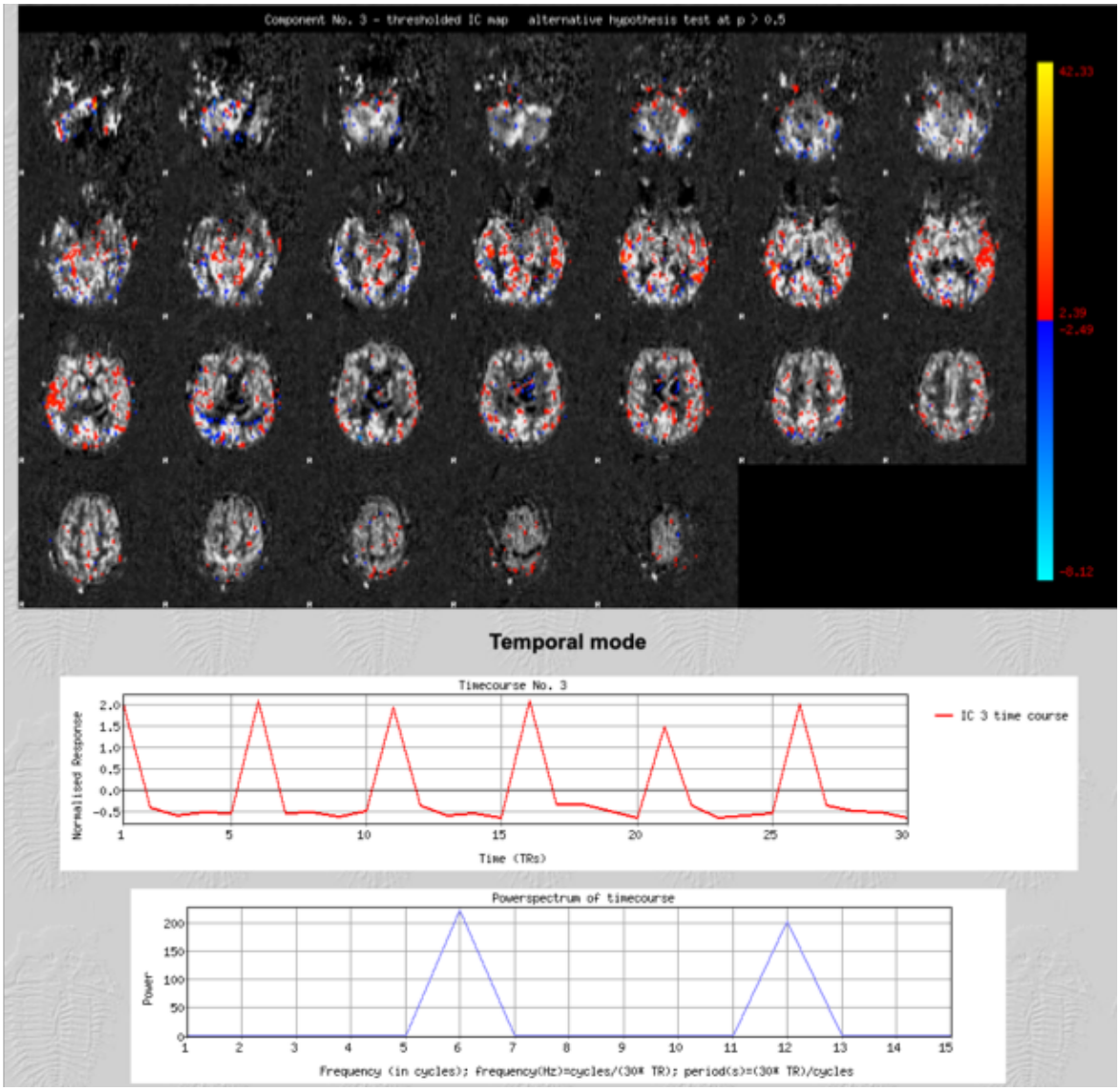


Figure 5-1 Representative Signal component. The spatial map (top) is consistent with the expected location of perfusion signal (i.e. grey matter); the time course (middle) is congruous with the post-labelling delays; most of the signal in the power spectrum (bottom) is at frequencies corresponding to the number of repetitions or its multiple. Patient age=86 years.

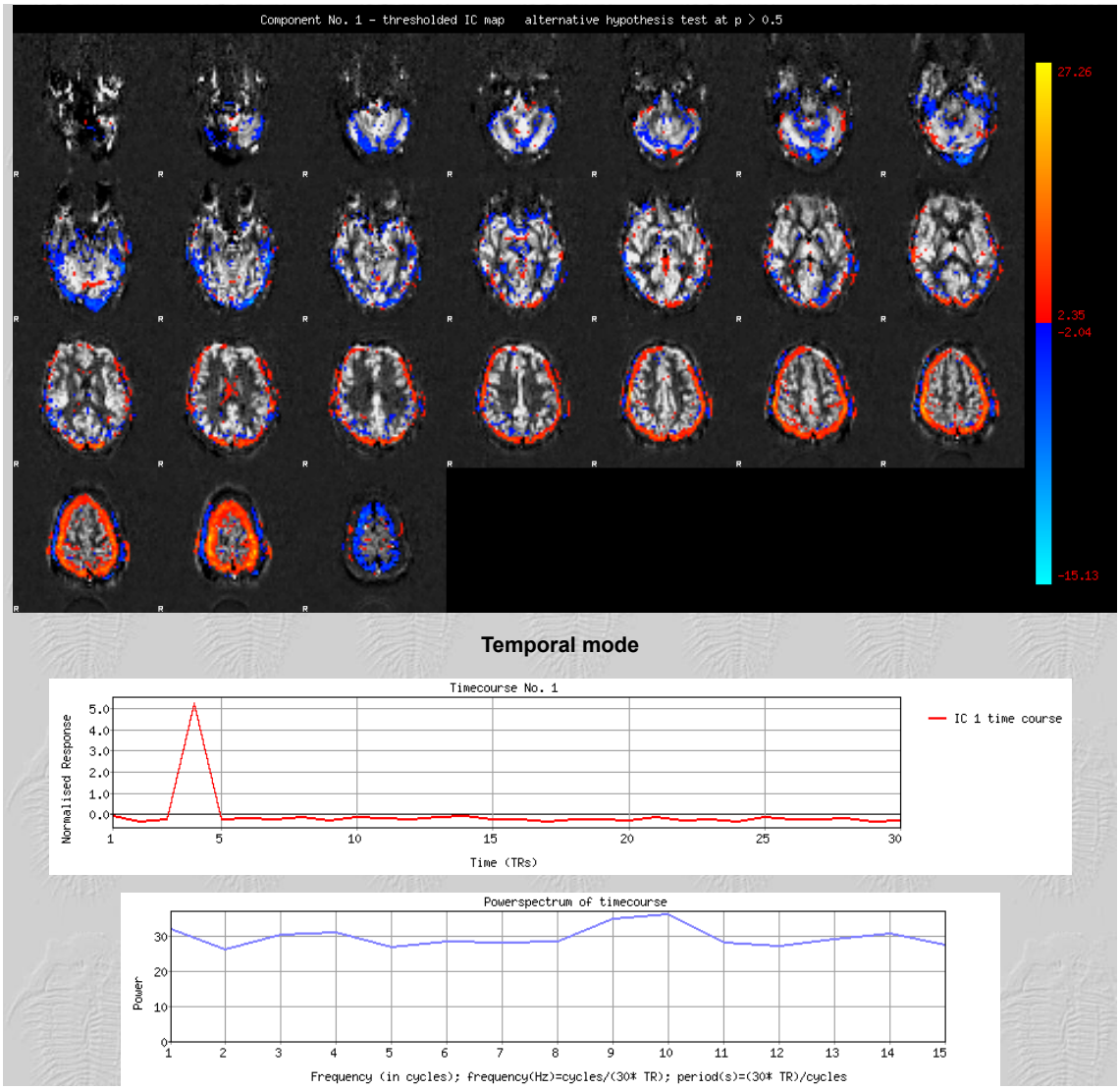


Figure 5-2 Representative Noise component. The spatial map (top) shows signal around the brain edges suggesting motion artefact. The time course is not consistent with the post-labelling delays. The signal in the power spectrum affects all frequencies equally.

2.3.2. Automated Independent Component classification and artefactual component regression

The automated classification and regression of components were obtained using a customized version of FMRIB's ICA-based X-noiseifier (FIX).[212] FIX extracts multiple spatial and temporal features for each component, each describing a different aspect of the data. These are fed into a multi-level classifier. Once trained using manually classified training datasets, FIX can then automatically classify new datasets.[212] A threshold is applied to FIX output to determine the binary classification of any given component. Changing the threshold shifts the balance between true positive ratio (TPR) and true negative ratio (TNR). For the purpose of this study, the optimal threshold was defined as the one that would grant the highest TNR while preserving a TPR above 90% (see Table 5-1).

Threshold	**1**	**2**	**5**	**10**	**20**	**30**	**40**	**50**
Median TPR	100	100	100	100	100	100.0	83.3	80
Median TNR	23.5	33.3	42.9	54.5	71.4	80	86.7	89.5

Table 5-1 FIX independent component classification performance. TPR = true positive rate, i.e., the percentage of true signals correctly classified. TNR = true negative rate, i.e., the percentage of true artefacts correctly classified. As the FIX threshold is lowered, TPR is maximized at the expense of lower TNR.

In order to optimize FIX for ASL data, it was custom-modified to identify as signal those ICs that had higher power in the frequencies that matched the specific ASL sequence PLD cycle frequency (6 cycles per scan). For more details on how FIX features were modified, see Table 5-2. In addition, FIX was automated to use the average motion parameters between the corresponding label and control images as motion parameters for each subtracted image.

This was required as motion correction was performed before label-control subtraction, whilst ICA was run on the subtracted data.

Feature Index	FIX (original version)	FIX (customized for ASL)
20–23	The ratio of the sum of power above f_{Hz} to the sum of power below f_{Hz} for f = 0.1, 0.15, 0.2 and 0.25	The ratio between N and D where N = (sum of power between 0 and (PLDcf- f_{cps})) + (sum of power between (PLDcf + f_{cps}) and (2*PLDcf - f_{cps})) + (sum of power between (2* PLDcf + f_{cps}) D = (sum of power between (PLDcf - f_{cps}) and (PLDcf + f_{cps})) + (sum of power between (2*PLDcf - f_{cps}) and (2*PLDcf + f_{cps})) for f = 1, 1.25, 1.5, 2
24–30	Percent of total power that falls in 0:0.01, 0.01:0.025, 0.025:0.05, 0.05:0.1, 0.1:0.15, 0.15:0.2 and 0.2:0.25 Hz bins	Percent of total power that falls in 0:(PLDcf- 0.5), (PLDcf- 0.5): (PLDcf), (PLDcf):(PLDcf+ 0.5), (PLDcf+0.5): (2*PLDcf- 0.5), (2*PLDcf-0.5): (2*PLDcf), (2*PLDcf+ 0.5): (2*PLDcf+ 0.5) and (2*PLDcf+ 0.5): (3*PLDcf- 0.5) cps bins

Table 5-2 Features modified in order optimize FIX for ASL. cps = cycles for scan, PLDcf = post labelling delay (PLD) cycle frequency (6 cps).

The labels generated during manual classification were used to create the required training dataset. When denoising ASL data obtained from a specific subject, all the labels derived from the same subject were excluded from the training dataset (leave-one-subject-out approach). As above, components were automatically regressed out of the data using the non-aggressive approach.

2.4. Alternative denoising methods used for comparison

2.4.1. aCompCor

aCompCor[205] is a Principal Component Analysis (PCA) based method developed to reduce noise in both BOLD and ASL based fMRI. Significant Principal Components are derived from noise regions-of-interest (ROI) composed primarily of white matter and cerebrospinal fluid. These components are then included as nuisance parameters within general linear models for BOLD and perfusion-based fMRI time-series data. aCompCor (available on https://nipype.readthedocs.io/en/latest/interfaces/generated/nipype.algorithms.confounds.html) was applied to the data used in this study after the pre-processing step described above in accordance with the user guide instructions.

2.4.2. Enhancement of Automated Blood Flow Estimates (ENABLE)

ENABLE is a multiparametric automated algorithm that identifies and removes poor quality difference images in multiple post-labelling delay (PLD) ASL as a means to improve the SNR. The quality criteria that ENABLE implements simultaneously are: the temporal contrast to noise ratio (tCNR, defined as the temporal mean of the 4D ASL subtracted dataset (ASL-sub) in the grey matter divided by the standard deviation of ASL-sub in non-brain voxels); the proportion of ASL-sub voxels in the grey matter significantly greater than zero; the coefficient of variation (CoV, defined as the ASL-sub spatial standard deviation divided by its spatial mean in the grey matter; and, the temporal SNR (tSNR, defined as the spatial mean of ASL-sub divided by its standard deviation in the grey matter).[124] ENABLE (available on https://asl-docs.readthedocs.io/en/latest/index.html) was applied to the data used in this study after the pre-processing step described above in accordance to the user guide instructions.[124]

2.5. Evaluation of the effects of denoising

Effects on ASL-sub variance: to test the effect of correction on ASL-sub, a voxel-wise variable, $\%\Delta STD_{map}$[213, 214] was calculated for every scan obtained. $\%\Delta STD_{map}$ was defined as:

$$\%\Delta STD_{map} = (STD\ (ASL\text{-}sub_{original}) - STD\ (ASL\text{-}sub_{corrected}))/STD\ (ASL\text{-}sub_{original}) \times 100$$

where STD is the standard deviation of each voxel over the volumes of the 4D ASL subtracted dataset. The %ΔSTD maps were then registered to the MNI152-2mm standard brain (using the non-linear transformation matrix obtained from registering the perfusion data to the MNI152-2mm standard brain) and averaged to generate an intensity map. ΔSTD maps were also thresholded (25%), binarised, and averaged to generate a probability map that would highlight those areas the ASL-sub variance was more frequently reduced across subjects.

Effects on the perfusion analysis: grey matter CBF, ATT and their respective intrasession variances were estimated before and after denoising using a spatially regularized Bayesian inference method (BASIL) that produces an estimate of both CBF and its associated variance at every voxel.[208] Mean CBF and mean ATT and their respective intrasession variances were compared in the grey matter across the different denoising strategies using an ANOVA for repeated measurements with multiple comparisons. In addition, mean CBF and its intrasession variance were computed before and after ICA-based denoising using different grey matter PVE thresholds (50, 70 and 90) to explore the effects of denoising in regions with increasingly smaller partial volume effects.

BASIL-generated z-statistics for the CBF fit were used as a marker of goodness-of-fit to the model parameters.[208, 215] The number of grey matter voxels having a z value < 2

(approximately < 5% confidence in fitted value) was compared across the different denoising strategies using an ANOVA for repeated measurements with multiple comparisons.

Effects on SNR estimates: SNR was defined to allow the direct comparison of the results with previous work using ENABLE.[124] CBF-SNR and ATT-SNR were estimated for each dataset by dividing (voxel-wise) the grey matter CBF (or ATT) values by the estimated standard deviation. SNR estimates were compared across different denoising strategies using an ANOVA for repeated measurements with multiple comparisons.

Effects on repeatability: to understand the effect of denoising on the repeatability of CBF measurements, each single session ASL dataset acquired was split into epochs comprising of one repetition for each post-labelling delay, before and after denoising. The grey matter CBF was estimated for each epoch. Repeatability was assessed using the coefficient of variation of these estimates (defined as the standard deviation divided by the mean; the lower the coefficient of variation, the higher the repeatability). The results were compared across different denoising strategies using an ANOVA for repeated measurements with multiple comparisons.

2.6. Evaluating the effects of varying the number of repetitions

Epochs were generated for each ASL dataset acquired before and after manual ICA-based denoising. An increasing number of repetitions were removed in a stepwise manner to understand how varying the number of repetitions acquired may impact SNR (the first repetitions to be removed were the last acquired). CBF-SNR was then estimated for each epoch and compared using an ANOVA for repeated measurements with multiple comparisons.

3. Results

3.1. Patients

72 scans were obtained from thirty consecutive patients with acute ischemic stroke (median age 77 years (IQR 70–82); 13 females (43%)). Patient characteristics are summarised in Table 5-3.

		Acute Stroke Patients
Number	**n**	30
Age	**Median (IQR)**	77 (70-82)
Sex	**n (%)**	F 13 (43%) M 17 (57%)
Presenting NIHSS	**Median (IQR)**	8 (5-13)
mRS pre-stroke	**Median (IQR)**	0 (0-1)
Hemisphere affected	**n (%)**	R 13 (43%) L 17 (57%)
r-tPA	**n (%)**	18 (60%)
MT	**n (%)**	3 (10%)

Table 5-3 Summary of patient demographic and clinical characteristics. NIHSS: National Institutes of Health Stroke Scale; mRS: modified Rankin scale; r-tPA: recombinant tissue plasminogen activator; MT: mechanical thrombectomy.

3.2. ICs classification and artefactual component regression

The mean number of single-subject ICs estimated by MELODIC was 19 (range 7-23).

The mean number of ICs manually classified as signal was 7 (range 3-14; inter-rater agreement ratio was 92%). The mean number of ICs classified as signal by FIX was 7 (range 2-16).

3.3. ENABLE

The mean number of volumes per patient scan classified as poor and subsequently removed from analysis was 1.7 (range 0-7).

3.4. Evaluation of the effects of denoising

Effect of correction on ASL-sub variance: following ICA-based denoising, individual average maps of %ΔSTD showed more frequent and pronounced changes around the brain edges and in the periventricular areas with an average decrease of 30-35% in the ASL-sub variance (Figure 5-3, right). When using aCompCor or ENABLE, the changes were similar although less frequent and less pronounced (Figure 5-3, middle and left).

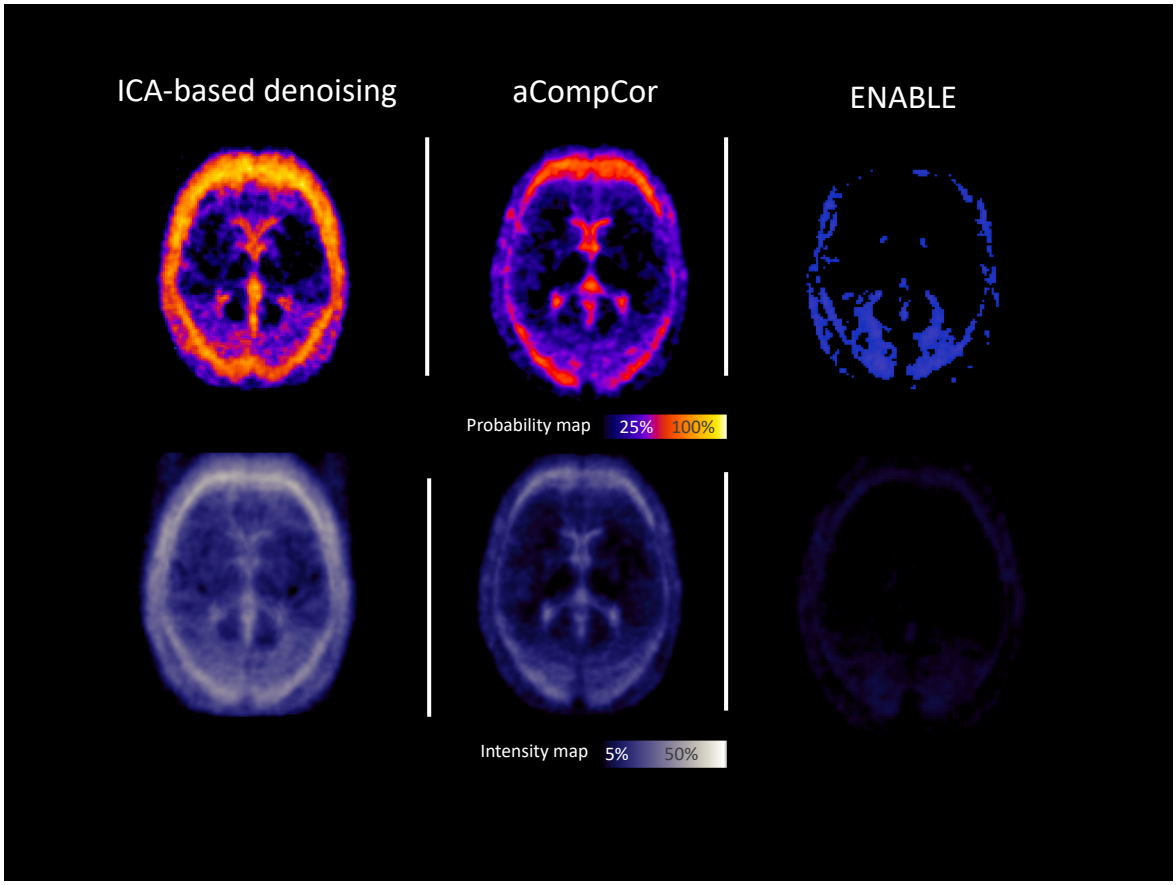


Figure 5-3 Spatial pattern of change in ASL-sub variance after denoising. Probability map (top), representing areas where the ASL-sub variance was affected more frequently in patients. Intensity map (bottom), representing average change in ASL-sub variance.

Effects on the perfusion analysis: the mean CBF and ATT values and their mean intra-session variances, before and after denoising are reported in Table 5-4,Figure 5-6 and Figure 5-7. Results from the multiple comparisons are listed in Table 5-5 and Table 5-6.

	CBF			ATT		
	Mean	**Variance**	**SNR**	**Mean**	**Variance**	**SNR**
Raw	31.8	68.8	4.2	1.38	0.49	2.9
ENABLE	33.9	70.4	4.3	1.39	0.46	3.1
aCompCor	34.9	59.8	5.0	1.45	0.36	4.2
MANUAL ICA	36.9	54.1	6.0	1.47	0.35	5.1
FIX ICA	36.7	54.7	5.9	1.46	0.35	5.0

Table 5-4 Group level results. Group level mean CBF(ATT), CBF (ATT) intrasession variance, and CBF (ATT) SNR before and after denoising

ICA-based denoising led to the greatest changes in the perfusion analysis. Compared to both raw data and data denoised using the other methods, mean CBF was significantly higher (mean difference vs raw data: 5.0 ml/100g/min, $p<0.001$: vs aCompCor 1.8 ml/100g/min, $p<0.01$; vs ENABLE 2.8 ml/100g/min, $p<0.001$; Figure 5-6, Table 5-5), whilst the mean CBF intra-session variance was lower (mean difference vs raw data: 21%, $p<0.001$, vs aCompCor 9%, $p<0.01$; vs ENABLE 18%, $p<0.001$; Figure 5-6, Table 5-5). There was no significant difference in either metric when the effects of manual and automated IC classification were compared. The use of aCompCor led to more modest changes in mean CBF (mean difference vs raw data: 3.2 ml/100g/min; $p<0.001$) and its intra-session variance (mean difference vs raw data: 17%, $p<0.001$; Figure 5-6, Table 5-5). The use of ENABLE resulted in an increase in mean CBF only (mean difference vs raw data: 1.5 ml/100g/min, $p<0.05$, Figure 5-6, Table 5-5).

The use of ICA-based denoising and aCompCor led to similar changes in ATT (mean difference vs raw data: 0.08s, $p<0.001$) and ATT intra-session variance (mean difference vs raw data: 28%, $p<0.001$; Figure 5-7, Table 5-6). There was no significant difference in either metric when the effects of manual and automated IC classification were compared. The use of ENABLE led to an increase in ATT intra-session variance only (mean relative difference: 5%, $p<0.001$, Figure 5-7, Table 5-6).

The changes in mean CBF and its intra-session variance following ICA-based denoising were significant across all grey matter PVE thresholds tested (see Figure 5-4).

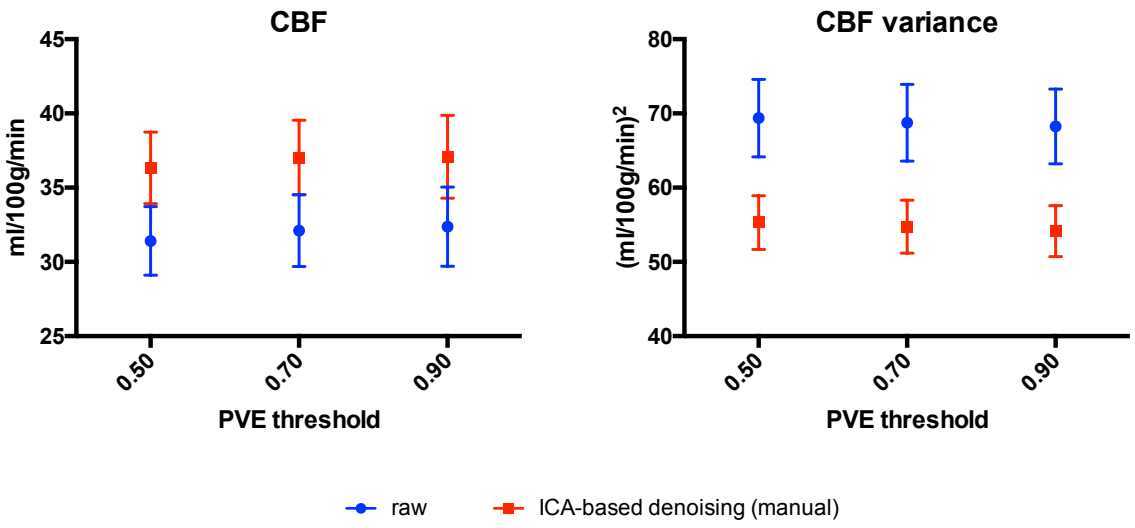


Figure 5-4 Effects of varying Partial Volume Estimates. The changes in mean CBF and its variance following ICA-based denoising compared to raw data were significant using gray matter PVE thresholds of 0.50, 0.70, and 0.90. PVE=partial volume estimate.

All denoising strategies led to a significant decrease in the number of poorly fitted voxels (z value < 2).[216] Compared to the raw data, this effect was greater following ICA-based denoising (14% decrease, $p<0.001$, Figure 5-5). There was no significant difference between manual and automated ICA-based denoising. The effects of aCompCor and ENABLE were more modest but still significant (aCompCor: 10% decrease, $p<0.001$; ENABLE: 8% decrease, $p<0.05$).

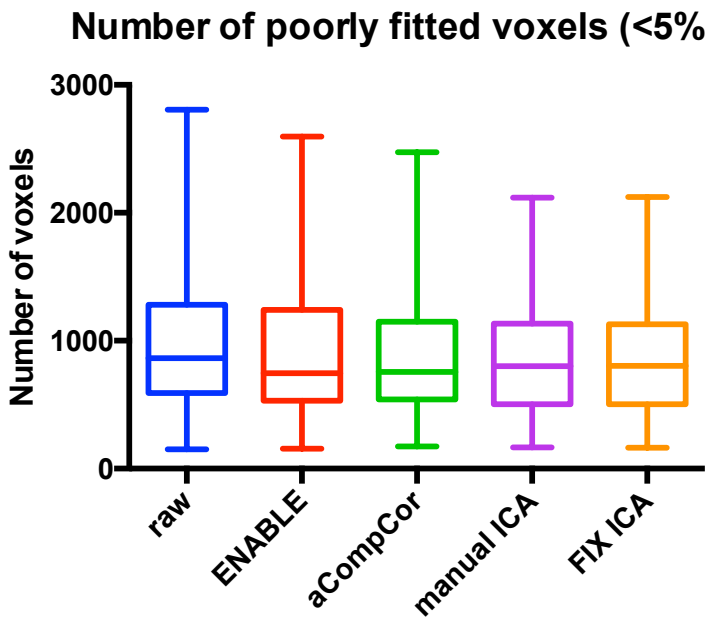


Figure 5-5 Effects on the number of poorly fitted voxels. All denoising strategies led to a significant decrease in the number of poorly fitted voxels (z value < 2). Compared to the raw data this effect was greater following ICA-based denoising ($p<0.001$). The effects of aCompCor and ENABLE were more modest but still significant (aCompCor $p<0.001$; ENABLE: $p<0.05$). manual ICA = manual ICA-based denoising; FIX ICA= automated ICA-based denoising.

Effects on SNR estimates: all denoising strategies led to a significant increase in both CBF- and ATT- SNR ($p<0.001$ Figure 5-6 and Figure 5-7; Table 5-5 and Table 5-6). The highest increase in SNR compared to raw data was observed following ICA-based denoising (40% increase in CBF-SNR, $p<0.001$, Figure 5-6, Table 5-5; manual and automated). There was no significant difference between manual and automated ICA-based denoising (Figure 5-6 and Figure 5-7, Table 5-5 and Table 5-6). The effects of aCompCor were more modest (20% increase in CBF-SNR, $p<0.001$, Figure 5-6, Table 5-5) whilst the use of ENABLE led to the smallest increase (4% increase in CBF-SNR, $p<0.001$, Figure 5-6, Table 5-5)

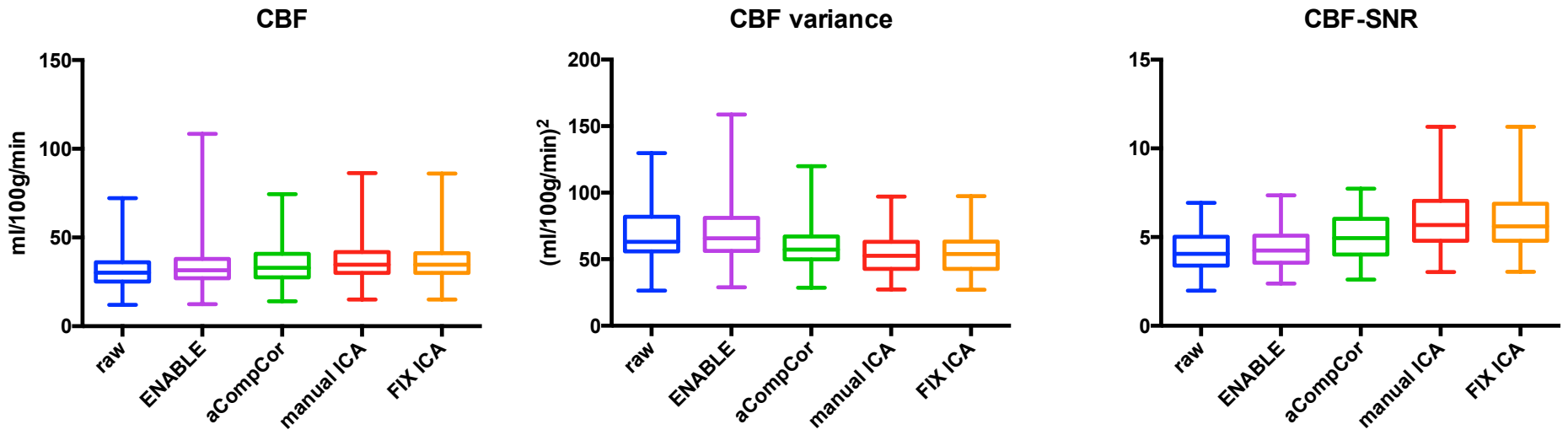


Figure 5-6 Effects on CBF. Grey matter mean CBF, CBF variance and CBF-SNR estimates. ICA-based denoising (manual and automated) led to significant increase in grey matter cerebral blood flow (CBF) estimates, significant decrease in CBF intra-session variance and to significant higher CBF-SNR. manual ICA = manual ICA-based denoising; FIX ICA= automated ICA-based denoising.

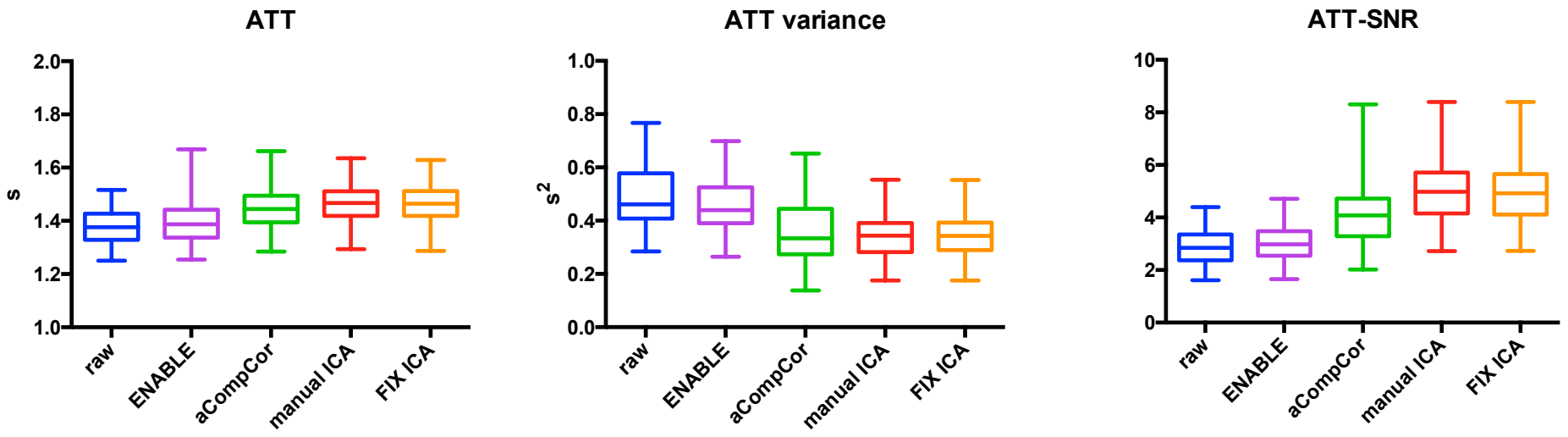


Figure 5-7 Effects on ATT. Grey matter ATT, ATT variance and ATT-SNR estimates. ICA-based denoising (manual and automated) led to significant increase in grey matter arterial transit time (ATT) estimates, decrease of ATT intra-session variance and to significant higher ATT-SNR. manual ICA = manual ICA-based denoising; FIX ICA= automated ICA-based denoising.

	CBF			CBF variance			CBF SNR		
Comparison	Mean Difference	95% CI	Summary	Mean Difference	95% CI	Summary	Mean Difference	95% CI	Summary
Raw vs ENABLE	-2.1	-4.0 to -0.2	*	-1.6	-4.6 to 1.3	ns	-0.2	-0.3 to -0.1	***
Raw vs aCompCor	-3.2	-3.9 to -2.4	****	9.0	6.2 to 11.8	****	-0.8	-0.9 to -0.7	****
raw vs MANUAL ICA	-5.1	-6.1 to -4.2	****	14.7	10.4 to 18.9	****	-1.8	-2.1 to -1.5	****
raw vs FIX ICA	-5.0	-5.9 to -4.1	****	14.1	9.8 to 18.4	****	-1.7	-2.0 to -1.5	****
ENABLE vs aCompCor	-1.1	-3.1 to 1.0	ns	10.7	6.7 to 14.6	****	-0.7	-0.8 to -0.5	****
ENABLE vs ANUAL ICA	-3.0	-4.6 to -1.5	****	16.3	11.1 to 21.5	****	-1.6	-1.9 to -1.4	****
ENABLE vs FIX ICA	-2.9	-4.4 to -1.4	****	15.8	10.6 to 21.0	****	-1.6	-1.8 to -1.3	****
aCompCor vs MANUAL ICA	-2.0	-3.3 to-0.7	***	5.7	2.2 to 9.1	***	-1.0	-1.2 to -0.7	****
aCompCor vs FIX ICA	-1.8	-3.0 to -0.6	**	5.1	1.6 to 8.6	**	-0.9	-1.2 to -0.6	****
MANUAL ICA vs FIX ICA	0.2	-0.1 to 0.4	ns	-0.5	-1.3 to 0.2	ns	0.08	-0.02 to 0.1	ns

Table 5-5 Results from the multiple comparison analysis (mean CBF, CBF intrasession variance, CBF-SNR). MANUAL ICA = manual ICA-based denoising; FIX ICA= automated ICA-based denoising

	ATT			ATT variance			ATT SNR		
Comparison	Mean Difference	95% CI	Summary	Mean Difference	95% CI	Summary	Mean Difference	95% CI	Summary
Raw vs ENABLE	-0.01	-0.03 to 0.005	ns	0.03	0.01 to 0.04	***	-0.2	-0.30 to -0.05	**
Raw vs aCompCor	-0.07	-0.09 to -0.04	****	0.13	0.12 to 0.14	****	-1.3	-1.6 to -1.0	****
raw vs MANUAL ICA	-0.09	-0.10 to -0.07	****	0.14	0.12 to 0.16	****	-2.2	-2.5 to -1.9	****
raw vs FIX ICA	-0.08	-0.10 to -0.07	****	0.14	0.12 to0.16	****	-2.1	-2.4 to -1.8	****
ENABLE vs aCompCor	-0.06	-0.09 to -0.03	****	0.10	0.08 to 0.12	****	-1.1	-1.5 to -0.8	****
ENABLE vs MANUAL ICA	-0.08	-0.10 to -0.05	****	0.11	0.09 to 0.13	****	-2.0	-2.4 to -1.7	****
ENABLE vs FIX ICA	-0.07	-0.09 to -0.05	****	0.11	0.09 to 0.13	****	-2.0	-2.3 to -1.6	****
aCompCor vs MANUAL ICA	-0.02	-0.05 to 0.01	ns	0.009	-0.01 to 0.03	ns	-0.9	-1.3 to -0.5	****
aCompCor vs FIX ICA	-0.01	-0.05 to 0.02	ns	0.007	-0.02 to 0.03	ns	-0.8	-1.2 to -0.4	****
MANUAL ICA vs FIX ICA	0.004	-0.002 to 0.01	ns	-0.002	-0.004 to 0.0009	ns	0.08	-0.02 to 0.1	ns

Table 5-6 Results from the multiple comparison analysis (mean ATT, ATT intrasession variance, ATT-SNR). MANUAL ICA = manual ICA-based denoising; FIX ICA= automated ICA-based denoising

Effect of correction on repeatability: repeatability was unaltered following the use of either aCompCor or ENABLE when compared to raw data. However, ICA-based denoising yielded significantly higher repeatability (p<0.05, Figure 5-8). There was no significant difference in repeatability between manual and automated ICA-based denoising (Figure 5-8).

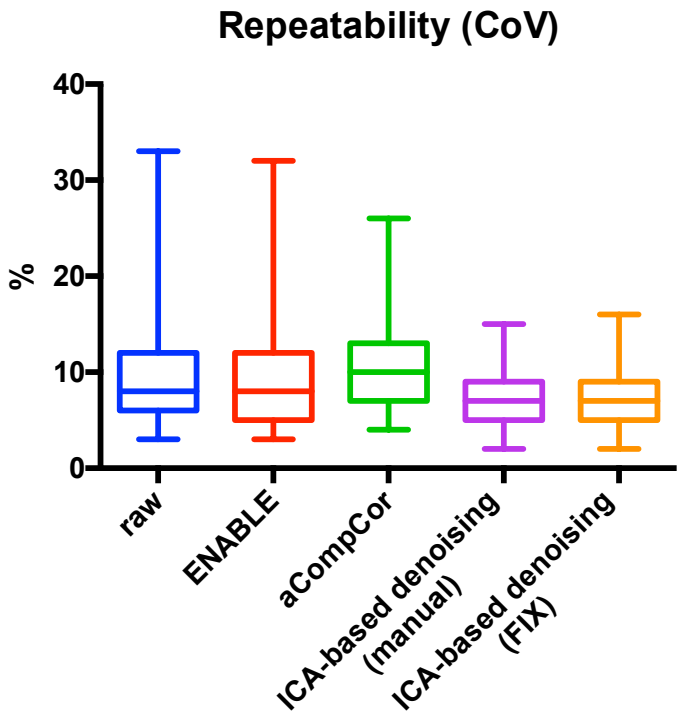


Figure 5-8 Effects on Repeatability. Data processed using ICA-based denoising (manual or automated) yielded significantly (p<0.05) higher repeatability compared to raw data (the lower the coefficient of variability, the higher the repeatability). manual ICA = manual ICA-based denoising; FIX ICA= automated ICA-based denoising.

3.5. Evaluating the effects of varying the number of repetitions

Decreasing the number of repetitions in the raw ASL data led to a drop in CBF-SNR, ranging from 4% (one repetition removed, p<0.001) to 21% (four repetitions removed, p<0.001). A similar effect was observed when removing repetitions from the manual ICA denoised ASL data. However, the CBF-SNR calculated in denoised data incorporating only 3, 4, or 5

repetitions was greater than the CBF-SNR calculated from the raw data with all repetitions included ($p<0.001$; Figure 5-9).

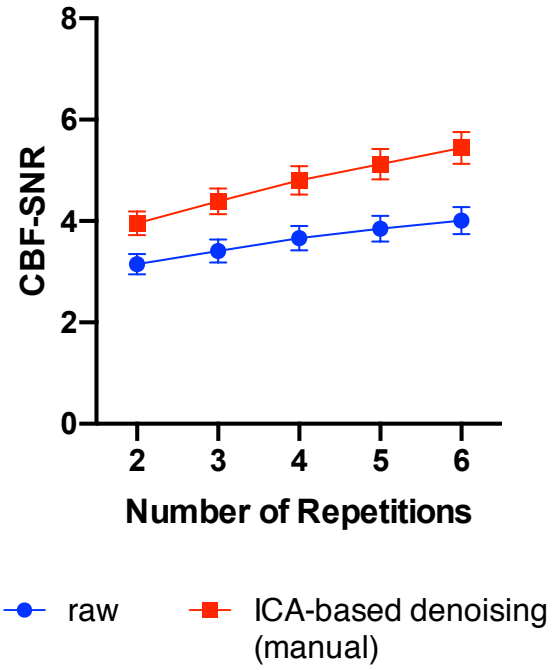


Figure 5-9 Effects of varying number of repetitions. Decreasing the number of repetitions led to a significant ($p<0.001$) drop in CBF-SNR in both raw ASL-data and data denoised using ICA (manual). Apart from epochs comprising only two repetitions, the CBF-SNR calculated in denoised data was always greater than the CBF-SNR calculated from the complete raw data ($p<0.001$ for epochs incorporating 3, 4, 5 and 6 repetitions).

4. Discussion

This study shows that the use of an ICA-based denoising approach results in lower CBF and ATT variance, increased SNR, and improved repeatability. These changes went beyond the effects of approaches using Principal Component Analysis (aCompCor) and removal of corrupt image volumes (ENABLE). Automating ICA denoising achieved near identical results to manual denoising across a broad range of metrics. Intriguingly, following ICA-based denoising, it was possible to obtain higher SNR levels compared to the full raw dataset using

only 50% of the data acquired, setting up the possibility of reducing acquisition times in acute stroke patients.

4.1. Impact of denoising ASL

An optimal approach to denoising ASL data should involve a simultaneous reduction in CBF and ATT variance alongside an improvement in repeatability with an associated increase in SNR (suggesting that the majority of signal has been preserved at the expense of noise removal). In this study, only the ICA-based approaches satisfied all these criteria. Further confidence that noise was removed was shown by the location of the changes in the ASL-sub variability matching expected sites of motion artefact (brain edges and periventricular areas). The increases seen in SNR were not only due to the reduction in variance but also due to an increase in CBF and ATT mean value that was seen across all denoising strategies. This was, at least in part, a reflection of the reduction in the number of poorly fitted voxels; the Bayesian CBF and ATT priors used in BASIL are both less than the overall mean CBF and ATT, regardless of denoising strategy. As data fidelity improves, the prior has less influence over the overall CBF and ATT estimates.[208, 216]

4.2. Comparison with ENABLE

Both component-based denoising approaches were superior to ENABLE, presumably due to their ability to remove noise across multiple volumes without having to discard entire volumes containing both signal and noise. In settings where a small number of repetitions are acquired, such as in this acute stroke study, ENABLE is disadvantaged as a denoising strategy as the concurrent removal of signal with noise has a greater marginal effect on the total signal available for analysis.

4.3. ICA vs PCA

The comparative performance of the two component-based approaches was in line with previous studies comparing the two in BOLD fMRI, where the denoising effects of aCompCor were more limited, especially in the presence of motion.[217, 218] This difference in effect appears to be related to inherent features of the approaches where different "rotation" criteria are used for determining the orientation of the basis vectors in their common solution space.[219] PCA-based strategies are better in removing the contributions of random noise; whilst ICA-based approaches are better suited in dealing with structured noise such as motion, respiratory and cardiac noise,[219, 220] major contributors of noise in acute stroke patients.[214]

4.4. Automating component classification

While manual IC classification has been widely used as the gold standard,[221,222] it is time-consuming, operator dependent and requires expert knowledge to separate signal and noise characteristics.[214,212] The customized version of FIX used here was able to achieve results comparable to manual ICA denoising, demonstrating that it is possible to automate this approach, overcoming these limitations. Moving to an automated approach may be challenging where the ASL data has been acquired with different scanners and/or different acquisition protocols. While the inherent structure of multi-PLD ASL data was exploited to help separate signal and noise components in this study, ICA denoising should also be beneficial in single-PLD ASL in the same it has been for BOLD fMRI. This requires further study.

5. Conclusion

This is the first work showing how ICA can be used to separate signal from noise in clinical ASL data. Ongoing work is being carried out to incorporate this strategy in large observation

cohort such the Whitehall-II imaging sub study and the Human Connectome Project (HCP) Aging subjects and the HCP Development subjects.

The removal of artefactual components improves data quality without increasing acquisition duration. In fact, this Chapter suggests that the acquisition time could be reduced by 50% without penalty to data quality, something that merits further investigation. Independent component classification and regression can be carried out either manually, following simple criteria, or automatically, through the use of FIX customized for ASL.

All further ASL data analyses in this thesis will use this approach.

Chapter 6.

Topological Data Analysis of Functional Connectivity

1. Introduction

The development of functional connectivity biomarkers of recovery for acute stroke has been flagged as a priority by the Stroke Recovery and Rehabilitation Roundtable.[84] rs-fMRI can provide insight on how the functional organisation of the brain has been affected and on the activation of compensatory mechanisms.[56] Incorporating this information could help improving stroke recovery prediction models.[56]

1.1. Stroke is heterogeneous

Most analyses using rs-fMRI localise changes occurring in specific brain regions or in how two specific brain regions are connected.[128, 130, 167] This is challenging in a general stroke population due to the heterogeneity of lesion location, size and number. The commonest way of minimising this variability is to group together patients presenting with similar symptoms.[128, 130, 167] The cost of this approach is the limited generalisability to a broader stroke population.

1.2. From a reductionist to a holistic view

As discussed in Chapter 1, the brain is a complex system. Focal injuries not only cause local dysfunction but disconnect, affecting the brain as a whole.[223] Analytic approaches less geared toward reductionism (i.e., reducing a system to its smaller constituent parts) and more toward complexity and how interactions in the network drive the system might better capture the changes in brain organization following stroke.

1.3. Topological Data Analysis

Topological data analysis (TDA)[224] is a novel analytical approach particularly well suited for the study of complex data. Compared to other approaches it allows to explore higher order relationships across brain regions. Another advantage TDA offers is that it allows the simultaneous investigation of both strong and weak connections. In contrast to graph theory, TDA does not require binarising matrices. Instead, it investigates connectivity over all possible thresholds.

When used in the analysis of brain networks, TDA can help to describe local data processing (cliques), and information-distributing paths (cycles), detecting changes in connectivity that are independent of location.[134] This approach may better capture the changes in compensatory mechanisms that underpin the potential for recovery following stroke.

1.4. Aims

The aim of this Chapter was to use TDA network biomarkers derived from rs-fMRI to study how changes in the brain's functional organisation related to recovery.

This included:

- investigating TDA metrics and their association with a number of demographic and imaging variables in a large, age appropriate and highly characterized imaging control population.
- using TDA metrics to detect changes in the brain functional organization in a heterogeneous cohort of stroke patients associated with recovery;
- exploring TDA metrics added valued in improving prognostic models at different time points.

2. Methods

2.1. Subjects

2.1.1. Control and chronic cerebrovascular cohort cohorts

Among general population large prospective observational cohorts with rs-fMRI imaging available, the Whitehall-II imaging sub-study was selected as a control group as it better matches the age (Human Connectome Projects age range: 21-35; UK-Biobank age range 40-69, Whitehall-II imaging sub-study 60-85) and prevalence of cardiovascular risk factors of a population of acute stroke patients. The Whitehall II study is a cohort of 10 308 British Civil Servants established in University College London in 1985 and followed-up for over 30 years. For the imaging sub-study, 800 participants were randomly selected from the parent study and underwent MRI scan at the FMRIB Centre, Oxford between 2012 and 2016. Informed consent was obtained from all participants. Ethical approval was granted by the *University of Oxford Central University / Medical Science Division Interdisciplinary Research Ethics Committee* (MSD/IDREC/2010/P17.2, MSD-IDREC-C1-2011-71). The study protocol has been described in detail previously.[225] Subjects with incomplete or poor-quality MRI data, presence of non-vascular neurological comorbidities, and a Montreal Cognitive Assessment (MoCA) < 26 were excluded from the analyses.

The control cohort was comprised of subjects included with no neurological comorbidities. The chronic cerebrovascular cohort (CCD) included subjects with a previous history of stroke or TIA.

2.1.2. Acute Stroke Patient cohort

Consecutive patients enrolled in the AMICI study from October 2013 to October 2019 with a clinical diagnosis of acute ischaemic stroke were eligible for this Chapter analyses.

To be included in this study a rs-fMRI had to be acquired at <24h and at 1-week (5-9 days) from stroke onset. Enrolment exclusion criteria included the presence of a contraindication for MRI and severely impaired conscious level (score >1 on question 1a of the National Institute for Health Stroke Scale-NIHSS). Treatment decisions (e.g. recanalization treatment) followed best practice and were carried previous to enrolment. Routine rehabilitation programs were initiated once patients were clinically stable.

Patients who were unable to tolerate the scan, or that experienced stroke recurrence, development of a symptomatic parenchymal hematoma (PH2 of the Heidelberg Bleeding Classification) or large hemispheric infarctions (LHI)[180] were removed from the analysis.

2.2. MRI data acquisition and analysis

In both cohorts, the imaging protocol included a resting state T2*-weighted scan, a T1-weighted MPRAGE and a T2-FLAIR. In stroke patients, diffusion-weighted imaging was also acquired. Arterial Spin Labelling (ASL) imaging was also collected in a subset of consecutive patients and controls.

The details of each BOLD sequence and scanner are reported in Table 6-1.

Dataset	Scanner	Acquisition Parameters
Whitehall II	3T Siemens Magnetom Verio (Erlangen, Germany)	voxel = 2 mm isotropic, TR = 1.3 s, multi-slice acceleration factor = 6, number of volumes = 460), acquisition time = 10:10
AMICI	3.0T Siemens Verio scanner (Siemens Healthcare, Erlangen, Germany).	voxel = 2.4 mm isotropic TR/TE=3000/40ms, number of volumes = 120, acquisition time = 6:00
AMICI	3.0T Siemens Verio scanner (Siemens Healthcare, Erlangen, Germany).	voxel = 2.4 mm isotropic TR/TE=735/39ms, MB=8, number of volumes = 490, acquisition time = 6:10

Table 6-1 Imaging protocols.

2.3. Clinical Procedures and Outcomes

Demographic and clinical information was collected for both controls and stroke patients upon enrolment.

In keeping with Chapter 3, overall recovery was defined as the change in NIHSS between <24h and 1-month. Acute recovery was defined as the change in NIHSS between <24h and 1-week. Sub-acute recovery at 1-month was defined as the change in NIHSS between 1-week and 1-month. Recovery in NIHSS (overall, 1-week, and 1 month) was also dichotomized using two thresholds (thresholds value: 4 for overall and 1-week recovery; 2 for 1-month recovery).

2.4. WMH volume and Cortical thickness

WMH segmentation was carried out using the Brain Intensity Abnormality Classification Algorithm (BIANCA) [185] on the FLAIR images collected.

Cortical thickness was estimated by processing the T1 images using Freesurfer.

2.5. Infarct volume

In stroke patients, infarct volume was defined at <24h using semiautomated delineation of apparent diffusion coefficient below an externally validated threshold of 620×10^{-6} mm^2/s.[172] (in keeping with the definition of infarct core in Chapter 3)

2.6. Perfusion metrics

ASL data underwent motion correction via rigid-body registration and brain extraction; FIX (FMRIB's ICA-based X-noisefier) was used to remove the artefactual components that reflected non-perfusion fluctuations. Registration between perfusion and structural images was

carried out using FLIRT (BBR option), which also allowed for simultaneous distortion correction using separately acquired fieldmaps.

CBF maps were then estimated using a spatially regularized Bayesian inference method (BASIL).[226] Mean grey matter perfusion was extracted for each subject; mean stroke lesion perfusion was obtained for each stroke patient (both at <24h and 1-week).

2.7. fMRI pre-processing and network modelling

In all subjects rs-fMRI scans were processed following the UK Biobank study pipeline.[227] rs-fMRI data were pre-processed using EPI distortion correction, rigid-body registration, brain extraction, Gaussian smoothing, high-pass temporal filtering (cut off = 100 s). FIX (FMRIB's ICA-based X-noisefier) was used to remove the artefactual components that reflected non-neuronal fluctuations.[214, 228, 229] The pre-processed and cleaned rs-fMRI scans were registered to standard space (MNI152) using FNIRT.

Nodes were generated by using (the first step of) a template-based dual regression.[230] The group-ICA spatial maps (dimensionality 100) derived from 4100 subjects enrolled in the UK Biobank study and publicly available online were mapped onto each subject's rs-fMRI data to derive subject-specific time series (i.e. one time series per node for each subject). The node time series were then used to estimate subject-specific network-matrices (NetMat). Network modelling was carried out using the FSLNets toolbox.[231] Of the 100 nodes, 45 were discarded as noise components (physiological noise, MRI or movement artefacts, white matter) and the remaining 55 nodes were used to create the network matrix.[232] To obtain a better estimate of the direct connections between nodes, we used partial correlation coefficients (with rho = 0.01 in Ridge Regression option in FSLNets) that were converted from Pearson correlation r-values into z-statistics with Fisher's transformation.

2.8. Topological Data Analysis metrics

To characterise the functional organisation of the brain using TDA, two properties, the Clique Maximum Size (CMS) and the Euler Entropy were computed for each subject as a function of the correlation strength. A greater CMS-slope expresses the overall presence of larger, more strongly connected cliques. Increases in the number of Topological Phase Transitions (nTPT) in the Euler Entropy are associated with the presence of larger, more strongly connected cycles.

TDA metrics were generated following Santos et al.[141] The filtration threshold $\varepsilon \in [0, 1]$ was defined so that two regions *i* and *j* are considered connected by an edge if the correlation strength $|Cij| > (1 - \varepsilon)$; for $\varepsilon = 1$ all regions in the brain are connected, while there are no connections if $\varepsilon = 0$.

The network topological organization of each individual was characterized as a function of ε. Due to the increasing (exponential) computational power requested when increasing ε, all analyses were limited to the largest threshold computable across all patients ($0<\varepsilon< 0.6$).

The number and size of cliques were computed for each value of ε using the Python Network X library software (https://networkx.github.io). The relationship between cliques maximum size (CMS) and correlation strength was expressed using the Sen slope (CMS-slope). To localize changes in cliques, the mean node participation rank (the number of k-cliques in which a node participates) was computed and normalized by dividing it by the total number of cliques.

Changes in cycles were detected using the number of Topological Phase Transitions (nTPT).[141] The Euler characteristic of the functional brain network of each individual was obtained by computing the alternate sum of the numbers of k-cliques (Clk) present for a given value of correlation threshold ε:

$$\chi = \sum_{k=1}^{N} (-1)^{k+1} Cl_k(\varepsilon)$$

The Euler Entropy (S_χ) is then obtained from χ :

$$S_\chi = \ln |\langle \chi \rangle|.$$

nTPT was defined as the number of times S_χ switched from positive to negative or vice versa.

The Euler characteristic can also be computed as the sum of the curvatures at each node.[141] This allows to localise the changes in connectivity driving the nTPT by computing for each node the curvature (k_i) of the participation rank:

$$\kappa_i = \sum_{k=1}^{k_{\max}} (-1)^{k+1} \frac{Cl_{ik}(\varepsilon)}{k}$$

2.9. Synthetics dataset of random networks

The synthetic dataset was obtained by generating 500 Erdös-Rényi graphs with the same size as the functional networks. Erdös-Rényi graphs represent random networks in which the uncorrelated connections between nodes occur with probability p. This allows expressing a function of the probability parameter $p \in [0, 1]$. If $p = 0$ no nodes are connected (empty graph), whereas if $p = 1$ all nodes are fully linked to each other (complete graph). The mean value of the Euler characteristic of Erdös-Rényi graphs with N nodes and linking probability p is exactly given by the following.

$$\langle \chi \rangle = \sum_{k=1}^{N} (-1)^{k+1} \binom{N}{k} p^{\binom{k}{2}}$$

2.10. Graph Theory metrics

Two graph theory metrics, small-worldness and modularity, were computed for each subject using the Network Toolbox (https://cran.r-project.org/web/packages/NetworkToolbox). Small-worldness was calculated using the random network option to compute the cross-correlation, whilst modularity was computed using the Louvain algorithm.

2.11. Statistical analysis

Demographics and clinical characteristics of the study cohort were summarized using descriptive statistics. The association between TDA metrics and demographic, clinical and imaging variables was explored using a Spearman correlation; p-values were adjusted for multiple comparisons via Bonferroni.

TDA metrics were compared across cohorts using an unpaired one-way ANOVA with multiple comparisons if normally distributed, and using the Kruskal–Wallis test when not.

Node participation rank and curvature normality ranges (99% CI) were generated using the values obtained from the Whitehall-II imaging subjects, to explore if there was a difference in the spatial distribution, for each node. Nodes were grouped in sub-networks using hierarchical clustering. To understand if some areas were more frequently abnormal, for each sub-network, the mean number of abnormal nodes was estimated in both controls and stroke patients (<24h and 1-week) and compared across groups and sub-networks using a Poisson generalized linear model.

fMRI networks were compared to random network both in terms of nTPT and curvature. Differences in nTPT were explored with a Kruskal–Wallis test. Changes in curvature across ε were summarized by generating a correlation matrix and computing the mean correlation.

The association between TDA metrics and recovery, and graph theory metrics (small-worldness and modularity), and recovery were explored using a Spearman correlation. Results were adjusted for multiple comparisons using Bonferroni. To explore the association between changes in specific edges and recovery each subject's NetMat was unwrapped into a single row and combined across subjects to create a Subject x Edges matrix. Each column (i.e. a given edge, estimated for all subjects) in this matrix was then correlated with recovery in a general linear model. The FSL randomize tool (with 5000 permutations) was used to correct for multiple comparisons controlling family-wise error across all edges.

To assess the additional value TDA descriptors hold in increasing prognostic accuracy, linear models were built using recovery (overall, acute, and sub-acute) as the dependent variables, and stroke lesion volume, NIHSS at time of scan (<24h or 1-week), recanalization treatment, age, cardiovascular risk factors as independent variables. TDA metrics associated with recovery were subsequently added as a covariate; its added value was estimated by comparing how strongly the model predicted recovery, with and without TDA metrics as a covariate. Logistic regression models were generated using dichotomized recovery (overall, acute, and sub-acute) as the dependent variable and stroke lesion volume, NIHSS at time of scan (<24h or 1-week), recanalization treatment, age, as the independent variables. TDA metrics associated with recovery were then added to the covariates; their added value was estimated by comparing the area under the curve (AUC) of the receiver operator curves (ROC) generated with and without TDA metric as a covariate. Model residuals were checked for normality. Multicollinearity was detected using variance inflation factors.

Linear model and logistic regression models predicting recovery were compared before and after adding TDA metrics using a log-likelihood test, and a chi-square test, respectively. In both instances. Results were adjusted for multiple comparisons using Bonferroni.

3. Results

3.1. Subjects

3.1.1. Control and chronic cerebrovascular cohort cohorts

503 subjects enrolled in the Whitehall-II imaging cohort met the inclusion criteria for the control cohort and 33 for the chronic cerebrovascular disease cohort (CCD).

3.1.2. Acute Stroke Patient cohort

Of the 83 acute stroke patients enrolled in the AMICI study and meeting the inclusion criteria, 4 were lost to follow-up (2 deaths, 2 declined); 6 were removed from all analyses due to the fMRI data collected not being analysable. The mean stroke lesion volume was 11.3 cm^3, ranging from 0 to 92.9 cm3.

ASL perfusion data were collected in 96 control subjects and 48 consecutive acute stroke patients, allowing to compare TDA metrics with CBF values.

Patients and control subjects characteristics are summarised in Table 6-2.

		Control Subjects	CCD Subjects	Acute Stroke Patients
n		503	33	72
Age	Mean (SD)	69.1 (4.8)	71.2 (5.0)	69.7 (16.00)
Sex	F %	20.7	12.1	38.0
	M %	79.3	87.9	62.0
Hypertension	**%**	29.8	66.7	52.1
Diabetes	**%**	6.4	6.1	8.5
AF	**%**			26.8
presenting NIHSS	Mean (SD)	n/a	n/a	7.0 (6.2)
mRS pre-stroke <3	%	n/a	n/a	13.9
r-tPA	**%**	n/a	n/a	46.5
MT	**%**	n/a	n/a	8.5

Table 6-2 Descriptive statistics. NIHSS: National Institutes of Health Stroke Scale; mRS: modified Rankin scale; r-tPA: recombinant tissue plasminogen activator; MT: mechanical thrombectomy.

3.2. Topological Data Analysis metrics

The TDA properties expressed in the control cohort significantly ($p<0.001$) differed from that of a synthetic dataset comprising of 500 random graphs (Erdös-Rényi, nodes: 55x55) (see Figure 6-1). In the control cohort, both metrics were consistent across subjects (see Figure 6-2). Both CMS-slope and nTPT were not significantly associated with demographic variables, cardiovascular risk factors, white matter hyperintensities volume or cortical thickness.

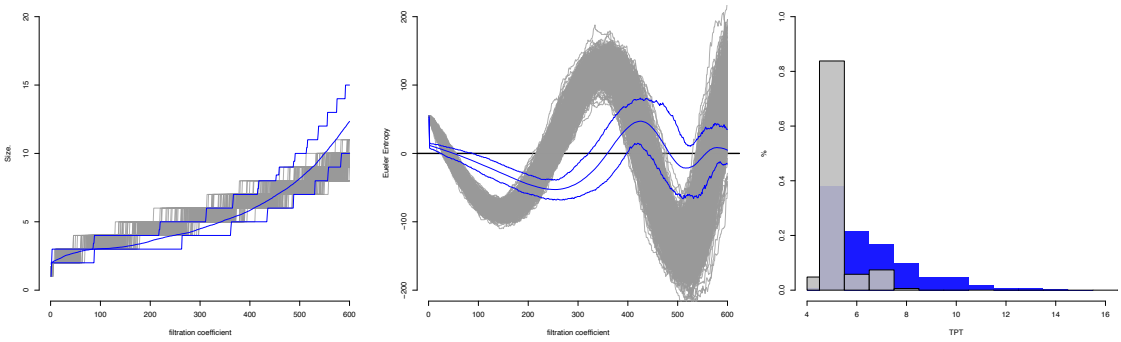


Figure 6-1 TDA descriptors in Erdős–Rényi networks. Cliques Maximum Size and Euler characteristic for 500 random networks (Erdős–Rényi). Gray: synthetic dataset of random matrices. Blue: control cohort.

Acute stroke patients exhibited significantly ($p< 0.001$) higher and more variable CMS-slope and nTPT values compared to control or CCD cohort subjects (see Figure 6-2). Although no difference was observed across timepoints at a group level, nTPT varied in the same subjects across time (correlation across timepoints: CMS-slope: 0.07, $p = 0.64$; nTPT: rho -0.04, $p = 0.76$). Both the CMS-slope and nTPT remained not associated with any demographic (age,

sex), clinical (NIHSS, AF, diabetes, hypertension) or imaging variables (cortical thickness, white matter volume, stroke lesion volume) tested.

In approximately 30% of the stroke patients in this study it was possible to observe, after an initial increase at <24h, a decrease in nTPT when rescanned at 1-week. In a second group of patients (30%) nTPT exhibited a different pattern, increasing in time.

No significant correlation was observed between TDA and perfusion metrics (mean grey matter CBF and mean stroke lesion CBF in stroke patients).

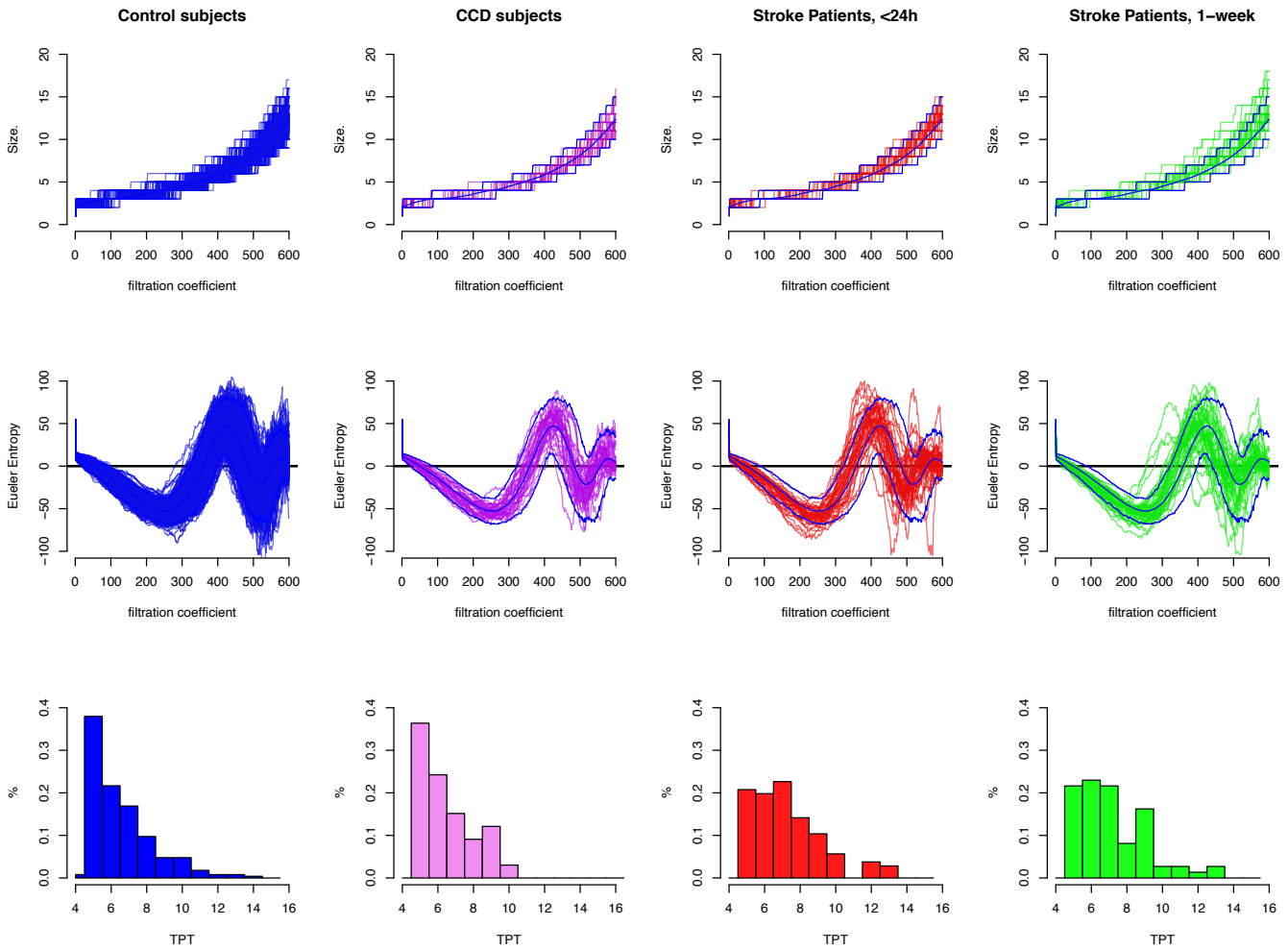


Figure 6-2 TDA descriptors in Controls and CCD subjects, and Acute Stroke patients (at <24h and 1 week). Top row: Cliques Max Size (CMS) as a function of the Filtration threshold (= 1- correlation strength). Middle row: Euler Entropy as a function of the Filtration threshold. Bottom row: Number of Topological Phase Transitions (nTPT) of the Euler Entropy. CCD: chronic cerebrovascular disease

	CMS-slope				nTPT			
	Controls		CCD		Controls		CCD	
	rho	p-value	rho	p-value	rho	p-value	rho	p-value
Age	-0.03	0.49	-0.28	0.12	0.01	0.79	-0.21	0.25
Sex	0.02	0.61	-0.08	0.65	-0.04	0.42	-0.43	0.01
Hypertension	0.02	0.70	-0.08	0.67	0.05	0.26	-0.02	0.89
MAP	0.08	0.07	0.03	0.87	0.04	0.34	-0.02	0.93
Diabetes	-0.10	0.02	-0.12	0.51	0.00	0.97	0.08	0.67
Smoker	-0.06	0.18	-0.22	0.21	-0.02	0.71	-0.20	0.26
CVD	0.00	0.92	0.07	0.68	-0.04	0.35	0.44	0.01
Cortical Thickness	0.00	0.95	0.10	0.57	0.03	0.55	-0.24	0.18
WMH-volume	0.05	0.31	0.09	0.64	0.10	0.03	0.10	0.60
Scanner	-0.09	0.05	-0.02	0.92	-0.03	0.46	0.42	0.02
Motion	-0.06	0.19	-0.19	0.30	-0.03	0.56	-0.07	0.70

Table 6-3 Association between demographic, clinical and imaging variables and TDA metrics in subjects enrolled in the Whitehall Imaging II cohort. CMS-slope: Clique Maximum Size slope; nTPT: number of Topological Phase Transitions; MAP: mean arterial pressure; CVD: cardiovascular disease. WMH: White Matter Hyperintensities. CCD: Chronic Cerebrovascular disease

	CMS-slope				nTPT			
	Stroke, < 24h		Stroke, 1-week		Stroke, < 24h		Stroke, 1-week	
	rho	p-value	rho	p-value	rho	p-value	rho	p-value
Age	0.04	0.82	-0.14	0.39	-0.06	0.65	-0.03	0.83
Sex	-0.10	0.53	-0.08	0.60	-0.14	0.24	0.04	0.74
Hypertension	-0.11	0.50	-0.22	0.16	-0.11	0.37	-0.13	0.29
MAP	0.25	0.11	-0.28	0.07	-0.02	0.86	-0.14	0.23
Diabetes	-0.13	0.41	-0.30	0.05	0.01	0.91	0.06	0.64
Smoker	-0.02	0.90	-0.05	0.74	-0.04	0.74	-0.15	0.23
AF	0.01	0.94	0.13	0.40	0.06	0.65	0.10	0.39
premorbid mRS	0.02	0.89	0.00	1.00	-0.07	0.59	0.10	0.39
NIHSS	0.15	0.34	-0.06	0.71	0.13	0.29	0.21	0.08
Infarct Volume	-0.09	0.59	0.11	0.48	0.08	0.50	0.08	0.51
Hemisphere affected	0.19	0.23	0.02	0.91	0.08	0.48	0.04	0.73
Cortical Thickness	0.03	0.85	0.11	0.55	0.03	0.84	-0.09	0.47
WMH-volume	0.09	0.06	0.09	0.06	0.09	0.06	0.09	0.06
Sequence	0.26	0.03	-0.05	0.68	0.26	0.03	-0.05	0.68
Motion	0.13	0.42	0.01	0.97	-0.16	0.22	0.19	0.14

Table 6-4 Association between demographic, clinical and imaging variables and TDA metrics in Acute Stroke Patients. CMS-slope: Cliques Maximum Size Slope; nTPT: number of Topological Phase Transitions; MAP: mean arterial pressure; AF: Atrial Fibrillation; NIHSS: National Institutes of Health Stroke Scale; mRS: modified Rankin scale; WMH: White Matter Hyperintensities.

3.3. Association with recovery and comparison with other fMRI metrics

In acute stroke patients, nTPT at <24h significantly correlated with overall recovery (rho 0.50, p<0.001, Table 6-5) and acute recovery (rho 0.59, p<0.001, Table 6-5). nTPT at 1-week significantly correlated with sub-acute recovery (rho 0.77, p<0.001, Table 6-5)). CMS-slope was not associated with recovery.

	Acute Recovery		Sub-acute Recovery		Overall recovery	
	rho	**p-value**	**rho**	**p-value**	**rho**	**p-value**
CMS-slope	0.18	0.31	0.11	0.54	0.22	0.21
nTPT	0.59	<0.001 ***	0.77	<0.001 ***	0.50	<0.001 ***
SW	-0.06	0.72	-0.13	0.47	0.00	0.98
Modularity	0.14	0.44	-0.36	0.05	0.08	0.65
Edges	*None found*		*None found*		*None found*	

Table 6-5 Association between functional MRI metrics and recovery. nTPT: number of Topological Phase Transitions, CMS-slope: Clique Maximum Size slope; SW: Small-Worldness.

The generalised linear model analysis, using each edge as a predictor variable did not yield any significant results; no edge was found to be significantly associated with recovery, at either timepoint.

Both modularity and small-worldness. were significantly lower in stroke patients (both at <24h and at 1-week) compared to control subjects (p<0.001). Neither metric was significantly associated with recovery (see Table 6-5).

3.4. Additional value in prediction clinical models

The addition of nTPT significantly improved all linear prediction models (overall recovery: from R^2 0.45 to 0.62, p<0.01; acute recovery: from R^2 0.31 to R^2 0.63, p<0.001; sub-acute

recovery: from R^2 0.14 to R^2 0.71, $p<0.001$; see Table 6-6 and Table 6-7). Among the other covariates, thrombectomy, premorbid mRS and NIHSS <24h were found to be significantly associated with overall recovery ($p<0.01$) and acute recovery, ($p<0.01$) but not with sub-acute recovery (see Table 6-6).

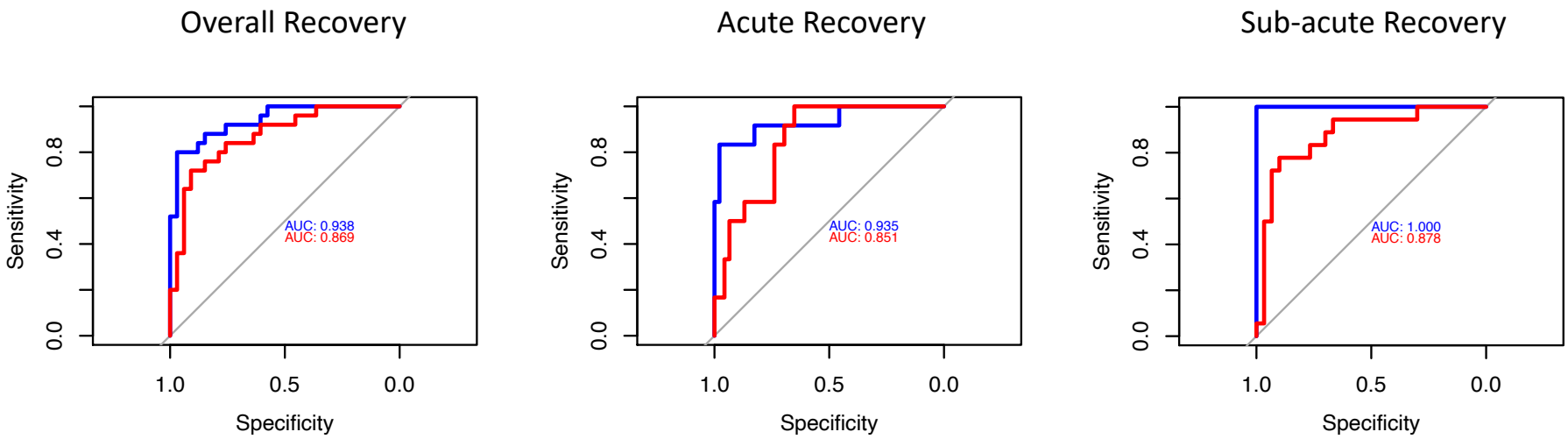
When dichotomizing recovery in NIHSS around a value of 4, nTPT significantly improved the AUC of the ROC curve from 0.87 to 0.94 when predicting overall recovery (see Figure 6-3); and from 0.85 to 0.94 when predicting acute recovery (see Figure 6-3). Changes in NIHSS were dichotomized around a value of 2 when predicting sub-acute recovery, The addition of nTPT improved the AUC from 0.88 to 1 (see Figure 6-3).

Parameter	Overall Recovery			Acute Recovery			Sub-acute Recovery		
	Estimate	Std.Error	p-value	Estimate	Std.Error	p-value	Estimate	Std.Error	p-value
AF	-0.43	0.48	0.37	0.12	0.41	0.77	-0.31	0.27	0.27
Age	0.00	0.01	0.97	0.02	0.01	0.20	0.00	0.01	0.93
nTPT	0.45	0.09	<0.001 ***	0.53	0.08	<0.001 ***	0.55	0.06	<0.001 ***
Lesion Volume	0.00	0.00	0.05	0.00	0.00	0.84	0.00	0.00	0.15
Diabetes	0.53	0.63	0.40	-0.35	0.55	0.53	0.41	0.40	0.31
Hemisphere (R)	0.42	0.38	0.28	-0.35	0.33	0.29	0.32	0.23	0.16
Hypertension	-0.58	0.37	0.12	-0.17	0.32	0.59	-0.23	0.23	0.32
NIHSS at time of scan	0.20	0.06	<0.01 **	0.14	0.05	<0.01 **	0.01	0.04	0.85
Premorbid mRS	-0.38	0.29	0.19	-0.94	0.25	0.00	0.00	0.17	0.99
Thrombectomy	1.92	0.75	0.01 **	1.57	0.65	0.02 *	0.08	0.53	0.88
rtPA	-0.46	0.36	0.21	-0.48	0.32	0.14	-0.12	0.26	0.64

Table 6-6 Predictive models of Recovery (linear models). NIHSS: National Institutes of Health Stroke Scale; mRS: modified Rankin scale; rtPA: recombinant tissue plasminogen activator; nTPT: number of Topological Phase Transitions

	R2 nTPT-	R2 nTPT+	p-value
Acute Recovery	0.31	0.63	<0.001***
Sub-acute Recovery	0.14	0.71	<0.001***
Overall recovery	0.45	0.62	<0.001**

Table 6-7 Change in R2 when adding nTPT to the linear model predicting recovery.



	AUC nTPT-	AUC nTPT+	p-value
Acute Recovery	0.85	0.94	<0.001***
Sub-acute Recovery	0.88	1.00	<0.001***
Overall recovery	0.87	0.94	<0.001**

Figure 6-3 ROC curves. Logistic regression models predicting recovery with nTPT (blue) and without nTPT (red). Overall Recovery was defined as an improvement in NIHSS of 4 or more between <24h and 1-month. Acute Recovery was defined as an improvement in NIHSS of 4 or more between <24h and 1-week. Changes in NIHSS were dichotomized around a value of 2 when predicting sub-acute recovery, due to the more modest recovery rate observed between 1-week and 1-month.

3.5. Localizing changes in connectivity

In control subjects, both the mean node participation-rank and curvature significantly varied across brain regions ($p<0.001$), ranging from 0.37% to 8.63%, and from -1.62 to 0.81, respectively.

Nodes presenting abnormal participation rank values were significantly more frequent in stroke patients compared to controls (increase in mean number of abnormal nodes for patient: <24h 1.2, $p<0.001$; 1-week 1.3, $p<0.001$; see Figure 6-4). It was possible to observe a similar behaviour for nodes presenting abnormal curvature (difference in mean number of abnormal nodes for patient: <24h 0.95, $p<0.001$, 1-week 0.55, $p<0.001$; see Figure 6-4).

Hierarchical clustering was run on the control cohort allowing to group nodes in 7 canonical sub-networks (see Figure 6-4 A). At <24h abnormal participation rank values were significantly more frequent in nodes belonging to the motor (32% $p<0.001$) and fronto-parietal sub-networks (40%, $p<0.001$). At 1-week abnormal participation node values were more frequently located in nodes belonging to the motor sub-network (60% patients, $p<0.001$); both at <24h and at 1-week the number of abnormal curvature nodes did not significantly vary across sub-networks.

In random networks the curvature of its nodes is identical at all correlation strengths. Therefore, curvature values vary in the same way in all nodes across correlation strength, resulting in a mean correlation across node curvatures of 1. Functional brain networks significantly differed from random networks (mean curvature correlation in controls: 0.44 CCD: 0.46, stroke <24h 0.45, stroke 1-week: 0.44); no significant difference in mean curvature correlation was observed across groups.

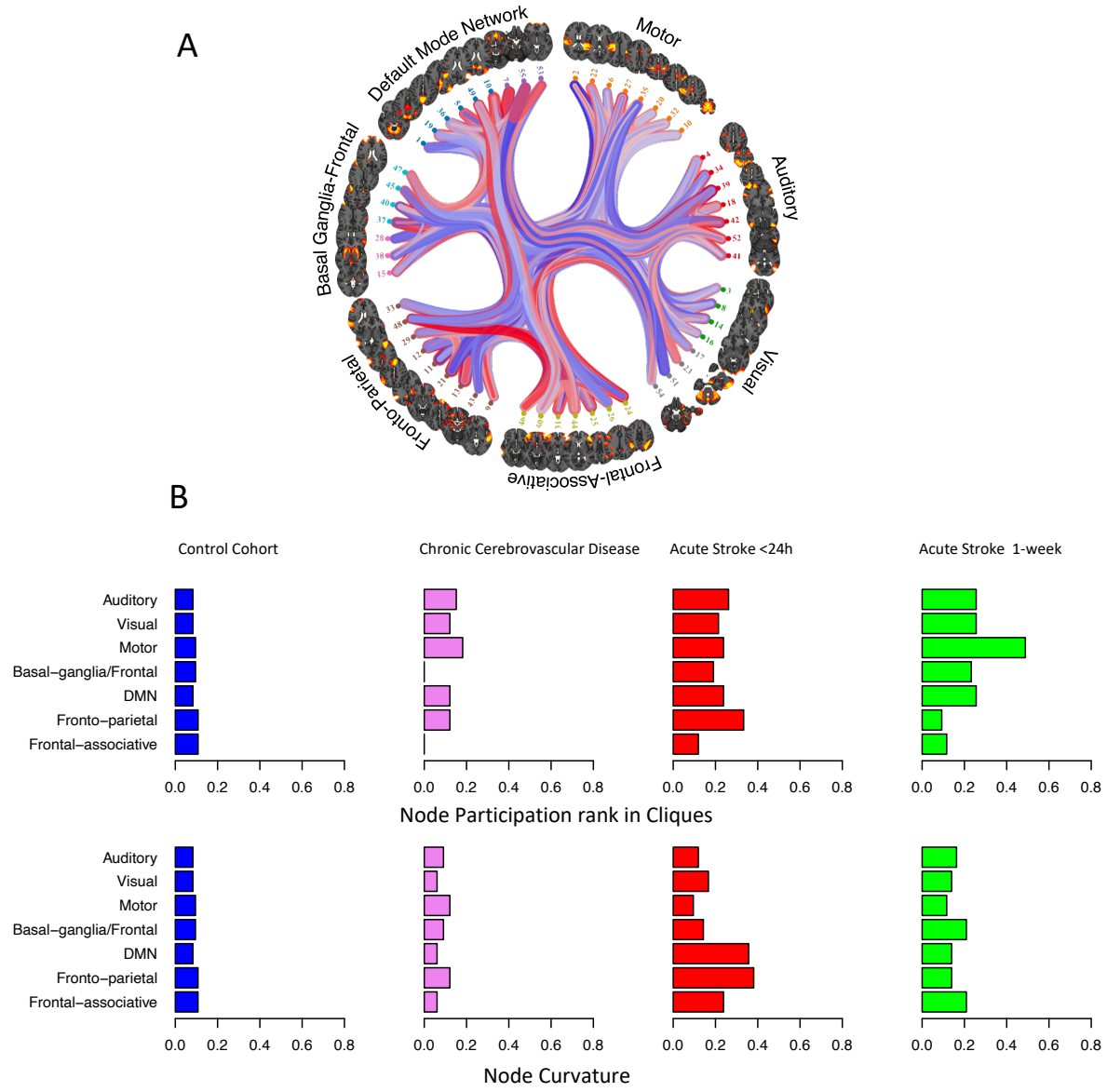


Figure 6-4 Changes in Participation Rank and Node Curvature. A) Hierarchical clustering of the 55 nodes in 7 known subnetworks using data obtained from the control cohort subjects. B) Number of outliers for subnetwork.

4. Discussion

TDA describes how the brain functional network is organised in cliques and cycles of different dimensions. The metrics implemented in this Chapter focus on the relationship between the size of these network structures and how strongly these are connected.

4.1. Control subjects

In subjects with no neurological comorbidities the topological organisation of the brain was found to be 1) consistent across individuals; and 2) significantly different from that of random networks. It was possible to observe higher order and more complex connections compared to chance. This is in line with previous works where algebraic topology was used to describe interactions across neurons.[135]

TDA metrics were not associated with age, cerebrovascular risk factors, or imaging metrics such as cortical thickness, white matter hyperintensities or cerebral perfusion. TDA metrics are known to be unaffected by small perturbations of a system.[224] These findings suggest that this also applies to the inter-individual differences across subjects with no neurological comorbidity.

4.2. CCD and Acute Stroke

In subjects with a past history of stroke or TIA (CCD), the brain topological organisation did not significantly vary from controls.

In acute stroke patients, both CMS-slope and nTPT were more variable and significantly higher than either control or CCD subjects. These findings suggest an acute increase respectively in local activity[134, 135] and global communication across the brain.[134, 135]

Increased connectivity and broader patterns of activation (typically involving contralesional or supplementary regions), have been well documented in previous fMRI and PET studies conducted in acute stroke.[56] TDA metrics did not correlate with any demographic, clinical (NIHSS, AF, diabetes, hypertension) or imaging variable (cortical thickness, white matter volume, stroke lesion volume, cerebral perfusion) tested.

4.3. nTPT is associated with recovery

nTPT, but not CMS-slope was found to be significantly associated with recovery. In stroke patients still symptomatic at the time of the scan, nTPT at <24h significantly correlated with overall and acute recovery; nTPT at 1-week significantly correlated with sub-acute recovery. The appearance of larger cycles is consistent with the recruitment of spared functional regions, a key mechanism underpinning early neurological recovery.[56] This is thought to be mediated by already existing multi-node connections that are normally suppressed due to the presence of more effective routes,[56, 233] and could explain how it was possible to observe increases in nTPT already hours after stroke onset.

4.4. nTPT improves prognostic models

The addition of nTPT significantly improved all linear prediction models. Among the other covariates, thrombectomy, premorbid mRS and NIHSS <24h were found to be significantly associated with overall and acute recovery, but not with sub-acute recovery. Recovery has been dichotomized in past studies and used as a binary variable.[190, 234] The addition of nTPT produced similar benefits when predicting recovery as a binary outcome.

4.5. Localising changes

Nodes presenting abnormal values were significantly more frequent in stroke patients compared to controls and involved all sub-networks. In a stroke population heterogenous for symptoms and lesion locations different sub-networks are likely to be recruited depending on the functional areas affected by the stroke lesion. These metrics might allow to further stratify patients according to which sub-networks were recruited rather than by presenting symptoms.

4.6. Longitudinal changes in connectivity

In CCD subjects the topological organisation of the brain did not significantly vary from controls. Although no difference was observed across timepoints at a group level, nTPT varied in the same subjects across time. Previous studies have suggested that recruitment is only the first stage of recovery;[235] this is followed by reorganization of the impaired area and restoration of activity around the lesion; activity is reduced to baseline levels as pathways become more efficient, mimicking the process of learning typically seen during development.[236] Meanwhile the activation of contralesional or supplementary regions is reduced or eliminated.[236] Consistent with this, in approximately 30% of the stroke patients in this study it was possible to observe, after an initial increase at <24h, a decrease in nTPT when rescanned at 1-week. In a second group of patients (30%) nTPT exhibited a different pattern, increasing in time. These patients typically exhibited a small nTPT at <24h and a more limited acute recovery. It is possible that in some patients the recruitment of new pathways might be more delayed. Alternatively, the changes observed might be secondary to rehabilitation. Learning new motor task has been shown to be associated with changes in cycles.[237] nTPT at <24h was more strongly associated with acute recovery than overall recovery, whilst nTPT at 1-week was more strongly associated with sub-acute recovery.

These findings might help to explain the presence of different recovery trajectories[17] and how these are determined in the early stage of stroke.

4.7. Limitations

This study presents some limitations: although neurological recovery is mediated by compensatory mechanisms, it can also result from the reperfusion of critically hypo-perfused but not yet infarcted tissue. In this Chapter, neither grey matter perfusion nor stroke lesion perfusion was associated with recovery or TDA metrics. Nevertheless, the BOLD signal is not independent of cerebral blood flow further studies are needed to clarify the relationship between the changes in connectivity observed and cerebral perfusion. There are some limitations when using the NIHSS to measure neurological recovery; NIHSS can be insensitive to small neurological changes, especially in posterior circulation or right hemisphere strokes. However, due to the acute nature of this study, where patients were scanned and examined in the early hours following stroke, the advantages the NIHSS offers, in particular its ability to rapidly test multiple neurological domains in a standardised and reliable way, exceeded these limitations.[238, 239]

5. Conclusions

The topological proprieties of the brain were found to be consistent across a large population of control subjects. In the cohort of acute stroke patients, the presence of larger and more strongly connected cycles measured using nTPT, was found to be an independent predictor of recovery, whereas local data processing, measured using CMS-slope was not. The appearance of larger cycles is in keeping with the recruitment of spared functional regions, a key mechanism underpinning early neurological recovery.

These results suggest that nTPT could be used to stratify patients based on their recovery potential, optimising patient selection for recovery trials and rationalising treatment decisions. Further work is required to validate these biomarkers.

In Chapter 8 the relationship between cerebral haemodynamics status and TDA metrics of functional connectivity will be further explored.

Chapter 7.

Local and Whole brain metrics of Residual Integrity

1. Introduction

The ability of the brain to function is enabled by its underlying structure. Sufficient neuronal resources are required for the brain to recover after injury. [223] For example, extensive damage to the corticospinal tract is associated with poor motor recovery.

Metrics estimating the residual integrity of the brain by quantifying infarcted tissue have shown limited value. Injury processes are not limited to the infarct,[14] but affect both peri-infarct tissue and more remote areas.[14] The degree of damage sustained by these regions contributes to symptom severity and the ability to recover. In contrast to infarcted tissue, part of the damage sustained by the peri-infarct is reversible. Within days to weeks from stroke onset the gradual restoration of the lost dendritic spines,[20, 21] and oedema resolution allow for a differential return of neuronal activation within the peri-infarct tissue.[20, 21, 43, 45] In addition, quantifying infarct is not sufficient. Its location and how this impacts the brain organisation as a whole are equally important.

MRI structural biomarkers can characterise the damage sustained both locally and at the whole-brain level, providing insight into the ability of patients to recover.

1.1. Characterising peri-infarct injury and residual integrity

Diffusion tensor imaging (DTI) allows estimating the microstructural integrity of the brain tissue at a voxel level. Fractional anisotropy in particular is sensitive to changes in axons and

dendrites integrity.[240] Imaging registration allows for the opportunity to quantify the degree of anatomical distortion secondary to oedema and haemorrhagic transformation.[86]

1.2. Whole-brain residual integrity

Probabilistic tractography provides insight into how white matter tracts connect different brain regions in a complex network (e.g. the structural connectome). Network analysis approaches can be used to generate summary measures describing how the brain organisation as a whole is impacted by stroke. In Chapter 6, the use of a Topological Data Analysis approach enabled the detections of functional connectivity patterns associated with recovery not detectable using more conventional approaches. Studying the changes in the brain structural organisation might benefit from a similar approach.

1.3. Aim

The aims of this Chapter were:

- to explore the relationship between recovery and markers of microstructural integrity in the peri-infarct;
- to investigate the relationship between recovery and the degree of anatomical distortion present at 1-week;
- to explore the ability of a TDA approach to describe changes in the brain structural organisation and how these relate to recovery.

2. Methods

2.1. Patients

Consecutive patients enrolled in the AMICI study from October 2013 to October 2019 with a diagnosis of stroke and an ischaemic lesion visible on DWI were eligible for this Chapter analyses.

Patients in which a DTI scan was obtained at <24h were included in microstructural and TDA analyses.

Patients still symptomatic at 1-week (NIHSS > 0) and in which follow-up imaging was obtained at 1-week were included in the analyses related to AD and recovery.

Patients that were unable to tolerate the scan or that experienced stroke recurrence, development of a symptomatic parenchymal hematoma (PH2 of the Heidelberg Bleeding Classification) or large hemispheric infarctions (LHI)[180] were removed from the analysis.

2.2. Control subjects

Consecutive subjects enrolled as controls for an observational imaging cohort study investigating acute hepatic encephalopathy were used as a control cohort, as they were scanned in the same facility using the same DTI sequence (see Table 7-1). The control cohort was comprised of patients attending the liver outpatient clinic at the John Radcliffe Hospital with cirrhosis but without overt clinical hepatic encephalopathy. Informed consent was obtained under research protocols agreed by the UK National Research Ethics Service committees (ref: 16/SC/0485).

2.3. Clinical Outcomes

In keeping with Chapter 3 overall recovery was defined as the change in NIHSS between <24h and 1-month. Acute recovery was defined as the change in NIHSS between <24h and 1-week. Sub-acute recovery at 1-month was defined as the change in NIHSS between 1-week and 1-month.

2.4. Image acquisition and pre-processing

Details related to the acquisition of DTI sequences are presented in Table 7-1. In 2019 the DTI sequence was updated to a multi-shell sequence, in line with the UK-BIOBANK imaging protocol.[227]

Dataset	Scanner	Acquisition Parameters
AMICI cohort	3.0T Siemens Verio scanner (Siemens Healthcare, Erlangen, Germany).	2.0x2.0x2.0mm 104x104x72 Directions=64 MB=4, b=0(5+3 phase-encoding-reversed) and b=1500
AMICI cohort (from AMICI 0208 onwards)	3.0T Siemens Verio scanner (Siemens Healthcare, Erlangen, Germany).	2.0x2.0x2.0mm 104x104x72 Directions=64 MB=4, b=0(5+3 phase-encoding-reversed), b=1000 and b2000
Control Cohort	3.0T Siemens Verio scanner (Siemens Healthcare, Erlangen, Germany).	2.0x2.0x2.0mm 104x104x72 Directions=64 MB=4, b=0(5+3 phase-encoding-reversed) and b=1500

Table 7-1. Imaging protocols.

DTI datasets were corrected for eddy currents and head motion. Structural T1-weighted anatomical images were processed using the FreeSurfer software package with standard procedures and parameters.

2.5. White matter hyperintensities volume and Cortical thickness.

WMH segmentation was carried out using the Brain Intensity Abnormality Classification Algorithm (BIANCA) [185] on the FLAIR images collected. Cortical thickness was estimated by processing the T1 images using FreeSurfer.

2.6. Infarct volume

At <24h, infarct volume was defined using semiautomated delineation of apparent diffusion coefficient below an externally validated threshold of 620×10^{-6} mm^2/s.[172]

At 1-week, the stroke lesion was defined by two stroke clinical research fellows, who independently defined stroke lesion on follow-up FLAIR. Any discrepancies (defined as Dice Similarity Index[173] <0.8) were resolved independently by a consultant neuroradiologist. Volumes were corrected for rAD.

2.7. Peri infarct FA and MD

Fractional anisotropy (FA) and mean diffusivity (MD) spatial maps were generated using FSL-DTIFIT.

In keeping with Chapter 3, peri-infarct ROIs were generated by dilating the infarct mask using a 3×3×3 kernel centred on each voxel of the infarct mask. The infarct mask was subtracted from the dilated mask to leave the peri-infarct ROI.[174] Peri-infarct at <24h was generated by dilating the <24h infarct mask. Peri-infarct at 1-week was generated by dilating the 1-week infarct mask.

2.8. Anatomical Distortion (AD)

Anatomical distortion (AD) was quantified using a registration-based approach.[86, 189] Briefly, follow-up MRI were registered to the baseline MRI using FMRIB's Linear Image Registration Tool (FLIRT), and FMRIB's Non-Linear Image Registration Tool (FNIRT).[9,10] The stroke lesion mask was corrected for AD by applying the non-linear registration warp and further refined by applying a CSF exclusion mask generated from the baseline scan.

AD was defined by subtracting the distortion-corrected mask from the uncorrected mask linearly registered to the baseline image. Relative AD (rAD) was obtained by dividing AD for the corrected infarct volume.

2.9. Network modelling

Undirected, weighted networks were constructed based on diffusion-tensor imaging and probabilistic tractography.

Network nodes were generated by parcellating the brain in 55 functional regions using a template derived from 4100 subjects enrolled in the UK Biobank study. Each spatial map was thresholded ($Z > 2.3$) and refined to delineate the grey-white matter boundary underlying the cortical areas to increase anatomical accuracy for DTI fibre tracking. Surface maps of the boundary between grey and white matter were generated by FreeSurfer. All resulting masks were visually checked for plausibility and accuracy.

Probabilistic tractography was applied to evaluate pairwise grey-matter structural connectivity. Tractography was estimated through FDT's probabilistic method with FDT's BEDPOST being used to assess default distributions of diffusion parameters at each voxel, and probabilistic tractography was performed using FDT's probtrackX (parameters: 5000 individual pathways

drawn through the probability distributions on principle fibre direction, curvature threshold set at 0.2, 200 maximum steps, step length 0.5 mm, and distance correction).

The weighted connectivity between the regions *i* and *j* was defined as the number of probabilistic streamlines arriving at region *j* when *i* was seeded, averaged with the number of probabilistic streamlines arriving at region *i* when *j* was seeded. The number of streamlines connecting each pair of regions was divided by the sum of the volumes of these regions, giving the number of connections per unit surface.

2.10. Topological Data Analysis metrics

TDA metrics were generated following Santos et al.[141] The filtration threshold $\varepsilon \in [0, 1]$ was defined so that two regions *i* and *j* are considered connected by an edge if the connection strength $|C_{ij}| > (1 - \varepsilon)$; for $\varepsilon = 1$ all regions in the brain are connected, while there are no connections if $\varepsilon = 0$.

The network topological organization of each individual was characterized as a function of ε. Due to the increasing (exponential) computational power requested when increasing ε, all analyses were limited to the largest threshold computable across all patients ($0<\varepsilon< 0.6$).

The number and size of cliques were computed for each value of ε using the Python Network X library software (https://networkx.github.io). The relationship between cliques maximum size (CMS) and correlation strength was expressed using the Sen slope (CMS-slope).

Changes in cycles were detected using the number of Topological Phase Transitions (nTPT).[141] The Euler characteristic of the functional brain network of each individual was obtained by computing the alternate sum of the numbers of k-cliques (Cl_k) present for a given value of correlation threshold ε:

$$\chi = \sum_{k=1}^{N} (-1)^{k+1} Cl_k(\varepsilon)$$

The Euler Entropy (S_χ) is then obtained from χ :

$$S_\chi = \ln |\langle \chi \rangle|.$$

nTPT was defined as the number of times S_χ switched from positive to negative or vice versa.

2.11. Graph Theory metrics

Two graph theory metrics, small-worldness and modularity, were computed for each subject using the Network Toolbox (https://cran.r-project.org/web/packages/NetworkToolbox). Small-worldness was calculated using the random network option to compute the cross-correlation, whilst modularity was computed using the Louvain algorithm.

2.12. Statistical analysis

Demographics and clinical characteristics were summarized using descriptive statistics. The association between demographic, clinical and imaging variables was explored using a Spearman correlation; p-values were adjusted for multiple comparisons via Bonferroni.

The association between imaging metrics and recovery was explored using a Spearman correlation; p-values were adjusted for multiple comparisons via Bonferroni.

To explore the association between changes in specific edges and recovery each subject's NetMat was unwrapped into a single row and combined across subjects to create a Subject x Edges matrix. Each column (i.e. a given edge, estimated for all subjects) in this matrix was then correlated with recovery in a general linear model. The FSL randomize tool (with 5000

permutations) was used to correct for multiple comparisons (controlling family-wise error) across all edges.

To assess if the imaging biomarkers were independent predictors of recovery, generalized linear models (GLM) were built using recovery (overall, acute, and sub-acute) as the dependent variables, and stroke lesion volume, NIHSS at time of scan (<24h or 1-week), recanalization treatment, age, cardiovascular risk factors as independent variables. Imaging metrics associated with recovery were subsequently added as a covariate. Logistic regression models were generated using dichotomized recovery (overall, acute, and sub-acute) as the dependent variable and stroke lesion volume, NIHSS at time of scan (<24h or 1-week), recanalization treatment, age, as the independent variables. Imaging metrics associated with recovery were then added to the covariates; their added value was estimated by comparing the area under the curve (AUC) of the receiver operator curves (ROC) generated with and without the imaging metric of interest as a covariate. Model residuals were checked for normality. Multicollinearity was detected using variance inflation factors.

Linear and logistic regression models predicting recovery were compared before and after adding the imaging metric of interest using a log-likelihood test, and a chi-square test, respectively. In both instances, p-values were adjusted for multiple comparisons via Bonferroni.

3. Results

3.1. Patients

Patients and control subjects' characteristics are summarised in Table 7-2

		Control Subjects	Acute Stroke Patients (DTI analyses)	Acute Stroke Patients (rAD analyses)
n		10	55	78
Age	Mean (SD)	63.9 (6.2)	73.2 (11.7)	72.1 (13.5)
Sex	F %	30.0	29.1	33.3
	M %	70.0	70.9	66.7
Hypertension	**%**	25.0	49.1	48.7
Diabetes	**%**	25.0	10.9	11.5
AF	**%**	0.0	32.7	30.8
presenting NIHSS	Mean (SD)	n/a	9.9 (7.1)	10.1 (7.3)
mRS pre-stroke < 3	%	n/a	98.2	98.7
r-tPA	**%**	n/a	63.6	46.2
MT	**%**	n/a	16.4	5.1

Table 7-2 Descriptive statistics. NIHSS: National Institutes of Health Stroke Scale; mRS: modified Rankin scale; r-tPA: recombinant tissue plasminogen activator; MT: mechanical thrombectomy.

3.2. Peri-infarct microstructural integrity

Following multiple comparison correction, it was not possible to observe any significant correlation between measures of microstructural integrity in the peri-infarct and recovery (overall, acute or sub-acute, see Table 7-3).

	Overall recovery		Acute Recovery		Sub-acute Recovery	
	rho	**p-value**	**rho**	**p-value**	**rho**	**p-value**
Peri-infarct FA	-0.35	0.04	-0.34	0.03	0.16	0.35
Peri-infarct MD	-0.24	0.15	-0.09	0.57	-0.27	0.11

Table 7-3 Association between DTI microstructural integrity metrics and recovery. Imaging at presentation was used to predict Overall and Acute Recovery. Imaging at 1-week was used to predict sub-acute recovery. FA fractional anisotropy. MD: Mean Diffusivity.

	Sub-acute Recovery	
	rho	p-value
rAD	0.45	<0.001 ***
Infarct Volume	0.38	<0.001 ***

Table 7-4 Association between rAD and Infarct Volume and Recovery. Imaging at 1-week was used to predict sub-acute recovery. rAD: relative anatomical distortion.

3.3. rAD

rAD at 1-week significantly correlated with sub-acute improvement (rho:-0.5, p-value < 0.001), see Table 7-4), infarct volume and NIHSS at time of scan (see.Table 7-5).

In multivariate analysis, rAD remained an independent predictor of subacute recovery. Infarct volume did not. The addition of rAD to both linear and a logistic regression model predicting sub-acute recovery significantly improved the models. The addition of nTPT improved the AUC from 0.79 to 0.90.

	rAD	
	rho	p-value
Age	0.01	0.93
Sex	-0.15	0.24
Hypertension	0.14	0.27
MAP	-0.10	0.44
Diabetes	0.24	0.06
Smoker	0.17	0.20
AF	-0.06	0.63
premorbid mRS	-0.21	0.11
NIHSS at scan	0.58	<0.001***
Infarct Volume	0.45	<0.001***
Hemisphere affected	0.08	0.53
Cortical Thickness	0.08	0.63
WMH-volume	-0.16	0.38
Motion	0.02	0.93

Table 7-5 Exploratory analysis. Association between demographic, clinical and imaging variables and rAD metrics in Acute Stroke Patients. MAP=mean arterial pressure; AF: Atrial Fibrillation; NIHSS: National Institutes of Health Stroke Scale; mRS: modified Rankin scale; WMH: White Matter Hyperintensities

Parameter	Sub-acute Recovery		
	Estimate	Std.Error	p-value
Age	0.02	0.02	0.29
NIHSS at time of scan	0.19	0.06	<0.001***
Diabetes	-1.37	0.75	0.08
AF	-0.08	0.49	0.87
Hypertension	0.05	0.46	0.92
Premorbid mRS	-0.45	0.29	0.13
Hemisphere (R)	1.14	0.45	0.02*
rAD	4.02	1.33	<0.001***
Infarct Volume	0.00	0.00	0.40
rtPA	0.23	0.43	0.60
Thrombectomy	0.35	1.04	0.74

Table 7-6 Predictive model of Recovery (linear model). NIHSS: National Institutes of Health Stroke Scale; mRS: modified Rankin scale; rtPA: recombinant tissue plasminogen activator; nTPT: number of Topological Phase Transitions

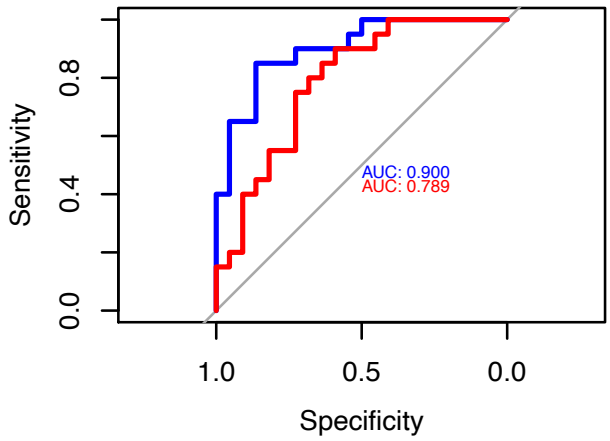


Figure 7-1 ROC curves. Logistic regression models predicting recovery with rAD (blue) and without rAD (red). Changes in NIHSS were dichotomized around a value of 2 when predicting sub-acute recovery.

3.4. Topological Data Analysis metrics

Neither CMS-slope nor the nTPT differed between the control and the acute stroke cohorts. CMS-slope was significantly associated with NIHSS at presentation, WMH-volume and cortical thickness. nTPT was not significantly associated with demographic variables, cardiovascular risk factors, white matter hyperintensities volume or cortical thickness.

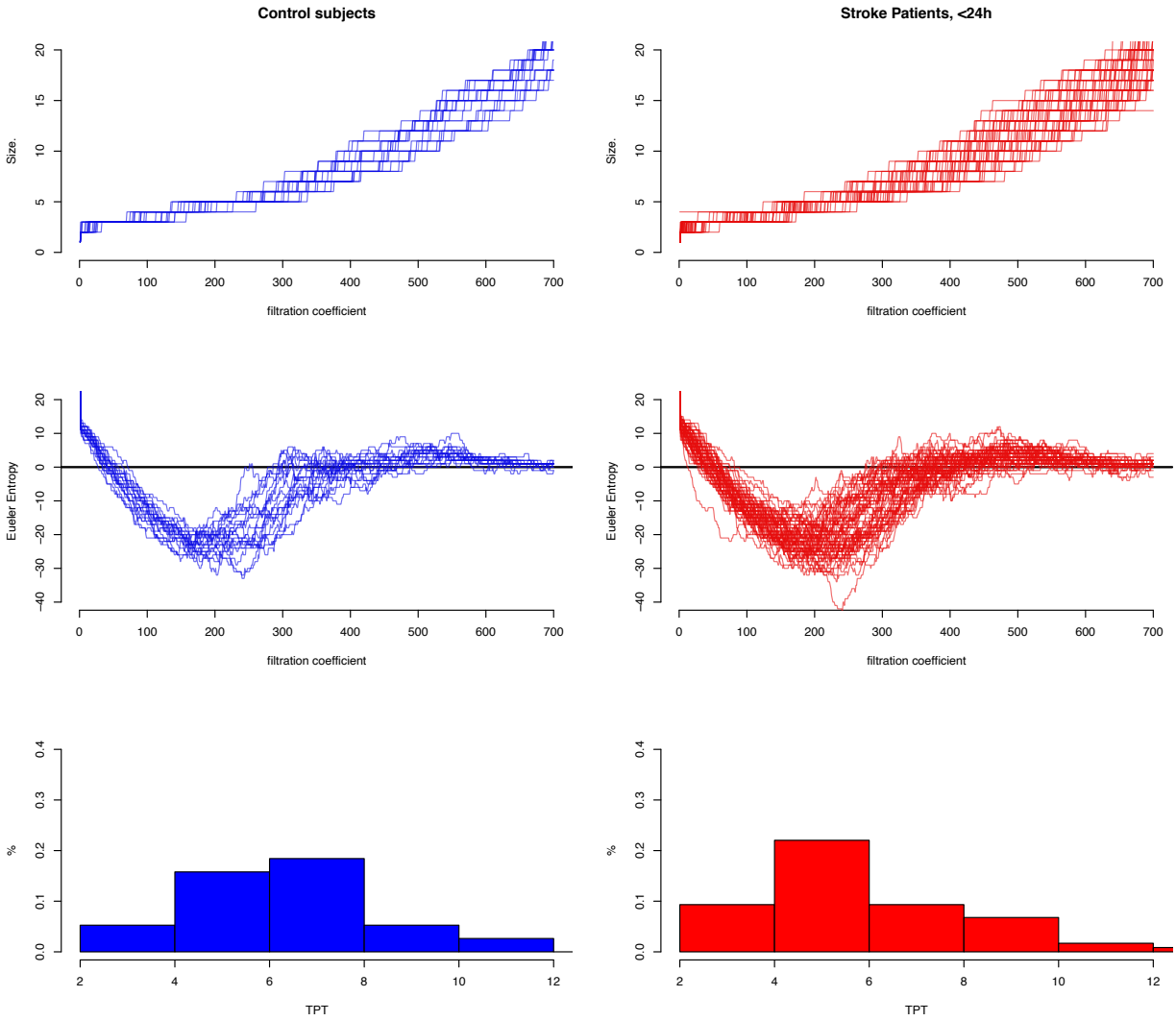


Figure 7-2 TDA descriptors in Controls and Acute Stroke patients Top row: Cliques Max Size (CMS) as a function of the Filtration threshold (= 1- connection strength). Middle row: Euler Entropy as a function of the Filtration threshold. Bottom row: Number of Topological Phase Transitions (nTPT) of the Euler Entropy. Blue=control subjects. Red= acute stroke patients.

3.4.1. Association with recovery and comparison with other network metrics

In acute stroke patients, nTPT at <24h significantly correlated with acute recovery (rho 0.53, p<0.001, see Table 7-7), but not overall recovery. CMS-slope was not associated with recovery (see Table 7-7).

	Acute Recovery		Overall recovery	
	rho	**p-value**	**rho**	**p-value**
CMS-slope	-0.28	0.07	-0.33	0.05
nTPT	0.58	<0.001 ***	0.32	0.06
SW	-0.15	0.34	0.11	0.51
Modularity	0.34	0.03	0.20	0.23
Edges	*None found*		*None found*	

Table 7-7 Association between Network Biomarkers and recovery. nTPT: number of Topological Phase Transitions, CMS-slope: Clique Maximum Size slope; SW: Small-Worldness.

The generalised linear model analysis, using each edge as a predictor variable did not yield any significant results; no edge was found to be significantly associated with recovery, at either timepoint. Neither modularity nor small-worldness was significantly associated with recovery (see Table 7-7).

	CMS-slope		nTPT	
	rho	**p-value**	**rho**	**p-value**
Age	-0.38	0.01	0.08	0.57
Sex	0.21	0.14	-0.03	0.86
Hypertension	-0.18	0.22	-0.07	0.62
MAP	0.12	0.43	0.01	0.96
Diabetes	-0.15	0.32	-0.01	0.94
Smoker	-0.11	0.52	0.15	0.37
AF	-0.17	0.25	-0.01	0.94
premorbid mRS	-0.24	0.10	0.08	0.57
NIHSS	-0.43	<0.001	0.11	0.46
Infarct Volume	-0.21	0.24	0.30	0.10
Hemisphere affected	-0.33	0.02	0.10	0.52
Cortical Thickness	0.44	<0.001	-0.07	0.68
WMH-volume	-0.63	<0.001	-0.01	0.94
Motion	0.10	0.56	0.05	0.75

Table 7-8 Association between demographic, clinical and imaging variables and TDA metrics in Acute Stroke Patients. CMS-slope: Cliques Maximum Size Slope; nTPT: number of Topological Phase Transitions; MAP=mean arterial pressure; AF: Atrial Fibrillation; NIHSS: National Institutes of Health Stroke Scale; mRS: modified Rankin scale; WMH: White Matter Hyperintensities

3.5. Additional value in prediction clinical models

In multivariate analysis nTPT was an independent predictor of recovery (acute and overall) The addition of nTPT significantly improved all linear prediction models (overall recovery: from R^2 0.33 to 0.55, $p<0.01$; acute recovery: from R^2 0.42 to R^2 0.65, $p<0.001$).

When dichotomizing recovery in NIHSS (around a value of 4), nTPT significantly improved the AUC of the ROC curve from 0.895 to 0.965 when predicting overall recovery; and from 0.861 to 0.922 when predicting acute recovery.

Parameter	Acute Recovery			Overall Recovery		
	Estimate	Std.Error	p-value	Estimate	Std.Error	p-value
AF	-2.37	0.96	0.02	-2.29	1.20	0.07
Age	0.03	0.04	0.46	0.02	0.06	0.71
Lesion Volume	0.00	0.00	0.04	0.00	0.00	0.31
Diabetes	1.46	1.81	0.43	2.12	2.26	0.36
Hemisphere (R)	2.13	0.93	0.03	2.90	1.21	0.03
Hypertension	-1.83	0.83	0.04	-1.67	1.09	0.14
NIHSS at time of scan	0.38	0.12	0.01	0.32	0.16	0.06
Premorbid mRS	-0.04	0.77	0.96	0.94	1.09	0.40
Thrombectomy	2.74	1.32	0.05	2.27	1.99	0.27
rtPA	1.62	0.90	0.09	1.45	1.15	0.22
nTPT	0.85	0.22	<0.001	0.84	0.28	0.01

Table 7-9 Predictive models of Recovery (linear models). NIHSS: National Institutes of Health Stroke Scale; mRS: modified Rankin scale; rtPA: recombinant tissue plasminogen activator; nTPT: number of Topological Phase Transitions

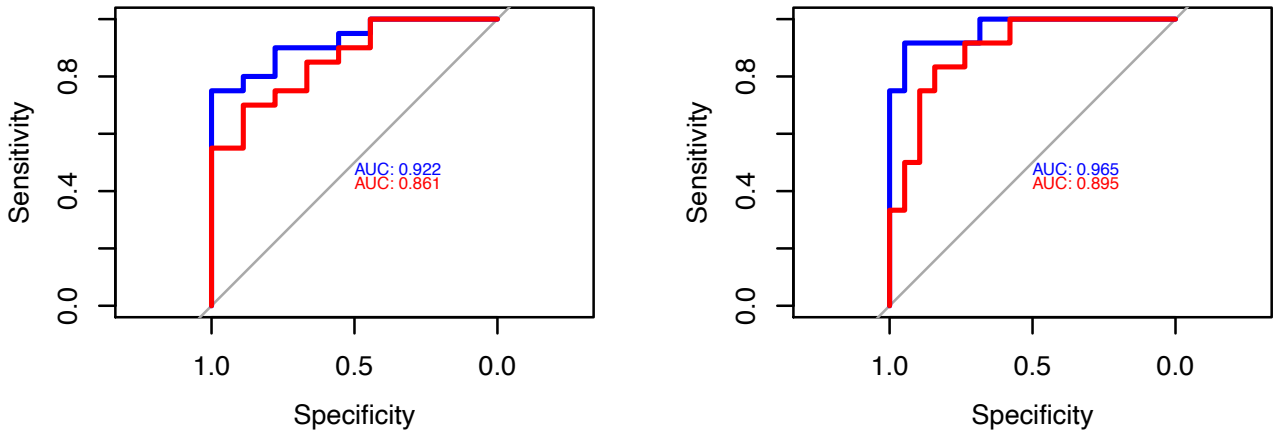


Figure 7-3 ROC curves. Logistic regression models predicting recovery with nTPT (blue) and without nTPT (red). Overall Recovery (left) was defined as an improvement in NIHSS of 4 or more between <24h and 1-month. Acute Recovery (right) was defined as an improvement in NIHSS of 4 or more between <24h and 1-week.

4. Discussion

In this Chapter, the relationship between the residual integrity of the brain and patients' ability to recover was explored. The local effects of stroke were assessed by measuring microstructural integrity and anatomical distortion. The impact of stroke on the whole brain architecture was explored by combining probabilistic tractography with a TDA approach.

4.1. Microstructural integrity of the Peri-infarct tissue

Measures of peri-infarct microstructural integrity were not significantly associated with recovery.

Although DTI metrics have been widely used for inferring microstructural changes related to plasticity and disease,[240] these are not specific to underlying microstructural features of axons and dendrites, and are often sensitive to tissue compartments other than neurites.[241] In acute stroke, the presence of vasogenic oedema, inflammation and changes in non-neuronal cell populations could affect DTI measurements.

More advanced modelling of the diffusion signal, requiring the acquisition of multi-shell DTI data with higher diffusion gradients might be able to better capture changes more specific to dendrites. In consideration of this, the DTI sequence acquired in the AMICI study was amended in 2019. However, due to the impact of the SARS-COVID pandemic on recruitment insufficient data was collected. As the AMICI study continues to enrol more patients it will be possible to further understand the relationship between microstructural integrity and recovery.

4.2. Oedema is an independent predictor of recovery

The presence of cerebral oedema at 1-week was both significantly associated with symptom severity (NIHSS at time of scan) and an independent predictor of recovery (sub-acute recovery).

Brain oedema is a well-recognized mechanism of secondary injury in acute stroke.[190, 242] Although the deleterious effect of swelling has mainly been recognized in cases of malignant infarction, recent studies have highlighted the broader clinical relevance of brain oedema in stroke populations. [243] In line with this, the results in this Chapter provide evidence for an association between oedema, severity of symptoms, and subsequent recovery in moderately sized stroke.

A possible interpretation of these findings is that the greater the contribution of oedema to symptom severity, the greater the improvement is following its resolution. Treatments aimed at reducing brain swelling[244] might be beneficial also in mild/moderate strokes populations, as they would enable to accelerate recovery rates and reduce discharge times. The relationship between recovery and anatomical distortion might also be driven by inflammation. Inflammation not only promotes tissue recovery[9, 14] but can contribute to tissue swelling [9, 14]

The results from this Chapter differ from the findings reported by Battey et al.,[243] where brain swelling was associated with worse outcome. There are a few key differences that might explain the difference in results.

First, the work from Battey et al. explored the relationship between absolute volume of oedema and final outcome (mRS at 3 months), and not improvement over time. Oedema volume strongly correlates with lesion volume, [243] which in turn is associated severity of symptoms and worse outcome. Additionally, in this Chapter, anatomical distortion was expressed relative

to the volume of infarct to capture the relationship between oedema and recovery independently from lesion size. Another important difference is that in Battey et al. work patients with mild strokes were not included and their results cannot be generalized to strokes with infarct volumes <10 mL or a National Institutes of Health Stroke Scale score <4, which are instead included in the AMICI cohort.

4.3. Residual integrity of the brain as a whole

TDA allowed the detection of patterns of connectivity associated with both symptom severity and recovery.

Changes in CMS-slope were associated with symptom severity, WMH burden and cortical atrophy. A greater CMS-slope indicates the presence of a larger number of brain regions strongly connected taking part in cliques. From a computational perspective, cliques represent highly interconnected structures for specialized data processing. A decrease in CMS slope would be in line with acute or chronic damage to the brain regions or the white matter tracts connecting these regions into cliques.

nTPT was an independent predictor of recovery. A higher nTPT indicates the presence of larger, more strongly connected cycles. Cycles represent paths along which data is disseminated to and collected from cliques.[134] Patients that presented with a smaller number of cycles showed a more limited ability to recover. Cycles may capture the presence (or absence) of the latent, multi-nodal connections that are recruited to compensate for the damage sustained following stroke.[14]

nTPT was more strongly associated with acute recovery than overall recovery. Recruitment is thought to play a bigger role during the first stage of recovery;[235] whilst subsequent recovery

is more likely mediated by reorganization of the impaired area and restoration of activity around the lesion.

The addition of nTPT significantly improved the prediction models tested, suggesting that nTPT could be used to stratify patients based on their recovery potential; this would allow to optimise patient selection for recovery trials and rationalise treatment decisions. Still, this finding requires confirmation from large scale trials.

4.4. Limitations

Although structural data might provide insight into the presence of multi-node paths, it is unable to provide information on their actual activation. The combined use of DTI and functional MRI might enable insight into what factors play a role in the recruitment of these compensatory circuits and how to enhance this mechanism of recovery.

An important limitation of all non-invasive brain mapping techniques is that they do not record microstructural information at the level of axons and synapses. Complementing connectivity studies of the human brain with animal studies might help to overcome this limitation.

It was not possible to observe a significant difference at a group level in nTPT between controls and acute stroke patients. Although this might suggest that nTPT is primarily driven by the state of the brain organisation prior to stroke, a larger population of control subjects is needed to clarify this and understand the relative contributions of chronic and acute injury.

5. Conclusions

Structural imaging can be used to estimate the effects of stroke both locally and on the whole brain.

Microstructural integrity metrics of the peri-infarct were not significantly associated with recovery. The presence of anatomical distortion (secondary to oedema) was associated with symptom severity and subsequent recovery. These finding suggest that treating oedema might improve the recovery rates in mild-moderate stroke populations.

The combination of TDA with DTI tractography allowed the detection, in a heterogeneous cohort of acute stroke patients, common patterns of connectivity associated with recovery that allowed to improve prediction models.

Chapter 8.

The impact of haemodynamic status on functional connectivity and oedema

1. Introduction

This Chapter aims at exploring the impact of haemodynamic status on TDA fMRI biomarkers and oedema.

1.1. Cerebral haemodynamics and functional connectivity

In Chapter 6, TDA biomarkers derived from fMRI were found to be independent predictors of recovery. These metrics might reflect neuronal compensatory mechanisms, such as the activation of latent redundant connections in the brain. However, neurological improvement can also result from the reperfusion of critically hypo-perfused tissue, and the BOLD contrast used in fMRI is inherently sensitive to alterations in cerebral blood flow.[106, 107]

Although ASL perfusion metrics were not associated with TDA metrics, ASL and BOLD might capture different aspects of cerebral perfusion. The difference in contrast agent employed by the two technologies has an impact on image intensity in different vessel types (arteries, veins, and capillaries).[245]

In ASL, the contrast agent (labelled water) is visible by the scanner as soon as it enters the brain. Due to magnetization decay, signal intensity is then progressively lost. After a theoretical bolus arrival time limit of approximately 3.5s, the signal is too low to allow ASL to measure perfusion.[246] As a consequence, ASL is unable to detect changes in the venous compartment

reliably. In rs-fMRI, the contrast agent is deoxyhaemoglobin (dHb). dHb allows for extended signal tracing, enabling both the study of venous circulation and the detection of longer delays in blood arrival.[109, 110, 245]However, arterial blood oxygenation is close to 100%. As a result, dHb is negligible in arteries, and therefore, arteries and arterioles are almost invisible to BOLD fMRI.[245, 247]

Extracting perfusion metrics directly from the BOLD signal and exploring their relationship with ASL, recovery and TDA functional connectivity metrics might provide additional insight on the findings obtained using fMRI in acute stroke patients.

1.2. Oedema formation

Many studies have suggested that oedema is caused by dysfunction of the neurovascular unit, loss of autoregulation, hyperaemia, and blood-brain barrier (BBB) breakdown.[108, 242] In addition, recent descriptions of the glymphatic system have suggested a novel hypothesis. The glymphatic system is a macroscopic waste clearance system that utilizes a system of interconnected perivascular channels to promote the elimination of soluble proteins and metabolites from the central nervous system.[248] Flow is transported through the perivascular pumping generated by the cardiac cycle.[249] Following stroke, a reduction in vessel diameter causes a relative increase in perivascular space size (PVS).[250] The reduced pressure in the expanding PVS would then cause an increase in the influx of CSF from the perivascular space into the parenchyma leading to brain swelling.[250] In addition, the impairment of the glymphatic system would hinder the efflux of the interstitial space fluid, further exacerbating the accumulation of fluid within the parenchyma.[250]

The haemodynamic metrics derived from BOLD and ASL might able to provide insight on the mechanisms underlying oedema. A more accurate understanding of oedema formation might help with patient selections for possible treatments.

1.3. Aims

The aims of this Chapter were:

- to compare BOLD and ASL perfusion metrics following acute stroke;
- to explore the relationship between BOLD perfusion metrics, recovery and TDA patterns of functional connectivity;
- to investigate the relationship between macrovascular status at 24h and oedema at 1-week.

2. Methods

2.1. Patients

Consecutive patients enrolled in the AMICI study from October 2013 to October 2019 with a diagnosis of ischaemic stroke and an ischaemic lesion visible on DWI were eligible for this Chapter analyses.

To be included in this analysis, rs-fMRI BOLD and ASL imaging had to be performed both at <24h and at 1-week (5-9 days) from stroke onset.

Patients that were unable to tolerate the scan or that experienced stroke recurrence, development of a symptomatic parenchymal hematoma (PH2 of the Heidelberg Bleeding Classification) or malignant MCA syndrome were not included in the analysis.

2.2. Image acquisition

Image acquisition parameters are detailed in Chapter 4 (ASL) and Chapter 6 (BOLD).

2.3. Clinical Outcomes

In keeping with the definition outlined in Chapter 3, overall recovery was defined as the change in NIHSS between <24h and 1-month. Acute recovery was defined as the change in NIHSS between <24h and 1-week. Sub-acute recovery at 1-month was defined as the change in NIHSS between 1-week and 1-month.

2.4. ROI

Infarct, peri-infarct and mirror ROIs have been defined in Chapter 3.

2.5. Imaging Outcomes

Relative anatomical distortion (rAD) and nTPT were defined in Chapter 4 and Chapter 6, respectively.

2.6. ASL analysis

ASL data underwent motion correction via rigid-body registration and brain extraction; FIX (FMRIB's ICA-based X-noisefier) was used to remove the artefactual components that reflected non-perfusion fluctuations as described in Chapter 4. Registration between perfusion and structural images was carried out using FLIRT (BBR option), which also allowed for simultaneous distortion correction using separately acquired fieldmaps.

CBF, ATT and aCBV maps were then estimated using a spatially regularized Bayesian inference method (BASIL).[226] rCBF, ΔATT and raCBV were obtained by correcting for mirror

ROIs (ΔATT was obtained by subtracting values; rCBF and raCBV were obtained by dividing values)

2.7. BOLD analysis

2.7.1. BOLD-perfusion metrics

BOLD lag maps were generated using *rapidtide*, a set of Python tools for finding time-lagged correlations (https://github.com/bbfrederick/rapidtide).

BOLD lag maps are generated by assigning each voxel the value of the time shift that achieves maximum cross-correlation between the reference time series and the voxel's time series. The time delay between every voxel's rs-BOLD signal and a reference signal is calculated to represent the blood arrival time at that voxel.[247]

A publicly available template[251] was used to extract the reference time series by averaging the BOLD signal across all voxels in the major venous sinuses. The venous sinus reference avoids the contamination of the BOLD delay assessment procedure by hypoperfused voxels because it extracts time courses from voxels outside the brain parenchyma.

MTT maps were generated by fitting a Gaussian curve to the correlation function and by estimating the area under the curve.[247]

Significance thresholds for the cross-correlation were set by *rapidtide* using a shuffling procedure (10,000 times) to calculate the distribution of null correlation values. To determine the offset associated with the highest correlation coefficient with the reference signal, we shifted the time course from −20 to +20 s. A very strict lower threshold of acceptance (=0.3) was implemented to control for spurious correlations.

Relative values (ΔLag, ΔMTT) were obtained by correcting for mirror ROIs (values were subtracted).

2.7.2. BOLD macrovascular metrics

- **BOLD amplitude**

The standard deviation of the BOLD signal was used to quantify the amplitude of the BOLD signal. Voxel-wise standard deviation maps were calculated after the following steps: rs-fMRI data were pre-processed using EPI distortion correction, rigid-body registration, brain extraction, Gaussian smoothing.

As the amplitude of the BOLD signal is dependent both on the number and size of the vessels, values in ROI were normalized by dividing for the mean BOLD-SD in the mirror mask.

- **Resistive and pulsatility index**

Cardiac waveforms were extracted from the fMRI data using *Happy*.[252] *Happy* determines the cardiac waveform over the time course of an fMRI dataset using slice selective averaging of fully unprocessed fMRI data. It exploits the nature of multislice imaging to extract this signal from the fMRI data itself. While any particular slice is recorded at the TR of the imaging experiment, slices are recorded much more quickly - typically from 10 to 20 Hz - sufficiently fast to fully sample the cardiac signal.[252]

After refining the initial cardiac wave estimate using a deep learning filter, the derived signal is used to construct a cardiac pulsation map over a single cycle of the cardiac waveform.

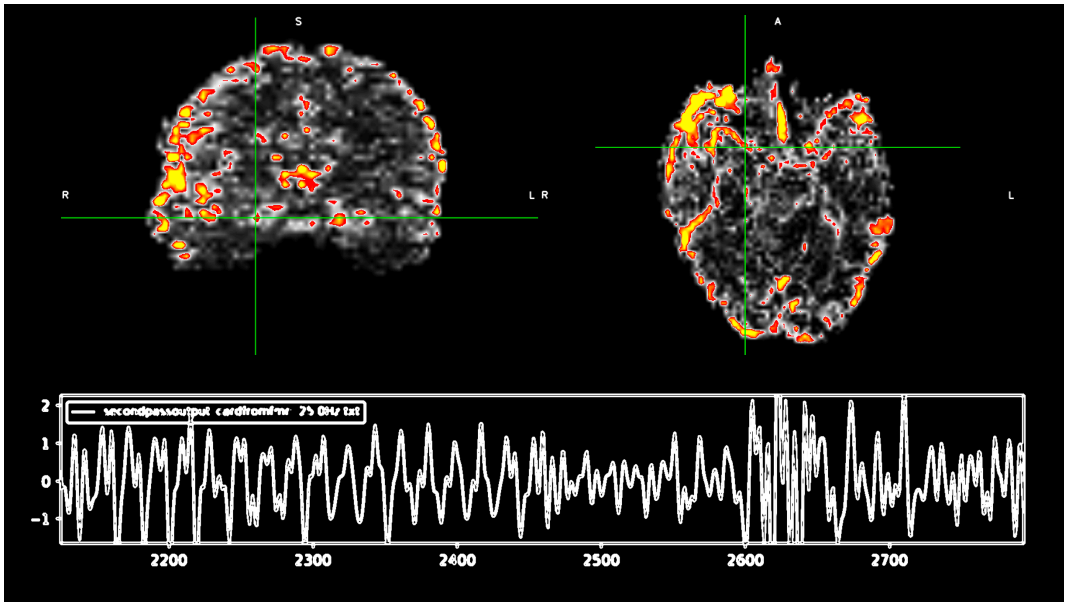


Figure 8-1 Representative cardiac signal. Representative cardiac signal extracted from the BOLD data of a single patient using Happy

The cardiac pulsation maps were then used to compute Pourcelot's Resistivity index (RI) and Gosling's Pulsatility index (PI) in the infarct ROI at <24h using the following equations:

$$RI = (P_{syst} - P_{diast})/P_{syst}$$

$$PI = (P_{syst} - P_{diast})/P_{mean}$$

where P_{syst} is the Peak systolic signal, P_{diast} is the Peak diastolic signal, and P_{mean} is the mean signal.

Relative values (rRI, rPI) were obtained by correcting for mirror ROIs.

2.8. Statistical analysis

Demographics and clinical characteristics of the patients included were summarized using descriptive statistics.

Perfusion metrics were compared across ROIs and across time using a paired one-way ANOVA with multiple comparisons if normally distributed, and using the Kruskal–Wallis test if not. The relationship between ASL and BOLD perfusion metrics was explored using a Spearman correlation. Results were adjusted for multiple comparisons via Bonferroni.

Spearman correlations were used to explore the relationship between perfusion metrics, nTPT and recovery. Results were adjusted for multiple comparisons via Bonferroni.

The association rSD at <24h and rAD at 1-week was explored using polynomial models. Results were adjusted for multiple comparisons via Bonferroni. A multivariate model was used to test if rSD was an independent predictor or rAD. Covariates were selected based on results from Chapter 5. Model residuals were checked for normality. Multicollinearity was detected using variance inflation factors.

3. Results

3.1. Patients

Among the ischemic stroke patients enrolled in the AMICI study, 34 met the inclusion criteria. Demographic and clinical characteristics are summarized in Table 8-1.

		Acute Stroke Patients
Number	n	34
Age	Mean (SD)	70.8 (14.9)
Female	n (%)	11 (32 %)
Hypertension	n (%)	16 (47 %)
Diabetes	n (%)	2 (6%)
AF	n (%)	13 (38%)
presenting NIHSS	Mean (SD)	9.6 (7.3)
mRS pre-stroke <3	n (%)	32 (94%)
r-tPA	n (%)	21 (62%)
MT	n (%)	5 (15%)

Table 8-1 Patient's summary characteristics.

3.2. ROI analysis

At both <24h and 1-week, there was greater variability in BOLD and ASL perfusion metrics in the infarct, peri-infarct, and mirror ROIs compared to the whole grey matter (see Figure 8-2).

After adjusting values using mirror-ROIs, at both <24h and 1-week, it was still possible to observe heterogeneity in the degree and rate of reperfusion in both infarct and peri-infarct regions (see Table 8-2, Figure 8-3). No significant difference was found when comparing at a group level BOLD od ASL perfusion metrics across ROIs or across time (see Table 8-2, Figure 8-3). No significant correlation was observed between ASL and BOLD perfusion metrics (see Figure 8-4).

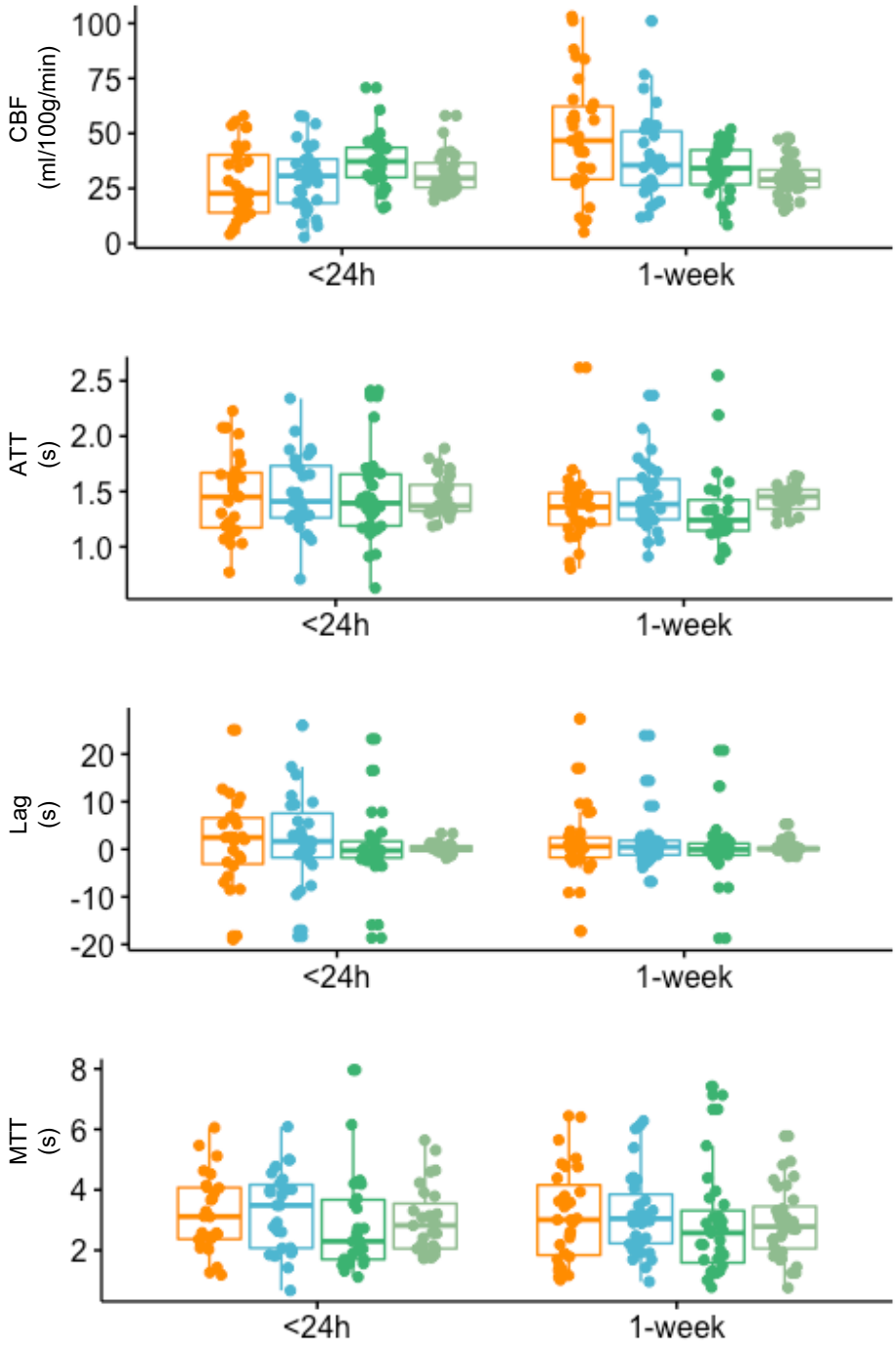


Figure 8-2 ROI analysis. BOLD and ASL perfusion related metrics in infarct, peri-infarct, mirror and grey matter at <24h and at 1-week; Orange = Infarct ROI; Blue = Peri-infarct ROI. Dark Green = Mirror Infarct ROI; Light Green = Grey Matter

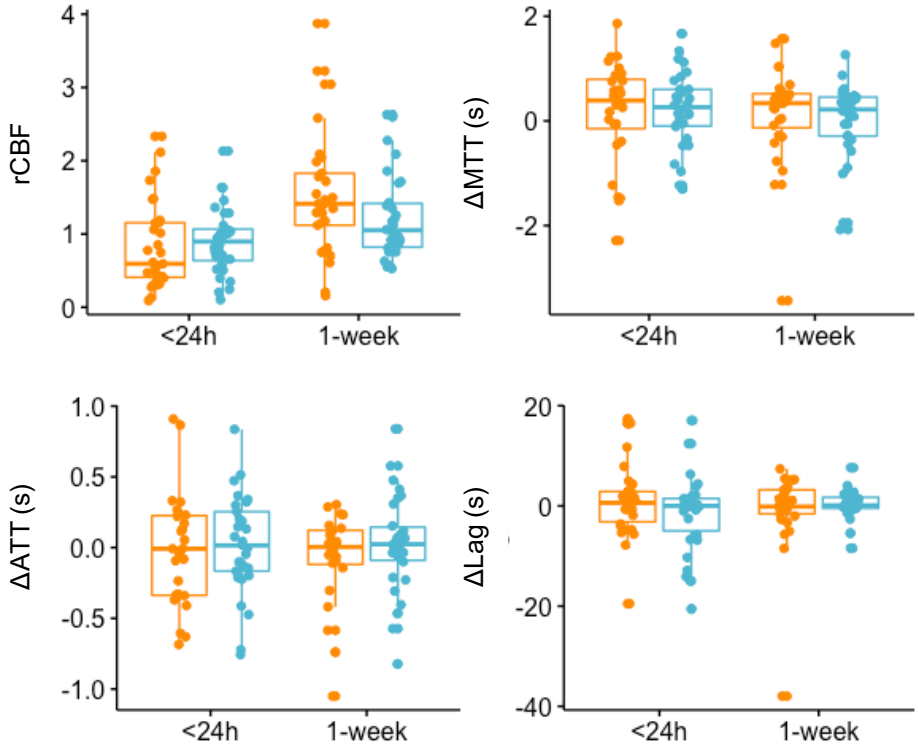


Figure 8-3 ROI analysis. BOLD and ASL perfusion values in Infarct and Peri-Infarct ROIs at <24h and at 1-week. Orange = Infarct ROI; Blue = Peri-infarct ROI.

	<24h		**1-week**	
	Infarct	**Peri-infarct**	**Infarct**	**Peri-infarct**
	Mean (SD)	Mean (SD)	Mean (SD)	Mean (SD)
rCBF	0.96 (0.76)	0.92 (0.70)	1.46 (0.75)	1.35 (0.69)
ΔATT	-0.01(0.48)	0.17 (0.39)	-0.04 (0.42)	-0.09 (0.28)
ΔLag	3.81 (11.00)	2.50 (10.80)	1.90 (6.87)	3.37 (6.39)
ΔMTT	0.26 (1.39)	0.17 (1.57)	0.18(0.68)	-0.01 (1.18)

Table 8-2 ROI analysis. BOLD and ASL perfusion values in Infarct and Peri-Infarct ROIs at <24h and at 1-week

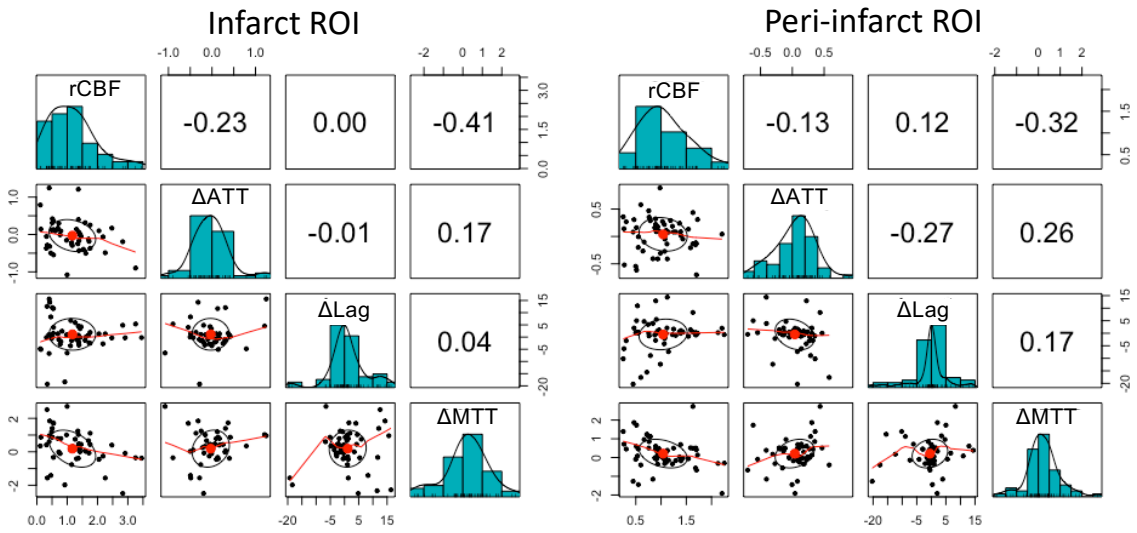


Figure 8-4 ROI correlation analysis. Spearman correlation between ASL and BOLD tissue-perfusion metrics in the infarct and in the Peri-infarct ROIs with corresponding Locally Weighted Scatterplot Smoothing (LOWESS)lines in red.

3.1. Peri-infarct perfusion and nTPT

No significant correlation was found between BOLD perfusion metrics and nTPTs

	nTPT <24h		nTPT 1-week	
	rho	**p-value**	**rho**	**p-value**
ΔLag infarct	-0.07	0.74	0.27	0.19
ΔMTT infarct	0.15	0.47	0.28	0.18
ΔLag Peri-infarct	0.17	0.38	0.29	0.42
ΔMTT Peri-infarct	0.26	0.18	-0.05	0.81

Table 8-3 ROI correlation analysis. Spearman correlation between BOLD tissue perfusion metrics and nTPT acquired at the same timepoint.

3.2. Peri-infarct perfusion and recovery

At 1-week, ΔLag and ΔMTT significantly correlated sub-acute recovery (see Table 8-4). The exploratory univariate analysis found that ΔLag and ΔMTT were associated with rAD, NIHSS at the time of the scan, infarct volume, and diabetes (see Table 8-5).

	Overall Recovery		Acute Recovery		Sub-acute Recovery	
	rho	**p-value**	**rho**	**p-value**	**rho**	**p-value**
rCBF	-0.24	0.41	0.18	0.34	-0.03	0.88
ΔATT	0.09	0.69	0.2	0.36	0.12	0.59
ΔLag	0.02	0.91	0.08	0.69	0.44	**<0.01** **
ΔMTT	0.08	0.69	0.18	0.35	0.35	**<0.01** **

Table 8-4 Association between perfusion metrics and recovery. Spearman correlation between perfusion and Overall, Acute and Sub-acute Recovery

	ΔLag		ΔMTT	
	rho	**p-value**	**rho**	**p-value**
Age	-0.17	0.39	-0.20	0.30
Sex	-0.11	0.57	0.02	0.93
NIHSS 1-week	0.35	<0.05 *	0.14	0.49
MAP	0.01	0.97	-0.12	0.54
Hypertension	0.09	0.64	-0.16	0.42
Diabetes	0.39	<0.05 *	0.33	0.09
Smoker	0.18	0.36	0.06	0.76
AF	-0.10	0.61	-0.16	0.39
r-tPA	-0.03	0.89	0.24	0.20
MT	0.11	0.56	0.16	0.40
Infarct volume	0.37	0.05	0.52	<0.01 **
rAD	0.57	<0.001 ***	0.51	<0.01 ***

Table 8-5 Exploratory analysis. Exploratory analysis between BOLD tissue-perfusion metrics at 1-week and clinical/imaging metrics.

3.2.1. Oedema

It was possible to observe a quadratic relationship between changes in the BOLD amplitude (rSD) at <24h and rAD at 1-week (see Figure 8-5). In multivariate analysis, the relationship between rSD and rAD remained significant after adjusting for other variables associated with oedema (see Chapter 7, Table 8-6).

The exploratory univariate analysis found that rSD at <24h to be associated with AF and ΔLag (see Table 8-7). At <24h, changes in RI but not in PI were significantly associated with rSD (see Table 8-7).

No significant relationship was found between raCBV at <24h and rAD at 1-week (see Figure 8-5).

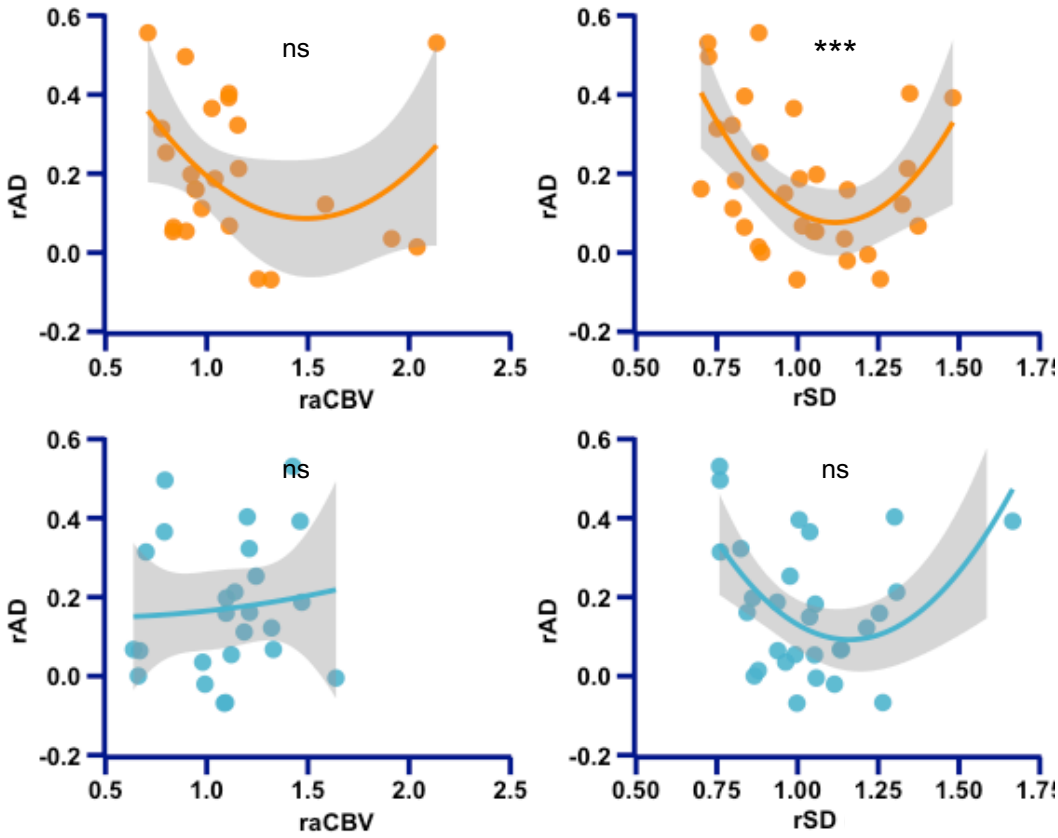


Figure 8-5 Relationship between rAD and macrovascular metrics. Orange = infarct ROI. Blue= peri-infarct ROI. *** p-value< 0.001

	Coefficient	Std. Error	Pr(>|t|)
Diabetes	0.29	0.11	0.02 *
MAP	0.00	0.00	0.05
Age	-0.01	0.00	0.02 *
Hypertension	0.03	0.06	0.59
rSD	-0.04	0.15	0.78
rSD^2	0.67	0.16	<0.001 ***
Infarct Volume	0.00	0.00	0.83
MT	-0.08	0.08	0.33
r- tPA	0.00	0.06	0.98

Table 8-6 Multivariate regression analysis. Multivariate regression with rAD as the dependent variable.

	rSD	
	rho	**p-value**
Age	0.03	0.85
Sex	0.09	0.63
NIHSS <24h	-0.01	0.98
MAP	0.09	0.61
Hypertension	0.16	0.39
Diabetes	0.10	0.59
Smoker	0.15	0.44
AF	0.39	**<0.05** *
r-tPA	0.09	0.63
MT	0.10	0.59
ADC lesion	-0.14	0.44
rCBF	-0.02	0.91
ΔATT	-0.19	0.36
ΔLag	0.37	**<0.05** *
ΔMTT	-0.05	0.81
raCBV	0.08	0.70
rRI	-0.37	**<0.05** *
rPI	-0.16	0.43

Table 8-7. Exploratory analysis. Exploratory analysis investigating the relationship between rSD and clinical/imaging variables

4. Discussion

4.1. BOLD vs ASL: ROI analysis

Although both BOLD and ASL showed a similar behaviour (relatively stable values in the grey matter and variable changes in infarct and peri-infarct ROIs), BOLD and ASL perfusion metrics did not correlate. The relative proportion of different blood vessel types in each voxel (artery, capillary and vein) and the different blood flow velocities in each of these vessel types are responsible for the discrepancies between ASL and BOLD derived metrics. The two imaging techniques likely describe different aspects of cerebral perfusion.

At both 24h and 1week, there was heterogeneity in the degree and rate of reperfusion within both infarct and peri-infarct regions. This variation was not a reflection of global changes as demonstrated by the relatively stable values in the grey matter; or a reflection of the different location of the infarct, as values were corrected for mirror ROIs.

The presence of variable patterns of reperfusion has been well documented in both clinical and preclinical studies.[253] A variety of factors may affect the degree of reperfusion in addition to the tissue state, including microvascular thrombi and endothelial dysfunction.[254, 255] Due to the great variability in reperfusion patterns, no significant difference was found when comparing at a group level perfusion metrics across ROIs or across time.

4.2. nTPT and BOLD perfusion metrics.

Although sLFO in rs-fMRI data can influence RSN analyses,[256] no direct association between perfusion metrics and nTPT was found. The different procedures adopted in this and the previous Chapter, including denoising, seed selection and cross-correlation, were all

fine-tuned to efficiently differentiate the sLFO from the low-frequency oscillations associated with neuronal activity.

4.3. BOLD perfusion metrics, recovery and oedema.

At 1-week, increased Lag and MTT in peri-infarct regions were associated with neurological impairment and subsequent recovery. No relationship was observed between ASL metrics and neurological improvement.

BOLD reflects tissue perfusion by red blood cells, whilst ASL reflects plasma perfusion.[109] These phenomena may be differentially affected in acute stroke, for example, due to progressive capillary constriction by pericytes, which can selectively prevent the passage of oxygen-carrying blood cells.[257] BOLD sensitivity to changes in oxygen delivery might better capture changes related to tissue dysfunction and its recovery. Other possible explanations are that the delays associated with severity and recovery were too long to be accurately captured by ASL; or that these delays mainly affect the blood flow from the capillary to the venous compartment.

Both Lag and MTT were found to be associated with increased values in rAD. Brain swelling can cause venous compression and increase resistance in the capillary and venous vasculature.[258] Microvascular dysfunction can directly contribute to symptom severity,[42] and recovery might reflect the restoration of microcirculation[42] following oedema resolution.

The relationship between recovery and abnormal perfusion status might also be driven by inflammation. Inflammation not only promotes tissue recovery,[9, 14] but can contribute to tissue swelling [9, 14] and cause increased vascular resistance through vasoconstriction and capillary thrombosis [259]

Finally, an increase in Lag and MTT might reflect angiogenesis, as the proliferation of endothelial cells and the formation of new vessels can increase the total resistance of the vascular bed of the afflicted artery.[260]

4.4. Macrovascular status and Oedema

A quadratic relationship was found between the amplitude of the BOLD signal in the first 24h and oedema at 1-week.

The amplitude of the BOLD signal is strongly associated with cerebral blood volume, which is dependent on both the size and number of vessels. Values were corrected for the contralateral ROI to capture changes related to vessel diameter rather than their number. Decreased rSD was found to be associated with longer Lag times, a pattern consistent with vasoconstriction.[118]

The results from this Chapter suggest that both vasoconstriction and vasodilation are linked to oedema formation. The ability to differentiate the dominant mechanism at a patient level would allow the development of different therapeutic strategies, allowing for the personalization of patient care.

In the glymphatic system, periventricular spaces form an interconnected hydraulic network, and flow is transported by means of perivascular pumping generated by the cardiac cycle.[249] Impairment of the glymphatic system would hinder the efflux of the interstitial space fluid, further exacerbating the accumulation of fluid within the parenchyma.[250] Nonetheless, the BOLD amplitude was found to be associated with changes in the resistive index rather than the pulsatility index. In line with evidence from preclinical studies,[250] the relationship between vessel status and oedema seems to be driven by changes in vessel diameter rather than abnormal pulsatility.[250]

No significant relationship was found between aCBV and oedema. In healthy brain parenchyma, aCBV is approximately 20–30% of the total CBV.[261] The effects of vasoconstriction or vasodilation might be more prominent in veins rather than in arteries. Another explanation is that the ASL sequence was optimized for perfusion quantification rather than studying the macrovascular circulation. As a result, the first PLD was acquired too late to accurately measure labelled blood in arteries, causing aCBV to be underestimated. Additionally, in areas critically hypoperfused the ASL signal might be insufficient to reliably characterize the arterial signal.

4.5. Limitations

A limitation of this study is the relatively small number of patients included. As a result, it was not possible to explore recovery using a multivariate approach. A second limitation is that the ASL sequence used in this study had a limited number of repetitions. Although the SNR is sufficient for estimating CBF, it might be still insufficient to accurately quantify ATT and aCBV.

4.6. Conclusions

No correlation was observed between TDA biomarkers of functional connectivity and perfusion metrics. The different procedures adopted allow to separately extract from the BOLD sequence different information. BOLD rs-fMRI an ideal technique to study the transition from injury to recovery.

At 1-week, abnormal perfusion patterns (increased BOLD Lag and MTT) in the peri-infarct areas were associated with symptoms severity, subsequent neurological improvement and presence of oedema. Further work is required to understand if this relationship is mediated by oedema resolution or inflammatory processes.

At <24h, both decreases and increases in the amplitude of the BOLD signal were independent predictors of oedema formation in the following week. These results suggest that both vasoconstriction and vasodilation might be linked to the development of oedema. Changes in the resistive index but not pulsatility index were found to be associated with changes in the BOLD amplitude, suggesting that the changes observed relate more to vessel diameter rather abnormal vessel pulsatility.

No relationship was found between ASL metrics and injury or recovery. ASL and BOLD describe different and possibly complementary aspects of cerebral circulation. Further work is required to understand if the discrepancy between the two imaging techniques is driven by the vessels primarily involved or if it is caused by ASL limitations in providing accurate descriptors in areas with low signal.

Chapter 9.

Summary and Conclusions

The aim of this Thesis was to investigate MRI biomarkers in the understanding of the transition from injury to recovery in a cohort of acute stroke patients. This Chapter summarises the findings presented in this Thesis and how they may help guide future work.

1. Summary

The systematic literature review (Chapter 2) highlighted how the majority of studies have focused on injury-related and specific brain region MRI biomarkers. These metrics are limited in their generalisability across stroke subgroups that differ according to symptoms, lesion location or recanalisation treatment. Whilst network biomarkers are a theoretically more generalisable alternative, there is only limited evidence of their use to date.

An additional finding was that only a minority of studies adopted strategies to minimise the confounding factors present in acute stroke patients. Lesion segmentation was mainly obtained through single rater manual delineation, despite being time-consuming and suffering from low reproducibility. Volumes and ROIs were rarely corrected for oedema. Sequences with low SNR (e.g. BOLD, ASL) were used for analysis without attempting to minimise the noise introduced by motion or vascular artefacts.

Chapters 4 and 5 focused on optimising and developing strategies to minimise these confounding factors. The machine learning approach presented in Chapter 4 accurately segmented acute stroke lesions whilst limiting the bias introduced by anatomical distortion. In Chapter 5, Independent Component Analysis (ICA) was used for the first time to denoise

clinical ASL data. A machine learning approach (FIX) was customised for ASL to classify and regress independent components. The removal of artefactual components improved data quality opening the possibility to reduce the duration of acquisition.

In Chapter 6, TDA network biomarkers derived from rs-fMRI were used to study how changes in the brain's functional organisation related to recovery. TDA can help to describe local data processing (cliques) and information-distributing paths (cycles), detecting changes in connectivity that are independent of location. The topological proprieties of the brain were found to be consistent across a large population of control subjects. In the cohort of acute stroke patients, the presence of larger and more strongly connected cycles measured using nTPT, was found to be an independent predictor of recovery, whereas local data processing, measured using CMS-slope was not. The appearance of larger cycles is in keeping with the recruitment of spared functional regions, a key mechanism underpinning early neurological recovery.

In Chapter 7, peri-infarct microstructural integrity measured using DTI was not significantly associated with recovery. The presence of anatomical distortion (mainly secondary to oedema) at 1-week was associated with both symptom severity and subsequent recovery. When TDA was used to analyse DTI tractography data, CMS-slope was associated with clinical measures of stroke severity (NIHSS) and measures of chronic injury (cortical atrophy and white matter hyperintensities), and nTPT was an independent predictor of recovery.

In Chapter 8 the relationship between perfusion and functional connectivity metrics was explored. BOLD and ASL perfusion metrics did not correlate either with themselves or nTPTs, supporting the observation that the relationship between TDA functional

connectivity metric and recovery is independent from the changes in cerebral perfusion following acute stroke.

In addition, the relationship between oedema and cerebral haemodynamics was explored using both ASL and BOLD. At presentation, BOLD metrics of both vasoconstriction and vasodilation independently predicted oedema formation, the latter providing supporting evidence for the glymphatic theory. At 1-week, the presence of oedema was associated with abnormalities in BOLD perfusion metrics, in keeping with either venous compression or with the vascular effect of the inflammatory response.

2. General considerations and future work

In this section future work about measurement accuracy, use of TDA analysis and the potential role to intervene on anatomical distortion will be discussed in turn.

There are some limitations common to imaging studies. Results are potentially subject to bias from patient dropout and loss to follow up. Despite best efforts to ensure all patients could return for follow up, death, clinical deterioration, and patient preference all accounted for some loss of data.

2.1. Minimising confounding factors

Minimising the potential confounding factors present in the early stroke stages enables the robust analysis and interpretation of results. Different strategies were successfully applied to this end.

BIANCA enabled the accurate segmentation of sub-acute stroke lesions. The use of volume-dependent settings led to a significant improvement in results. Although BIANCA

performance was validated using an external dataset, the cohort of patients used was not representative of the general stroke population, as all patients included had proximal occlusions treated with mechanical thrombectomy. Ongoing work is being currently carried out to test this strategy using a deep learning approach in a larger and more representative cohort of patients with multimodal imaging (CT and MRI).

ICA denoising improved the quality of both rs-fMRI BOLD and ASL perfusion data acquired. Ongoing work is being carried out to incorporate the ICA-based denoising I developed in the processing pipeline for ASL data in large observation cohorts such as the Whitehall-II imaging sub-study, the Human Connectome Project (HCP) Aging subjects, and the HCP Development subjects.

2.2. TDA network biomarkers

TDA outperformed more traditional network analysis strategies. Analyses geared less toward reductionism (i.e., reducing a system to its smaller constituent parts) and more toward complexity and how interactions in the network drive the system are likely to better capture the brain functional and structural organisation (and how this is affected by stroke).

2.2.1. Improving prediction models using TDA metrics

TDA biomarkers were independent predictors of recovery, and their addition significantly improved the prediction models tested. These metrics require validation in large prospective cohorts of stroke patients.

If validated, nTPT could be used in Phase III trials to exclude patients that would recover regardless of intervention, leading to an increase in effect size. Alternatively, these markers could be used to detect the presence of imbalances in treatments arms of a recovery trial.

2.2.2. The relationship between Structural-Functional connectivity

Due to the SARS-COVID pandemic, it was only possible to acquire both BOLD and DTI data in a small number of patients. This is unfortunate as it seems likely that nTPT derived from DTI data are informative of the presence of compensatory paths, whilst nTPT derived from rs-fMRI provides insight into their activation. Combining these two different TDA metrics might better capture who has the capacity recover with or without intervention. These metrics could be used to study treatment response in Phase II trials investigating interventions aimed at maximising the activation of existent compensatory pathways. Phase II studies could implement nTPT to understand if these markers can select patient more responsive to treatment.

2.2.3. Stratifying patients based on the area recruited to compensate

Patient stratification for recovery interventions is usually carried out based on patient symptoms or lesion location. TDA offers a different way to stratify patients, given it was possible to localise the regions contributing to the changes observed in nTPT using node curvature. This information could be used to focus on augmenting the compensatory response, or to stratify patients based on what specific brain regions/sub-networks are recruited to compensate. This might better select patients for specific recovery interventions (e.g. trans-cranial magnetic stimulation).

2.3. Anatomical Distortion

This Thesis' results provide evidence for an association between oedema, symptom severity, and subsequent recovery in moderately sized stroke.

A possible interpretation of these findings is that the greater the contribution of oedema to symptom severity, the greater the improvement is following its resolution. Although the deleterious effect of swelling has mainly been recognized in cases of malignant infarction, recent studies have highlighted the broader clinical relevance of brain oedema in stroke populations. [243] Treatments aimed at reducing brain swelling[244] might be beneficial in mild/moderate strokes populations, as they would enable to accelerate recovery rates and reduce discharge times.

Nonetheless, the relationship between rAD and recovery could also be a reflection of the inflammatory response, as the latter can both cause oedema[9, 14] and trigger tissue recovery mechanisms.[9, 14]A greater understanding of how post-stroke oedema reflects the balance of injury and repair mechanisms is needed to guide what treatment might be appropriate and when following acute stroke.

Validating these findings in large longitudinal prospective studies would allow to better understand the role of oedema. Anatomical distortion can be estimated using imaging acquired in routine practice (both MRI and CT), allowing this method to be easily incorporated in multi-centre studies. The effect of anatomical distortion might be better captured by taking in account the eloquence of the affected area. Image registration techniques might enable to measure oedema contribution using TDA structural connectivity metrics.

A more accurate understanding mechanism underlying oedema formation and their prevalence might help with patient selections for treatment. The results from this Thesis suggest that both vasoconstriction and vasodilation at <24h are linked to oedema formation, suggesting the presence of different mechanisms driving oedema (hyperaemia or glymphatic theory dysfunction).

2.3.1. Stratifying patients based on oedema formation mechanism

The presence of different mechanisms driving oedema might explain the variable response to antioedema strategies,[262, 263] as these interventions are likely to target only one of these two mechanisms. The ability to differentiate the dominant mechanism at a patient level would allow the development of different therapeutic strategies, allowing for the personalisation of patient care. This might also have repercussion on strategies aimed at preventing haemorrhagic conversion. Recent insights into the pathophysiology of oedema in stroke suggest that ischemic oedema and haemorrhagic conversion likely arise from similar processes of microvascular dysfunction.[242] BOLD MRI might be able to select patients at higher risk of neurovascular dysfunction that might better respond to treatments targeting these phenomena.

Appendix A: Example Search Strategy used in Chapter 2

Database: Embase 1974 to present

Search Strategy: (23/01/20)

---

1 exp *cerebrovascular disease/ (333569)

2 exp cerebrovascular disease/ (616636)

3 exp *basal ganglion hemorrhage/ (302)

4 exp basal ganglion hemorrhage/ (739)

5 exp *brain ischemia/ (91017)

6 exp brain ischemia/ (180368)

7 exp *cerebrovascular accident/ (79167)

8 exp cerebrovascular accident/ (202216)

9 exp *hypoxic ischemic encephalopathy/ (3369)

10 exp hypoxic ischemic encephalopathy/ (7008)

11 exp *thromboembolism/ (199941)

12 exp thromboembolism/ (468018)

13 exp *brain hemorrhage/ (52141)

14 exp brain hemorrhage/ (135048)

15 (stroke* or poststroke or post-stroke or cerebrovasc$ or brain vasc$ or cerebral vasc$ or cva$ or apoplex$ or isch?emi$ attack$).tw. (456240)

16 ((lacunar or cortical) adj5 infarct$).tw. (7291)

17 ((isch?emic or apoplectic) adj5 (event or events or insult or attack$)).tw. (44267)

18 2 or 4 or 6 or 8 or 10 or 12 or 14 or 15 or 16 or 17 (1174938)

19 1 or 3 or 5 or 7 or 9 or 11 or 13 or 15 or 16 or 17 (812173)

20 exp nuclear magnetic resonance imaging/ (925618)

21 exp *nuclear magnetic resonance imaging/ (237363)

22 (magnetic resonance adj3 imag*).ti,ab. (299306)

23 mri.ti,ab. (399777)

24 mr.ti,ab. (177981)

25 fmrib.ti,ab. (473)

26 fmri.ti,ab. (54846)

27 resting state.ti,ab. (25874)

28 dti.ti,ab. (16025)

29 diffusion tensor imaging.ti,ab. (17500)

30 blood oxygen level dependent.ti,ab. (4745)

31 bold.ti,ab. (16093)

32 tractography.ti,ab. (7382)

33 functional connectivity.ti,ab. (22113)
34 connectivity.ti,ab. (66758)
35 exp *neuroimaging/ (23062)
36 exp neuroimaging/ (132163)
37 neuroimaging.ti,ab. (65150)
38 neuro-imaging.ti,ab. (1756)
39 (brain* adj3 imag*).ti,ab. (50566)
40 20 or 22 or 23 or 24 or 25 or 26 or 27 or 28 or 29 or 30 or 31 or 32 or 33 or 34 or 35 or 36 or 37 or 38 or 39 (1161109)
41 21 or 22 or 23 or 24 or 25 or 26 or 27 or 28 or 29 or 30 or 31 or 32 or 33 or 34 or 35 or 36 or 37 or 38 or 39 (888952)
42 recover*.ti,ab. (822119)
43 modified rankin scale.ti,ab. (14497)
44 function*.ti,ab. (4406060)
45 exp *aphasia/ (12582)
46 exp aphasia/ (27939)
47 *anomia/ (533)
48 anomia/ (1490)
49 *hemiplegia/ (6085)
50 hemiplegia/ (16793)
51 *hemianopia/ (1012)
52 hemianopia/ (4482)
53 *paresis/ (1753)
54 paresis/ (8985)
55 exp *dysphagia/ (16412)
56 exp dysphagia/ (69536)
57 exp *dysarthria/ (1999)
58 exp dysarthria/ (17493)
59 *pseudobulbar palsy/ (180)
60 pseudobulbar palsy/ (617)
61 *spasticity/ (7940)
62 spasticity/ (22266)
63 (aphasi$ or apraxi$ or dysphasi$ or dysphagi$ or deglutition disorder$ or swallow$ disorder$ or dysarthri$ or hemipleg$ or hemipar$ or paresis or paretic or hemianop$ or hemineglect or spasticity or anomi$ or dysnomi$ or acquired brain injur$ or hemiball$).tw. (146535)
64 ((unilateral or visual or hemispatial or attentional or spatial) adj5 neglect).tw. (3530)
65 42 or 43 or 44 or 45 or 47 or 49 or 51 or 53 or 55 or 57 or 59 or 61 or 63 or 64 (5149322)
66 42 or 43 or 44 or 46 or 48 or 50 or 52 or 54 or 56 or 58 or 60 or 62 or 63 or 64 (5195424)
67 18 and 40 and 66 (45298)

68 19 and 41 and 65 (28743)

69 (exp animals/ or nonhuman/) not human/ (6424282)

70 68 not 69 (26621)

****

Appendix B: Studies included in Chapter 2

1. Vora NA, Shook SJ, Schumacher HC, et al. A 5-item scale to predict stroke outcome after cortical middle cerebral artery territory infarction: validation from results of the Diffusion and Perfusion Imaging Evaluation for Understanding Stroke Evolution (DEFUSE) Study. Stroke 2011; 42: 645-649. DOI: https://dx.doi.org/10.1161/STROKEAHA.110.596312.

2. Yu X, Jiaerken Y, Xu X, et al. Abnormal corpus callosum induced by diabetes impairs sensorimotor connectivity in patients after acute stroke. European Radiology 2019; 29: 115-123. DOI: http://dx.doi.org/10.1007/s00330-018-5576-y.

3. Puig J, Pedraza S, Blasco G, et al. Acute damage to the posterior limb of the internal capsule on diffusion tensor tractography as an early imaging predictor of motor outcome after stroke. AJNR American journal of neuroradiology 2011; 32: 857-863. DOI: https://dx.doi.org/10.3174/ajnr.A2400.

4. Moulton E, Magno S, Valabregue R, et al. Acute Diffusivity Biomarkers for Prediction of Motor and Language Outcome in Mild-to-Severe Stroke Patients. Stroke 2019; 50: 2050-2056. DOI: http://dx.doi.org/10.1161/STROKEAHA.119.024946.

5. Lee J, Park E, Lee A, et al. Alteration and Role of Interhemispheric and Intrahemispheric Connectivity in Motor Network After Stroke. Brain Topography 2018; 31: 708-719. DOI: http://dx.doi.org/10.1007/s10548-018-0644-9.

6. Lee M, Saver JL, Hao Q, et al. Anterior choroidal artery ischaemic patterns predict outcome of carotid occlusion. Journal of Neurology, Neurosurgery and Psychiatry 2012; 83: 586-590. DOI: http://dx.doi.org/10.1136/jnnp-2011-301493.

7. Benghanem S, Rosso C, Arbizu C, et al. Aphasia outcome: the interactions between initial severity, lesion size and location. Journal of Neurology 2019; 266: 1303-1309. DOI: http://dx.doi.org/10.1007/s00415-019-09259-3.

8. Zhong G, Yan S, Zhang S, et al. Association between Leukoaraiosis and Poor Outcome is not due to Reperfusion Inefficiency after Intravenous Thrombolysis. Translational stroke research 2016; 7: 439-445. DOI: https://dx.doi.org/10.1007/s12975-016-0473-7.

9. De Havenon A, Haynor DR, Tirschwell DL, et al. Association of collateral blood vessels detected by arterial spin labeling magnetic resonance imaging with neurological outcome after ischemic stroke. JAMA Neurology 2017; 74: 453-458. DOI: http://dx.doi.org/10.1001/jamaneurol.2016.4491.

10. Mucke J, Mohlenbruch M, Kickingereder P, et al. Asymmetry of deep medullary veins on susceptibility weighted MRI in patients with acute MCA stroke is associated with poor outcome. PLoS ONE 2015; 10: e0120801. DOI: http://dx.doi.org/10.1371/journal.pone.0120801.

11. Liu G, Peng K, Dang C, et al. Axial diffusivity changes in the motor pathway above stroke foci and functional recovery after subcortical infarction. Restorative Neurology and Neuroscience 2018; 36: 173-182. DOI: http://dx.doi.org/10.3233/RNN-170747.

12. Yu X, Xu X, Jackson A, et al. Blood Brain Barrier Disruption in Diabetic Stroke Related to Unfavorable Outcome. Cerebrovascular diseases (Basel, Switzerland) 2016; 42: 49-56. DOI: https://dx.doi.org/10.1159/000444809.

13. Garg R, Liebling S, Maas M, et al. Blood pressure control, decreased diffusion on mri, and outcomes after intracerebral hemorrhage. Neurocritical Care 2011; 15: S76. DOI: http://dx.doi.org/10.1007/s12028-011-9625-5.

14. Lasek-Bal A, Kidon J, Blaszczyszyn M, et al. BOLD fMRI signal in stroke patients and its importance for prognosis in the subacute disease period - Preliminary report. Neurologia i Neurochirurgia Polska 2018; 52: 341-346. DOI: http://dx.doi.org/10.1016/j.pjnns.2017.12.006.

15. Cho TH, Nighoghossian N, Tahon F, et al. Brain stem diffusion-weighted imaging lesion score: a potential marker of outcome in acute basilar artery occlusion. American Journal of Neuroradiology 2009; 30: 194-198. DOI: http://dx.doi.org/10.3174/ajnr.A1278.

16. Vural A, Gocmen R, Oguz KK, et al. Bright and dark vessels on stroke imaging: Different sides of the same coin? Diagnostic and Interventional Radiology 2016; 22: 284-290. DOI: http://dx.doi.org/10.5152/dir.2015.15271.

17. Kim W-J, Kim JH, Ko Y, et al. Can early ischemic lesion recurrence on diffusion-weighted MRI affect functional outcome after acute ischemic stroke? Journal of clinical neurology (Seoul, Korea) 2010; 6: 19-26. DOI: https://dx.doi.org/10.3988/jcn.2010.6.1.19.

18. Chi NF, Ku HL, Chen DYT, et al. Cerebral Motor Functional Connectivity at the Acute Stage: An Outcome Predictor of Ischemic Stroke. Scientific reports 2018; 8: 16803. DOI: http://dx.doi.org/10.1038/s41598-018-35192-y.

19. Liou LM, Chen CF, Guo YC, et al. Cerebral white matter hyperintensities predict functional stroke outcome. Cerebrovascular Diseases 2010; 29: 22-27. DOI: http://dx.doi.org/10.1159/000255970.

20. Barrett KM, Ding YH, Wagner DP, et al. Change in diffusion-weighted imaging infarct volume predicts neurologic outcome at 90 days results of the acute stroke accurate prediction (ASAP) trial serial imaging substudy. Stroke 2009; 40: 2422-2427. DOI: http://dx.doi.org/10.1161/STROKEAHA.109.548933.

21. Sagnier S, Okubo G, Catheline G, et al. Chronic Cortical Cerebral Microinfarcts Slow Down Cognitive Recovery after Acute Ischemic Stroke. Stroke 2019; 50: 1430-1436. DOI: http://dx.doi.org/10.1161/STROKEAHA.118.024672.

22. Held V, Szabo K, Bazner H, et al. Chronic Small Vessel Disease Affects Clinical Outcome in Patients with Acute Striatocapsular Stroke. Cerebrovascular Diseases 2011; 33: 86-91. DOI: http://dx.doi.org/10.1159/000333431.

23. Apoil M, Turc G, Tisserand M, et al. Clinical and magnetic resonance imaging predictors of very early neurological response to intravenous thrombolysis in patients with middle cerebral artery occlusion. Journal of the American Heart Association 2013; 2: e000511. DOI: http://dx.doi.org/10.1161/JAHA.113.000511.

24. Kimura K, Sakamoto Y, Iguchi Y, et al. Clinical and MRI scale to predict very poor outcome in tissue plasminogen activator patients. European Neurology 2011; 65: 291-295. DOI: http://dx.doi.org/10.1159/000327690.

25. Ebinger M, Ostwaldt AC, Galinovic I, et al. Clinical and radiological courses do not differ between fluid-attenuated inversion recovery-positive and negative patients with stroke after thrombolysis. Stroke 2010; 41: 1823-1825. DOI: http://dx.doi.org/10.1161/STROKEAHA.110.583971.

26. Nickel A, Cheng B, Pinnschmidt H, et al. Clinical outcome of isolated cerebellar stroke-A prospective observational study. Frontiers in Neurology 2018; 9: 580. DOI: http://dx.doi.org/10.3389/fneur.2018.00580.

27. Kaesmacher J, Kreiser K, Manning NW, et al. Clinical outcome prediction after thrombectomy of proximal middle cerebral artery occlusions by the appearance of lenticulostriate arteries on magnetic resonance angiography: A retrospective analysis. Journal of Cerebral Blood Flow and Metabolism 2018; 38: 1911-1923. DOI: http://dx.doi.org/10.1177/0271678X17719790.

28. Kim SE, Lee BI, Kim SE, et al. Clinical Significance of Fluid-Attenuated Inversion Recovery Vascular Hyperintensities in Borderzone Infarcts. Stroke 2016; 47: 1548-1554. DOI: https://dx.doi.org/10.1161/STROKEAHA.115.012285.

29. Legrand L, Naggara O, Turc G, et al. Clot burden score on admission T2*-MRI predicts recanalization in acute stroke. Stroke 2013; 44: 1878-1884. DOI: http://dx.doi.org/10.1161/STROKEAHA.113.001026.

30. Jiang L, Su HB, Zhang YD, et al. Collateral vessels on magnetic resonance angiography in endovascular-treated acute ischemic stroke patients associated with clinical outcomes. Oncotarget 2017; 8: 81529-81537. DOI: http://dx.doi.org/10.18632/oncotarget.21081.

31. Findlater SE, Hawe RL, Mazerolle EL, et al. Comparing CST Lesion Metrics as Biomarkers for Recovery of Motor and Proprioceptive Impairments After Stroke. Neurorehabilitation and Neural Repair 2019; 33: 848-861. DOI: http://dx.doi.org/10.1177/1545968319868714.

32. Bivard A, Yassi N, Krishnamurthy V, et al. A comprehensive analysis of metabolic changes in the salvaged penumbra. Neuroradiology 2016; 58: 409-415. DOI: http://dx.doi.org/10.1007/s00234-015-1638-x.

33. Lindow J, Domin M, Grothe M, et al. Connectivity-based predictions of hand motor outcome for patients at the subacute stage after stroke. Frontiers in Human Neuroscience 2016; 10: 101. DOI: http://dx.doi.org/10.3389/fnhum.2016.00101.

34. Thamm T, Guo J, Rosenberg J, et al. Contralateral Hemispheric Cerebral Blood Flow Measured With Arterial Spin Labeling Can Predict Outcome in Acute Stroke. Stroke 2019; 50: 3408-3415. DOI: http://dx.doi.org/10.1161/STROKEAHA.119.026499.

35. Wen H, Alshikho MJ, Wang Y, et al. Correlation of Fractional Anisotropy With Motor Recovery in Patients With Stroke After Postacute Rehabilitation. Archives of Physical Medicine and Rehabilitation 2016; 97: 1487-1495. DOI: http://dx.doi.org/10.1016/j.apmr.2016.04.010.

36. Groisser BN, Copen WA, Singhal AB, et al. Corticospinal tract diffusion abnormalities early after stroke predict motor outcome. Neurorehabilitation and Neural Repair 2014; 28: 751-760. DOI: http://dx.doi.org/10.1177/1545968314521896.

37. Lin DJ, Cloutier AM, Erler KS, et al. Corticospinal Tract Injury Estimated From Acute Stroke Imaging Predicts Upper Extremity Motor Recovery After Stroke. Stroke 2019; 50: 3569-3577. DOI: http://dx.doi.org/10.1161/STROKEAHA.119.025898.

38. Feng W, Wang J, Chhatbar PY, et al. Corticospinal tract lesion load: An imaging biomarker for stroke motor outcomes. Annals of Neurology 2015; 78: 860-870. DOI: http://dx.doi.org/10.1002/ana.24510.

39. Terasawa Y, Kimura K, Iguchi Y, et al. Could clinical diffusion-mismatch determined using DWI ASPECTS predict neurological improvement after thrombolysis before 3 h after acute stroke? Journal of Neurology, Neurosurgery and Psychiatry 2010; 81: 864-868. DOI: http://dx.doi.org/10.1136/jnnp.2009.190140.

40. Sakuta K, Saji N, Aoki J, et al. Decrease of hyperintense vessels on fluid-attenuated inversion recovery predicts good outcome in t-PA patients. Cerebrovascular Diseases 2016; 41: 211-218. DOI: http://dx.doi.org/10.1159/000443533.

41. Maraka S, Jiang Q, Jafari-Khouzani K, et al. Degree of corticospinal tract damage correlates with motor function after stroke. Annals of clinical and translational neurology 2014; 1: 891-899. DOI: https://dx.doi.org/10.1002/acn3.132.

42. Liu Y, Zhang M, Chen Y, et al. The degree of leukoaraiosis predicts clinical outcomes and prognosis in patients with middle cerebral artery occlusion after intravenous thrombolysis. Brain Research 2018; 1681: 28-33. DOI: http://dx.doi.org/10.1016/j.brainres.2017.12.033.

43. Doughty C, Wang J, Feng W, et al. Detection and Predictive Value of Fractional Anisotropy Changes of the Corticospinal Tract in the Acute Phase of a Stroke. Stroke 2016; 47: 1520-1526. DOI: https://dx.doi.org/10.1161/STROKEAHA.115.012088.

44. Thamm T, Zweynert S, Piper SK, et al. Diagnostic and prognostic benefit of arterial spin labeling in subacute stroke. Brain and Behavior 2019; 9: e01271. DOI: http://dx.doi.org/10.1002/brb3.1271.

45. Hawe RL, Findlater SE, Kenzie JM, et al. Differential Impact of Acute Lesions Versus White Matter Hyperintensities on Stroke Recovery. Journal of the American Heart Association 2018; 7: e009360. DOI: https://dx.doi.org/10.1161/JAHA.118.009360.

46. Song TJ, Kim J, Lee HS, et al. Differential impact of unrecognised brain infarction on stroke outcome in non-valvular atrial fibrillation. Thrombosis and haemostasis 2014; 112: 1312-1318. DOI: https://dx.doi.org/10.1160/TH14-02-0176.

47. Baik M, Kim K, Yoo J, et al. Differential impact of white matter hyperintensities on long-term outcomes in ischemic stroke patients with large artery atherosclerosis. PloS one 2017; 12: e0189611. DOI: https://dx.doi.org/10.1371/journal.pone.0189611.

48. Rost NS, Cougo P, Lorenzano S, et al. Diffuse microvascular dysfunction and loss of white matter integrity predict poor outcomes in patients with acute ischemic stroke. Journal of Cerebral Blood Flow and Metabolism 2018; 38: 75-86. DOI: http://dx.doi.org/10.1177/0271678X17706449.

49. Reineck LA, Agarwal S and Hillis AE. "Diffusion-clinical mismatch" is associated with potential for early recovery of aphasia. Neurology 2005; 64: 828-833. DOI: http://dx.doi.org/10.1212/01.WNL.0000152983.52869.51.

50. Tei H, Uchiyama S, Usui T, et al. Diffusion-weighted ASPECTS as an independent marker for predicting functional outcome. Journal of Neurology 2011; 258: 559-565. DOI: http://dx.doi.org/10.1007/s00415-010-5787-x.

51. Jeong JY, Han SK, Shin DH, et al. Diffusion-weighted imaging-fluid-attenuated inversion recovery mismatch is associated with better neurologic response to intravenous thrombolytic therapy in acute ischemic stroke patients. Clinical and experimental emergency medicine 2015; 2: 31-37.

52. Karameshev A, Arnold M, Schroth G, et al. Diffusion-weighted MRI helps predict outcome in basilar artery occlusion patients treated with intra-arterial thrombolysis. Cerebrovascular Diseases 2011; 32: 393-400. DOI: http://dx.doi.org/10.1159/000330644.

53. Yang H, Shen R, Jin Z, et al. Dilated Virchow-Robin Spaces in First-Ever Lacunar Stroke Patients: Topography and Clinical Correlations. Journal of Stroke and Cerebrovascular Diseases 2016; 25: 306-311. DOI: http://dx.doi.org/10.1016/j.jstrokecerebrovasdis.2015.09.034.

54. Song J, Ma Z, Meng H, et al. Distal hyperintense vessels alleviate insula infarction in proximal middle cerebral artery occlusion. International Journal of Neuroscience 2016; 126: 1030-1035. DOI: http://dx.doi.org/10.3109/00207454.2015.1102139.

55. Huang X, Liu W, Zhu W, et al. Distal hyperintense vessels on FLAIR: a prognostic indicator of acute ischemic stroke. European neurology 2012; 68: 214-220. DOI: https://dx.doi.org/10.1159/000340021.

56. Liu D, Scalzo F, Starkman S, et al. DWI Lesion Patterns Predict Outcome in Stroke Patients with Thrombolysis. Cerebrovascular Diseases 2015; 40: 279-285. DOI: http://dx.doi.org/10.1159/000441153.

57. Aoki J, Kimura K, Shibazaki K, et al. DWI-ASPECTS as a predictor of dramatic recovery after intravenous recombinant tissue plasminogen activator administration in

patients with middle cerebral artery occlusion. Stroke 2013; 44: 534-537. 2012/12/06. DOI: 10.1161/strokeaha.112.675470.

58. Rehme AK, Eickhoff SB, Wang LE, et al. Dynamic causal modeling of cortical activity from the acute to the chronic stage after stroke. NeuroImage 2011; 55: 1147-1158. DOI: http://dx.doi.org/10.1016/j.neuroimage.2011.01.014.

59. Hu J, Du J, Xu Q, et al. Dynamic network analysis reveals altered temporal variability in brain regions after stroke: A longitudinal resting-state fMRI study. Neural Plasticity 2018; 2018: 9394156. DOI: http://dx.doi.org/10.1155/2018/9394156.

60. Simpkins AN, Dias C, Norato G, et al. Early Change in Stroke Size Performs Best in Predicting Response to Therapy. Cerebrovascular diseases (Basel, Switzerland) 2017; 44: 141-149. DOI: https://dx.doi.org/10.1159/000477945.

61. Yang H, Ma N, Liu L, et al. Early Diffusion-Weighted Imaging Brain Stem Score for Acute Basilar Artery Occlusion Treated with Mechanical Thrombectomy. Journal of stroke and cerebrovascular diseases : the official journal of National Stroke Association 2018; 27: 2822-2828. DOI: https://dx.doi.org/10.1016/j.jstrokecerebrovasdis.2018.06.019.

62. Bigourdan A, Munsch F, Coupe P, et al. Early fiber number ratio is a surrogate of corticospinal tract integrity and predicts motor recovery after stroke. Stroke 2016; 47: 1053-1059. DOI: http://dx.doi.org/10.1161/STROKEAHA.115.011576.

63. Saur D, Ronneberger O, Kummerer D, et al. Early functional magnetic resonance imaging activations predict language outcome after stroke. Brain 2010; 133: 1252-1264. DOI: http://dx.doi.org/10.1093/brain/awq021.

64. Du J, Yang F, Zhang Z, et al. Early functional MRI activation predicts motor outcome after ischemic stroke: a longitudinal, multimodal study. Brain Imaging and Behavior 2018; 12: 1804-1813. DOI: http://dx.doi.org/10.1007/s11682-018-9851-y.

65. Marshall RS, Zarahn E, Alon L, et al. Early imaging correlates of subsequent motor recovery after stroke. Annals of Neurology 2009; 65: 596-602. DOI: http://dx.doi.org/10.1002/ana.21636.

66. Cho KH, Kwon SU, Lee DH, et al. Early infarct growth predicts long-term clinical outcome after thrombolysis. Journal of the Neurological Sciences 2012; 316: 99-103. DOI: http://dx.doi.org/10.1016/j.jns.2012.01.015.

67. Kim SM, Kwon SU, Kim JS, et al. Early infarct growth predicts long-term clinical outcome in ischemic stroke. Journal of the Neurological Sciences 2014; 347: 205-209. DOI: http://dx.doi.org/10.1016/j.jns.2014.09.048.

68. Abela E, Missimer JH, Pastore-Wapp M, et al. Early prediction of long-term tactile object recognition performance after sensorimotor stroke. Cortex 2019; 115: 264-279. DOI: http://dx.doi.org/10.1016/j.cortex.2019.01.018.

69. Tanriverdi Z, Gocmen R, Oguz KK, et al. Elevations in Tissue Fluid-Attenuated Inversion Recovery Signal Are Related to Good Functional Outcome after Thrombolytic

Treatment. Journal of Stroke and Cerebrovascular Diseases 2016; 25: 480-483. DOI: http://dx.doi.org/10.1016/j.jstrokecerebrovasdis.2015.10.024.

70. Luo G, Mo D, Tong X, et al. Factors Associated with 90-Day Outcomes of Patients with Acute Posterior Circulation Stroke Treated By Mechanical Thrombectomy. World Neurosurgery 2018; 109: e318-e328. DOI: http://dx.doi.org/10.1016/j.wneu.2017.09.171.

71. Zaidi SF, Aghaebrahim A, Urra X, et al. Final infarct volume is a stronger predictor of outcome than recanalization in patients with proximal middle cerebral artery occlusion treated with endovascular therapy. Stroke 2012; 43: 3238-3244. DOI: http://dx.doi.org/10.1161/STROKEAHA.112.671594.

72. Jiang L, Peng M, Geng W, et al. FLAIR hyperintensities-DWI mismatch in acute stroke: associations with DWI volume and functional outcome. Brain Imaging and Behavior 2019. DOI: http://dx.doi.org/10.1007/s11682-019-00156-x.

73. Wang Y, Zhou Z and Ding S. FLAIR vascular hyperintensity-DWI mismatch most likely to benefit from recanalization and good outcome after stroke. Medicine (United States) 2020; 99: e18665. DOI: http://dx.doi.org/10.1097/MD.0000000000018665.

74. Ebinger M, Kufner A, Galinovic I, et al. Fluid-attenuated inversion recovery images and stroke outcome after thrombolysis. Stroke 2011. DOI: http://dx.doi.org/10.1161/STROKEAHA.111.632026.

75. Dong X and Nao J. Fluid-attenuated inversion recovery vascular hyperintensities in anterior circulation acute ischemic stroke: associations with cortical brain infarct volume and 90-day prognosis. Neurological sciences : official journal of the Italian Neurological Society and of the Italian Society of Clinical Neurophysiology 2019; 40: 1675-1682. DOI: https://dx.doi.org/10.1007/s10072-019-03909-0.

76. Legrand L, Tisserand M, Turc G, et al. Fluid-Attenuated Inversion Recovery Vascular Hyperintensities-Diffusion-Weighted Imaging Mismatch Identifies Acute Stroke Patients Most Likely to Benefit from Recanalization. Stroke 2016; 47: 424-427. DOI: http://dx.doi.org/10.1161/STROKEAHA.115.010999.

77. Liu D, Scalzo F, Rao NM, et al. Fluid-attenuated inversion recovery vascular hyperintensity topography, novel imaging marker for revascularization in middle cerebral artery occlusion. Stroke 2016; 47: 2763-2769. DOI: http://dx.doi.org/10.1161/STROKEAHA.116.013953.

78. Olindo S, Chausson N, Joux J, et al. Fluid-attenuated inversion recovery vascular hyperintensity: An early predictor of clinical outcome in proximal middle cerebral artery occlusion. Archives of Neurology 2012; 69: 1462-1468. DOI: http://dx.doi.org/10.1001/archneurol.2012.1310.

79. Tsai YH, Hsu LM, Weng HH, et al. Functional diffusion map as an imaging predictor of functional outcome in patients with primary intracerebral haemorrhage. British Journal of Radiology 2013; 86: 20110644. DOI: http://dx.doi.org/10.1259/bjr.20110644.

80. Li Y, Chen Z, Su X, et al. Functional lateralization in cingulate cortex predicts motor recovery after basal ganglia stroke. Neuroscience Letters 2016; 613: 6-12. DOI: http://dx.doi.org/10.1016/j.neulet.2015.12.051.

81. Samuelsson M, Soderfeldt B and Olsson GB. Functional outcome in patients with lacunar infarction. Stroke 1996; 27: 842-846. DOI: http://dx.doi.org/10.1161/01.STR.27.5.842.

82. Lee J, Lee M, Kim DS, et al. Functional reorganization and prediction of motor recovery after a stroke: A graph theoretical analysis of functional networks. Restorative Neurology and Neuroscience 2015; 33: 785-793. DOI: http://dx.doi.org/10.3233/RNN-140467.

83. Kufner A, Galinovic I, Ambrosi V, et al. Hyperintense vessels on FLAIR: Hemodynamic correlates and response to thrombolysis. American Journal of Neuroradiology 2015; 36: 1426-1430. DOI: http://dx.doi.org/10.3174/ajnr.A4320.

84. Nave AH, Kufner A, Bücke P, et al. Hyperintense Vessels, Collateralization, and Functional Outcome in Patients With Stroke Receiving Endovascular Treatment. Stroke 2018; 49: 675-681. 2018/02/21. DOI: 10.1161/strokeaha.117.019588.

85. Luby M, Warach SJ, Nadareishvili Z, et al. Immediate changes in stroke lesion volumes post thrombolysis predict clinical outcome. Stroke 2014; 45: 3275-3279. DOI: http://dx.doi.org/10.1161/STROKEAHA.114.006082.

86. Olivot JM, Sissani L, Meseguer E, et al. Impact of Initial Diffusion-Weighted Imaging Lesion Growth Rate on the Success of Endovascular Reperfusion Therapy. Stroke 2016; 47: 2305-2310. DOI: http://dx.doi.org/10.1161/STROKEAHA.116.013916.

87. Huang YH, Xia ZX, Wei W, et al. The impact of leucoaraiosis on neurological function recovery in elderly patients with acute cerebral infarction: Clinical study involving 279 Chinese patients. Journal of International Medical Research 2014; 42: 857-862. DOI: http://dx.doi.org/10.1177/0300060513507386.

88. Choi K-H, Kim J-H, Kang K-W, et al. Impact of Microbleeds on Outcome Following Recanalization in Patients With Acute Ischemic Stroke. Stroke 2018: STROKEAHA118023084. DOI: https://dx.doi.org/10.1161/STROKEAHA.118.023084.

89. Chung JW, Kim JY, Park HK, et al. Impact of the Penumbral Pattern on Clinical Outcome in Patients with Successful Endovascular Revascularization. Journal of Stroke and Cerebrovascular Diseases 2017; 26: 360-367. DOI: http://dx.doi.org/10.1016/j.jstrokecerebrovasdis.2016.09.031.

90. Rehme AK, Volz LJ, Feis DL, et al. Individual prediction of chronic motor outcome in the acute post-stroke stage: Behavioral parameters versus functional imaging. Human Brain Mapping 2015; 36: 4553-4565. DOI: http://dx.doi.org/10.1002/hbm.22936.

91. Lee K-J, Jung K-H, Byun J-I, et al. Infarct pattern and clinical outcome in acute ischemic stroke following middle cerebral artery occlusion. Cerebrovascular diseases (Basel, Switzerland) 2014; 38: 31-38. DOI: https://dx.doi.org/10.1159/000364939.

92. Yamashita Y, Wada I, Horiba M, et al. Influence of cerebral white matter lesions on the activities of daily living of older patients with mild stroke. Geriatrics & gerontology international 2016; 16: 942-947. DOI: https://dx.doi.org/10.1111/ggi.12580.

93. Derex L, Nighoghossian N, Hermier M, et al. Influence of pretreatment MRI parameters on clinical outcome, recanalization and infarct size in 49 stroke patients treated by intravenous tissue plasminogen activator. Journal of the Neurological Sciences 2004; 225: 3-9. DOI: http://dx.doi.org/10.1016/j.jns.2004.05.020.

94. Son S, Kim YW, Oh MK, et al. Initial factors affecting the clinical outcome after successful recanalization via MR-based mechanical thrombectomy in patients with acute ischemic stroke due to basilar artery occlusion. Journal of NeuroInterventional Surgery 2016; 8: 889-893. DOI: http://dx.doi.org/10.1136/neurintsurg-2015-011912.

95. Etherton MR, Wu O, Cougo P, et al. Integrity of normal-appearing white matter and functional outcomes after acute ischemic stroke. Neurology 2017; 88: 1701-1708. DOI: http://dx.doi.org/10.1212/WNL.0000000000003890.

96. Zhang X, Zhang S, Chen Q, et al. Ipsilateral prominent thalamostriate vein on susceptibility-weighted imaging predicts poor outcome after intravenous thrombolysis in acute ischemic stroke. American Journal of Neuroradiology 2017; 38: 875-881. DOI: http://dx.doi.org/10.3174/ajnr.A5135.

97. Sanak D, Horak D, Kral M, et al. Is clinical-diffusion mismatch associated with good clinical outcome in acute stroke patients treated with intravenous thrombolysis? Ceska a Slovenska Neurologie a Neurochirurgie 2009; 72: 548-552.

98. Wardlaw JM, Keir SL, Bastin ME, et al. Is diffusion imaging appearance an independent predictor of outcome after ischemic stroke? Neurology 2002; 59: 1381-1387. DOI: http://dx.doi.org/10.1212/01.WNL.0000032495.71720.C3.

99. Boccuni L, Meyer S, Kessner SS, et al. Is There Full or Proportional Somatosensory Recovery in the Upper Limb After Stroke? Investigating Behavioral Outcome and Neural Correlates. Neurorehabilitation and Neural Repair 2018; 32: 691-700. DOI: http://dx.doi.org/10.1177/1545968318787060.

100. Yoo J, Choi JW, Lee S-J, et al. Ischemic Diffusion Lesion Reversal After Endovascular Treatment. Stroke 2019; 50: 1504-1509. DOI: https://dx.doi.org/10.1161/STROKEAHA.118.024263.

101. Kaya D, Dincer A, Arman F, et al. Ischemic involvement of the primary motor cortex is a prognostic factor in acute stroke. International Journal of Stroke 2015; 10: 1277-1283. DOI: http://dx.doi.org/10.1111/j.1747-4949.2011.00640.x.

102. Bentley P, Kumar G, Rinne P, et al. Lesion locations influencing baseline severity and early recovery in ischaemic stroke. European Journal of Neurology 2014; 21: 1226-1232. DOI: http://dx.doi.org/10.1111/ene.12464.

103. Liu Y, Gong P, Sun H, et al. Leukoaraiosis is associated with poor outcomes after successful recanalization for large vessel occlusion stroke. Neurological Sciences 2019; 40: 585-591. DOI: http://dx.doi.org/10.1007/s10072-018-3698-2.

104. Zhang Z, Ren W, Shao B, et al. Leukoaraiosis is associated with worse short-term functional and cognitive recovery after minor stroke. Neurologia Medico-Chirurgica 2017; 57: 136-143. DOI: http://dx.doi.org/10.2176/nmc.oa.2016-0188.

105. Choi JH, Bae HJ and Cha JK. Leukoaraiosis on magnetic resonance imaging is related to long-term poor functional outcome after thrombolysis in acute ischemic stroke. Journal of Korean Neurosurgical Society 2011; 50: 75-80. DOI: http://dx.doi.org/10.3340/jkns.2011.50.2.75.

106. Park CH, Chang WH, Ohn SH, et al. Longitudinal changes of resting-state functional connectivity during motor recovery after stroke. Stroke 2011; 42: 1357-1362. DOI: http://dx.doi.org/10.1161/STROKEAHA.110.596155.

107. Guggisberg AG, Nicolo P, Cohen LG, et al. Longitudinal Structural and Functional Differences Between Proportional and Poor Motor Recovery After Stroke. Neurorehabilitation and Neural Repair 2017; 31: 1029-1041. DOI: http://dx.doi.org/10.1177/1545968317740634.

108. Ma C, Liu A, Li Z, et al. Longitudinal study of diffusion tensor imaging properties of affected cortical spinal tracts in acute and chronic hemorrhagic stroke. Journal of Clinical Neuroscience 2014; 21: 1388-1392. DOI: https://doi.org/10.1016/j.jocn.2013.11.032.

109. Turc G, Apoil M, Naggara O, et al. Magnetic resonance imaging-DRAGON score: 3-month outcome prediction after intravenous thrombolysis for anterior circulation stroke. Stroke 2013; 44: 1323-1328. DOI: http://dx.doi.org/10.1161/STROKEAHA.111.000127.

110. Jang SH, Bai D, Su MS, et al. Motor outcome prediction using diffusion tensor tractography in pontine infarct. Annals of Neurology 2008; 64: 460-465. DOI: http://dx.doi.org/10.1002/ana.21444.

111. Kim EH, Lee J and Jang SH. Motor outcome prediction using diffusion tensor tractography of the corticospinal tract in large middle cerebral artery territory infarct. NeuroRehabilitation 2013; 32: 583-590. DOI: http://dx.doi.org/10.3233/NRE-130880.

112. Weller P, Wittsack HJ, Siebler M, et al. Motor recovery as assessed with isometric finger movements and perfusion magnetic resonance imaging after acute ischemic stroke. Neurorehabilitation and Neural Repair 2006; 20: 390-397. DOI: http://dx.doi.org/10.1177/1545968305285037.

113. Liu G, Tan S, Dang C, et al. Motor Recovery Prediction with Clinical Assessment and Local Diffusion Homogeneity after Acute Subcortical Infarction. Stroke 2017; 48: 2121-2128. DOI: http://dx.doi.org/10.1161/STROKEAHA.117.017060.

114. Hand PJ, Wardlaw JM, Rivers CS, et al. MR diffusion-weighted imaging and outcome prediction after ischemic stroke. Neurology 2006; 66: 1159-1163. DOI: http://dx.doi.org/10.1212/01.wnl.0000202524.43850.81.

115. Nagel S, Herweh C, Kohrmann M, et al. MRI in patients with acute basilar artery occlusion - DWI lesion scoring is an independent predictor of outcome. International Journal of Stroke 2012; 7: 282-288. DOI: http://dx.doi.org/10.1111/j.1747-4949.2011.00705.x.

116. Moulton E, Valabregue R, Lehericy S, et al. Multivariate prediction of functional outcome using lesion topography characterized by acute diffusion tensor imaging. NeuroImage: Clinical 2019; 23: 101821. DOI: http://dx.doi.org/10.1016/j.nicl.2019.101821.

117. Payabvash S, Benson JC, Tyan AE, et al. Multivariate Prognostic Model of Acute Stroke Combining Admission Infarct Location and Symptom Severity: A Proof-of-Concept Study. Journal of Stroke and Cerebrovascular Diseases 2018; 27: 936-944. DOI: http://dx.doi.org/10.1016/j.jstrokecerebrovasdis.2017.10.034.

118. Granziera C, Daducci A, Meskaldji DE, et al. A new early and automated MRI-based predictor of motor improvement after stroke. Neurology 2012; 79: 39-46. DOI: http://dx.doi.org/10.1212/WNL.0b013e31825f25e7.

119. Khatri P, Conaway MR, Johnston KC, et al. Ninety-day outcome rates of a prospective cohort of consecutive patients with mild ischemic stroke. Stroke 2012; 43: 560-562. DOI: https://dx.doi.org/10.1161/STROKEAHA.110.593897.

120. Yoon W, Kim SK, Heo TW, et al. Outcomes are not different between patients with intermediate and high dwi-aspects after stent-retriever thrombectomy. Stroke 2016; 47.

121. Nadareishvili Z, Simpkins AN, Hitomi E, et al. Post-stroke blood-brain barrier disruption and poor functional outcome in patients receiving thrombolytic therapy. Cerebrovascular Diseases 2019; 47: 135-142. DOI: http://dx.doi.org/10.1159/000499666.

122. Ichijo M, Miki K, Ishibashi S, et al. Posterior cerebral artery laterality on magnetic resonance angiography predicts long-term functional outcome in middle cerebral artery occlusion. Stroke 2013; 44: 512-515. DOI: http://dx.doi.org/10.1161/STROKEAHA.112.674101.

123. Mundiyanapurath S, Mohlenbruch M, Ringleb PA, et al. Posterior circulation acute stroke prognosis early computed tomography score using hypointense vessels on susceptibility weighted imaging independently predicts outcome in patients with basilar artery occlusion. PLoS ONE 2015; 10: e0132587. DOI: http://dx.doi.org/10.1371/journal.pone.0132587.

124. Tei H, Uchiyama S, Usui T, et al. Posterior circulation ASPECTS on diffusion-weighted MRI can be a powerful marker for predicting functional outcome. Journal of neurology 2010; 257: 767-773. DOI: https://dx.doi.org/10.1007/s00415-009-5406-x.

125. Gomez-Choco M, Mengual JJ, Rodriguez-Antiguedad J, et al. Pre-Existing Cerebral Small Vessel Disease Limits Early Recovery in Patients with Acute Lacunar Infarct. Journal of Stroke and Cerebrovascular Diseases 2019; 28: 104312. DOI: http://dx.doi.org/10.1016/j.jstrokecerebrovasdis.2019.104312.

126. Lin SF, Chen CI, Hu HH, et al. Predicting functional outcomes of posterior circulation acute ischemic stroke in first 36 h of stroke onset. Journal of Neurology 2018; 265: 926-932. DOI: http://dx.doi.org/10.1007/s00415-018-8746-6.

127. Schiemanck SK, Kwakkel G, Post MWM, et al. Predicting long-term independency in activities of daily living after middle cerebral artery stroke: Does information from MRI have added predictive value compared with clinical information? Stroke 2006; 37: 1050-1054. DOI: http://dx.doi.org/10.1161/01.STR.0000206462.09410.6f.

128. Buch ER, Rizk S, Nicolo P, et al. Predicting motor improvement after stroke with clinical assessment and diffusion tensor imaging. Neurology 2016; 86: 1924-1925. DOI: https://dx.doi.org/10.1212/WNL.0000000000002675.

129. Puig J, Blasco G, Terceno M, et al. Predicting motor outcome in acute intracerebral hemorrhage. American Journal of Neuroradiology 2019; 40: 769-775. DOI: http://dx.doi.org/10.3174/ajnr.A6038.

130. Kuzu Y, Inoue T, Kanbara Y, et al. Prediction of motor function outcome after intracerebral hemorrhage using fractional anisotropy calculated from diffusion tensor imaging. Cerebrovascular Diseases 2012; 33: 566-573. DOI: http://dx.doi.org/10.1159/000338904.

131. Zarahn E, Alon L, Ryan SL, et al. Prediction of motor recovery using initial impairment and fMRI 48 h poststroke. Cerebral Cortex 2011; 21: 2712-2721. DOI: http://dx.doi.org/10.1093/cercor/bhr047.

132. Yamamoto N, Satomi J, Izumi Y, et al. Predictors of a Favorable Outcome after Recanalization in Patients with Cerebral Major Vessel Occlusion. Journal of stroke and cerebrovascular diseases : the official journal of National Stroke Association 2015; 24: 2793-2799. DOI: https://dx.doi.org/10.1016/j.jstrokecerebrovasdis.2015.08.012.

133. Sanak D, Herzig R, Zapletalova J, et al. Predictors of good clinical outcome in acute stroke patients treated with intravenous thrombolysis. Acta neurologica Scandinavica 2011; 123: 339-344. DOI: https://dx.doi.org/10.1111/j.1600-0404.2010.01401.x.

134. Yoon W, Kim SK, Heo TW, et al. Predictors of Good Outcome After Stent-Retriever Thrombectomy in Acute Basilar Artery Occlusion. Stroke 2015; 46: 2972-2975. DOI: https://dx.doi.org/10.1161/STROKEAHA.115.010840.

135. Man S, Aoki J, Hussain MS, et al. Predictors of infarct growth after endovascular therapy for acute ischemic stroke. Journal of Stroke and Cerebrovascular Diseases 2015; 24: 401-407. DOI: http://dx.doi.org/10.1016/j.jstrokecerebrovasdis.2014.09.004.

136. Li CC, Hao XZ, Tian JQ, et al. Predictors of short-term outcome in patients with acute middle cerebral artery occlusion: Unsuitability of fluid-attenuated inversion recovery vascular hyperintensity scores. Neural Regeneration Research 2018; 13: 69-76. DOI: http://dx.doi.org/10.4103/1673-5374.224375.

137. Qu JF, Chen YK, Zhong HH, et al. Preexisting Cerebral Abnormalities and Functional Outcomes After Acute Ischemic Stroke. Journal of Geriatric Psychiatry and Neurology 2019; 32: 327-335. DOI: http://dx.doi.org/10.1177/0891988719862631.

138. Boccuni L, Meyer S, D'Cruz N, et al. Premotor dorsal white matter integrity for the prediction of upper limb motor impairment after stroke. Scientific reports 2019; 9: 19712. DOI: http://dx.doi.org/10.1038/s41598-019-56334-w.

139. Kawano H, Hirano T, Inatomi Y, et al. Presence of deep white matter lesions on diffusion-weighted imaging is a negative predictor of early dramatic improvement after intravenous tissue plasminogen activator thrombolysis. Cerebrovascular Diseases 2010; 30: 230-236. DOI: http://dx.doi.org/10.1159/000317183.

140. Nezu T, Koga M, Kimura K, et al. Pretreatment ASPECTS on DWI predicts 3-month outcome following rt-PA: SAMURAI rt-PA Registry. Neurology 2010; 75: 555-561. DOI: http://dx.doi.org/10.1212/WNL.0b013e3181eccf78.

141. Kruetzelmann A, Kohrmann M, Sobesky J, et al. Pretreatment diffusion-weighted imaging lesion volume predicts favorable outcome after intravenous thrombolysis with tissue-type plasminogen activator in acute ischemic stroke. Stroke 2011; 42: 1251-1254. DOI: http://dx.doi.org/10.1161/STROKEAHA.110.600148.

142. Kim HS, Lee DH, Choi CG, et al. Progression of middle cerebral artery susceptibility sign on T2*-weighted images: its effect on recanalization and clinical outcome after thrombolysis. AJR American journal of roentgenology 2006; 187: W650-657. DOI: http://dx.doi.org/10.2214/AJR.05.0447.

143. Yu X, Yuan L, Jackson A, et al. Prominence of medullary veins on susceptibility-weighted images provides prognostic information in patients with subacute stroke. American Journal of Neuroradiology 2016; 37: 423-429. DOI: http://dx.doi.org/10.3174/ajnr.A4541.

144. Wang Y, Shi T, Chen B, et al. Prominent Hypointense Vessel Sign on Susceptibility-Weighted Imaging Is Associated with Clinical Outcome in Acute Ischaemic Stroke. European Neurology 2018; 79: 231-239. DOI: http://dx.doi.org/10.1159/000488587.

145. Chen CY, Chen CI, Tsai FY, et al. Prominent vessel sign on susceptibility-weighted imaging in acute stroke: Prediction of infarct growth and clinical outcome. PLoS ONE 2015; 10: e0131118. DOI: http://dx.doi.org/10.1371/journal.pone.0131118.

146. Smith MC, Byblow WD, Barber PA, et al. Proportional Recovery from Lower Limb Motor Impairment after Stroke. Stroke 2017; 48: 1400-1403. DOI: http://dx.doi.org/10.1161/STROKEAHA.116.016478.

147. Lim HS, Kim SM and Kang DW. Quantitative Predictive Models for the Degree of Disability After Acute Ischemic Stroke. Journal of Clinical Pharmacology 2018; 58: 549-557. DOI: http://dx.doi.org/10.1002/jcph.1039.

148. Binkofski F, Seitz RJ, Hacklander T, et al. Recovery of motor functions following hemiparetic stroke: A clinical and magnetic resonance-morphometric study. Cerebrovascular Diseases 2001; 11: 273-281. DOI: http://dx.doi.org/10.1159/000047650.

149. Lee J, Park E, Lee A, et al. Recovery-related indicators of motor network plasticity according to impairment severity after stroke. European Journal of Neurology 2017; 24: 1290-1299. DOI: http://dx.doi.org/10.1111/ene.13377.

150. Yu J, Wang L, Li Z, et al. Related Factors of Asymmetrical Vein Sign in Acute Middle Cerebral Artery Stroke and Correlation with Clinical Outcome. Journal of Stroke and Cerebrovascular Diseases 2017; 26: 2346-2353. DOI: http://dx.doi.org/10.1016/j.jstrokecerebrovasdis.2017.05.023.

151. Cheng L, Wu Z, Sun J, et al. Reorganization of Motor Execution Networks During Sub-Acute Phase After Stroke. IEEE transactions on neural systems and rehabilitation engineering : a publication of the IEEE Engineering in Medicine and Biology Society 2015; 23: 713-723. DOI: http://dx.doi.org/10.1109/TNSRE.2015.2401978.

152. Puig J, Blasco G, Alberich-Bayarri A, et al. Resting-state functional connectivity magnetic resonance imaging and outcome after acute stroke. Stroke 2018; 49: 2353-2360. DOI: http://dx.doi.org/10.1161/STROKEAHA.118.021319.

153. Keser Z, Sebastian R, Hasan KM, et al. Right Hemispheric Homologous Language Pathways Negatively Predicts Poststroke Naming Recovery. Stroke 2019: STROKEAHA119028293. DOI: http://dx.doi.org/10.1161/STROKEAHA.119.028293.

154. Rehme AK, Fink GR, Von Cramon DY, et al. The role of the contralesional motor cortex for motor recovery in the early days after stroke assessed with longitudinal fMRI. Cerebral Cortex 2011; 21: 756-768. DOI: http://dx.doi.org/10.1093/cercor/bhq140.

155. Qu JF, Chen YK, Luo GP, et al. Severe lesions involving cortical cholinergic pathways predict poorer functional outcome in acute ischemic stroke. Stroke 2018; 49: 2983-2989. DOI: http://dx.doi.org/10.1161/STROKEAHA.118.023196.

156. Arsava EM, Rahman R, Rosand J, et al. Severity of leukoaraiosis correlates with clinical outcome after ischemic stroke. Neurology 2009; 72: 1403-1410. DOI: http://dx.doi.org/10.1212/WNL.0b013e3181a18823.

157. Giurgiutiu DV, Yoo AJ, Fitzpatrick K, et al. Severity of leukoaraiosis, leptomeningeal collaterals, and clinical outcomes after intra-arterial therapy in patients with acute ischemic stroke. Journal of NeuroInterventional Surgery 2015; 7: 326-330. DOI: http://dx.doi.org/10.1136/neurintsurg-2013-011083.

158. Ichijo M, Iwasawa E, Numasawa Y, et al. Significance of development and reversion of collaterals on mri in early neurologic improvement and long-term functional outcome after intravenous thrombolysis for ischemic stroke. American Journal of Neuroradiology 2015; 36: 1839-1845. DOI: http://dx.doi.org/10.3174/ajnr.A4384.

159. Kimura K, Sakamoto Y, Iguchi Y, et al. A simple clinical and MRI scale to predict good outcome in t-PA patients. Neurological Research 2011; 33: 1038-1043. DOI: http://dx.doi.org/10.1179/1743132811Y.0000000031.

160. Bivard A, Krishnamurthy V, Stanwell P, et al. Spectroscopy of reperfused tissue after stroke reveals heightened metabolism in patients with good clinical outcomes. Journal of Cerebral Blood Flow and Metabolism 2014. DOI: http://dx.doi.org/10.1038/jcbfm.2014.166.

161. Munsch F, Sagnier S, Asselineau J, et al. Stroke location is an independent predictor of cognitive outcome. Stroke 2016; 47: 66-73. DOI: http://dx.doi.org/10.1161/STROKEAHA.115.011242.

162. Ryu WS, Woo SH, Schellingerhout D, et al. Stroke outcomes are worse with larger leukoaraiosis volumes. Brain 2017; 140: 158-170. DOI: http://dx.doi.org/10.1093/brain/aww259.

163. Bang OY, Liebeskind DS, Saver JL, et al. Stunned brain syndrome: Serial diffusion perfusion MRI of delayed recovery following revascularisation for acute ischaemic stroke. Journal of Neurology, Neurosurgery and Psychiatry 2011; 82: 27-32. DOI: http://dx.doi.org/10.1136/jnnp.2010.209155.

164. Tateishi Y, Hamabe J, Kanamoto T, et al. Subacute lesion volume as a potential prognostic biomarker for acute ischemic stroke after intravenous thrombolysis. Journal of the Neurological Sciences 2016; 369: 77-81. DOI: http://dx.doi.org/10.1016/j.jns.2016.08.006.

165. Kim SJ, Ha YS, Ryoo S, et al. Sulcal effacement on fluid attenuation inversion recovery magnetic resonance imaging in hyperacute stroke: association with collateral flow and clinical outcomes. Stroke 2012; 43: 386-392. DOI: https://dx.doi.org/10.1161/STROKEAHA.111.638106.

166. Aoki J, Kimura K, Shibazaki K, et al. The susceptibility vessel sign at the proximal M1: A strong predictor for poor outcome after intravenous thrombolysis. Journal of the Neurological Sciences 2015; 348: 195-200. DOI: http://dx.doi.org/10.1016/j.jns.2014.12.002.

167. Bourcier R, Hassen WB, Soize S, et al. Susceptibility vessel sign on MRI predicts better clinical outcome in patients with anterior circulation acute stroke treated with stent retriever as first-line strategy. Journal of NeuroInterventional Surgery 2019; 11: 328-333. DOI: http://dx.doi.org/10.1136/neurintsurg-2018-014217.

168. Bourcier R, Volpi S, Guyomarch B, et al. Susceptibility vessel sign on MRI predicts favorable clinical outcome in patients with anterior circulation acute stroke treated with mechanical thrombectomy. American Journal of Neuroradiology 2015; 36: 2346-2353. DOI: http://dx.doi.org/10.3174/ajnr.A4483.

169. Liu H, Mei W, Huang Y, et al. Susceptibility vessel sign predicts poor clinical outcome for acute stroke patients untreated by thrombolysis. Experimental and Therapeutic Medicine 2017; 14: 5207-5213. DOI: http://dx.doi.org/10.3892/etm.2017.5195.

170. Dejobert M, Cazals X, Annan M, et al. Susceptibility-Diffusion Mismatch in Hyperacute Stroke: Correlation with Perfusion-Diffusion Mismatch and Clinical Outcome. Journal of Stroke and Cerebrovascular Diseases 2016; 25: 1760-1766. DOI: http://dx.doi.org/10.1016/j.jstrokecerebrovasdis.2016.02.025.

171. Payabvash S, Taleb S, Benson JC, et al. Susceptibility-diffusion mismatch in middle cerebral artery territory acute ischemic stroke: Clinical and imaging implications. Acta Radiologica 2017; 58: 876-882. DOI: http://dx.doi.org/10.1177/0284185116675658.

172. Lou M, Chen Z, Wan J, et al. Susceptibility-diffusion mismatch predicts thrombolytic outcomes: A retrospective cohort study. American Journal of Neuroradiology 2014; 35: 2061-2067. DOI: http://dx.doi.org/10.3174/ajnr.A4017.

173. Payabvash S, Benson JC, Taleb S, et al. Susceptible vessel sign: identification of arterial occlusion and clinical implications in acute ischaemic stroke. Clin Radiol 2017; 72: 116-122. 2016/11/28. DOI: 10.1016/j.crad.2016.11.001.

174. Huo Y-C, Li Q, Zhang W-Y, et al. Total Small Vessel Disease Burden Predicts Functional Outcome in Patients With Acute Ischemic Stroke. Frontiers in neurology 2019; 10: 808. DOI: https://dx.doi.org/10.3389/fneur.2019.00808.

175. Kunimatsu A, Itoh D, Nakata Y, et al. Utilization of diffusion tensor tractography in combination with spatial normalization to assess involvement of the corticospinal tract in capsular/pericapsular stroke: Feasibility and clinical implications. Journal of Magnetic Resonance Imaging 2007; 26: 1399-1404. DOI: http://dx.doi.org/10.1002/jmri.20945.

176. Johnston KC, Wagner DP, Wang XQ, et al. Validation of an acute ischemic stroke model: Does diffusion-weighted imaging lesion volume offer a clinically significant improvement in prediction of outcome? Stroke 2007; 38: 1820-1825. DOI: http://dx.doi.org/10.1161/STROKEAHA.106.479154.

177. Chung JW, Kim KJ, Noh WY, et al. Validation of FLAIR hyperintense lesions as imaging biomarkers to predict the outcome of acute stroke after intra-arterial thrombolysis following intravenous tissue plasminogen activator. Cerebrovascular Diseases 2013; 35: 461-468. DOI: http://dx.doi.org/10.1159/000350201.

178. Lazar RM, Speizer AE, Festa JR, et al. Variability in language recovery after first-time stroke. Journal of neurology, neurosurgery, and psychiatry 2008; 79: 530-534.

179. Dunn LE, Schweber AB, Manson DK, et al. Variability in Motor and Language Recovery during the Acute Stroke Period. Cerebrovascular diseases extra 2016; 6: 12-21. DOI: https://dx.doi.org/10.1159/000444149.

180. Hinkle JL. Variables explaining functional recovery following motor stroke. The Journal of neuroscience nursing : journal of the American Association of Neuroscience Nurses 2006; 38: 6-12.

181. Renu A, Laredo C, Lopez-Rueda A, et al. Vessel Wall Enhancement and Blood-Cerebrospinal Fluid Barrier Disruption after Mechanical Thrombectomy in Acute Ischemic

Stroke. Stroke 2017; 48: 651-657. DOI: http://dx.doi.org/10.1161/STROKEAHA.116.015648.

182. Tsai Y-H, Hsu L-M, Weng H-H, et al. Voxel-based analysis of apparent diffusion coefficient in perihaematomal oedema: associated factors and outcome predictive value for intracerebral haemorrhage. BMJ open 2011; 1: e000230. DOI: https://dx.doi.org/10.1136/bmjopen-2011-000230.

183. Mechtouff L, Nighoghossian N, Amaz C, et al. White matter burden does not influence the outcome of mechanical thrombectomy. Journal of Neurology 2019. DOI: http://dx.doi.org/10.1007/s00415-019-09624-2.

184. Kang HJ, Stewart R, Park MS, et al. White matter hyperintensities and functional outcomes at 2 weeks and 1 year after stroke. Cerebrovascular Diseases 2013; 35: 138-145. DOI: http://dx.doi.org/10.1159/000346604.

185. Helenius J, Mayasi Y and Henninger N. White matter hyperintensity lesion burden is associated with the infarct volume and 90-day outcome in small subcortical infarcts. Acta neurologica Scandinavica 2017; 135: 585-592. DOI: https://dx.doi.org/10.1111/ane.12670.

186. Atchaneeyasakul K, Leslie-Mazwi T, Donahue K, et al. White matter hyperintensity volume and outcome of mechanical thrombectomy with stentriever in acute ischemic stroke. Stroke 2017; 48: 2892-2894. DOI: http://dx.doi.org/10.1161/STROKEAHA.117.018653.

187. Patti J, Helenius J, Puri AS, et al. White Matter Hyperintensity-Adjusted Critical Infarct Thresholds to Predict a Favorable 90-Day Outcome. Stroke 2016; 47: 2526-2533. DOI: http://dx.doi.org/10.1161/STROKEAHA.116.013982.

188. Yu X, Song R, Jiaerken Y, et al. White matter injury induced by diabetes in acute stroke is clinically relevant: A preliminary study. Diabetes and Vascular Disease Research 2016; 14: 40-46. DOI: http://dx.doi.org/10.1177/1479164116675491.

189. Leonards CO, Ipsen N, Malzahn U, et al. White matter lesion severity in mild acute ischemic stroke patients and functional outcome after 1 year. Stroke 2012; 43: 3046-3051. DOI: http://dx.doi.org/10.1161/STROKEAHA.111.646554.

190. Kamakura CK, Ueno Y, Sakai Y, et al. White matter lesions and cognitive impairment may be related to recovery from unilateral spatial neglect after stroke. Journal of the Neurological Sciences 2017; 379: 241-246. DOI: http://dx.doi.org/10.1016/j.jns.2017.06.021

Appendix C: Studies included in Chapter 2

Reference	Study Size	Time acquired	Biomarker	Biomarker Class	Sequence	Imaging type	Restricted for Location	Restricted for Symptoms	Restricted for Treatment	Outcome Scale	Domain Specific	Outcome Time	Prospective	Pre-planned	Predictor
Abela et al. , 2018	116	H	Collaterals	I	FLAIR	R	Y	Y	N	mRS	N	3m	Y	N	Y
Aoki et al. , 2011	87	A	Collaterals	I	FLAIR	R	Y	N	Y	mRS	N	3m	Y	N	Y
Bigourdan et al. , 2010	59	H	Collaterals	I	FLAIR	R	Y	Y	N	mRS	N	3m	Y	Y	N
Bigourdan et al. , 2010	59	H	Collaterals	I	FLAIR/DWI	R	Y	Y	N	mRS	N	3m	Y	Y	Y
Cho et al. , 2019	105	H	Collaterals	I	FLAIR	R	Y	Y	N	mRS	N	3m	Y	N	Y
De¬†Havenon et al. , 2017	60	H	Collaterals	I	DWI	R	Y	N	N	mRS	N	D	Y	N	Y
Du et al. , 2009	160	A	Collaterals	I	FLAIR	R	N	Y	N	mRS	N	3m	Y	Y	Y
Ebinger et al. , 2016	164	H	Collaterals	I	FLAIR/DWI	R	Y	Y	N	mRS	N	3m	N	N	Y
Garg et al. , 2011	76	H	Collaterals	I	MRA	R	Y	Y	N	mRS	N	3m	N	N	Y

Hu et al. , 2018	114	S	Collaterals	I	FLAIR/DWI	R	Y	Y	N	mRS	N	3m	N	N	Y
Huang et al. , 2012	90	H	Collaterals	I	FLAIR	R	N	Y	N	mRS	N	3m	Y	Y	Y
Ichijo et al. , 2016	77	H	Collaterals	I	ASL	R	Y	Y	N	mRS	N	3m	Y	Y	Y
Jiang et al. , 2011	57	H	Collaterals	I	FLAIR	R	Y	Y	N	mRS	N	3m	Y	N	N
Kim et al. , 2016	62	H	Collaterals	I	FLAIR	R	Y	Y	N	mRS	N	3m	Y	N	N
Lasek-Bal et al. , 2018	48	H	Collaterals	I	FLAIR/MRA	R	Y	Y	N	NIHSS/mRS	N	1w	N	N	Y
Liu et al. , 2015	50	H	Collaterals	I	FLAIR	R	N	N	N	NIHSS/mRS	N	D	N	N	Y
Liu et al. , 2018	55	H	Collaterals	I	MRA	R	Y	Y	N	mRS	N	3m	Y	N	Y
Luo et al. , 2019	38	A	Collaterals	I	FLAIR	R	Y	Y	N	mRS	N	3m	Y	Y	N
Marshall et al. , 2014	101	H	Collaterals	I	FLAIR	R	Y	Y	N	mRS	N	3m	Y	N	Y
Mucke et al. , 2015	38	A	Collaterals	I	ASL	R	N	N	N	mRS	N	D	N	N	Y
Rehme et al. , 2018	118	H	Collaterals	I	FLAIR	R	Y	Y	N	mRS	N	3m	N	N	Y
Saur et al. , 2010	72	H	Collaterals	I	DWI/FLAIR	R	Y	Y	N	mRS	N	3m	Y	N	Y
Saur et al. , 2010	72	H	Collaterals	I	FLAIR	R	Y	Y	N	mRS	N	3m	Y	N	Y
Simpkins et al. , 2018	54	H	Collaterals	I	FLAIR	R	Y	Y	N	mRS	N	3m	N	N	Y
Tanriverdi et al. , 2012	76	A	Collaterals	I	FLAIR	R	Y	Y	N	NIHSS	N	D	Y	N	Y
Turc et al. , 2013	75	A	Collaterals	I	MRA	R	Y	Y	N	mRS	N	3m	N	N	Y
Wang et al. , 2020	50	H	Collaterals	I	FLAIR/DWI	R	N	Y	N	NIHSS	N	1w	N	N	Y
Yang et al. , 2016	65	A	Collaterals	I	FLAIR	R	Y	Y	N	mRS	N	3m	N	N	Y
Yu et al. , 2016	50	H	Collaterals	I	MRA	R	Y	Y	N	mRS	N	>3 m	N	N	Y
Zaidi et al. , 2012	139	H	Collaterals	I	FLAIR	R	Y	Y	N	mRS	N	3m	Y	N	Y
Chen et al. , 2017	71	A	Infarct Growth	I	DWI	R	Y	Y	N	mRS	N	3m	Y	N	Y
Choi et al. , 2017	786	S	Infarct Growth	I	DWI	R	N	Y	N	mRS	N	>3 m	Y	N	N

Kim et al. , 2018	169	A	Infarct Growth	I	DWI	R	N	N	N	mRS	N	3m	Y	Y	Y
Lim et al. , 2017	405	A	Infarct Growth	I	DWI	R	N	N	N	mRS	N	3m	Y	Y	Y
Moulton et al. , 2012	404	A	Infarct Growth	I	DWI	R	Y	Y	N	mRS	N	3m	N	N	Y
Smith et al. , 2001	136	A	Infarct Growth	I	DWI	R	N	N	N	mRS	N	3m	Y	Y	Y
Tanriverdi et al. , 2012	76	A	Infarct Growth	I	DWI	R	Y	Y	N	NIHSS	N	D	Y	N	Y
Wang et al. , 2015	409	A	Infarct Growth	I	DWI	R	N	N	N	mRS	N	3m	Y	Y	Y
Weller et al. , 2006	58	H	Infarct Growth	I	DWI	R	N	N	N	NIHSS	N	1w	Y	Y	Y
Yu et al. , 2015	81	A	Infarct Growth	I	DWI	R	Y	Y	N	mRS	N	3m	Y	N	Y
H et al. , 2019	47	H	Infarct Severity	I	DWI	R	Y	N	N	mRS	N	>3 m	Y	Y	N
Nagel et al. , 2018	108	A	Infarct Severity	I	DWI	R	N	N	N	mRS	N	>3 m	Y	Y	N
Olindo et al. , 2016	166	H	Infarct Severity	I	DWI	R	Y	Y	N	mRS	N	3m	Y	N	Y
Payabvash et al. , 2016	82	H	Infarct Severity	I	DWI	R	N	N	N	mRS	N	3m	Y	Y	N
Arsava et al. , 2015	132	A	Lesion Size	I	DWI	R	Y	N	N	mRS	N	3m	Y	Y	Y
Bentley et al. , 2017	75	S	Lesion Size	I	FLAIR	R	Y	N	N	BI	N	>3 m	Y	Y	N
Bigourdan et al. , 2010	59	H	Lesion Size	I	DWI	R	Y	Y	N	mRS	N	3m	Y	Y	Y
Boccuni et al. , 2015	35	S	Lesion Size	I	DWI	R	Y	N	Y	TOR	Y	>3 m	Y	Y	N
Buch et al. , 2012	54	H	Lesion Size	I	DWI	R	N	Y	N	NIHSS/mRS	N	3m	Y	N	N
Cho et al. , 2019	105	H	Lesion Size	I	DWI	R	Y	Y	N	mRS	N	3m	Y	N	N
Choi et al. , 2010	66	H	Lesion Size	I	DWI	R	Y	Y	N	NIHSS	N	1w	Y	Y	Y
Chung et al. , 2015	35	H	Lesion Size	I	DWI	R	Y	Y	N	mRS	N	3m	N	N	Y
Derex et al. , 2017	22	H	Lesion Size	I	DWI	R	Y	Y	N	mRS	N	3m	N	N	Y
Doughty et al. , 2016	184	H	Lesion Size	I	DWI	R	N	N	N	mRS	N	3m	Y	N	N
Etherton et al. , 2009	50	H	Lesion Size	I	DWI	R	Y	Y	N	mRS	N	3m	N	N	Y
Findlater et al. , 2019	117	A	Lesion Size	I	DWI	R	Y	N	N	FMA/mRS	Y	>3 m	Y	Y	N

Gomez-Choco et al. , 2006	124	A	Lesion Size	I	DWI	R	Y	Y	N	mRS	N	3m	N	N	N
Granziera et al. , 2012	34	S	Lesion Size	I	DWI	R	Y	N	Y	FMA	Y	3m	Y	Y	N
Guggisberg et al. , 2013	117	H	Lesion Size	I	DWI	R	N	Y	N	mRS	N	3m	Y	Y	N
H et al. , 2019	47	H	Lesion Size	I	DWI	R	Y	N	N	mRS	N	>3 m	Y	Y	N
Held et al. , 2011	60	A	Lesion Size	I	DWI	R	Y	N	N	NIHSS	Y	3m	Y	N	N
Huang et al. , 2012	90	H	Lesion Size	I	DWI	R	N	Y	N	mRS	N	3m	Y	Y	Y
Ichijo et al. , 2010	174	H	Lesion Size	I	DWI	R	N	Y	N	mRS	N	3m	Y	N	Y
Jang et al. , 2006	177	A	Lesion Size	I	DWI	R	N	Y	N	mRS	N	3m	Y	N	Y
Jian-Feng¬†Qu¬† et al. , 2009	50	H	Lesion Size	I	DWI	R	Y	N	N	mRS	N	3m	Y	N	Y
Keser et al. , 2019	69	H	Lesion Size	I	DWI	R	Y	Y	N	mRS	N	3m	Y	Y	Y
Khatri et al. , 2019	85	A	Lesion Size	I	DWI	R	Y	Y	N	mRS	N	3m	N	N	N
Kim et al. , 2013	125	A	Lesion Size	I	DWI	R	Y	Y	N	mRS	N	3m	N	N	Y
Kim et al. , 2016	62	H	Lesion Size	I	DWI	R	Y	Y	N	mRS	N	3m	Y	N	Y
Kim et al. , 2016	43	H	Lesion Size	I	DWI	R	Y	N	Y	NIHSS	Y	3m	Y	Y	Y
Kim et al. , 2017	69	A	Lesion Size	I	FLAIR	R	Y	N	Y	robotic and clinical score (motor/proprioceptive)	Y	3m	Y	N	Y
Kufner et al. , 2014	29	H	Lesion Size	I	DWI	R	Y	Y	N	mRS	N	3m	Y	Y	Y
Kuzu et al. , 2015	648	H	Lesion Size	I	DWI	R	N	N	N	composite clinical score	N	3m	Y	Y	N
Lee et al. , 2014	228	H	Lesion Size	I	DWI	R	Y	Y	N	mRS	N	3m	Y	N	Y
Lee et al. , 2015	105	H	Lesion Size	I	DWI	R	N	Y	N	mRS	N	3m	Y	Y	N
Li et al. , 2019	414	A	Lesion Size	I	DWI	R	Y	N	N	mRS	N	3m	Y	N	Y
Lin et al. , 2016	69	A	Lesion Size	I	DWI	R	Y	Y	N	NIHSS/mRS	N	3m	Y	N	Y
Liu et al. , 2012	196	A	Lesion Size	I	DWI	R	Y	Y	N	mRS	N	3m	Y	N	Y
Liu et al. , 2018	55	H	Lesion Size	I	DWI	R	Y	Y	N	mRS	N	3m	Y	N	N
Luby et al. , 2018	350	H	Lesion Size	I	DWI	R	Y	N	N	mRS	N	3m	N	N	Y

Luo et al. , 2019	38	A	Lesion Size	I	DWI	R	Y	Y	N	mRS	N	3m	Y	Y	N
Ma et al. , 2008	15	A	Lesion Size	I	DWI	R	Y	N	N	MICARS	Y	3m	Y	Y	Y
Man et al. , 2019	74	A	Lesion Size	I	DWI	R	Y	N	N	mRS	N	3m	Y	N	Y
Moulton et al. , 2012	404	A	Lesion Size	I	DWI	R	Y	Y	N	mRS	N	3m	N	N	Y
Mundiyanapurath et al. , 2019	43	A	Lesion Size	I	DWI	R	Y	Y	N	mRS	N	3m	N	N	N
Nadareishvili et al. , 2015	246	A	Lesion Size	I	DWI	R	N	N	N	ADL	N	>3 m	Y	Y	Y
Nagel et al. , 2018	108	A	Lesion Size	I	DWI	R	N	N	N	mRS	N	>3 m	Y	Y	N
Nave et al. , 2016	186	H	Lesion Size	I	DWI	R	Y	Y	N	NIHSS	N	1w	N	N	Y
Olivot et al. , 2017	23	H	Lesion Size	I	DWI	R	Y	Y	N	mRS	N	3m	N	N	Y
Park et al. , 2014	129	A	Lesion Size	I	DWI	R	Y	N	N	mRS	N	1m	Y	N	Y
Payabvash et al. , 2016	82	H	Lesion Size	I	DWI	R	N	N	N	mRS	N	3m	Y	Y	N
Puig et al. , 2011	161	H	Lesion Size	I	DWI	R	Y	Y	N	mRS	N	3m	N	N	N
Puig et al. , 2018	50	H	Lesion Size	I	DWI	R	Y	Y	N	mRS	N	3m	N	N	Y
Rehme et al. , 2016	164	H	Lesion Size	I	DWI	R	N	Y	N	NIHSS/mRS	N	3m	N	N	Y
Samuelsson et al. , 2015	73	A	Lesion Size	I	DWI	R	Y	N	Y	AHS	Y	3m	N	N	Y
Sanak et al. , 2015	60	A	Lesion Size	I	DWI	R	N	N	N	FIM	Y	3m	Y	Y	N
Sanak et al. , 2018	477	H	Lesion Size	I	DWI	R	N	Y	N	mRS	N	3m	N	N	Y
Saur et al. , 2010	72	H	Lesion Size	I	DWI	R	Y	Y	N	mRS	N	3m	Y	N	Y
Schiemanck et al. , 2019	164	S	Lesion Size	I	DWI	R	N	Y	N	mRS	N	3m	Y	N	Y
Simpkins et al. , 2018	54	H	Lesion Size	I	DWI	R	Y	Y	N	mRS	N	3m	N	N	Y
Son et al. , 2017	125	A	Lesion Size	I	DWI	R	Y	N	N	mRS	N	3m	Y	N	Y
Tei et al. , 2018	52	A	Lesion Size	I	PD	R	N	N	Y	composite clinical score	Y	1m	Y	Y	N
Thamm et al. , 2019	47	A	Lesion Size	I	DWI	R	N	N	N	mRS	N	>3 m	Y	Y	N
Turc et al. , 2013	75	A	Lesion Size	I	DWI	R	Y	Y	N	mRS	N	3m	N	N	Y

Weller et al. , 2006	58	H	Lesion Size	I	DWI	R	N	N	N	NIHSS	N	1w	Y	Y	N
Yamamoto et al. , 2015	34	A	Lesion Size	I	DWI	R	N	N	Y	FMA/WAB/BNT	Y	1w	Y	Y	N
Yamashita et al. , 2016	171	H	Lesion Size	I	DWI	R	Y	Y	N	mRS	N	3m	N	N	N
Yoo et al. , 2014	550	A	Lesion Size	I	DWI	R	N	N	N	NIHSS	N	1w	N	N	Y
Yoon et al. , 2018	293	H	Lesion Size	I	DWI	R	Y	Y	N	mRS	N	3m	N	N	N
Zarahn et al. , 2011	22	A	Lesion Size	I	DWI	R	N	N	Y	langauge battery	Y	3m	Y	Y	N
Zhang et al. , 2002	83	H	Lesion Size	I	DWI	R	Y	Y	N	NIHSS	N	1w	N	N	Y
Doughty et al. , 2016	184	H	Microstructure	I	DWI	R	N	N	N	mRS	N	3m	Y	N	Y
Khatri et al. , 2019	85	A	Microstructure	I	DTI	A	Y	Y	N	mRS	N	3m	N	N	N
Qu et al. , 2010	305	A	Microstructure	I	DTI	A	Y	N	N	mRS	N	3m	Y	N	Y
Bentley et al. , 2017	75	S	multiple tracts/areas	I	FLAIR	R	Y	N	N	BI	N	>3 m	Y	Y	N
Thamm et al. , 2019	47	A	multiple tracts/areas	I	DWI	R	N	N	N	mRS	N	>3 m	Y	Y	Y
Wardlaw et al. , 2019	172	H	multiple tracts/areas	I	DWI	R	Y	Y	N	mRS	N	3m	Y	N	Y
Zhang et al. , 2011	289	A	multiple tracts/areas	I	DWI	R	Y	N	N	mRS	N	3m	Y	Y	N
Choi et al. , 2010	66	H	Occlusion	I	SWI	R	Y	Y	N	NIHSS	N	1w	Y	Y	Y
Choi et al. , 2010	66	H	Occlusion	I	MRA	R	Y	Y	N	NIHSS	N	1w	Y	Y	Y
Gomez-Choco et al. , 2006	124	A	Occlusion	I	MRA	R	Y	Y	N	mRS	N	3m	N	N	N
Guggisberg et al. , 2013	117	H	Occlusion	I	MRA	R	N	Y	N	mRS	N	3m	Y	Y	Y
Guggisberg et al. , 2013	117	H	Occlusion	I	SWI	R	N	Y	N	mRS	N	3m	Y	Y	Y
H et al. , 2019	47	H	Occlusion	I	MRA	R	Y	N	N	mRS	N	>3 m	Y	Y	N
Helenius et al. , 2019	213	H	Occlusion	I	SWI	R	N	N	N	mRS	N	3m	N	N	N
Jang et al. , 2006	177	A	Occlusion	I	SWI	R	N	Y	N	mRS	N	3m	Y	N	Y
Kang et al. , 2016	116	A	Occlusion	I	SWI/DWI	R	Y	Y	N	mRS	N	3m	N	N	Y
Kim et al. , 2013	125	A	Occlusion	I	MRA	R	Y	Y	N	mRS	N	3m	N	N	N

Kruetzelmann et al. , 2006	33	H	Occlusion	I	SWI	R	Y	Y	N	mRS	N	3m	N	N	N
Kruetzelmann et al. , 2006	33	H	Occlusion	I	SWI	R	Y	Y	N	mRS	N	3m	N	N	Y
Lee et al. , 2014	228	H	Occlusion	I	MRA	R	Y	Y	N	mRS	N	3m	Y	N	Y
Lee et al. , 2015	105	H	Occlusion	I	MRA	R	N	Y	N	mRS	N	3m	Y	Y	Y
Mechtouff et al. , 2017	70	H	Occlusion	I	SWI	R	N	Y	N	mRS	N	3m	N	N	Y
Nezu et al. , 2018	109	H	Occlusion	I	MRA	R	N	Y	N	mRS	N	3m	N	N	N
Park et al. , 2014	129	A	Occlusion	I	MRA	R	Y	N	N	mRS	N	1m	Y	N	Y
Puig et al. , 2011	161	H	Occlusion	I	SWI	R	Y	Y	N	mRS	N	3m	N	N	Y
Sanak et al. , 2018	477	H	Occlusion	I	MRA	R	N	Y	N	mRS	N	3m	N	N	Y
Tsai et al. , 2011	217	H	Occlusion	I	SWI	R	Y	Y	N	NIHSS/mRS	N	3m	Y	N	Y
Baik et al. , 2017	46	H	Oedema	I	DWI/FLAIR	R	N	N	N	mRS	N	>3 m	Y	Y	Y
Doughty et al. , 2016	184	H	Oedema	I	PWI	R	N	N	N	mRS	N	3m	Y	N	N
Hawe et al. , 2018	58	A	Oedema	I	MRI + gad	R	Y	Y	N	mRS	N	3m	N	N	Y
Maraka et al. , 2014	95	S	Oedema	I	DWI	R	N	N	N	mRS	N	3m	Y	Y	Y
Sakuta et al. , 2016	62	A	Oedema	I	MRI + gad	R	Y	Y	N	mRS	N	3m	Y	Y	Y
Song et al. , 2014	60	A	Oedema	I	MRI + gad	R	Y	Y	N	mRS	N	3m	Y	Y	Y
Thamm et al. , 2019	47	A	Oedema	I	DWI	R	N	N	N	mRS	N	>3 m	Y	Y	Y
Huang et al. , 2012	90	H	other	I	FLAIR	R	N	Y	N	mRS	N	3m	Y	Y	Y
Tsai et al. , 2013	114	A	other	I	DWI	R	Y	N	N	mRS	N	3m	N	N	Y
Boccuni et al. , 2010	110	A	Penumbra MRS	I	MRS	A	Y	N	N	mRS	N	3m	Y	Y	Y
Kawano et al. , 2011	60	A	Penumbra MRS	I	MRS	A	Y	Y	N	mRS	N	3m	Y	Y	Y
Chen et al. , 2017	71	A	Penumbra Perfusion	I	PWI	R	Y	Y	N	mRS	N	3m	Y	N	Y
Giurgiutiu et al. , 2014	36	H	Penumbra Perfusion	I	PWI	R	N	N	Y	ESC	N	D	Y	Y	Y
H et al. , 2019	47	H	Penumbra Perfusion	I	PWI	R	Y	N	N	mRS	N	>3 m	Y	Y	N

Ichijo et al. , 2010	174	H	Penumbra Perfusion	I	PWI	R	N	Y	N	mRS	N	3m	Y	N	N
Kawano et al. , 2011	60	A	Penumbra Perfusion	I	ASL	R	Y	Y	N	mRS	N	3m	Y	Y	Y
Kim et al. , 2016	62	H	Penumbra Perfusion	I	PWI	R	Y	Y	N	mRS	N	3m	Y	N	Y
Lin et al. , 2016	69	A	Penumbra Perfusion	I	PWI	R	Y	Y	N	NIHSS/mRS	N	3m	Y	N	Y
Munsch et al. , 2016	38	A	Penumbra Perfusion	I	ASL	R	Y	N	N	mRS	N	D	Y	Y	Y
Nezu et al. , 2018	109	H	Penumbra Perfusion	I	PWI	R	N	Y	N	mRS	N	3m	N	N	N
Weller et al. , 2006	58	H	Penumbra Perfusion	I	PWI	R	N	N	N	NIHSS	N	1w	Y	Y	N
Benghanem et al. , 2019	71	H	Penumbra Volume	I	DWI	R	Y	Y	N	NIHSS	N	1w	Y	Y	Y
Bivard et al. , 2017	121	H	Penumbra Volume	I	DWI/PWI	R	Y	Y	N	mRS	N	3m	Y	N	Y
Buch et al. , 2012	54	H	Penumbra Volume	I	SWI/DWI	R	N	Y	N	NIHSS/mRS	N	3m	Y	N	Y
H et al. , 2019	47	H	Penumbra Volume	I	DWI/PWI	R	Y	N	N	mRS	N	>3 m	Y	Y	N
Kamakura et al. , 2017	150	H	Penumbra Volume	I	SWI/DWI	R	Y	N	N	mRS	N	3m	Y	N	Y
Lee et al. , 2012	23	H	Penumbra Volume	I	DWI	R	Y	N	N	langauge battery	Y	1w	Y	N	Y
Leonards et al. , 2012	88	H	Penumbra Volume	I	SWI/PWI	R	Y	Y	N	mRS	N	3m	Y	Y	N
Leonards et al. , 2012	88	H	Penumbra Volume	I	SWI/DWI	R	Y	Y	N	mRS	N	3m	Y	Y	N
Terasawa et al. , 2010	51	H	Penumbra Volume	I	FLAIR/DWI	R	N	Y	N	NIHSS	N	1w	N	N	N
Zhong et al. , 2016	92	H	Penumbra Volume	I	DWI	R	N	Y	N	NIHSS	N	1w	N	N	Y
Aoki et al. , 2013	73	H	SVD	I	FLAIR	R	Y	Y	N	mRS	N	3m	Y	N	N
Arsava et al. , 2015	132	A	SVD	I	FLAIR	R	Y	N	N	mRS	N	3m	Y	Y	Y
Bang et al. , 2012	187	S	SVD	I	FLAIR	R	N	N	N	mRS/BI	N	1m	Y	Y	Y
Bentley et al. , 2017	75	S	SVD	I	FLAIR	R	Y	N	N	BI	N	>3 m	Y	Y	N
Bourcier et al. , 2016	631	A	SVD	I	FLAIR	R	Y	N	N	NIHSS/mRS	N	3m	Y	N	Y
Bourcier et al. , 2017	538	A	SVD	I	FLAIR	R	N	N	N	mRS	N	3m	Y	N	N
Chung et al. , 2017	416	A	SVD	I	FLAIR	R	N	N	N	mRS	N	3m	Y	N	Y

Dejobert et al. , 2015	81	A	SVD	I	FLAIR	R	Y	N	N	OHS	N	>3 m	Y	Y	Y
Doughty et al. , 2016	184	H	SVD	I	FLAIR	R	N	N	N	mRS	N	3m	Y	N	N
Dunn et al. , 2019	56	H	SVD	I	FLAIR	R	Y	Y	N	mRS	N	3m	N	N	N
Hinkle et al. , 2013	101	A	SVD	I	FLAIR	R	N	N	N	mRS	N	>3 m	Y	N	Y
Huang et al. , 2007	4424	S	SVD	I	FLAIR	R	N	N	N	NIHSS/mRS	N	>3 m	Y	N	Y
Huo et al. , 2019	5035	A	SVD	I	Lesion Size	R	N	N	N	mRS	N	3m	Y	Y	NA
Huo et al. , 2019	5035	A	SVD	I	FLAIR	R	N	N	N	mRS	N	3m	Y	Y	Y
Johnston et al. , 2007	279	H	SVD	I	FLAIR	R	N	N	N	NIHSS/mRS	N	D	Y	Y	Y
Kim et al. , 2017	62	S	SVD	I	FLAIR	R	Y	N	N	mRS	N	D	Y	N	Y
Kim et al. , 2017	69	A	SVD	I	FLAIR	R	Y	N	Y	robotic and clinical score (motor/proprioceptive)	Y	3m	Y	N	Y
Kunimatsu et al. , 2016	97	S	SVD	I	FLAIR	R	Y	Y	N	mRS	N	3m	N	N	Y
Lazar et al. , 2011	408	A	SVD	I	FLAIR	R	N	N	N	NIHSS/mRS/BI	N	1m	Y	Y	Y
Li et al. , 2019	414	A	SVD	I	FLAIR	R	Y	N	N	mRS	N	3m	Y	N	Y
Liu et al. , 2014	426	H	SVD	I	FLAIR	R	Y	Y	N	mRS	N	>3 m	Y	Y	Y
Liu et al. , 2015	217	A	SVD	I	FLAIR	R	N	N	N	NIHSS/MMSE	Y	1m	Y	Y	Y
Lou et al. , 2018	44	S	SVD	I	FLAIR	R	N	N	N	ADL	N	D	Y	N	Y
Man et al. , 2019	74	A	SVD	I	FLAIR	R	Y	N	N	mRS	N	3m	Y	N	Y
Nadareishvili et al. , 2015	246	A	SVD	I	FLAIR	R	N	N	N	ADL	N	>3 m	Y	Y	Y
Payabvash et al. , 2011	97	A	SVD	I	FLAIR	R	Y	Y	N	mRS	N	3m	Y	N	Y
Payabvash et al. , 2014	667	H	SVD	I	SWI	R	N	Y	N	mRS	N	3m	Y	Y	Y
Rehme et al. , 2007	240	H	SVD	I	FLAIR	R	N	Y	N	mRS	N	>3 m	Y	N	Y
Rehme et al. , 2016	164	H	SVD	I	FLAIR	R	N	Y	N	NIHSS/mRS	N	3m	N	N	N

Renu et al. , 2019	18	A	SVD	I	FLAIR	R	Y	N	Y	BIT	Y	1m	N	N	Y
Ryu et al. , 2016	79	H	SVD	I	FLAIR	R	Y	Y	N	mRS	N	3m	Y	N	Y
Tateishi et al. , 2019	199	S	SVD	I	FLAIR/T1	R	Y	N	Y	ZCT	Y	>3 m	Y	Y	Y
Yoon et al. , 2018	293	H	SVD	I	FLAIR	R	Y	Y	N	mRS	N	3m	N	N	N
Zhang et al. , 2002	83	H	SVD	I	DWI	R	Y	Y	N	NIHSS	N	1w	N	N	Y
Atchaneeyasakul et al. , 2012	86	A	SVS-v	I	SWI	R	Y	N	N	NIHSS/mRS	N	D	N	N	Y
Derex et al. , 2017	22	H	SVS-v	I	SWI	R	Y	Y	N	mRS	N	3m	N	N	N
Gomez-Choco et al. , 2006	124	A	SVS-v	I	SWI	R	Y	Y	N	mRS	N	3m	N	N	Y
Liu et al. , 2015	50	H	SVS-v	I	SWI	R	N	N	N	NIHSS/mRS	N	D	N	N	Y
Mundiyanapurath et al. , 2019	43	A	SVS-v	I	SWI	R	Y	Y	N	mRS	N	3m	N	N	Y
Nezu et al. , 2018	109	H	SVS-v	I	SWI	R	N	Y	N	mRS	N	3m	N	N	Y
Patti et al. , 2017	40	A	SVS-v	I	SWI	R	Y	N	N	mRS	N	3m	N	N	Y
Yu et al. , 2016	22	A	SVS-v	I	SWI	R	Y	N	N	NIHSS	N	1w	Y	Y	Y
Reineck et al. , 2005	21	S	activation-language	S	fmri (task)	A	Y	N	Y	LRS	Y	>3 m	Y	N	Y
Bivard et al. , 2016	19	S	activation-motor	S	fmri	A	Y	N	Y	FMA	Y	3m	Y	Y	Y
Cho et al. , 2009	10	A	activation-motor	S	fmri (task)	A	N	N	Y	ARAT/grip strength	Y	>3 m	N	N	Y
Granziera et al. , 2012	34	S	activation-motor	S	fmri (task)	A	Y	N	Y	FMA	Y	3m	Y	Y	Y
Kimura et al. , 2011	23	A	activation-motor	S	fmri (task)	A	N	N	Y	FMA	Y	3m	Y	Y	Y
Lee et al. , 2018	11	A	activation-motor	S	fmri (task)	A	N	N	Y	ARAT/grip strength	Y	1m	Y	Y	N
Moulton et al. , 2019	30	A	activation-motor	S	fmri (task)	A	N	N	Y	FMA	Y	3m	Y	Y	N
Puig et al. , 2011	21	S	activation-motor	S	fmri (task)	A	Y	N	Y	ARAT/grip strength	Y	>3 m	Y	N	Y
Vora et al. , 2011	13	A	activation-motor	S	fmri (task)	A	N	N	N	mRS	N	1m	Y	Y	N
Yu et al. , 2019	9	S	activation-motor	S	fmri (task)	A	Y	N	Y	FMA	Y	1m	Y	Y	N

Apoil et al. , 2013	43	S	CST	S	DTI	A	N	N	N	MRFS/FIM	Y	D	N	N	Y
Barrett et al. , 2009	43	S	CST	S	DTI	A	Y	N	Y	FMA	Y	3m	Y	Y	Y
Chi et al. , 2018	25	S	CST	S	DTI	A	Y	N	Y	MI/MBC/FAC	Y	>3 m	Y	Y	Y
Ebinger et al. , 2010	58	A	CST	S	DTI	A	Y	N	Y	FMA	Y	3m	Y	N	Y
Ebinger et al. , 2010	58	A	CST	S	DTI	A	Y	N	Y	FMA	Y	3m	Y	N	Y
Feng et al. , 2015	27	A	CST	S	DWI	R	N	N	Y	FMA	Y	>3 m	Y	Y	Y
Findlater et al. , 2019	117	A	CST	S	DTI	A	Y	N	N	FMA/mRS	Y	>3 m	Y	Y	Y
Granziera et al. , 2012	34	S	CST	S	DTI	A	Y	N	Y	FMA	Y	3m	Y	Y	N
Groisser et al. , 2014	23	S	CST	S	T1	R	N	N	Y	FMA	Y	3m	Y	Y	N
Held et al. , 2011	60	S	CST	S	DTI	A	Y	N	N	NIHSS	Y	3m	Y	N	N
Held et al. , 2011	60	A	CST	S	DTI	A	Y	N	N	NIHSS	Y	3m	Y	N	Y
Jiang et al. , 2017	17	A	CST	S	DTI	A	N	N	N	FMA	Y	3m	Y	Y	Y
Kaesmacher et al. , 2018	25	S	CST	S	DTI	A	Y	N	N	FMA	Y	3m	Y	Y	Y
Kim et al. , 2010	76	A	CST	S	DWI	R	N	N	Y	FMA	Y	3m	Y	Y	Y
Kim et al. , 2016	43	H	CST	S	DTI	A	Y	N	Y	NIHSS	Y	3m	Y	Y	Y
Kimura et al. , 2011	10	A	CST	S	DTI	A	Y	N	Y	MI/NHPT/grip strength	Y	>3 m	Y	Y	Y
Legr et al. , 2013	23	A	CST	S	DTI	A	N	Y	N	NIHSS/MF	Y	3m	Y	Y	Y
Lin et al. , 2019	14	S	CST	S	DWI	R	Y	N	N	MMT	Y	D	Y	Y	Y
Lindow et al. , 2016	50	A	CST	S	DTI	A	Y	Y	N	FMA	Y	3m	Y	Y	Y
Liou et al. , 2010	37	S	CST	S	DTI	A	Y	N	Y	MI/MBC/FAC	Y	>3 m	N	N	Y
Liou et al. , 2010	37	S	CST	S	DTI	A	Y	N	Y	MI/MBC/FAC	Y	>3 m	N	N	Y
Nickel et al. , 2018	23	H	CST	S	DTI	A	N	N	N	MFS	Y	3m	Y	Y	Y
Sagnier et al. , 2019	17	A	CST	S	DTI	A	Y	Y	Y	JTT/grip strength	Y	3m	N	N	Y

Sagnier et al. , 2019	28	A	CST	S	DTI	A	Y	Y	Y	composite clinical score	Y	3m	N	N	Y
Thamm et al. , 2019	149	A	CST	S	DWI	R	Y	N	Y	robotic and clinical score (motor/proprioceptive)	Y	>3 m	Y	Y	Y
Vural et al. , 2016	48	S	CST	S	DWI	R	N	N	Y	FMA	Y	3m	Y	Y	Y
Wen et al. , 2016	32	A	CST	S	DWI	R	N	N	Y	rNSA	Y	>3 m	Y	N	N
Li et al. , 2015	10	S	language tract/area	S	DTI	A	Y	N	Y	BNT	Y	>3 m	Y	Y	N
Li et al. , 2015	10	S	language tract/area	S	DTI	A	Y	N	Y	BNT	Y	>3 m	Y	Y	N
Sagnier et al. , 2019	28	A	language tract/area	S	DTI	A	Y	Y	Y	AHS	Y	3m	N	N	Y
Samuelsson et al. , 2015	73	A	language tract/area	S	DWI	R	Y	N	Y	AHS	Y	3m	N	N	Y
Boccuni et al. , 2015	35	S	multiple tracts/areas	S	DWI	R	Y	N	Y	TOR	Y	>3 m	Y	Y	Y
Kaya et al. , 2019	198	H	multiple tracts/areas	S	DWI	R	N	N	N	mRS	N	3m	Y	N	Y
Kim et al. , 2016	43	H	multiple tracts/areas	S	DTI	A	Y	N	Y	NIHSS	Y	3m	Y	Y	Y
Liu et al. , 2019	302	A	multiple tracts/areas	S	DWI	R	N	N	N	mRS	N	>3 m	Y	Y	Y
Yoo et al. , 2014	550	A	multiple tracts/areas	S	DWI	R	N	N	N	NIHSS	N	1w	N	N	Y
Binkofski et al. , 2017	22	A	other motor tract/area	S	DTI	A	Y	Y	Y	FMA	Y	3m	Y	Y	N
Lee et al. , 2015	12	A	other motor tract/area	S	DTI	A	Y	N	N	NIHSS	Y	>3 m	Y	Y	Y
Yu et al. , 2018	65	A	other motor tract/area	S	DWI	R	Y	N	Y	NIHSS	N	3m	Y	Y	Y
Cheng et al. , 2019	18	A	other tract/area	S	DTI	A	Y	N	N	mRS	N	3m	Y	Y	Y
Liu et al. , 2019	302	A	other tract/area	S	DWI	R	N	N	N	mRS	N	>3 m	Y	Y	Y
Wen et al. , 2016	32	A	other tract/area	S	DWI	R	N	N	Y	rNSA	Y	>3 m	Y	N	N
Jeong et al. , 2015	67	A	Specific Connection	N	fmri	A	Y	N	N	mRS	N	3m	Y	Y	Y
Karameshev et al. , 2011	17	S	Specific Connection	N	fmri	A	N	N	Y	MI/BB	Y	>3 m	Y	Y	N

Karameshev et al. , 2011	17	S	Specific Connection	N	DTI	A	N	N	Y	MI/BB	Y	>3 m	Y	Y	Y
Rost et al. , 2018	26	A	Specific Connection	N	fmri	A	Y	Y	N	mRS	N	3m	Y	Y	Y
Song et al. , 2016	37	A	Specific Connection	N	fmri	A	Y	N	N	mRS	N	3m	Y	Y	Y
Tei et al. , 2011	81	S	Specific Connection	N	fmri	A	N	N	N	FMA	Y	3m	Y	Y	Y
Yang et al. , 2016	12	S	Specific Connection	N	fmri	A	Y	N	Y	FMA	Y	>3 m	Y	Y	Y
Dong et al. , 2019	12	S	Whole network/subnetwork	N	fmri	A	Y	N	Y	FMA	Y	3m	Y	Y	Y
Legr et al. , 2012	30	S	Whole network/subnetwork	N	fmri	A	N	N	Y	FMA	N	3m	Y	Y	Y
Liu et al. , 2013	5	S	Whole network/subnetwork	N	fmri (task)	A	N	N	Y	FMA	Y	3m	Y	Y	Y

H: Hyperacute, A: Acute. S: Subacute. Acronyms are listed in the Abbreviation table.

Appendix D

OPEN

Quantifying Infarct Growth and Secondary Injury Volumes
Comparing Multimodal Image Registration Measures

George W.J. Harston, DPhil; Davide Carone, MD; Fintan Sheerin, MA; Mark Jenkinson, DPhil; James Kennedy, FRCP

Background and Purpose—Lesion expansion in the week after acute stroke involves both infarct growth (IG) and anatomic distortion (AD) because of edema and hemorrhage. Enabling separate quantification would allow clinical trials targeting these distinct pathological processes. We developed an objective and automated approach to quantify these processes at 24 hours and 1 week.

Methods—Patients with acute ischemic stroke were scanned at presentation, 24 hours, and 1 week in a magnetic resonance imaging (MRI) cohort study. IG and AD were calculated from follow-up lesion masks after linear and nonlinear registration to a presenting MRI scan. Performance of IG and AD was compared with edema quantified using cerebrospinal fluid displacement. The use of alternative reference images to define AD, including template MRI, mirrored MRI, and presenting computed tomographic scan, was explored.

Results—Thirty-seven patients with nonlacunar stroke were included. AD was responsible for 20% and 36% of lesion expansion at 24 hours (n=30) and 1 week (n=28). Registration-defined IG and AD compared favorably with edema quantified using cerebrospinal fluid displacement, particularly at smaller infarct volumes. Presenting computed tomographic imaging was the preferred alternative reference image to presenting MRI for measuring AD.

Conclusions—The contributions of IG and AD to lesion expansion can be measured separately over time through the use of image registration. This approach can be used to combine imaging outcome data from computed tomography and MRI. **(*Stroke*. 2018;49:1647-1655. DOI: 10.1161/STROKEAHA.118.020788.)**

Key Words: edema ■ follow-up studies ■ humans ■ magnetic resonance imaging ■ stroke ■ tomography, X-ray computed

Downloaded from http://ahajournals.org by on June 18, 2021

With the widespread adoption of mechanical thrombectomy into clinical practice, there is renewed interest in strategies to mitigate secondary injury for patients with acute ischemic stroke, including neuroprotection and minimizing vasogenic edema.[1,2] Lesion expansion after the ischemic insult is because of a combination of infarct growth (IG), which is associated with poor long-term clinical outcomes[3,4] and anatomic distortion (AD) because of cerebral edema and hemorrhagic transformation—the major cause of neurological deterioration and death in the days after the event.[5–7] Quantifying IG and AD separately poses significant challenges and limits the opportunity for clinical trials to assess treatment efficacy.

The most common approaches to defining IG in trials have used either differences in measured infarct volumes between time points or the identification of regions of new infarction after linear image registration.[8,9] Both will be confounded by AD because of edema or hemorrhage included in the volume. To minimize confounding, IG has been defined using extension into new anatomic territories.[10,11] However, moving away from a volume-based approach compromises the ability to demonstrate a potential treatment effect.

Quantification of edema is similarly challenging. Current strategies involve labor intensive and subjective methodology defining regions on a slice-by-slice basis,[12–14] measures of midline shift insensitive to submassive distortions,[2] or inferences about focal edema from changes in whole brain or cerebrospinal fluid (CSF) volumes, which have produced inconsistent results and a fixed error that limits their use in smaller infarcts.[15,16] Despite these challenges, the importance of AD has been highlighted by manual quantification of brain swelling, which has identified >11 mL volume as the threshold with greatest sensitivity and specificity for predicting poor outcome.[11]

Image registration has been key in the interpretation and design of acute stroke trials.[17–19] Although linear registration is a well-suited approach within a time point when there are

Received January 15, 2018; final revision received May 1, 2018; accepted May 14, 2018.

From the Radcliffe Department of Medicine, Acute Vascular Imaging Centre (G.W.J.H., D.C., F.S., J.K.) and Nuffield Department of Clinical Neurosciences, Wellcome Centre for Integrative Neuroimaging (M.J.), University of Oxford, United Kingdom.

Presented in part at the International Stroke Conference, Houston, TX, February 21–24, 2017.

The online-only Data Supplement is available with this article at https://www.ahajournals.org/doi/suppl/10.1161/STROKEAHA.118.020788.

Correspondence to George W.J. Harston, DPhil, Department of Medicine, Acute Vascular Imaging Centre, Level 2, John Radcliffe Hospital, University of Oxford, Oxford OX39DU, United Kingdom. E-mail george.harston@rdm.ox.ac.uk

© 2018 The Authors. *Stroke* is published on behalf of the American Heart Association, Inc., by Wolters Kluwer Health, Inc. This is an open access article under the terms of the Creative Commons Attribution License, which permits use, distribution, and reproduction in any medium, provided that the original work is properly cited.

Appendix E

NeuroImage: Clinical 16 (2017) 23–31

Contents lists available at ScienceDirect

NeuroImage: Clinical

journal homepage: www.elsevier.com/locate/ynicl

Impact of automated ICA-based denoising of fMRI data in acute stroke patients

D. Carone[a,b], R. Licenik[a,c], S. Suri[d], L. Griffanti[e], N. Filippini[f], J. Kennedy[a,*]

[a] Acute Vascular Imaging Centre, Radcliffe Department of Medicine, University of Oxford, Oxford, United Kingdom
[b] Laboratory of Experimental Stroke Research, Department of Surgery and Translational Medicine, University of Milano Bicocca, Milan Center of Neuroscience, Monza, Italy
[c] Department of Social Medicine and Public Health, Faculty of Medicine, Palacky University, Olomouc, Czech Republic
[d] Department of Psychiatry, Warneford Hospital, University of Oxford, Oxford, United Kingdom
[e] Oxford Centre of Functional MRI of the Brain, Nuffield Department of Clinical Neurosciences, University of Oxford, Oxford, United Kingdom
[f] Nuffield Department of Clinical Neurosciences, West Wing level 6, JR hospital, Oxford, United Kingdom

ARTICLE INFO

Keywords:
Independent component analysis
fMRI
Acute stroke
Denoising
BOLD
Resting state

ABSTRACT

Different strategies have been developed using Independent Component Analysis (ICA) to automatically de-noise fMRI data, either focusing on removing only certain components (e.g. motion-ICA-AROMA, Pruim et al., 2015a) or using more complex classifiers to remove multiple types of noise components (e.g. FIX, Salimi-Khorshidi et al., 2014 Griffanti et al., 2014). However, denoising data obtained in an acute setting might prove challenging: the presence of multiple noise sources may not allow focused strategies to clean the data enough and the heterogeneity in the data may be so great to critically undermine complex approaches. The purpose of this study was to explore what automated ICA based approach would better cope with these limitations when cleaning fMRI data obtained from acute stroke patients.

The performance of a focused classifier (ICA-AROMA) and a complex classifier (FIX) approaches were compared using data obtained from twenty consecutive acute lacunar stroke patients using metrics determining RSN identification, RSN reproducibility, changes in the BOLD variance, differences in the estimation of functional connectivity and loss of temporal degrees of freedom.

The use of generic-trained FIX resulted in misclassification of components and significant loss of signal (< 80%), and was not explored further. Both ICA-AROMA and patient-trained FIX based denoising approaches resulted in significantly improved RSN reproducibility ($p < 0.001$), localized reduction in BOLD variance consistent with noise removal, and significant changes in functional connectivity ($p < 0.001$). Patient-trained FIX resulted in higher RSN identifiability ($p < 0.001$) and wider changes both in the BOLD variance and in functional connectivity compared to ICA-AROMA.

The success of ICA-AROMA suggests that by focusing on selected components the full automation can deliver meaningful data for analysis even in population with multiple sources of noise. However, the time invested to train FIX with appropriate patient data proved valuable, particularly in improving the signal-to-noise ratio.

1. Introduction

After acute brain injury, brain plasticity and reorganization underlie functional recovery, and improvement is mediated by adaptations in brain network connectivity (Andrews, 1991). Resting-state functional MRI (rs-fMRI) allows detailed investigation of these changes providing potentially useful information to guide treatment. The minimal demands on the patient during scanning makes the technique an ideal and increasingly used choice in acute clinical settings (Ovadia-Caro et al., 2014).

However, overcoming the contribution of noise in the acquisition of rs-fMRI data is important in limiting false observations and reliably estimating functional connectivity in Resting State Networks (RSN) (Raichle and Snyder, 2007; Friston et al., 1996; Dagli et al., 1999; Glover et al., 2000; Windischberger et al., 2002). Independent component analysis (ICA) can be used to reliably separate signal from noise, enabling artefacts to be regressed out of the data thereby allowing a significant improvement on results obtained with traditional pre-processing (Stone et al., 2002; Thomas et al., 2002; Kochiyama et al., 2005; McKeown et al., 2005; Zou et al., 2009; Zuo and Xing, 2014). While

* Corresponding author at: AVIC, University of Oxford, Level 2, John Radcliffe Hospital, Headington, Oxford OX3 9DU, United Kingdom.
E-mail address: James.Kennedy@rdm.ox.ac.uk (J. Kennedy).

http://dx.doi.org/10.1016/j.nicl.2017.06.033
Received 10 January 2017; Received in revised form 15 June 2017; Accepted 29 June 2017
Available online 30 June 2017
2213-1582/ © 2017 The Authors. Published by Elsevier Inc. This is an open access article under the CC BY license (http://creativecommons.org/licenses/BY/4.0/).

References

1. Feigin VL, Lawes CM, Bennett DA, et al. Worldwide stroke incidence and early case fatality reported in 56 population-based studies: a systematic review. *Lancet Neurol* 2009; 8: 355-369. 2009/02/24. DOI: 10.1016/s1474-4422(09)70025-0.

2. Office. NA. Reducing Brain Damage: Faster access to better stroke care. *NAO, London* 2005. .

3. Youman P, Wilson K, Harraf F, et al. The economic burden of stroke in the United Kingdom. *PharmacoEconomics* 2003; 21 Suppl 1: 43-50. 2003/03/22.

4. Ovadia-Caro S, Margulies DS and Villringer A. The value of resting-state functional magnetic resonance imaging in stroke. *Stroke; a journal of cerebral circulation* 2014; 45: 2818-2824. DOI: 10.1161/STROKEAHA.114.003689.

5. Counsell C, Dennis M, McDowall M, et al. Predicting outcome after acute and subacute stroke: development and validation of new prognostic models. *Stroke; a journal of cerebral circulation* 2002; 33: 1041-1047. 2002/04/06.

6. O'Collins VE, Macleod MR, Donnan GA, et al. 1,026 experimental treatments in acute stroke. *Annals of neurology* 2006; 59: 467-477. 2006/02/03. DOI: 10.1002/ana.20741.

7. Cramer SC and Chopp M. Recovery recapitulates ontogeny. *Trends in neurosciences* 2000; 23: 265-271. 2000/06/06.

8. Hoffmann TC and Walker MF. 'TIDieR-ing up' the reporting of interventions in stroke research: the importance of knowing what is in the 'black box'. *International journal of stroke : official journal of the International Stroke Society* 2015; 10: 657-658. 2015/06/23. DOI: 10.1111/ijs.12524.

9. Lo EH. A new penumbra: transitioning from injury into repair after stroke. *Nat Med* 2008; 14: 497-500. 2008/05/09. DOI: 10.1038/nm1735.

10. Bernhardt J, Hayward KS, Kwakkel G, et al. Agreed definitions and a shared vision for new standards in stroke recovery research: The Stroke Recovery and Rehabilitation Roundtable taskforce. *International Journal of Stroke* 2017; 12: 444-450. DOI: 10.1177/1747493017711816.

11. Biernaskie J, Chernenko G and Corbett D. Efficacy of rehabilitative experience declines with time after focal ischemic brain injury. *The Journal of neuroscience : the official journal of the Society for Neuroscience* 2004; 24: 1245-1254. 2004/02/06. DOI: 10.1523/jneurosci.3834-03.2004.

12. Burke E and Cramer SC. Biomarkers and predictors of restorative therapy effects after stroke. *Current neurology and neuroscience reports* 2013; 13: 329. 2013/01/10. DOI: 10.1007/s11910-012-0329-9.

13. Dirnagl U, Iadecola C and Moskowitz MA. Pathobiology of ischaemic stroke: an integrated view. *Trends Neurosci* 1999; 22: 391-397. Research Support, Non-U.S. Gov't Research Support, U.S. Gov't, P.H.S. Review 1999/08/11.

14. Carmichael ST. The 3 Rs of Stroke Biology: Radial, Relayed, and Regenerative. *Neurotherapeutics* 2016; 13: 348-359. 2015/11/26. DOI: 10.1007/s13311-015-0408-0.

15. Astrup J, Siesjö BK and Symon L. Thresholds in cerebral ischemia - the ischemic penumbra. *Stroke; a journal of cerebral circulation* 1981; 12: 723-725. 1981/11/01. DOI: 10.1161/01.str.12.6.723.

16. Eltzschig HK and Eckle T. Ischemia and reperfusion--from mechanism to translation. *Nat Med* 2011; 17: 1391-1401. Research Support, N.I.H., Extramural Research Support, Non-U.S. Gov't Review 2011/11/09. DOI: 10.1038/nm.2507.

17. Schofield ZV, Woodruff TM, Halai R, et al. Neutrophils--a key component of ischemia-reperfusion injury. *Shock* 2013; 40: 463-470. 2013/10/04. DOI: 10.1097/shk.0000000000000044.

18. Heiss WD. The ischemic penumbra: how does tissue injury evolve? *Ann N Y Acad Sci* 2012; 1268: 26-34. 2012/09/22. DOI: 10.1111/j.1749-6632.2012.06668.x.

19. Pietrobon D and Moskowitz MA. Chaos and commotion in the wake of cortical spreading depression and spreading depolarizations. *Nature reviews Neuroscience* 2014; 15: 379-393. 2014/05/27. DOI: 10.1038/nrn3770.

20. Brown CE, Aminoltejari K, Erb H, et al. In Vivo Voltage-Sensitive Dye Imaging in Adult Mice Reveals That Somatosensory Maps Lost to Stroke Are Replaced over Weeks by New Structural and Functional Circuits with Prolonged Modes of Activation within Both the Peri-Infarct Zone and Distant Sites. *The Journal of Neuroscience* 2009; 29: 1719-1734. DOI: 10.1523/jneurosci.4249-08.2009.

21. Mostany R, Chowdhury TG, Johnston DG, et al. Local hemodynamics dictate long-term dendritic plasticity in peri-infarct cortex. *The Journal of neuroscience : the official journal of the Society for Neuroscience* 2010; 30: 14116-14126. 2010/10/22. DOI: 10.1523/jneurosci.3908-10.2010.

22. Hossmann KA. The two pathophysiologies of focal brain ischemia: implications for translational stroke research. *J Cereb Blood Flow Metab* 2012 2012/01/12. DOI: jcbfm2011186 [pii]10.1038/jcbfm.2011.186.

23. Duering M, Righart R, Wollenweber FA, et al. Acute infarcts cause focal thinning in remote cortex via degeneration of connecting fiber tracts. *Neurology* 2015; 84: 1685-1692.

2015/03/27. DOI: 10.1212/wnl.0000000000001502.

24. He BJ, Snyder AZ, Vincent JL, et al. Breakdown of functional connectivity in frontoparietal networks underlies behavioral deficits in spatial neglect. *Neuron* 2007; 53: 905-918. 2007/03/16. DOI: 10.1016/j.neuron.2007.02.013.

25. Corbetta M, Ramsey L, Callejas A, et al. Common behavioral clusters and subcortical anatomy in stroke. *Neuron* 2015; 85: 927-941. 2015/03/06. DOI: 10.1016/j.neuron.2015.02.027.

26. Nomura EM, Gratton C, Visser RM, et al. Double dissociation of two cognitive control networks in patients with focal brain lesions. *Proceedings of the National Academy of Sciences* 2010; 107: 12017-12022. DOI: 10.1073/pnas.1002431107.

27. Le Belle JE, Orozco NM, Paucar AA, et al. Proliferative Neural Stem Cells Have High Endogenous ROS Levels that Regulate Self-Renewal and Neurogenesis in a PI3K/Akt-Dependant Manner. *Cell Stem Cell* 2011; 8: 59-71. DOI: 10.1016/j.stem.2010.11.028.

28. Hu Q, Liang X, Chen D, et al. Delayed hyperbaric oxygen therapy promotes neurogenesis through reactive oxygen species/hypoxia-inducible factor-1α/β-catenin pathway in middle cerebral artery occlusion rats. *Stroke; a journal of cerebral circulation* 2014; 45: 1807-1814. 2014/04/24. DOI: 10.1161/strokeaha.114.005116.

29. Ekdahl CT, Kokaia Z and Lindvall O. Brain inflammation and adult neurogenesis: the dual role of microglia. *Neuroscience* 2009; 158: 1021-1029. 2008/07/30. DOI: 10.1016/j.neuroscience.2008.06.052.

30. Withers GS, Higgins D, Charette M, et al. Bone morphogenetic protein-7 enhances dendritic growth and receptivity to innervation in cultured hippocampal neurons. *Eur J Neurosci* 2000; 12: 106-116. 2000/01/29. DOI: 10.1046/j.1460-9568.2000.00889.x.

31. Gertz K, Kronenberg G, Kälin RE, et al. Essential role of interleukin-6 in post-stroke angiogenesis. *Brain : a journal of neurology* 2012; 135: 1964-1980. 2012/04/12. DOI: 10.1093/brain/aws075.

32. Liu XS, Zhang ZG, Zhang RL, et al. Chemokine ligand 2 (CCL2) induces migration and differentiation of subventricular zone cells after stroke. *J Neurosci Res* 2007; 85: 2120-2125. 2007/05/19. DOI: 10.1002/jnr.21359.

33. Yan YP, Sailor KA, Lang BT, et al. Monocyte chemoattractant protein-1 plays a critical role in neuroblast migration after focal cerebral ischemia. *Journal of cerebral blood flow and metabolism : official journal of the International Society of Cerebral Blood Flow and Metabolism* 2007; 27: 1213-1224. 2006/12/28. DOI: 10.1038/sj.jcbfm.9600432.

34. Keyvani K, Bosse F, Reinecke S, et al. Postlesional transcriptional regulation of metabotropic glutamate receptors: implications for plasticity and excitotoxicity. *Acta Neuropathologica* 2001; 101: 79-84. DOI: 10.1007/s004010000339.

35. Kitagawa K. CREB and cAMP response element-mediated gene expression in the ischemic brain. *The FEBS Journal* 2007; 274: 3210-3217. DOI: https://doi.org/10.1111/j.1742-4658.2007.05890.x.

36. Carmichael ST and Chesselet MF. Synchronous neuronal activity is a signal for axonal sprouting after cortical lesions in the adult. *The Journal of neuroscience : the official journal of the Society for Neuroscience* 2002; 22: 6062-6070. 2002/07/18. DOI: 10.1523/jneurosci.22-14-06062.2002.

37. Grefkes C and Fink GR. Connectivity-based approaches in stroke and recovery of function. *The Lancet Neurology* 2014; 13: 206-216. DOI: https://doi.org/10.1016/S1474-4422(13)70264-3.

38. Bernhardt J, Hayward KS, Kwakkel G, et al. Agreed definitions and a shared vision for new standards in stroke recovery research: The Stroke Recovery and Rehabilitation Roundtable taskforce. *International journal of stroke : official journal of the International Stroke Society* 2017; 12: 444-450. 2017/07/13. DOI: 10.1177/1747493017711816.

39. Murphy TH and Corbett D. Plasticity during stroke recovery: from synapse to behaviour. *Nature Reviews Neuroscience* 2009; 10: 861-872. DOI: 10.1038/nrn2735.

40. Brumm KP, Perthen JE, Liu TT, et al. An arterial spin labeling investigation of cerebral blood flow deficits in chronic stroke survivors. *NeuroImage* 2010; 51: 995-1005. 2010/03/10. DOI: 10.1016/j.neuroimage.2010.03.008.

41. Hillis AE. Magnetic resonance perfusion imaging in the study of language. *Brain and Language* 2007; 102: 165-175. DOI: https://doi.org/10.1016/j.bandl.2006.04.016.

42. Hillis AE. Pharmacological, surgical, and neurovascular interventions to augment acute aphasia recovery. *Am J Phys Med Rehabil* 2007; 86: 426-434. 2007/05/23. DOI: 10.1097/PHM.0b013e31805ba094.

43. Mostany R, Chowdhury TG, Johnston DG, et al. Local Hemodynamics Dictate Long-Term Dendritic Plasticity in Peri-Infarct Cortex. *The Journal of Neuroscience* 2010; 30: 14116-14126. DOI: 10.1523/jneurosci.3908-10.2010.

44. Mostany R, Chowdhury TG, Johnston DG, et al. Local hemodynamics dictate long-term dendritic plasticity in peri-infarct cortex. *The Journal of neuroscience : the official journal of the Society for Neuroscience* 2010; 30: 14116-14126. DOI: 10.1523/JNEUROSCI.3908-10.2010.

45. Lim DH, LeDue JM, Mohajerani MH, et al. Optogenetic mapping after stroke reveals network-wide scaling of functional connections and heterogeneous recovery of the peri-infarct. *The Journal of neuroscience : the official journal of the Society for Neuroscience* 2014; 34: 16455-16466. 2014/12/05. DOI: 10.1523/jneurosci.3384-14.2014.

46. Mohajerani MH, Aminoltejari K and Murphy TH. Targeted mini-strokes produce

changes in interhemispheric sensory signal processing that are indicative of disinhibition within minutes. *Proceedings of the National Academy of Sciences* 2011; 108: E183-E191. DOI: 10.1073/pnas.1101914108.

47. Jacobs K and Donoghue J. Reshaping the cortical motor map by unmasking latent intracortical connections. *Science* 1991; 251: 944-947. DOI: 10.1126/science.2000496.

48. O'Shea J, Johansen-Berg H, Trief D, et al. Functionally specific reorganization in human premotor cortex. *Neuron* 2007; 54: 479-490. 2007/05/08. DOI: 10.1016/j.neuron.2007.04.021.

49. Reis J, Swayne OB, Vandermeeren Y, et al. Contribution of transcranial magnetic stimulation to the understanding of cortical mechanisms involved in motor control. *The Journal of physiology* 2008; 586: 325-351. 2007/11/03. DOI: 10.1113/jphysiol.2007.144824.

50. Deiber MP, Wise SP, Honda M, et al. Frontal and parietal networks for conditional motor learning: a positron emission tomography study. *Journal of neurophysiology* 1997; 78: 977-991. 1997/08/01. DOI: 10.1152/jn.1997.78.2.977.

51. Penhune VB and Doyon J. Cerebellum and M1 interaction during early learning of timed motor sequences. *NeuroImage* 2005; 26: 801-812. 2005/06/16. DOI: 10.1016/j.neuroimage.2005.02.041.

52. Dancause N, Barbay S, Frost SB, et al. Extensive Cortical Rewiring after Brain Injury. *The Journal of Neuroscience* 2005; 25: 10167-10179. DOI: 10.1523/jneurosci.3256-05.2005.

53. Overman JJ, Clarkson AN, Wanner IB, et al. A role for ephrin-A5 in axonal sprouting, recovery, and activity-dependent plasticity after stroke. *Proceedings of the National Academy of Sciences* 2012; 109: E2230-E2239. DOI: 10.1073/pnas.1204386109.

54. Hinman JD, Rasband MN and Carmichael ST. Remodeling of the axon initial segment after focal cortical and white matter stroke. *Stroke; a journal of cerebral circulation* 2013; 44: 182-189. 2012/12/13. DOI: 10.1161/strokeaha.112.668749.

55. Silasi G and Murphy Timothy H. Stroke and the Connectome: How Connectivity Guides Therapeutic Intervention. *Neuron* 2014; 83: 1354-1368. DOI: https://doi.org/10.1016/j.neuron.2014.08.052.

56. Crofts A, Kelly ME and Gibson CL. Imaging Functional Recovery Following Ischemic Stroke: Clinical and Preclinical fMRI Studies. *J Neuroimaging* 2020; 30: 5-14. 2019/10/13. DOI: 10.1111/jon.12668.

57. Biernaskie J, Szymanska A, Windle V, et al. Bi-hemispheric contribution to functional motor recovery of the affected forelimb following focal ischemic brain injury in rats. *European Journal of Neuroscience* 2005; 21: 989-999. DOI: https://doi.org/10.1111/j.1460-

9568.2005.03899.x.

58. Zeiler SR, Gibson EM, Hoesch RE, et al. Medial premotor cortex shows a reduction in inhibitory markers and mediates recovery in a mouse model of focal stroke. *Stroke; a journal of cerebral circulation* 2013; 44: 483-489. 2013/01/17. DOI: 10.1161/strokeaha.112.676940.

59. Takatsuru Y, Fukumoto D, Yoshitomo M, et al. Neuronal Circuit Remodeling in the Contralateral Cortical Hemisphere during Functional Recovery from Cerebral Infarction. *The Journal of Neuroscience* 2009; 29: 10081-10086. DOI: 10.1523/jneurosci.1638-09.2009.

60. Ohab JJ and Carmichael ST. Poststroke neurogenesis: emerging principles of migration and localization of immature neurons. *Neuroscientist* 2008; 14: 369-380. 2007/11/21. DOI: 10.1177/1073858407309545.

61. Lichtenwalner RJ and Parent JM. Adult neurogenesis and the ischemic forebrain. *Journal of cerebral blood flow and metabolism : official journal of the International Society of Cerebral Blood Flow and Metabolism* 2006; 26: 1-20. 2005/06/17. DOI: 10.1038/sj.jcbfm.9600170.

62. Krupinski J, Kaluza J, Kumar P, et al. Role of angiogenesis in patients with cerebral ischemic stroke. *Stroke; a journal of cerebral circulation* 1994; 25: 1794-1798. 1994/09/01. DOI: 10.1161/01.str.25.9.1794.

63. Stinear CM. Prediction of motor recovery after stroke: advances in biomarkers. *The Lancet Neurology* 2017; 16: 826-836. DOI: https://doi.org/10.1016/S1474-4422(17)30283-1.

64. Bernhardt J, Borschmann K, Boyd L, et al. Moving rehabilitation research forward: Developing consensus statements for rehabilitation and recovery research. *International Journal of Stroke* 2016; 11: 454-458. DOI: 10.1177/1747493016643851.

65. Burke E and Cramer SC. Biomarkers and Predictors of Restorative Therapy Effects After Stroke. *Current Neurology and Neuroscience Reports* 2013; 13: 329. DOI: 10.1007/s11910-012-0329-9.

66. Wadden KP, Woodward TS, Metzak PD, et al. Compensatory motor network connectivity is associated with motor sequence learning after subcortical stroke. *Behavioural brain research* 2015; 286: 136-145. 2015/03/12. DOI: 10.1016/j.bbr.2015.02.054.

67. Cramer SC, Wolf SL, Saver JL, et al. The Utility of Domain-Specific End Points in Acute Stroke Trials. *Stroke; a journal of cerebral circulation* 2021; 52: 1154-1161. 2021/02/11. DOI: 10.1161/strokeaha.120.031939.

68. Whiteley W, Wardlaw J, Dennis M, et al. The use of blood biomarkers to predict

poor outcome after acute transient ischemic attack or ischemic stroke. *Stroke; a journal of cerebral circulation* 2012; 43: 86-91. 2011/10/25. DOI: 10.1161/strokeaha.111.634089.

69. Lindgren A and Maguire J. Stroke Recovery Genetics. *Stroke; a journal of cerebral circulation* 2016; 47: 2427-2434. 2016/08/16. DOI: 10.1161/strokeaha.116.010648.

70. Stinear CM, Barber PA, Petoe M, et al. The PREP algorithm predicts potential for upper limb recovery after stroke. *Brain : a journal of neurology* 2012; 135: 2527-2535. 2012/06/13. DOI: 10.1093/brain/aws146.

71. Byblow WD, Stinear CM, Barber PA, et al. Proportional recovery after stroke depends on corticomotor integrity. *Ann Neurol* 2015; 78: 848-859. 2015/07/08. DOI: 10.1002/ana.24472.

72. Rabiller G, He JW, Nishijima Y, et al. Perturbation of Brain Oscillations after Ischemic Stroke: A Potential Biomarker for Post-Stroke Function and Therapy. *Int J Mol Sci* 2015; 16: 25605-25640. 2015/10/31. DOI: 10.3390/ijms161025605.

73. Paggiaro A, Birbaumer N, Cavinato M, et al. Magnetoencephalography in Stroke Recovery and Rehabilitation. *Front Neurol* 2016; 7: 35. 2016/04/12. DOI: 10.3389/fneur.2016.00035.

74. Minematsu K, Li L, Fisher M, et al. Diffusion-weighted magnetic resonance imaging: rapid and quantitative detection of focal brain ischemia. *Neurology* 1992; 42: 235-240. 1992/01/01.

75. Buxton RB, Frank LR, Wong EC, et al. A general kinetic model for quantitative perfusion imaging with arterial spin labeling. *Magn Reson Med* 1998; 40: 383-396. 1998/09/04.

76. Zhou J, Payen JF, Wilson DA, et al. Using the amide proton signals of intracellular proteins and peptides to detect pH effects in MRI. *Nat Med* 2003; 9: 1085-1090. Research Support, Non-U.S. Gov't Research Support, U.S. Gov't, P.H.S. 2003/07/23. DOI: 10.1038/nm907.

77. Ogawa S, Lee TM, Kay AR, et al. Brain magnetic resonance imaging with contrast dependent on blood oxygenation. *Proceedings of the National Academy of Sciences of the United States of America* 1990; 87: 9868-9872. 1990/12/01. DOI: 10.1073/pnas.87.24.9868.

78. Radda GK. The use of NMR spectroscopy for the understanding of disease. *Science* 1986; 233: 640-645. Research Support, Non-U.S. Gov't Research Support, U.S. Gov't, P.H.S. 1986/08/08.

79. Brown RW. *Magnetic resonance imaging : physical principles and sequence design*. Hoboken, New Jersey: Wiley-Blackwell, 2014.

80. Le Bihan D, Mangin JF, Poupon C, et al. Diffusion tensor imaging: concepts and applications. *J Magn Reson Imaging* 2001; 13: 534-546.

81. Le Bihan D, Mangin J-F, Poupon C, et al. Diffusion tensor imaging: Concepts and applications. *Journal of Magnetic Resonance Imaging* 2001; 13: 534-546. DOI: https://doi.org/10.1002/jmri.1076.

82. Le Bihan D and Johansen-Berg H. Diffusion MRI at 25: Exploring brain tissue structure and function. *NeuroImage* 2012; 61: 324-341. DOI: https://doi.org/10.1016/j.neuroimage.2011.11.006.

83. Alexander LD, Black SE, Gao F, et al. Correlating lesion size and location to deficits after ischemic stroke: the influence of accounting for altered peri-necrotic tissue and incidental silent infarcts. *Behavioral and Brain Functions* 2010; 6: 6. DOI: 10.1186/1744-9081-6-6.

84. Boyd LA, Hayward KS, Ward NS, et al. Biomarkers of stroke recovery: Consensus-based core recommendations from the Stroke Recovery and Rehabilitation Roundtable. *International journal of stroke : official journal of the International Stroke Society* 2017; 12: 480-493. 2017/07/13. DOI: 10.1177/1747493017714176.

85. Boyd LA, Hayward KS, Ward NS, et al. Biomarkers of Stroke Recovery: Consensus-Based Core Recommendations from the Stroke Recovery and Rehabilitation Roundtable. *Neurorehabilitation and neural repair* 2017; 31: 864-876. 2017/12/14. DOI: 10.1177/1545968317732680.

86. Harston GWJ, Carone D, Sheerin F, et al. Quantifying Infarct Growth and Secondary Injury Volumes: Comparing Multimodal Image Registration Measures. *Stroke; a journal of cerebral circulation* 2018; 49: 1647-1655. 2018/06/14. DOI: 10.1161/strokeaha.118.020788.

87. Mori S and Zhang J. Principles of Diffusion Tensor Imaging and Its Applications to Basic Neuroscience Research. *Neuron* 2006; 51: 527-539. DOI: https://doi.org/10.1016/j.neuron.2006.08.012.

88. Buxton RB. Quantifying CBF with arterial spin labeling. *J Magn Reson Imaging* 2005; 22: 723-726. DOI: 10.1002/jmri.20462.

89. Markus HS. Cerebral perfusion and stroke. *J Neurol Neurosurg Psychiatry* 2004; 75: 353-361. 2004/02/18.

90. Kane I, Carpenter T, Chappell F, et al. Comparison of 10 different magnetic resonance perfusion imaging processing methods in acute ischemic stroke: effect on lesion size, proportion of patients with diffusion/perfusion mismatch, clinical scores, and radiologic outcomes. *Stroke* 2007; 38: 3158-3164. DOI: 10.1161/STROKEAHA.107.483842.

91. Alsop DC, Detre JA, Golay X, et al. Recommended implementation of arterial spin-

labeled perfusion MRI for clinical applications: A consensus of the ISMRM perfusion study group and the European consortium for ASL in dementia. *Magn Reson Med* 2014 2014/04/10. DOI: 10.1002/mrm.25197.

92. Kanal E and Tweedle MF. Residual or retained gadolinium: practical implications for radiologists and our patients. *Radiology* 2015; 275: 630-634. 2015/05/06. DOI: 10.1148/radiol.2015150805.

93. Essig M, Shiroishi MS, Nguyen TB, et al. Perfusion MRI: the five most frequently asked technical questions. *AJR Am J Roentgenol* 2013; 200: 24-34. DOI: 10.2214/AJR.12.9543.

94. Alsop DC, Detre JA, Golay X, et al. Recommended implementation of arterial spin-labeled perfusion MRI for clinical applications: A consensus of the ISMRM perfusion study group and the European consortium for ASL in dementia. *Magnetic Resonance in Medicine* 2015; 73: spcone-spcone. DOI: 10.1002/mrm.25607.

95. Alsop DC and Detre JA. Reduced transit-time sensitivity in noninvasive magnetic resonance imaging of human cerebral blood flow. *J Cereb Blood Flow Metab* 1996; 16: 1236-1249. 1996/11/01. DOI: 10.1097/00004647-199611000-00019.

96. Zaharchuk G. Arterial Spin Labeling for Acute Stroke: Practical Considerations. *Transl Stroke Res* 2012; 3: 228-235. DOI: 10.1007/s12975-012-0159-8.

97. Ogawa S, Lee TM, Nayak AS, et al. Oxygenation-sensitive contrast in magnetic resonance image of rodent brain at high magnetic fields. *Magnetic resonance in medicine* 1990; 14: 68-78. 1990/04/01. DOI: 10.1002/mrm.1910140108.

98. Ogawa S and Lee TM. Magnetic resonance imaging of blood vessels at high fields: in vivo and in vitro measurements and image simulation. *Magnetic resonance in medicine* 1990; 16: 9-18. 1990/10/01. DOI: 10.1002/mrm.1910160103.

99. Bandettini PA, Wong EC, Hinks RS, et al. Time course EPI of human brain function during task activation. *Magnetic resonance in medicine* 1992; 25: 390-397. 1992/06/01. DOI: 10.1002/mrm.1910250220.

100. Ogawa S, Tank DW, Menon R, et al. Intrinsic signal changes accompanying sensory stimulation: functional brain mapping with magnetic resonance imaging. *Proceedings of the National Academy of Sciences of the United States of America* 1992; 89: 5951-5955. 1992/07/01. DOI: 10.1073/pnas.89.13.5951.

101. Buxton RB and Frank LR. A model for the coupling between cerebral blood flow and oxygen metabolism during neural stimulation. *Journal of cerebral blood flow and metabolism : official journal of the International Society of Cerebral Blood Flow and Metabolism* 1997; 17: 64-72. 1997/01/01. DOI: 10.1097/00004647-199701000-00009.

102. Grefkes C and Fink GR. Connectivity-based approaches in stroke and recovery of

function. *Lancet Neurol* 2014; 13: 206-216. 2014/01/25. DOI: 10.1016/s1474-4422(13)70264-3.

103. Biswal B, Zerrin Yetkin F, Haughton VM, et al. Functional connectivity in the motor cortex of resting human brain using echo-planar mri. *Magnetic resonance in medicine* 1995; 34: 537-541. DOI: https://doi.org/10.1002/mrm.1910340409.

104. Grefkes C and Fink GR. Reorganization of cerebral networks after stroke: new insights from neuroimaging with connectivity approaches. *Brain : a journal of neurology* 2011; 134: 1264-1276. DOI: 10.1093/brain/awr033.

105. Andrews RJ. Transhemispheric diaschisis. A review and comment. *Stroke; a journal of cerebral circulation* 1991; 22: 943-949.

106. Buxton RB, Uludağ K, Dubowitz DJ, et al. Modeling the hemodynamic response to brain activation. *NeuroImage* 2004; 23 Suppl 1: S220-233. 2004/10/27. DOI: 10.1016/j.neuroimage.2004.07.013.

107. D'Esposito M, Deouell LY and Gazzaley A. Alterations in the BOLD fMRI signal with ageing and disease: a challenge for neuroimaging. *Nature reviews Neuroscience* 2003; 4: 863-872. 2003/11/05. DOI: 10.1038/nrn1246.

108. Klatzo I. Pathophysiological aspects of brain edema. *Acta Neuropathol* 1987; 72: 236-239. 1987/01/01. DOI: 10.1007/bf00691095.

109. Khalil AA, Ostwaldt AC, Nierhaus T, et al. Relationship Between Changes in the Temporal Dynamics of the Blood-Oxygen-Level-Dependent Signal and Hypoperfusion in Acute Ischemic Stroke. *Stroke; a journal of cerebral circulation* 2017; 48: 925-931. 2017/03/10. DOI: 10.1161/strokeaha.116.015566.

110. Khalil AA, Villringer K, Fiebach JB, et al. Non-invasive monitoring of longitudinal changes in cerebral hemodynamics in acute ischemic stroke using BOLD signal delay. *Journal of cerebral blood flow and metabolism : official journal of the International Society of Cerebral Blood Flow and Metabolism* 2020; 40: 23-34. 2018/10/20. DOI: 10.1177/0271678x18803951.

111. Lv Y, Margulies DS, Cameron Craddock R, et al. Identifying the perfusion deficit in acute stroke with resting-state functional magnetic resonance imaging. *Annals of Neurology* 2013; 73: 136-140. DOI: https://doi.org/10.1002/ana.23763.

112. Christen T, Jahanian H, Ni WW, et al. Noncontrast mapping of arterial delay and functional connectivity using resting-state functional MRI: A study in Moyamoya patients. *Journal of Magnetic Resonance Imaging* 2015; 41: 424-430. DOI: https://doi.org/10.1002/jmri.24558.

113. Siegel JS, Snyder AZ, Ramsey L, et al. The effects of hemodynamic lag on functional connectivity and behavior after stroke. *Journal of cerebral blood flow and metabolism :*

official journal of the International Society of Cerebral Blood Flow and Metabolism 2016; 36: 2162-2176. 2015/12/15. DOI: 10.1177/0271678x15614846.

114. Vigneau-Roy N, Bernier M, Descoteaux M, et al. Regional variations in vascular density correlate with resting-state and task-evoked blood oxygen level-dependent signal amplitude. *Human brain mapping* 2014; 35: 1906-1920. 2013/07/12. DOI: 10.1002/hbm.22301.

115. Mandell DM, Han JS, Poublanc J, et al. Mapping cerebrovascular reactivity using blood oxygen level-dependent MRI in Patients with arterial steno-occlusive disease: comparison with arterial spin labeling MRI. *Stroke; a journal of cerebral circulation* 2008; 39: 2021-2028. 2008/05/03. DOI: 10.1161/strokeaha.107.506709.

116. Golestani AM, Wei LL and Chen JJ. Quantitative mapping of cerebrovascular reactivity using resting-state BOLD fMRI: Validation in healthy adults. *NeuroImage* 2016; 138: 147-163. 2016/05/15. DOI: 10.1016/j.neuroimage.2016.05.025.

117. Smeeing DP, Hendrikse J, Petersen ET, et al. Arterial Spin Labeling and Blood Oxygen Level-Dependent MRI Cerebrovascular Reactivity in Cerebrovascular Disease: A Systematic Review and Meta-Analysis. *Cerebrovascular diseases* 2016; 42: 288-307. 2016/05/31. DOI: 10.1159/000446081.

118. Yang HS, Liang Z, Yao JF, et al. Vascular effects of caffeine found in BOLD fMRI. *J Neurosci Res* 2019; 97: 456-466. 2018/11/30. DOI: 10.1002/jnr.24360.

119. Rack-Gomer AL, Liau J and Liu TT. Caffeine reduces resting-state BOLD functional connectivity in the motor cortex. *NeuroImage* 2009; 46: 56-63. 2009/05/22. DOI: 10.1016/j.neuroimage.2009.02.001.

120. Atwi S, Robertson AD, Theyers AE, et al. Cardiac-Related Pulsatility in the Insula Is Directly Associated With Middle Cerebral Artery Pulsatility Index. *J Magn Reson Imaging* 2020; 51: 1454-1462. 2019/11/02. DOI: 10.1002/jmri.26950.

121. Pedersen PM, Jorgensen HS, Nakayama H, et al. Aphasia in acute stroke: incidence, determinants, and recovery. *Annals of neurology* 1995; 38: 659-666. 1995/10/01. DOI: 10.1002/ana.410380416.

122. Engstrom G, Hedblad B, Juul-Moller S, et al. Cardiac Arrhythmias and Stroke : Increased Risk in Men With High Frequency of Atrial Ectopic Beats. *Stroke; a journal of cerebral circulation* 2000; 31: 2925-2929. DOI: 10.1161/01.str.31.12.2925.

123. Nogues MA and Benarroch E. Abnormalities of respiratory control and the respiratory motor unit. *Neurologist* 2008; 14: 273-288. DOI: 10.1097/NRL.0b013e318173e830.

124. Shirzadi Z, Stefanovic B, Chappell MA, et al. Enhancement of automated blood flow estimates (ENABLE) from arterial spin-labeled MRI. *Journal of magnetic resonance imaging*

: JMRI 2018; 47: 647-655. 2017/07/07. DOI: 10.1002/jmri.25807.

125. Tan H, Maldjian JA, Pollock JM, et al. A fast, effective filtering method for improving clinical pulsed arterial spin labeling MRI. *Journal of magnetic resonance imaging : JMRI* 2009; 29: 1134-1139. 2009/04/24. DOI: 10.1002/jmri.21721.

126. Stone JV, Porrill J, Porter NR, et al. Spatiotemporal independent component analysis of event-related fMRI data using skewed probability density functions. *NeuroImage* 2002; 15: 407-421. 2002/01/19. DOI: 10.1006/nimg.2001.0986.

127. Thomas CG, Harshman RA and Menon RS. Noise reduction in BOLD-based fMRI using component analysis. *NeuroImage* 2002; 17: 1521-1537. 2002/11/05.

128. Bullmore E and Sporns O. Complex brain networks: graph theoretical analysis of structural and functional systems. *Nature reviews Neuroscience* 2009; 10: 186-198. 2009/02/05. DOI: 10.1038/nrn2575.

129. Sporns O. Graph theory methods: applications in brain networks. *Dialogues Clin Neurosci* 2018; 20: 111-121. DOI: 10.31887/DCNS.2018.20.2/osporns.

130. Bassett DS and Bullmore E. Small-world brain networks. *Neuroscientist* 2006; 12: 512-523. 2006/11/03. DOI: 10.1177/1073858406293182.

131. Watts DJ and Strogatz SH. Collective dynamics of 'small-world' networks. *Nature* 1998; 393: 440-442. DOI: 10.1038/30918.

132. Battiston F, Cencetti G, Iacopini I, et al. Networks beyond pairwise interactions: Structure and dynamics. *Physics Reports* 2020; 874: 1-92. DOI: https://doi.org/10.1016/j.physrep.2020.05.004.

133. Carlsson G. Topological methods for data modelling. *Nature Reviews Physics* 2020; 2: 697-708. DOI: 10.1038/s42254-020-00249-3.

134. Sizemore AE, Giusti C, Kahn A, et al. Cliques and cavities in the human connectome. *J Comput Neurosci* 2018; 44: 115-145. 2017/11/16. DOI: 10.1007/s10827-017-0672-6.

135. Reimann MW, Nolte M, Scolamiero M, et al. Cliques of Neurons Bound into Cavities Provide a Missing Link between Structure and Function. *Frontiers in Computational Neuroscience* 2017; 11. Original Research. DOI: 10.3389/fncom.2017.00048.

136. Carlsson G. Topology and data. *BULLETIN (New Series) OF THE AMERICAN MATHEMATICAL SOCIETY* 2009; 46.

137. Zomorodian AJ. *Topology for computing*. Cambridge: Cambridge University Press, 2009.

138. Expert P, Lord L-D, Kringelbach ML, et al. Editorial: Topological Neuroscience.

Network Neuroscience 2019; 3: 653-655. DOI: 10.1162/netn_e_00096.

139. Petri G, Expert P, Turkheimer F, et al. Homological scaffolds of brain functional networks. *J R Soc Interface* 2014; 11: 20140873. 2014/11/18. DOI: 10.1098/rsif.2014.0873.

140. Gracia-Tabuenca Z, Díaz-Patiño JC, Arelio I, et al. Topological Data Analysis Reveals Robust Alterations in the Whole-Brain and Frontal Lobe Functional Connectomes in Attention-Deficit/Hyperactivity Disorder. *eneuro* 2020; 7: ENEURO.0543-0519.2020. DOI: 10.1523/eneuro.0543-19.2020.

141. Santos FAN, Raposo EP, Coutinho-Filho MD, et al. Topological phase transitions in functional brain networks. *Phys Rev E* 2019; 100: 032414. 2019/10/24. DOI: 10.1103/PhysRevE.100.032414.

142. Lee J VY, Zafarmand M, Bossuyt P. Quality Assessment of Prognostic Accuracy Studies (QUAPAS): an extension of the Quality Assessment of Diagnostic Accuracy Studies (QUADAS-2) tool for systematic reviews of prognostic test accuracy studies *Cochrane Database of Systematic Reviews* 2020. DOI: 10.1002/14651858.Cd201901.

143. Whiting PF, Rutjes AW, Westwood ME, et al. QUADAS-2: a revised tool for the quality assessment of diagnostic accuracy studies. *Ann Intern Med* 2011; 155: 529-536. 2011/10/19. DOI: 10.7326/0003-4819-155-8-201110180-00009.

144. Moher D, Liberati A, Tetzlaff J, et al. Preferred reporting items for systematic reviews and meta-analyses: the PRISMA statement. *PLoS Med* 2009; 6: e1000097. 2009/07/22. DOI: 10.1371/journal.pmed.1000097.

145. Johnston KC, Wagner DP, Wang XQ, et al. Validation of an acute ischemic stroke model: does diffusion-weighted imaging lesion volume offer a clinically significant improvement in prediction of outcome? *Stroke; a journal of cerebral circulation* 2007; 38: 1820-1825. 2007/04/21. DOI: 10.1161/strokeaha.106.479154.

146. Wardlaw JM, Keir SL, Bastin ME, et al. Is diffusion imaging appearance an independent predictor of outcome after ischemic stroke? *Neurology* 2002; 59: 1381-1387. 2002/11/13. DOI: 10.1212/01.wnl.0000032495.71720.c3.

147. Lin SF, Chen CI, Hu HH, et al. Predicting functional outcomes of posterior circulation acute ischemic stroke in first 36 h of stroke onset. *Journal of neurology* 2018; 265: 926-932. 2018/02/20. DOI: 10.1007/s00415-018-8746-6.

148. Nagel S, Herweh C, Köhrmann M, et al. MRI in patients with acute basilar artery occlusion - DWI lesion scoring is an independent predictor of outcome. *International journal of stroke : official journal of the International Stroke Society* 2012; 7: 282-288. 2011/12/14. DOI: 10.1111/j.1747-4949.2011.00705.x.

149. Tei H, Uchiyama S, Usui T, et al. Posterior circulation ASPECTS on diffusion-weighted MRI can be a powerful marker for predicting functional outcome. *Journal of neurology*

2010; 257: 767-773. 2009/11/28. DOI: 10.1007/s00415-009-5406-x.

150. Turc G, Apoil M, Naggara O, et al. Magnetic Resonance Imaging-DRAGON score: 3-month outcome prediction after intravenous thrombolysis for anterior circulation stroke. *Stroke; a journal of cerebral circulation* 2013; 44: 1323-1328. 2013/03/14. DOI: 10.1161/strokeaha.111.000127.

151. Nezu T, Koga M, Kimura K, et al. Pretreatment ASPECTS on DWI predicts 3-month outcome following rt-PA: SAMURAI rt-PA Registry. *Neurology* 2010; 75: 555-561. 2010/08/11. DOI: 10.1212/WNL.0b013e3181eccf78.

152. Ryu WS, Woo SH, Schellingerhout D, et al. Stroke outcomes are worse with larger leukoaraiosis volumes. *Brain : a journal of neurology* 2017; 140: 158-170. 2016/12/23. DOI: 10.1093/brain/aww259.

153. Gómez-Choco M, Mengual JJ, Rodríguez-Antigüedad J, et al. Pre-Existing Cerebral Small Vessel Disease Limits Early Recovery in Patients with Acute Lacunar Infarct. *Journal of stroke and cerebrovascular diseases : the official journal of National Stroke Association* 2019; 28: 104312. 2019/08/10. DOI: 10.1016/j.jstrokecerebrovasdis.2019.104312.

154. Etherton MR, Wu O, Cougo P, et al. Integrity of normal-appearing white matter and functional outcomes after acute ischemic stroke. *Neurology* 2017; 88: 1701-1708. 2017/04/07. DOI: 10.1212/wnl.0000000000003890.

155. Findlater SE, Hawe RL, Mazerolle EL, et al. Comparing CST Lesion Metrics as Biomarkers for Recovery of Motor and Proprioceptive Impairments After Stroke. *Neurorehabilitation and neural repair* 2019; 33: 848-861. 2019/08/23. DOI: 10.1177/1545968319868714.

156. Lasek-Bal A, Kidoń J, Błaszczyszyn M, et al. BOLD fMRI signal in stroke patients and its importance for prognosis in the subacute disease period - Preliminary report. *Neurol Neurochir Pol* 2018; 52: 341-346. 2018/01/14. DOI: 10.1016/j.pjnns.2017.12.006.

157. Du J, Yang F, Zhang Z, et al. Early functional MRI activation predicts motor outcome after ischemic stroke: a longitudinal, multimodal study. *Brain Imaging Behav* 2018; 12: 1804-1813. 2018/05/17. DOI: 10.1007/s11682-018-9851-y.

158. Abela E, Missimer JH, Pastore-Wapp M, et al. Early prediction of long-term tactile object recognition performance after sensorimotor stroke. *Cortex* 2019; 115: 264-279. 2019/03/16. DOI: 10.1016/j.cortex.2019.01.018.

159. Chi NF, Ku HL, Chen DY, et al. Cerebral Motor Functional Connectivity at the Acute Stage: An Outcome Predictor of Ischemic Stroke. *Sci Rep* 2018; 8: 16803. 2018/11/16. DOI: 10.1038/s41598-018-35192-y.

160. Lee J, Park E, Lee A, et al. Alteration and Role of Interhemispheric and Intrahemispheric Connectivity in Motor Network After Stroke. *Brain topography* 2018; 31:

708-719. 2018/04/20. DOI: 10.1007/s10548-018-0644-9.

161. Lee J, Park E, Lee A, et al. Recovery-related indicators of motor network plasticity according to impairment severity after stroke. *Eur J Neurol* 2017; 24: 1290-1299. 2017/08/24. DOI: 10.1111/ene.13377.

162. Lee J, Lee M, Kim DS, et al. Functional reorganization and prediction of motor recovery after a stroke: A graph theoretical analysis of functional networks. *Restor Neurol Neurosci* 2015; 33: 785-793. 2015/10/21. DOI: 10.3233/rnn-140467.

163. Wilke M, de Haan B, Juenger H, et al. Manual, semi-automated, and automated delineation of chronic brain lesions: a comparison of methods. *NeuroImage* 2011; 56: 2038-2046. DOI: 10.1016/j.neuroimage.2011.04.014.

164. Neumann AB, Jonsdottir KY, Mouridsen K, et al. Interrater agreement for final infarct MRI lesion delineation. *Stroke; a journal of cerebral circulation* 2009; 40: 3768-3771. Comparative Study Multicenter Study Research Support, Non-U.S. Gov't 2009/10/03. DOI: 10.1161/STROKEAHA.108.545368.

165. Muir KW, Buchan A, von Kummer R, et al. Imaging of acute stroke. *Lancet Neurol* 2006; 5: 755-768. 2006/08/18. DOI: 10.1016/s1474-4422(06)70545-2.

166. Sudlow CL and Warlow CP. Comparable studies of the incidence of stroke and its pathological types: results from an international collaboration. International Stroke Incidence Collaboration. *Stroke; a journal of cerebral circulation* 1997; 28: 491-499. 1997/03/01. DOI: 10.1161/01.str.28.3.491.

167. Bullmore ET and Bassett DS. Brain graphs: graphical models of the human brain connectome. *Annu Rev Clin Psychol* 2011; 7: 113-140. 2010/12/07. DOI: 10.1146/annurev-clinpsy-040510-143934.

168. Merino JG, Lattimore SU and Warach S. Telephone Assessment of Stroke Outcome Is Reliable. *Stroke* 2005; 36: 232-233. DOI: 10.1161/01.STR.0000153055.43138.2f.

169. Smith SM, Jenkinson M, Woolrich MW, et al. Advances in functional and structural MR image analysis and implementation as FSL. *Neuroimage* 2004; 23 Suppl 1: S208-219. Research Support, Non-U.S. Gov't Review 2004/10/27. DOI: 10.1016/j.neuroimage.2004.07.051.

170. Woolrich MW, Jbabdi S, Patenaude B, et al. Bayesian analysis of neuroimaging data in FSL. *Neuroimage* 2009; 45: S173-186. Research Support, Non-U.S. Gov't 2008/12/09. DOI: 10.1016/j.neuroimage.2008.10.055.

171. Jenkinson M, Beckmann CF, Behrens TE, et al. FSL. *NeuroImage* 2012; 62: 782-790. 2011/10/08. DOI: 10.1016/j.neuroimage.2011.09.015.

172. Purushotham A, Campbell BC, Straka M, et al. Apparent diffusion coefficient

threshold for delineation of ischemic core. *International journal of stroke : official journal of the International Stroke Society* 2015; 10: 348-353. 2013/06/28. DOI: 10.1111/ijs.12068.

173. Maier O, Menze BH, von der Gablentz J, et al. ISLES 2015 - A public evaluation benchmark for ischemic stroke lesion segmentation from multispectral MRI. *Med Image Anal* 2017; 35: 250-269. DOI: 10.1016/j.media.2016.07.009.

174. Harston GW, Okell TW, Sheerin F, et al. Quantification of Serial Cerebral Blood Flow in Acute Stroke Using Arterial Spin Labeling. *Stroke; a journal of cerebral circulation* 2017; 48: 123-130. 2016/11/24. DOI: 10.1161/strokeaha.116.014707.

175. Zhang Y, Brady M and Smith S. Segmentation of brain MR images through a hidden Markov random field model and the expectation-maximization algorithm. *IEEE transactions on medical imaging* 2001; 20: 45-57. 2001/04/11. DOI: 10.1109/42.906424.

176. Desikan RS, Segonne F, Fischl B, et al. An automated labeling system for subdividing the human cerebral cortex on MRI scans into gyral based regions of interest. *Neuroimage* 2006; 31: 968-980. Research Support, N.I.H., Extramural Research Support, Non-U.S. Gov't 2006/03/15. DOI: 10.1016/j.neuroimage.2006.01.021.

177. Lyden P, Lu M, Jackson C, et al. Underlying structure of the National Institutes of Health Stroke Scale: results of a factor analysis. NINDS tPA Stroke Trial Investigators. *Stroke; a journal of cerebral circulation* 1999; 30: 2347-2354. 1999/11/05. DOI: 10.1161/01.str.30.11.2347.

178. Harrison JK, McArthur KS and Quinn TJ. Assessment scales in stroke: clinimetric and clinical considerations. *Clin Interv Aging* 2013; 8: 201-211. 2013/02/27. DOI: 10.2147/cia.S32405.

179. Kasner SE. Clinical interpretation and use of stroke scales. *Lancet Neurol* 2006; 5: 603-612. 2006/06/20. DOI: 10.1016/s1474-4422(06)70495-1.

180. Wijdicks EF, Sheth KN, Carter BS, et al. Recommendations for the management of cerebral and cerebellar infarction with swelling: a statement for healthcare professionals from the American Heart Association/American Stroke Association. *Stroke; a journal of cerebral circulation* 2014; 45: 1222-1238. 2014/02/01. DOI: 10.1161/01.str.0000441965.15164.d6.

181. Lansberg MG, Straka M, Kemp S, et al. MRI profile and response to endovascular reperfusion after stroke (DEFUSE 2): a prospective cohort study. *Lancet Neurol* 2012; 11: 860-867. Comparative Study Multicenter Study Research Support, N.I.H., Extramural 2012/09/08. DOI: 10.1016/S1474-4422(12)70203-X.

182. Kidwell CS, Jahan R, Gornbein J, et al. A trial of imaging selection and endovascular treatment for ischemic stroke. *N Engl J Med* 2013; 368: 914-923. Clinical Trial, Phase IIMulticenter Study Randomized Controlled Trial Research Support, N.I.H., Extramural Research Support, Non-U.S. Gov't 2013/02/12. DOI: 10.1056/NEJMoa1212793.

183. Davis SM, Donnan GA, Parsons MW, et al. Effects of alteplase beyond 3 h after stroke in the Echoplanar Imaging Thrombolytic Evaluation Trial (EPITHET): a placebo-controlled randomised trial. *Lancet Neurol* 2008; 7: 299-309. Clinical Trial, Phase IIRandomized Controlled Trial Research Support, Non-U.S. Gov't.

184. Rekik I, Allassonniere S, Carpenter TK, et al. Corrigendum to "Medical image analysis methods in MR/CT-imaged acute-subacute ischemic stroke lesion: Segmentation, prediction and insights into dynamic evolution simulation models. A critical appraisal" [NeuroImage: Clinical 1 (2012) 164-178]. *NeuroImage Clinical* 2013; 2: 600. DOI: 10.1016/j.nicl.2013.04.013.

185. Griffanti L, Zamboni G, Khan A, et al. BIANCA (Brain Intensity AbNormality Classification Algorithm): A new tool for automated segmentation of white matter hyperintensities. *Neuroimage* 2016; 141: 191-205. DOI: 10.1016/j.neuroimage.2016.07.018.

186. Zamboni G, Griffanti L, Jenkinson M, et al. White Matter Imaging Correlates of Early Cognitive Impairment Detected by the Montreal Cognitive Assessment After Transient Ischemic Attack and Minor Stroke. *Stroke; a journal of cerebral circulation* 2017; 48: 1539-1547. DOI: 10.1161/STROKEAHA.116.016044.

187. Weeda MM, Brouwer I, de Vos ML, et al. Comparing lesion segmentation methods in multiple sclerosis: Input from one manually delineated subject is sufficient for accurate lesion segmentation. *Neuroimage Clin* 2019; 24: 102074. 2019/11/18. DOI: 10.1016/j.nicl.2019.102074.

188. Broocks G, Flottmann F, Scheibel A, et al. Quantitative Lesion Water Uptake in Acute Stroke Computed Tomography Is a Predictor of Malignant Infarction. *Stroke; a journal of cerebral circulation* 2018; 49: 1906-1912. 2018/07/07. DOI: 10.1161/strokeaha.118.020507.

189. Harston GW, Minks D, Sheerin F, et al. Optimizing image registration and infarct definition in stroke research. *Ann Clin Transl Neurol* 2017; 4: 166-174. 2017/03/10. DOI: 10.1002/acn3.388.

190. Kimberly WT, Bevers MB, von Kummer R, et al. Effect of IV glyburide on adjudicated edema endpoints in the GAMES-RP Trial. *Neurology* 2018; 91: e2163-e2169. DOI: 10.1212/wnl.0000000000006618.

191. Wu O, Winzeck S, Giese AK, et al. Big Data Approaches to Phenotyping Acute Ischemic Stroke Using Automated Lesion Segmentation of Multi-Center Magnetic Resonance Imaging Data. *Stroke; a journal of cerebral circulation* 2019; 50: 1734-1741. 2019/06/11. DOI: 10.1161/strokeaha.119.025373.

192. Dyrby TB, Rostrup E, Baaré WF, et al. Segmentation of age-related white matter changes in a clinical multi-center study. *NeuroImage* 2008; 41: 335-345. 2008/04/09. DOI: 10.1016/j.neuroimage.2008.02.024.

193. Sundaresan V, Zamboni G, Le Heron C, et al. Automated lesion segmentation with BIANCA: Impact of population-level features, classification algorithm and locally adaptive thresholding. *NeuroImage* 2019; 202: 116056. 2019/08/04. DOI: 10.1016/j.neuroimage.2019.116056.

194. Wei H, Jia FM, Yin HX, et al. Decompressive hemicraniectomy versus medical treatment of malignant middle cerebral artery infarction: a systematic review and meta-analysis. *Biosci Rep* 2020; 40 2019/12/20. DOI: 10.1042/bsr20191448.

195. Detre JA, Leigh JS, Williams DS, et al. Perfusion imaging. *Magnetic Resonance in Medicine* 1992; 23: 37-45. DOI: 10.1002/mrm.1910230106.

196. Wang DJ, Alger JR, Qiao JX, et al. Multi-delay multi-parametric arterial spin-labeled perfusion MRI in acute ischemic stroke - Comparison with dynamic susceptibility contrast enhanced perfusion imaging. *NeuroImage Clinical* 2013; 3: 1-7. 2013/10/26. DOI: 10.1016/j.nicl.2013.06.017.

197. Okell TW, Chappell MA, Kelly ME, et al. Cerebral blood flow quantification using vessel-encoded arterial spin labeling. *Journal of cerebral blood flow and metabolism : official journal of the International Society of Cerebral Blood Flow and Metabolism* 2013; 33: 1716-1724. 2013/08/08. DOI: 10.1038/jcbfm.2013.129.

198. Grade M, Hernandez Tamames JA, Pizzini FB, et al. A neuroradiologist's guide to arterial spin labeling MRI in clinical practice. *Neuroradiology* 2015; 57: 1181-1202. 2015/09/10. DOI: 10.1007/s00234-015-1571-z.

199. Kochiyama T MT, Okada T, Yonekura Y, Matsumura M, Sadato N. . Removing the effects of task-related motion using independent-component analysis.. *Neuroimage* 2005; 25: 802–814.

200. McKeown M, Hu YJ and Jane Wang Z. ICA Denoising for Event-Related fMRI Studies. *Conference proceedings : Annual International Conference of the IEEE Engineering in Medicine and Biology Society IEEE Engineering in Medicine and Biology Society Annual Conference* 2005; 1: 157-161. 2007/02/07. DOI: 10.1109/IEMBS.2005.1616366.

201. Zou Q WC, Stein EA, Zang Y, Yang Y. . Static and dynamic characteristics of cerebral blood flow during the resting state. . *NeuroImage* 2009; 48: 515–524.

202. Arfanakis K, Cordes D, Haughton VM, et al. Independent component analysis applied to diffusion tensor MRI. *Magn Reson Med* 2002; 47: 354-363.

203. Calamante F, Morup M and Hansen LK. Defining a local arterial input function for perfusion MRI using independent component analysis. *Magnetic Resonance in Medicine* 2004; 52: 789-797. DOI: 10.1002/mrm.20227.

204. Wells JA, Thomas DL, King MD, et al. Reduction of errors in ASL cerebral perfusion and arterial transit time maps using image de-noising. *Magn Reson Med* 2010; 64: 715-724.

DOI: 10.1002/mrm.22319.

205. Behzadi Y, Restom K, Liau J, et al. A component based noise correction method (CompCor) for BOLD and perfusion based fMRI. *NeuroImage* 2007; 37: 90-101. 2007/06/15. DOI: 10.1016/j.neuroimage.2007.04.042.

206. Jenkinson M, Bannister P, Brady M, et al. Improved optimization for the robust and accurate linear registration and motion correction of brain images. *NeuroImage* 2002; 17: 825-841. 2002/10/16.

207. Smith SM. Fast robust automated brain extraction. *Human brain mapping* 2002; 17: 143-155. 2002/10/23. DOI: 10.1002/hbm.10062.

208. Chappell MA GA, Whitcher B, Woolrich MW. Variational Bayesian inference for a non-linear forward model. *IEEE Transactions on Signal Processing* 2009; 57: 223-236.

209. Jenkinson M and Smith S. A global optimisation method for robust affine registration of brain images. *Medical image analysis* 2001; 5: 143-156. 2001/08/23.

210. Beckmann CF and Smith SM. Probabilistic independent component analysis for functional magnetic resonance imaging. *IEEE transactions on medical imaging* 2004; 23: 137-152. 2004/02/18. DOI: 10.1109/TMI.2003.822821.

211. Griffanti L S-KG, Beckmann CF, Auerbach EJ, Douaud G, Sexton CE, Zsoldos E, Ebmeier KP, Filippini N, Mackay CE, Moeller S, Xu J, Yacoub E, Baselli G, Ugurbil K, Miller KL, Smith SM. I. ICA-based artefact removal and accelerated fMRI acquisition for improved resting state network imaging. *Neuroimage* 2014; 95: 232-247.

212. Salimi-Khorshidi G, Douaud, G., Beckmann, C.F., Glasser, M., Griffanti, L., Smith, S. M. Automatic denoising of functional MRI data: combining independent component analysis and hierarchical fusion of classifiers. . *NeuroImage* 2014; 90: 449–468.

213. Khalili-Mahani N, Chang C, van Osch MJ, et al. The impact of "physiological correction" on functional connectivity analysis of pharmacological resting state fMRI. *NeuroImage* 2013; 65: 499-510. 2012/10/02. DOI: 10.1016/j.neuroimage.2012.09.044.

214. Carone D, Licenik R, Suri S, et al. Impact of automated ICA-based denoising of fMRI data in acute stroke patients. *Neuroimage Clin* 2017; 16: 23-31. 2017/07/25. DOI: 10.1016/j.nicl.2017.06.033.

215. MacIntosh BJ, Filippini N, Chappell MA, et al. Assessment of arterial arrival times derived from multiple inversion time pulsed arterial spin labeling MRI. *Magnetic resonance in medicine* 2010; 63: 641-647. 2010/02/11. DOI: 10.1002/mrm.22256.

216. Gardener AG and Jezzard P. Investigating white matter perfusion using optimal sampling strategy arterial spin labeling at 7 Tesla. *Magnetic resonance in medicine* 2015; 73: 2243-2248. 2014/06/24. DOI: 10.1002/mrm.25333.

217. Pruim RHR, Mennes M, Buitelaar JK, et al. Evaluation of ICA-AROMA and alternative strategies for motion artifact removal in resting state fMRI. *NeuroImage* 2015; 112: 278-287. 2015/03/17. DOI: 10.1016/j.neuroimage.2015.02.063.

218. Parkes L, Fulcher B, Yucel M, et al. An evaluation of the efficacy, reliability, and sensitivity of motion correction strategies for resting-state functional MRI. *NeuroImage* 2018; 171: 415-436. 2017/12/27. DOI: 10.1016/j.neuroimage.2017.12.073.

219. James GA, Lu ZL, VanMeter JW, et al. Changes in resting state effective connectivity in the motor network following rehabilitation of upper extremity poststroke paresis. *Topics in stroke rehabilitation* 2009; 16: 270-281. 2009/09/11. DOI: 10.1310/tsr1604-270.

220. Biswal BB and Ulmer JL. Blind source separation of multiple signal sources of fMRI data sets using independent component analysis. *Journal of computer assisted tomography* 1999; 23: 265-271. 1999/03/30.

221. De Martino F, Gentile F, Esposito F, et al. Classification of fMRI independent components using IC-fingerprints and support vector machine classifiers. *NeuroImage* 2007; 34: 177-194. 2006/10/31. DOI: 10.1016/j.neuroimage.2006.08.041.

222. Rummel C, Verma RK, Schopf V, et al. Time course based artifact identification for independent components of resting-state FMRI. *Frontiers in human neuroscience* 2013; 7: 214. 2013/06/05. DOI: 10.3389/fnhum.2013.00214.

223. Veldsman M and Brodtmann A. Disconnectomics: Stroke-related disconnection and dysfunction in distributed brain networks. *International Journal of Stroke* 2019; 14: 6-8. DOI: 10.1177/1747493018806166.

224. Carlsson G. *BULLETIN (New Series) OF THE AMERICAN MATHEMATICAL SOCIETY* 2009; 46.

225. Filippini N, Zsoldos E, Haapakoski R, et al. Study protocol: the Whitehall II imaging sub-study. *BMC Psychiatry* 2014; 14: 159. DOI: 10.1186/1471-244X-14-159.

226. Chappell MA, Groves AR, Whitcher B, et al. Variational Bayesian Inference for a Nonlinear Forward Model. *IEEE Transactions on Signal Processing* 2009; 57: 223-236. DOI: 10.1109/TSP.2008.2005752.

227. Alfaro-Almagro F, Jenkinson M, Bangerter NK, et al. Image processing and Quality Control for the first 10,000 brain imaging datasets from UK Biobank. *NeuroImage* 2018; 166: 400-424. 2017/10/29. DOI: 10.1016/j.neuroimage.2017.10.034.

228. Griffanti L, Salimi-Khorshidi G, Beckmann CF, et al. ICA-based artefact removal and accelerated fMRI acquisition for improved resting state network imaging. *NeuroImage* 2014; 95: 232-247. 2014/03/25. DOI: 10.1016/j.neuroimage.2014.03.034.

229. Salimi-Khorshidi G, Douaud G, Beckmann CF, et al. Automatic denoising of

functional MRI data: combining independent component analysis and hierarchical fusion of classifiers. *NeuroImage* 2014; 90: 449-468. 2014/01/07. DOI: 10.1016/j.neuroimage.2013.11.046.

230. Filippini N, MacIntosh BJ, Hough MG, et al. Distinct patterns of brain activity in young carriers of the APOE-epsilon4 allele. *Proceedings of the National Academy of Sciences of the United States of America* 2009; 106: 7209-7214. DOI: 10.1073/pnas.0811879106.

231. Smith SM, Beckmann CF, Andersson J, et al. Resting-state fMRI in the Human Connectome Project. *NeuroImage* 2013; 80: 144-168. 2013/05/25. DOI: 10.1016/j.neuroimage.2013.05.039.

232. Miller KL, Alfaro-Almagro F, Bangerter NK, et al. Multimodal population brain imaging in the UK Biobank prospective epidemiological study. *Nat Neurosci* 2016; 19: 1523-1536. 2016/10/28. DOI: 10.1038/nn.4393.

233. Manganotti P, Patuzzo S, Cortese F, et al. Motor disinhibition in affected and unaffected hemisphere in the early period of recovery after stroke. *Clinical neurophysiology : official journal of the International Federation of Clinical Neurophysiology* 2002; 113: 936-943. 2002/06/06. DOI: 10.1016/s1388-2457(02)00062-7.

234. National Institute of Neurological D and Stroke rt PASSG. Tissue plasminogen activator for acute ischemic stroke. *The New England journal of medicine* 1995; 333: 1581-1587. DOI: 10.1056/NEJM199512143332401.

235. Nelles G, Spiekramann G, Jueptner M, et al. Evolution of functional reorganization in hemiplegic stroke: a serial positron emission tomographic activation study. *Ann Neurol* 1999; 46: 901-909. 1999/12/10. DOI: 10.1002/1531-8249(199912)46:6<901::aid-ana13>3.0.co;2-7.

236. Feydy A, Carlier R, Roby-Brami A, et al. Longitudinal study of motor recovery after stroke: recruitment and focusing of brain activation. *Stroke; a journal of cerebral circulation* 2002; 33: 1610-1617. 2002/06/08. DOI: 10.1161/01.str.0000017100.68294.52.

237. Stolz BJ, Harrington HA and Porter MA. Persistent homology of time-dependent functional networks constructed from coupled time series. *Chaos* 2017; 27: 047410. 2017/05/01. DOI: 10.1063/1.4978997.

238. Schlegel DJ, Tanne D, Demchuk AM, et al. Prediction of hospital disposition after thrombolysis for acute ischemic stroke using the National Institutes of Health Stroke Scale. *Arch Neurol* 2004; 61: 1061-1064. 2004/07/21. DOI: 10.1001/archneur.61.7.1061.

239. Demaerschalk BM, Vegunta S, Vargas BB, et al. Reliability of real-time video smartphone for assessing National Institutes of Health Stroke Scale scores in acute stroke patients. *Stroke; a journal of cerebral circulation* 2012; 43: 3271-3277. 2012/11/20. DOI: 10.1161/strokeaha.112.669150.

240. Heidi Johansen-Berg TEJB. Diffusion MRI: From Quantitative Measurement to In vivo Neuroanatomy: Second Edition. 2013: 1–614.

241. Pierpaoli C and Basser PJ. Toward a quantitative assessment of diffusion anisotropy. *Magnetic resonance in medicine* 1996; 36: 893-906. DOI: https://doi.org/10.1002/mrm.1910360612.

242. Simard JM, Kent TA, Chen M, et al. Brain oedema in focal ischaemia: molecular pathophysiology and theoretical implications. *Lancet Neurol* 2007; 6: 258-268. 2007/02/17. DOI: 10.1016/s1474-4422(07)70055-8.

243. Battey TW, Karki M, Singhal AB, et al. Brain edema predicts outcome after nonlacunar ischemic stroke. *Stroke; a journal of cerebral circulation* 2014; 45: 3643-3648. 2014/10/23. DOI: 10.1161/strokeaha.114.006884.

244. Sheth KN, Elm JJ, Molyneaux BJ, et al. Safety and efficacy of intravenous glyburide on brain swelling after large hemispheric infarction (GAMES-RP): a randomised, double-blind, placebo-controlled phase 2 trial. *The Lancet Neurology* 2016; 15: 1160-1169. DOI: 10.1016/S1474-4422(16)30196-X.

245. Tong Y, Lindsey KP, Hocke LM, et al. Perfusion information extracted from resting state functional magnetic resonance imaging. *Journal of cerebral blood flow and metabolism : official journal of the International Society of Cerebral Blood Flow and Metabolism* 2017; 37: 564-576. 2016/02/14. DOI: 10.1177/0271678x16631755.

246. Zaharchuk G. Arterial spin labeling for acute stroke: practical considerations. *Transl Stroke Res* 2012; 3: 228-235. 2012/06/01. DOI: 10.1007/s12975-012-0159-8.

247. Tong Y and Frederick Bd. Tracking cerebral blood flow in BOLD fMRI using recursively generated regressors. *Human brain mapping* 2014; 35: 5471-5485. DOI: https://doi.org/10.1002/hbm.22564.

248. Jessen NA, Munk AS, Lundgaard I, et al. The Glymphatic System: A Beginner's Guide. *Neurochem Res* 2015; 40: 2583-2599. 2015/05/08. DOI: 10.1007/s11064-015-1581-6.

249. Mestre H, Tithof J, Du T, et al. Flow of cerebrospinal fluid is driven by arterial pulsations and is reduced in hypertension. *Nature Communications* 2018; 9: 4878. DOI: 10.1038/s41467-018-07318-3.

250. Mestre H, Du T, Sweeney AM, et al. Cerebrospinal fluid influx drives acute ischemic tissue swelling. *Science* 2020; 367: eaax7171. DOI: 10.1126/science.aax7171.

251. Bernier M, Cunnane SC and Whittingstall K. The morphology of the human cerebrovascular system. *Human brain mapping* 2018; 39: 4962-4975. DOI: https://doi.org/10.1002/hbm.24337.

252. Aslan S, Hocke L, Schwarz N, et al. Extraction of the cardiac waveform from

simultaneous multislice fMRI data using slice sorted averaging and a deep learning reconstruction filter. *NeuroImage* 2019; 198: 303-316. 2019/05/28. DOI: 10.1016/j.neuroimage.2019.05.049.

253. Heiss WD, Grond M, Thiel A, et al. Tissue at risk of infarction rescued by early reperfusion: A positron emission tomography study in systemic recombinant tissue plasminogen activator thrombolysis of acute stroke. *J Cereb Blood Flow Metab* 1998; 18: 1298-1307. Article.

254. del Zoppo GJ and Hallenbeck JM. Advances in the vascular pathophysiology of ischemic stroke. *Thromb Res* 2000; 98: 73-81. Research Support, U.S. Gov't, P.H.S.Review 2000/05/17.

255. Molina CA and Alvarez-Sabín J. Recanalization and Reperfusion Therapies for Acute Ischemic Stroke. *Cerebrovasc Dis* 2009; 27: 162-167.

256. Tong Y, Hocke LM, Fan X, et al. Can apparent resting state connectivity arise from systemic fluctuations? *Frontiers in human neuroscience* 2015; 9: 285. 2015/06/02. DOI: 10.3389/fnhum.2015.00285.

257. Hall CN, Reynell C, Gesslein B, et al. Capillary pericytes regulate cerebral blood flow in health and disease. *Nature* 2014; 508: 55-60. 2014/03/29. DOI: 10.1038/nature13165.

258. Tong LS, Guo ZN, Ou YB, et al. Cerebral venous collaterals: A new fort for fighting ischemic stroke? *Progress in neurobiology* 2018; 163-164: 172-193. 2017/12/05. DOI: 10.1016/j.pneurobio.2017.11.001.

259. Vila E and Salaices M. Cytokines and vascular reactivity in resistance arteries. *American Journal of Physiology-Heart and Circulatory Physiology* 2005; 288: H1016-H1021. DOI: 10.1152/ajpheart.00779.2004.

260. Liu J, Wang Y, Akamatsu Y, et al. Vascular remodeling after ischemic stroke: mechanisms and therapeutic potentials. *Progress in neurobiology* 2014; 115: 138-156. 2013/12/03. DOI: 10.1016/j.pneurobio.2013.11.004.

261. van Zijl PC, Eleff SM, Ulatowski JA, et al. Quantitative assessment of blood flow, blood volume and blood oxygenation effects in functional magnetic resonance imaging. *Nat Med* 1998; 4: 159-167. 1998/02/14. DOI: 10.1038/nm0298-159.

262. Yao Y, Zhang Y, Liao X, et al. Potential Therapies for Cerebral Edema After Ischemic Stroke: A Mini Review. *Frontiers in Aging Neuroscience* 2021; 12. Mini Review. DOI: 10.3389/fnagi.2020.618819.

263. Bardutzky J and Schwab S. Antiedema Therapy in Ischemic Stroke. *Stroke; a journal of cerebral circulation* 2007; 38: 3084-3094. DOI: doi:10.1161/STROKEAHA.107.490193.